SEPTEMBER, 1951

Journal of METALS

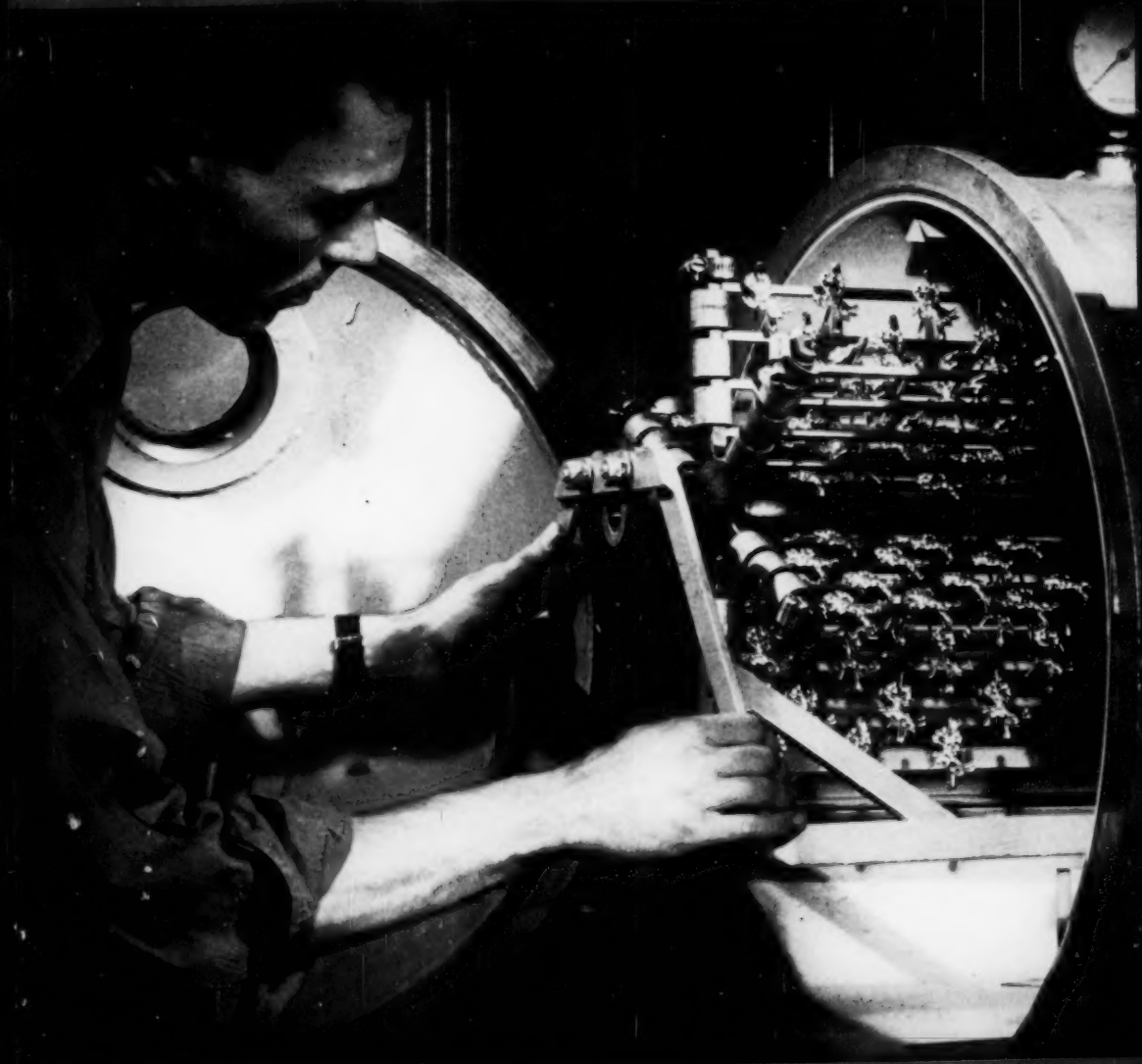

September JOURNAL OF METALS Highlights:

"Electrolytic Probe for Underground Corrosion Studies," - p. 706
"Nickel—A JOURNAL OF METALS Industry Report," - p. 712
"Gases in High Density Metal Powder Compacts," - p. 774

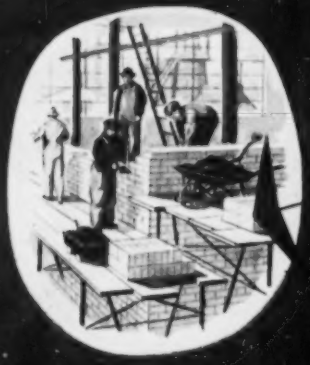

for maximum furnace life

THERE is no *one* bonding mortar that is best for all conditions. Harbison-Walker manufactures more than a score of different classes and types, each of which has definite fields of applications. From this complete line, there can be selected the brand that will insure greatest economy, minimum maintenance and maximum furnace life for any service.

Harbison-Walker mortar materials comprise

Air-Setting cements for making brick joints which remain strong over the temperature range of their utility.

Hot-Setting mortars to provide a bond which is firm and impermeable at high temperatures, and also flexible to permit relief of stresses caused by expansion.

Developed through research, these mortars have the optimum combinations of properties such as workability, water retention, thermal expansion, strength, refractoriness, impermeability and resistance to fluxes and gases. Great care has been given to achieve a nicely adjusted balance in each Harbison-Walker brand.

Harbison-Walker representatives welcome the opportunity to assist you in the selection of bonding materials that will provide the best service and economy in your furnaces.

To secure full benefit from the superior properties of refractory brick an equally superior bond is essential.

HARBISON-WALKER BONDS

for every service

AIR-SETTING	Harwaco Bond Coralite Bonding Mortar Korundal Bonding Mortar	High-Alumina
	Firebond—Siliceous	
	Thermolith—Chrome Base	
	Periklase Bonding Mortar H-W Forsterite	Basic
HOT-SETTING	Ankorite—High-Alumina	
	H-W Fine Ground Fire Clays H-W Super Duty-Mortar H-W Special Mortar Mix	Alumina-Silica
	Vega Bond Starbond Star Silica Cement H-W Coke Oven Silica Cement	Siliceous
	H-W 20 Bonding Mortar H-W 26 Bonding Mortar H-W 444 Bonding Mortar	For Insulating Brick
	H-W Furnace Magnesite H-W Special Furnace Chrome	Basic

HARBISON-WALKER

REFRACTORIES COMPANY

AND SUBSIDIARIES

World's Largest Producer of Refractories

General Offices: **PITTSBURGH 22, PENNA.**

Journal of METALS

VOL. 3, NO. 9 SEPTEMBER, 1951

Published to provide a continuing, authoritative, and up-to-date record of technological, engineering, and economic progress in all branches of the metals industry by the

Metals Branch

American Institute of Mining and Metallurgical Engineers, Inc.
29 West 39th Street, New York 18

THOMAS E. LLOYD
Manager of Publications
Editor, Journal of Metals

A. S. COHAN — Associate Editor

D. G. GARRETT — MARGARET BAGG
Assistant Editors

GRACE PUGSLEY — Production Manager

W. J. SEWING — Asst. Prod. Mgr.

METALS BRANCH COUNCIL

C. C. Long — Chairman
E. O. Kirkendall — Secretary
R. M. Brick — IMD Chairman
T. L. Joseph — ISD Chairman
O. C. Ralston — EMD Chairman
M. Gensamer — D. S. Eppelsheimer
H. K. Work — Evan Just

TECHNICAL PUBLICATIONS COMMITTEE

F. B. Foley — Chairman
E. J. Kennedy, Jr. — Secretary

AUXILIARY PUBLICATIONS COMMITTEE CHAIRMEN

F. N. Rhines — Institute of Metals Div.
F. M. Washburn — Iron & Steel Div.
Philip T. Stroup — Extract. Metal Div.

JAMES A. STANGARONE
Advertising Manager
New York

B. C. SNELL
Regional Manager, Pittsburgh
1110 McDonald Place, Sewickly, Pa.

The AIME Publishes:
Journal of Metals
Mining Engineering
Journal of Petroleum Technology

COVER

Vacuum metallizing is a method of depositing thin coats of metallics on base materials by metal evaporation in a vacuum. Almost any material can be coated. Complete surfaces can be coated, coating can be selective, and continuous roll coating is possible. This photo, made at F. J. Stokes Machine Co., shows costume jewelry mounted on a special jig, being coated with gold. Vacuum metallized parts require no finishing or buffing.

FEATURES AND NEWS

Journal of Metals Reporter	703	Meet the Authors	692
Titanium Capacity to Be Increased	705	IMD Fall Meeting	809
Research and Development Requirements	705	New Products	698
Employment Service	700	Coming Events	694
		Personals	811
		New Members	812

TECHNICAL ARTICLES

Electrolytic Probe for Underground Corrosion Studies — W. Beck — 706
Nickel, A Report to Industry — J. V. Beall — 712
European Research on Low Shaft Blast Furnace — 720

TRANSACTIONS

Grain Structure of Al-Killed, Low Carbon Steel Sheets — R. L. Solter, C. W. Beattie — 721
Isothermal Formation of Martensite at Subzero Temperatures in a High Cr Steel — S. C. Das Gupta, B. S. Lement — 727
Desulphurization of Pig Iron with Pulverized Lime — Bo Kalling, C. Danielsson, Ottar Dragge — 732
Kalling-Domnarfvet Process at Surahammar Works — Sven Forander — 739
A Corrected CO/CO_2 Ratio for Blast Furnaces — S. T. Killian — 742
Burst Phenomenon in the Martensitic Transformation — E. S. Machlin, Morris Cohen — 746
Fundamental Effects of Cold Working on the Creep Resistance of an Austenitic Alloy — D. N. Frey, J. W. Freeman — 755
Thermal Variation of Young's Modulus in Some Fe-Ni-Mo Alloys — M. E. Fine, W. C. Ellis — 761
Effect of Rate of Cooling on the Alpha-Beta Transformation in Ti and Ti-Mo Alloys — Pol Duwez — 765
Crystal Structure of Ti_5Si_3, Ti_5Ge_3, and Ti_5Sn_3 — P. Pietrokowsky, Pol Duwez — 772
Role of Gases in the Production of High Density Powder Compacts — D. Warren, J. F. Libsch — 774
Constitution and Precipitation-Hardening Properties of Cu-Rich Cu-Sn-Be Alloys — R. A. Cresswell, J. W. Cuthbertson — 782
Lattice Parameter of InSb — T. S. Liu, E. A. Peretti — 791
Creep Behavior of Zn Modified by Cu in the Surface Layer — M. R. Pickus, E. R. Parker — 792
Equilibrium Relations in Mg-Al-Mn Alloys — B. J. Nelson — 797
Crystal Structure of UAl$_4$ — B. S. Borie, Jr. — 800
Solidification of Pb-Sn Alloy Droplets — J. H. Holloman, D. Turnbull — 803
Creep Characteristics of Some Platinum Metals at 1382°F — R. H. Atkinson, D. E. Furman — 806
Deformation Texture of Body-Centered Cubic Metal Wires — W. R. Hibbard, Jr., A. E. Roswell, A. E. Schuetz — 808

Published the first day of each month by the American Institute of Mining and Metallurgical Engineers, Inc., 29 West 39th Street, New York 18, N. Y. Telephone: PEnnsylvania 6-9220. Subscription $8 per year for non-AIME members in United States and North, South and Central America; $9, foreign; $6 for AIME members, or $4 additional in combination with a subscription to "Mining Engineering" or "Journal of Petroleum Technology". Single copies, 75 cents; special issues, $1.50. . . . The AIME is not responsible for any statement made or opinion expressed in its publications. . . .

Copyright 1951 by the American Institute of Mining and Metallurgical Engineers, Inc. . . .

Registered cable address, AIME New York . . . Indexed in Engineering Index, Industrial Arts Index and Chemical Abstracts . . . Reentered as second-class matter Sept. 21, 1949, at the post office at New York, N. Y., under the Act of March 3, 1879. Additional entry established at Manchester, N. H.

Are you taking full advantage of the constantly growing range of forgings? Typical is this aluminum alloy forging with a projected area of more than 1,000 square inches used in the wing structure of a modern military bomber. Such forgings are today made possible by the use of the largest die forging press in America (18,000 tons). For hammer or press die forgings of aluminum, magnesium or steel, Wyman-Gordon engineers are ready to serve you—there is no substitute for Wyman-Gordon experience.

Standard of the Industry for More Than Sixty Years

WYMAN-GORDON

FORGINGS OF ALUMINUM • MAGNESIUM • STEEL

WORCESTER, MASSACHUSETTS

HARVEY, ILLINOIS DETROIT, MICHIGAN

War on waste!

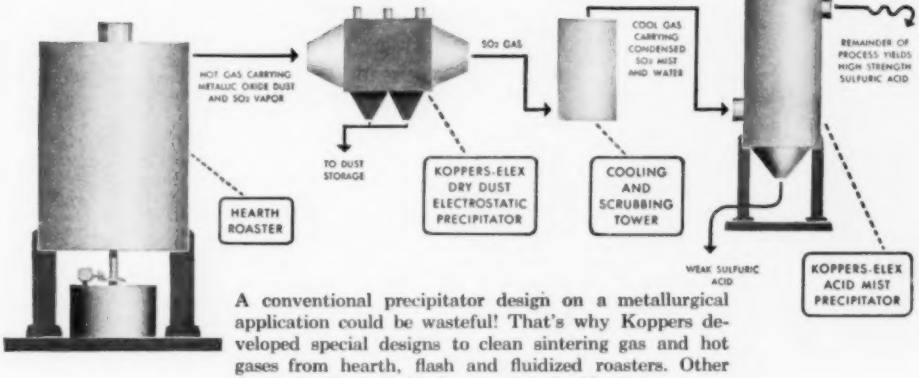
HOT GAS CARRYING METALLIC OXIDE DUST AND SO2 VAPOR
SO2 GAS
COOL GAS CARRYING CONDENSED SO3 MIST AND WATER
REMAINDER OF PROCESS YIELDS HIGH STRENGTH SULFURIC ACID
TO DUST STORAGE
HEARTH ROASTER
KOPPERS-ELEX DRY DUST ELECTROSTATIC PRECIPITATOR
COOLING AND SCRUBBING TOWER
WEAK SULFURIC ACID
KOPPERS-ELEX ACID MIST PRECIPITATOR

A conventional precipitator design on a metallurgical application could be wasteful! That's why Koppers developed special designs to clean sintering gas and hot gases from hearth, flash and fluidized roasters. Other types are also available for removal of acid mists.

Koppers-Elex Electrostatic Precipitators offer Guaranteed Rates of Recovery and Nuisance Abatement!

HERE'S THE RECORD*

Koppers engineers analyze each metallurgical gas cleaning and recovery problem individually. Then, based on extensive experience, they give you a specific recommendation of the amount of recovery that can be economically combined with the degree of gas cleaning you require.

A PROFITABLE INVESTMENT . . . that's the report about Koppers-Elex electrostatic precipitators on zinc roaster and acid mist applications. Not only is recovery guaranteed to any efficiency you specify . . . but proper engineering protects you against failure during overloads and production peaks!

Only Koppers gives you the drag scraper which provides continuous dust removal and eliminates plugged hoppers and bothersome dust build-up. Separately energized multiple series fields provide maximum collection of very fine particles . . . and protect your investment because outage of one field does not halt the gas-cleaning action of the precipitator!

Hundreds of Elex precipitators are in use today all over the world. Koppers-Elex electrostatic precipitators are designed, engineered, fabricated and erected under one contract by the Koppers Company . . . and each installation comes complete with "packaged" mechanical or vacuum tube power packs. If you have a gas-cleaning problem, write to: Koppers Company, Inc., Precipitator Dept., 269 Scott St., Baltimore 3, Md.

***Guaranteed:** Koppers-Elex precipitators are guaranteed to equal or better (under tests made by your own personnel) any efficiency or residual content you specify.

KOPPERS

Koppers-Elex ELECTROSTATIC PRECIPITATORS

Meet The Authors

R. L. SOLTER

R. L. Solter (p. 721), born in Wichita, Kans., received his B.A. in chemistry from University of Wichita in 1934. Since 1935, he has been associated with research div. of Armco Steel Corp., where he is now supervisor of research engineering.

C. W. BEATTIE

C. W. Beattie (p. 721), senior research engineer, has been with the research div. of Armco Steel Corp. since 1937. Born in Virginia, he studied at University of Illinois, and was awarded his B.S. degree. His hobbies are golf and bowling.

S. C. DAS GUPTA

S. C. Das Gupta (p. 727), born in Barisal, East Pakistan, studied at Scottish Church College, the Bengal Engineering College, Calcutta University, Calcutta, India, and the Missouri School of Mines and Metallurgy. He is presently working for his Ph.D. in metallurgy at University of Notre Dame. His hobby is photography.

B. S. LEMENT

B. S. Lement (p. 727), who received S.B. and Sc.D. degrees from Massachusetts Institute of Technology, is now on the research staff of dept. of metallurgy at that school. He has also been connected with Watertown Arsenal, and the Universities of Massachusetts and Notre Dame. This member of AIME, ASM, and Sigma Xi enjoys tennis, chess, and bridge.

J. F. Libsch (p. 774), who received S.B., S.M., and Sc.D. degrees from Massachusetts Institute of Technology, has served as Captain, Army Ordnance, Springfield Armory, is now associate professor of metallurgy and director of magnetics project at Lehigh University and consultant to Lepel High Frequency Laboratory. This AIME member also belongs to ASM and Sigma Xi.

J. W. Freeman (p. 755) is research engineer and associate professor of metallurgy at University of Michigan, where he received his B.S., M.S.E. and Ph.D. degrees. He has been working in research on metals at high temperatures since 1933, particularly for aircraft, petroleum, and steam-power applications. He is a member of AIME, ASM, ASTM, British Iron & Steel Institute, and Institute of Metals. Camping, trout fishing, and hunting are his hobbies.

T. S. Liu (p. 791) was born in Hankow, China, and is a graduate of Tangshan Engineering College, China, and Missouri School of Mines. He was foundry metallurgist at Puchen Locomotive Works, China, and is now working toward his Ph.D. at University of Notre Dame. Record collecting is the hobby of this AIME and ASM member.

B. J. Nelson (p. 797), a graduate of University of Kentucky, was research assistant at Carnegie Institute of Technology, research metallurgist at University of Chicago, and is now research metallurgist, Aluminum Research Laboratories, Aluminum Co. of America. Music, choral singing, hunting, and gardening occupy the spare time of this AIME member.

E. R. Parker (p. 792), professor of metallurgy, University of California, is a graduate of Colorado School of Mines. From 1935 to 1944 he was research metallurgist for General Electric Co. He holds membership in AIME, ASM, AWS, and American Physical Society.

J. H. Hollomon (p. 803) has published about 37 papers on metallurgy, 14 of which were presented before AIME. He received his B.S. and Ph.D. degrees from Massachusetts Institute of Technology, and was an instructor at Harvard University. He has been with General Electric Research Laboratory since 1946, where he is now assistant manager, metallurgy and ceramics dept. A member of AIME and numerous societies in this country and abroad, his hobbies are reading and music.

D. Turnbull (p. 803), born in Stark County, Ill., went to Monmouth College (B.S. 1936) and the University of Illinois (Ph.D. 1939). He was an instructor and assistant professor of physical chemistry at Case Institute of Technology from 1939 to 1946; re-

J. F. LIBSCH

J. W. FREEMAN

T. S. LIU

B. J. NELSON

PROFESSIONAL SERVICES

Limited to AIME members, or to companies that have at least one AIME member on their staffs. Rates $40 per year per inch.

MAX STERN
Consulting Engineer
Expert for Scrap Recovery and Shipwrecking — Modernization of Plants and Yards for Ferrous and Nonferrous Metal Scrap
150 Broadway New York 7, N. Y.

ST & CO.
ENGINEERS
CONSULTANTS
METALLURGISTS
Small Jobs Welcomed
SAM TOUR & CO., INC.
Laboratories and offices
44 Trinity Place, New York 6, N. Y.
Testing—Certifying
American Standards Testing Bureau, Inc.

R. S. DEAN LABORATORIES, INC.
Consulting, Research Development Chemistry, Electrochemistry, & Metallurgy Laboratory Research on a Contract Basis
5810—47TH AVENUE AP-2821
RIVERDALE, MD.

LEWIS B. LINDEMUTH
Consulting Engineer
140 CEDAR STREET, NEW YORK 6, N. Y.
STEEL PRODUCTION

Authors

R. H. ATKINSON

D. E. FURMAN

search associate at General Electric Research Labs from 1946 to 1950; and head of the chemical, metallurgy and structures div., GE Research Labs from 1950 to the present time. He has written several papers for AIME in the past.

R. H. Atkinson (p. 806) was born in England and educated at Cambridge University. He has been assistant refinery manager, Mond Nickel Co.; chief research chemist, Inco of Canada, Ltd.; and research chemist, Merck & Co. Now research metallurgist, International Nickel Co., he has 28 years of experience with the platinum metals. An AIME member, he was Jubilee Memorial Lecturer of Society of Chemical Industry in 1940. Gardening is his hobby.

D. E. Furman (p. 806) received his B.M.E. degree from New York University, and is research metallurgist for International Nickel Co., Inc., where he specializes in stainless and heat resisting alloys.

B. S. Borie, Jr. (p. 800) was associated with Westinghouse Electric Co. and is now at Oak Ridge National Laboratory. He graduated from Southwestern Louisiana Institute, where he served as instructor, and Tulane University. His hobbies are tennis and music.

Sven Fornander (p. 739), research manager, Surahammars Bruks AB, Sweden, will become director of research, Jernkontoret, Stockholm, in 1952. A graduate of Royal Institute of Technology, Stockholm, this AIME member enjoys fly fishing.

W. R. Hibbard, Jr. (p. 808) has served as Lt. Cdr., Bureau of Ships, associate professor of metallurgy at Yale University, and is now research associate for General Electric Co. Tennis, golf, and gardening occupy the spare time of this member of AIME.

D. N. Frey (p. 755), a graduate of Michigan State College and University of Michigan with B.S., M.S.E., and Ph.D. degrees, is assistant professor at University of Michigan. A member of AIME, his spare time is spent raising his three children.

A COMPLETE LINE OF

PRECISION INSTRUMENTS for Metallographers

NEW DESK-TYPE METALLOGRAPH

Years ahead in simplicity and ease of operation. Perform *every* operation while sitting comfortably at a modern desk . . . compose the picture on a screen directly in front of you . . . focus camera automatically while examining specimen through the microscope . . . take notes, change magnification, adjust the lamp, make the exposure—all with unbelievable speed, ease, and precision. Other features: monocular or binocular bodies, revolving objective turret, two lamps—visual and photographic, "autofocus" coarse adjustment stop.

SPENCER METALLURGICAL MICROSCOPES

From this complete line of Spencer Metallurgical Microscopes you can select an instrument that exactly meets your needs. Here are some of the many outstanding features for convenience and speed in operation:

- **Americote Optics** eliminate reflections and provide added contrast.
- **Wide Range Adjustable Stage** handles unusually large or small specimens.
- **Large, Sturdy, Research-Type Stand** with micrometer screw fine adjustment . . . interchangeable body tubes.
- **Brilliant, Uniform Illumination** from a vertical illuminator that is simple to operate, sturdy, and always cool enough to handle.
- **Variety of Equipment** for teaching, routine examinations, and research.

SPENCER STEREOSCOPIC MICROSCOPES

Two distinct advantages are offered by these instruments:

1. The image is erect and a wide field of view is provided.
2. The image has depth and shows the specimen in three-dimensional perspective.

These are real advantages in studying surface characteristics and examining parts.

No. 26 is designed for examining small specimens.

No. 23 (illustrated) for large objects. No. 353 lamp provides an adaptable source of illumination.

SPENCER BIERBAUM MICROCHARACTER

This is a precision instrument for determining the hardness of small areas, particles, and microscopic constituents in metals. A highly polished and lubricated specimen is moved by micrometer feed beneath an accurately ground diamond point. The pressure is precisely controlled so that hardness can be determined by the width of the resulting cut when measured under the microscope.

For further information about these and other Spencer Instruments write Dept. W-182

American Optical COMPANY

INSTRUMENT DIVISION • BUFFALO 15, NEW YORK

FOR INCREASED PRODUCTION

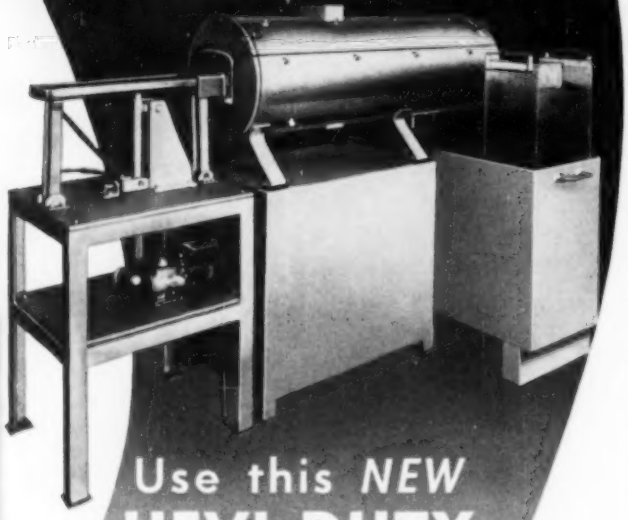

Use this *NEW*
HEVI DUTY
SHAKER HEARTH
FURNACE

DESIGNED specifically for production heat treating of small parts, these Hevi Duty Shaker Hearth furnaces have proved themselves to be versatile in their application.

Bright Carburizing, Cyaniding and Hardening processes are easily performed using the proper atmosphere in the alloy retort. Close control of case depths can be maintained.

Because the work drops directly into the quench tank a few pieces at a time, a most satisfactory quench results with a minimum of quenching medium.

Write for bulletin HD-850.

HEVI DUTY ELECTRIC COMPANY
HEAT TREATING FURNACES HEVI-DUTY ELECTRIC EXCLUSIVELY
DRY TYPE TRANSFORMERS — CONSTANT CURRENT REGULATORS
MILWAUKEE 1, WISCONSIN

— Coming Events —

Sept. 13-15, AIME, Industrial Minerals Div., fall meeting, University of West Virginia, Morgantown, W. Va.

Sept. 19, AIME, Carlsbad, Potash Section, Riverside Country Club, Carlsbad, N. Mex.

Sept. 30, AIME, Utah Section, Newhouse Hotel, Salt Lake City.

Sept. 25-28, ASME, fall meeting, Radisson Hotel, Minneapolis.

Oct. 1-4, Assn. of Iron & Steel Engineers, annual convention, Hotel Sherman, Chicago.

Oct. 3-5, AIME, petroleum branch, fall meeting, Oklahoma City.

Oct. 10-11, AIME, Southwestern and Western Sections, Open Hearth Committee, joint meeting. Oct. 10, plant trip, Colorado Fuel & Iron Co., Pueblo. Oct. 11, Broadmoor Hotel, Colorado Springs.

Oct. 10-12, Electrochemical Society, autumn national convention, Hotel Statler, Detroit.

Oct. 11-12, Joint Fuels Conference, AIME Coal Division, ASME Fuel Section, Roanoke Hotel, Roanoke, Va.

Oct. 12, AIME, Eastern Section, Open Hearth Committee, Warwick Hotel, Philadelphia.

Oct. 12-14, Metal Treating Institute, annual meeting, Detroit.

Oct. 15-17, AIME, Institute of Metals Div., fall meeting, Detroit-Leland Hotel, Detroit.

Oct. 15-19, National Metal Congress & Exposition, Detroit.

Oct. 18-19, Scientific Apparatus Makers Assn., mid-year meeting, industrial instrument section, Seaview Country Club, Absecon, N. J.

Oct. 18-20, National Assn. of Corrosion Engineers, south central region, Corpus Christi, Texas.

Oct. 19-20, Engineers' Council for Professional Development, annual meeting, Hotel Statler, Boston.

Oct. 22, AIME, Chicago Section, Open Hearth Committee, Phil Schmidt's, Chicago.

Oct. 22-24, American Mining Congress, Metal and Nonmetallic Mining Convention, Biltmore Hotel, Los Angeles.

Oct. 25-26, AIME, Los Angeles Section, fall meeting, Los Angeles.

Oct. 26-27, AIME, National Openhearth Committee, Southern Ohio Section, Deshler-Wallick Hotel, Columbus, Ohio.

Oct. 29-Nov. 3, AIME, fall meeting, Mexico City.

Nov. 2, AIME, Pittsburgh Local Section and Open Hearth Local Section, annual off-the-record meeting, William Penn Hotel, Pittsburgh.

Nov. 25-30, ASME, annual meeting, Chalfonte-Haddon Hall, Atlantic City.

Nov. 28-30, Scientific Apparatus Makers Assn., midyear meeting, laboratory apparatus, optical, nautical, aeronautical, and military instrument sections, Hotel New Yorker, New York.

Nov. 29, AIME, Buffalo Section, Open Hearth Committee, Statler Hotel, Buffalo, N. Y.

Dec. 2-5, American Institute of Chemical Engineers, annual meeting, Chalfonte-Haddon Hall, Atlantic City.

Dec. 6-8, AIME, Electric Furnace Conference, William Penn Hotel, Pittsburgh.

Jan. 16-18, 1952, Society of Plastic Engineers, Inc., annual national technical conference, Edgewater Beach Hotel, Chicago.

Feb. 18-21, AIME, annual meeting, Hotel Statler, New York.

Mar. 3-7, ASTM, spring meeting and committee week, Hotel Statler, Cleveland.

Apr. 23-26, AIME, New England Regional Conference, Kenmore Hotel, Boston.

June 23-27, ASTM, 50th anniversary meeting, Hotel Statler, New York.

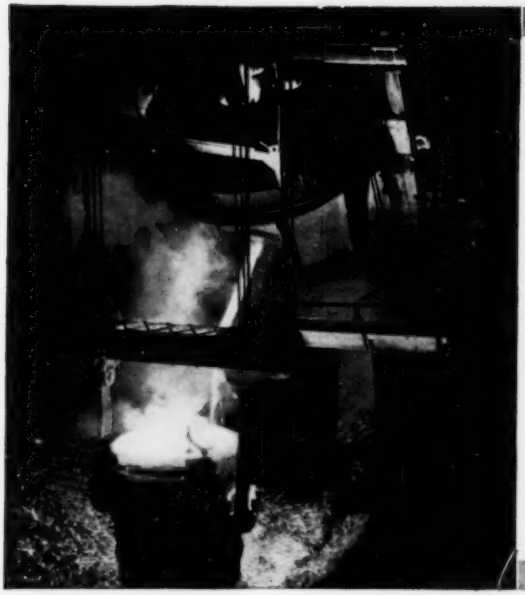

Heroult

ELECTRIC MELTING FURNACE

. . . as ever, the dependable furnace for the production of high-grade stainless, alloy and rimming steels.

Removable roof of new design now available for the larger furnaces.

AMERICAN BRIDGE COMPANY
General Offices: Frick Building, Pittsburgh, Pa.

Contracting Offices in New York, Philadelphia, Chicago, San Francisco and other principal cities
United States Steel Export Company, New York

USS

AMERICAN BRIDGE

UNITED STATES STEEL

FOR SALE

I.L.S. Metalloscope, with Camera, Illuminating Unit, Objectives and Eye Pieces.

Also

Three-Disc Polishing Table.
Condition equal to new equipment.

—— • ——

Factory in New York City discontinuing metallurgy.

—— • ——

Write to JOURNAL OF METALS, Box H-12, for detailed list of accessories or appointment to examine.

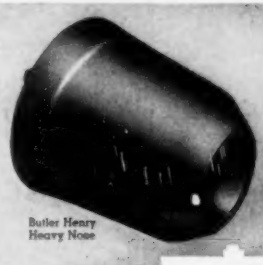

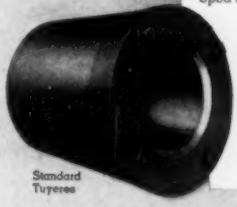

Blast Furnace TUYERES

Made to quality standards developed through years of specialization in the manufacture of Blast Furnace Copper Castings.

Licensed manufacturers of all leading designs.

Phone, wire or send specifications for estimates.

SMEETH-HARWOOD COMPANY
3401-09 West Cermak Road, Chicago 8, Illinois

Superior* Blast Furnace Copper Castings *Exclusively

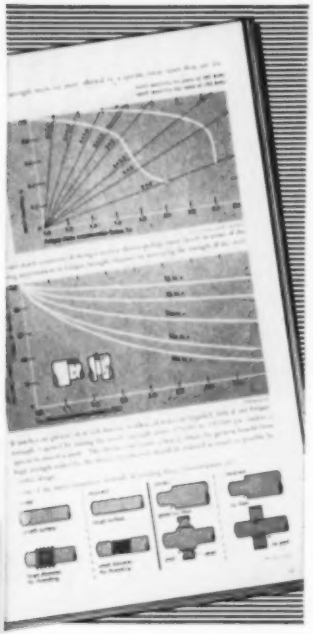

Every designer must be something of a metallurgist

Here are 72 pages packed with information of vital significance to engineers faced with the design, selection and treatment of steel components to give a specified service at minimum cost.

Besides dealing with scientific design, the book gives important metallurgical data, all compiled from the designer's viewpoint. Free on request.

Climax Molybdenum Company
500 Fifth Avenue · New York City

Please send your
FREE BOOKLET
3 KEYS TO SATISFACTION

Name.....
Position.....
Company.....
Address.....
JM-9 © F 22

Industrial Notes . . . . .

- Wheeling Steel Corp. will spend $24 million by the end of 1953 for modernization of its cold reduced sheet facilities, reconditioning two bessemer converters, and installing improved materials handling and annealing capacity at Steubenville, Ohio; mine mechanization and building a new coal washer at Harmarville, Pa.; and installing a new continuous galvanizing line at Martins Ferry, Ohio. Since 1946, Wheeling has invested more than $70 million in new plant and plant improvement.

- Admiral Corp. has started a long-range $7 million expansion program. Included in the program are a $2 million building for defense work, a $1.5 million building in Chicago, and a $1 million factory building at Galesburg, Ill. The program will be financed from existing capital.

- Solvay Process Div., Allied Chemical & Dye Corp., will expand its Baton Rouge, La., soda ash plant. Cost of buildings, equipment, and facilities will exceed $15 million, including some equipment at the company's limestone quarry in Illinois. A new pilot plant was recently completed, costing about $350,000, at Hopewell, Va., that will serve as a bridge between laboratory findings and full-scale plants.

- Georgia Power Co., will start construction in the fall of a $20 million steam-electric generating station on the Coosa River. Designed for future expansion, the plant will have an initial installation of two 100,000 kw units.

- Pacific Steel Co. of Chile will build a new battery of 13 chemical-recovery coke ovens at its plant near Huachipato, Chile. Design and materials for the new ovens will be supplied by Koppers Co., Inc., and will be of the same type as the present battery of 57.

- Ansco will build a warehouse, a pilot casting plant, and addition to the power plant as part of its $4 million expansion program. The two-story pilot casting plant will be the major part of the program.

- Chevrolet Div., General Motors, announced a $20,800,000 expansion program of its Buffalo, N. Y., operations, including three buildings that will house an engine plant, a forge plant, and a foundry. The facilities will augment present manufacturing capacity in Buffalo for production of the Wright R-3350 aviation engine.

- Columbia Steel Co.'s expansion of sheet and tin plate capacity is about 50 pct completed. When completed, the added facilities will increase tin plate output from 200,000 to 350,000 tons a year, and sheet production from 125,000 to 190,000 tons. Cost has been estimated between $25 and $30 million.

- Shell Chemical Corp. will build a new synthetic ammonia plant at its petro-chemical manufacturing operations at Dominguez, Calif. Natural gas will be the raw material, and the expansion will be completed in 1952.

- Aluminum Co. of America will build the first aluminum metal producing plant to use lignite for fuel at one of several locations about 60 miles south of Waco, Texas. The plant will cost more than $80 million, and have a capacity of 170 million lb per year. The project is scheduled for completion in late 1952. Two high-cost noncommercial aluminum plants, Badin, N. C., and Massena, N. Y., were re-activated by Alcoa. Final costs of Alcoa's present expansion program is estimated about $250 million, which is in addition to $300 million spent on finishing capacity since the end of World War II.

- Aluminum Co. of Canada has started a $160 million construction program at three sites in northern British Columbia as part of a three-year 150,000 metric ton annual production goal.

- Ford Motor Co. has started a $43 million expansion and modernization program of steel operations at Rouge plant that will increase the company's annual finished steel output by 190,000 tons a year, or 18 pct. The program includes 37 new coke ovens, a sinter plant, pig casting equipment, openhearth and rolling mill improvements.

- Battelle Memorial Institute will establish a European branch in 1952.

- Consolidated Vultee Aircraft Corp. started work in August on a guided missile plant that it will operate for the Navy. The plant and equipment will cost more than $50 million, and be the first integrated mass production facility for guided missiles.

- Tenn-Tex Alloy & Chemical Corp., a new company, will erect a $1 million plant at Houston, Texas, for production of ferromanganese, ferrosilicon, and other alloys required in steel production. The bulk of production of about 2000 tons a month will go to Sheffield Steel Corp.

Advertisement

ELECTROMET Data Sheet

A Digest of the Production, Properties, and Uses of Steels and Other Metals

Published by Electro Metallurgical Company, a Division of Union Carbide and Carbon Corporation, 30 East 42nd Street, New York 17, N. Y. • In Canada: Electro Metallurgical Company of Canada, Limited, Welland, Ontario

High-Chromium, High-Carbon Iron

. . . the Iron That Hardens as it Wears

In many applications involving extreme abrasion, ordinary work-hardening alloys are not suitable. This is because most of these alloys require a definite pounding action for a martensite transformation, and the scouring action of an abrasive is not sufficient for development of high wear resistance. For this reason, high-chromium, high-carbon irons were developed — irons that wear-harden.

Chromium Content of Irons Ranges from 24 to 30 Per Cent

These irons are made in the electric furnace and have the following composition range:

Chromium	26 to 28 per cent
Carbon	2.60 to 2.80 per cent
Manganese	0.50 to 1.25 per cent
Silicon	0.25 to 0.75 per cent
Sulphur	max. 0.05 per cent
Phosphorus	max. 0.05 per cent
Nickel	minimum
Iron	balance

Irons of this composition are readily castable by steel casting techniques.

Development of Greater Wear Resistance by Heat Treatment

Structurally, these irons consist of primary iron-chromium carbides in a matrix of iron-chromium solid solution and secondary iron-chromium carbides. They are hard in the as-cast condition (500 to 550 Brinell), but when they are given an austenitization heat-treatment they develop much higher hardness (about 600 Brinell), and also have greatly improved wear resistance. Austenitization consists of heating these irons to a temperature of about 2012 deg. F. for an hour, then allowing them to cool in air. This heat-treatment promotes the formation of very unstable austenite—austenite that will transform to a harder martensitic end-product even under rubbing or mild impingement action. Austenitization has been found to be far more effective in increasing wear resistance than the promotion of unstable austenite by the addition of ferrite-forming alloying elements.

High-chromium, high-carbon irons can also be annealed to sufficiently low-hardness values for grinding or simple machining. Hardnesses as low as 350 to 450 Brinell can be obtained by heating the castings to temperatures of 1400 to 1450 deg. F. for 12 to 24 hours, then allowing them to cool in air.

Irons Have Wear Resistance Many Times That of Other Alloys

Austenitized high-chromium irons have been known to last as much as 21 times longer than other wear-resistant alloys in applications involving extreme frictional abrasion. These applications include sand-blast nozzles and liners, pantograph contact shoes, grinding disks, pulleys, chute-liner plates, dredge-pump liners, and rollers for crushing various hard materials.

In a recent test, high-chromium iron was compared to special wear-resistant steel castings as the material for hammers in a machine that was used to crush abrasive material. The chrome-iron hammers were found to have almost 7 times the wear resistance of the steel castings.

Fig. 1. After crushing the same amount of abrasive material in a hammer mill, the badly worn steel casting (left) had a weight loss of 37 per cent while the high-chromium iron casting (right) lost only 5.5 per cent.

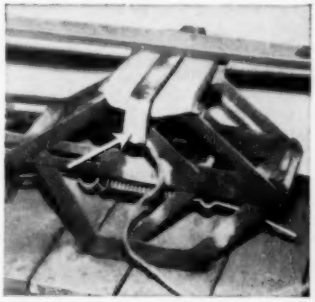

Fig. 2. This chrome-iron pantograph shoe had a service life of about 10 years. A tool steel that was used in similar service wore out in about 3 or 4 months; copper lasted about 24 hours.

When thoroughly backed up with zinc, the iron also has enough shock resistance to be used effectively as crushing hammers and jaw plates for many severe rock-handling jobs.

Metallurgical Service Available

For years, ELECTROMET high-carbon ferrochrome has been used to make chromium additions to abrasion-resistant high-chromium irons. If you should have any questions about either the production or use of these irons, write to the nearest ELECTROMET office. Our metallurgists will be glad to give many valuable suggestions and recommendations on how to make or use this iron most effectively.

Write for a free copy of the ELECTROMET publication, "Abrasion-Resistant High-Chromium Iron." This booklet is a collection of some of the best available information on how to make and to use abrasion-resistant iron castings most efficiently.

The term "Electromet" is a registered trademark of Union Carbide and Carbon Corporation.

New Products

New Products | New Literature | New Services

For Further Information or Literature on any Product, Fill in the Coupon and Send to JOURNAL OF METALS
Students are Requested to Apply Directly to Manufacturers for Bulletins and Information

1—ARCH CONNECTIONS: Open-hearth arch connections that are a simplification of fan-tail arch connections have been developed by *Geo. P. Reintjes Co.* Primarily developed for open hearths, this construction is applicable for use in glass tanks, reverberatory furnaces or other types of melting furnaces. The arch connection can be applied to practically any furnace where suspended fan-tail nosing and the chill walls meet. It can be built of alumina, silica or metal-clad basic refractories, all suspended from the same structure.

2—CAPACITOR MOTORS: Line of single-phase capacitor motors offered by *General Electric Co.* has been extended to include a totally enclosed fan-cooled construction. Available in ratings of 1, 1½, 2, 3, and 5 hp the new line was developed for use where extra severe conditions of dirt, grit, or moisture are encountered. Except for the 5-hp size, that uses 230 v, the new motors operate on 115/230 v, 60 cycle power supply.

3—GRINDING SPEED CALCULATOR: Grinding wheel speeds in rpm or sfpm and wheel diameters are determined easily with slide rule type calculator. By setting in any two of the above factors on slide rule, third element can be read directly. Available from *Electro Refractories & Abrasives Corp.*, data imprinted on the calculator include inch and centimeter scales and table of maximum operating speeds for Electro resin-bonded high speed grinding wheels.

4—AIR GRINDER: Air grinder announced by *Ingersoll-Rand* has an added safety device to prevent overspeed operation. It has special application in foundries, steel mills, general manufacturing and metalworking plants where hand grinding is required for snagging, trimming, smoothing, etc. It is available for 8 in., 6 in. or 5 in. wheels running at respective motor speeds of 3100, 4100 and 4500 rpm. It also has a multiple exhaust system. There are four exhaust positions, 90° apart that direct the exhaust away from the work.

5—PACKAGED DRYING UNIT: Unit consisting of a rotary dryer with driver, screw feeder, air heater, fan and dust collector integrally mounted on a steel frame is available from *Patterson Foundry & Machine Co.* Materials to be dried are fed continuously by means of a special feeder directly to the sanitary interior of the dryer and a uniformly dried product is discharged continuously.

6—STEAM GENERATOR: Model 4740 developed to supply large quantities of hi-pressure dry steam to supply processing steam, operate pile driving, heating, and 600 lb pressure is announced by *Vapor Heating Corp.* The machine is 52 in. wide, 76 in. long, and 78 in. high.

7—CERAMIC STRAINER: New foundry ceramic strainer core has been announced by the *American Clay Forming Co.* Machine-made under high pressures, these cores are fired to temperatures above 2400°F. They fit into the gate of the mold and strain the molten metal as it flows through the holes of the strainer core.

8—GAS DUST ANALYZER: An instrument designed to record the amount of total suspended solids or dust particles in gas streams, such as blast furnace gas lines, fly-ash in boiler smokestacks, has been developed by *General Power Plant Corp.* The gas sample is introduced into the center of the main tube and flows either way to the exhausts where it is burned. The outlet is large in relation to the inlet because it is necessary to keep the pressure constant in the sampling. Use of large exhausts keeps the sampling tube at practically atmospheric pressure.

9—SYNCROGEAR MOTOR: A new principle in geared motors has been developed by *U. S. Electrical Motors* in type GL Syncrogear. Two secondary pinions are used to drive the output gear thereby doubling the effective torque rating of conventional single pinion and gear units.

10—FILTER CLOTHS: High strength, resistance to practically all acids, salts, and solvents are advantages claimed for synthetic filter fabrics offered by *Filtration Engineers, Inc.'s Filtration Fabrics Div.* Fabrics are available as yard goods or tailored to fit all types of pressure and vacuum filters, centrifuges, and dry filtration equipment.

11—FOSCOAT PROCESS: A new metal treating chemical process that extends lubrication limits in cold working of steel has been announced by *Pennsylvania Salt Mfg. Co.* It consists of compatible cleaning, pickling and application of a new phosphate coating and specially developed lubricants to steel. The process has been employed in conjunction with all grades of plain carbon and SAE alloy steels, as well as some medium alloy grades.

12—REFRACTORY PATCHING MACHINE: A redesigned Bondact machine is available from *Eastern Clay Products, Inc.* Air placement of refractory patching materials is accomplished by ramming them into position by air pressure. A larger hopper provides capacity for the refractory being applied. Improved control of the pressure makes possible a more exacting control over the moisture content of the patch. Gages are grouped together to simplify operations.

13—QUENCH-CONVEY UNIT: Quenching and conveying equipment designed for continuous heat treating of individual pieces has been marketed by *Klaas Machine & Mfg. Co.* The quenching medium is recirculated and cooled. The metal belt allows the parts to drain as they

Journal of Metals **September**
29 West 39th St.
New York 18, N. Y.

Please send me — More Information ☐ Free Literature ☐ Price Data ☐ — on items indicated

1	2	3	4	5	6	7	8	9	10
11	12	13	14	15	16	17	18	19	20
21	22	23	24	25	26	27	28	29	30
31	32	33	34	35	36	37	38	39	40

Name ..... Title .....
Company .....
Street .....
City and Zone ..... State .....

move out of the bath up an incline, driven by a self-contained power unit. Dimensions: 8 ft long x 2 ft wide x 4 ft high.

14—VACUUM LEAK DETECTOR: A new, sensitive leak detector for vacuum systems down to 1 micron Hg has been announced by *Distillation Products Industries*. In operation, the sensitive tube of the detector is sealed into the system and the system is pumped down to a moderate vacuum. A jet of gas is then directed against portions of the system suspected of leaking, and when a leak is hit there is a deflection of the meter needle because gas entering the system increases the ability of the hot platinum anode in the tube to emit positive ions. The detector appeals particularly to those who have only occasional need for a leak detector.

15—THIN STEEL: A new, thin electrical steel has been developed by *Armco Steel Corp.*, known as Tran-Cor T-O-S. It can be operated at high inductions, 20 pct higher than any Ni-Fe alloy. Thinner than most electrical steels, it is intended for use in wound-type transformers and reactors that operate at 400 cycles. Minimum permeability at 18 kilogausses is 1800, volume resistivity is 47 micohm-cm, and it has a lamination factor of 95 pct solid.

Free Literature

20—ALLOY STEEL TUBING: Assistance in solving problems, involving use of alternate grades of medium carbon or full hardening grades of tubing steels, is offered in bulletin TDC 141 published by *Babcock & Wilcox Tube Co.* Condensed data on microstructure, critical points, effect of alloy elements, forging, machining are presented in bulletin.

21—FLOW RATIO CONTROLLER: Unusual features of *Fischer & Porter Co.'s* automatic flow ratio control systems are described in Catalog 53. Principle of operation is described as well as fundamental reasons for improved ratio control. Typical installations are shown and applications listed.

22—STAINLESS STEELS: A 12-p. booklet "Guide to Type 430 Stainless Steels as Alternates of the 18-8 Series" has been released by *Republic Steel Corp.* It is designed to help manufacturers affected by defense restrictions on the use of chromium-nickel stainless steel. Data are given concerning performance under corrosive conditions and the mechanical properties related to high temperature uses.

23—CONVEYOR BELT CLEANER: A spring-type cleaner devised for cleaning conveyor belts is described in brochure available from *Stephens-Adamson Mfg. Co.* Self aligning, spring steel wiper blades set perpendicular to the belt surface, but diagonal to belt travel, wipe the belt clean and dry as it passes. The wiper has an independent mounting assembly and can be easily adapted to fit existing conveyor installations.

24—TURBINE-TYPE PUMPS: A catalog describing APH-APK vertical turbine-type pumps has been prepared by *Ingersoll-Rand Co.* These pumps are particularly applicable to bulk liquid transfer, dewatering and similar services where suction is taken from an open source. They range in size from 6 to 30 in. for capacities to 15,000 gpm and pressures to 250 psi.

25—SPECIMEN MOUNT PRESS: A new bulletin describing AB speed press features use of preheated premolds, rapid closing and universal application for thermosetting or thermoplastic materials in three sizes. *Buehler Ltd.*

26—CASTINGS: A new folder on Colmonoy castings may be obtained from *Diamonds & Tools, Inc.* Special castings are made for various wear resistant parts where either hand welding or sprayweld process is not feasible.

27—COLD STRIP MILL: Technical report describing and illustrating Y-type reversing cold strip mill is being distributed by *Mackintosh-Hemphill Co.* The mill is available in widths ranging from 16 to 66 in. or larger. Booklet discusses mill design, roll arrangement and tentative gage reduction schedules. Each major component part of the mill is described.

28—IRON CORE MAGNET: A paper reviewing the development of an improved iron core magnet for general laboratory use may be obtained from *Arthur D. Little, Inc.* The paper presents design considerations and operating characteristics (with curves) for a research electromagnet having a wide range of application.

29—FOUNDRY PRACTICE: Booklet #101 issued by *Foundry Services, Inc.* describes and illustrates various experiments, the results of which are helpful to practical foundrymen.

30—STOPPER HEADS: A new composition has been developed by *Electro Refractories & Abrasives Corp.* that gives assurance from troublesome internal leakage-source cracks in steel ladle stoppers. Booklet S-750 lists advantages of these stopper heads for open hearth, electric furnace, and steel foundry practice.

31—ELECTROSTATIC PRECIPITATOR: Brochure available from *Koppers Co., Inc.*, describes this precipitator for cleaning blast furnace gas. The cleaners are available in vertical and horizontal types and gas is cleaned to residuals better than 0.001 grains per cu ft. They are used by various industries such as cement and gypsum, aluminum plants, metallurgical plants for electric and roasting furnace gases, coke ovens, and chemical and electro-chemical plants.

32—STAINLESS STEEL HANDBOOK: New data and handbook on stainless steels has been released by *Allegheny Ludlum Steel Corp.*

33—CERROMATRIX: The Cerromatrix method of punch and die setting is described in a 20-p. manual available from *Cerro de Pasco Corp.* Practical information on die design and manufacture is included, along with line and photographic illustrations.

34—DYNOPTIC LABROSCOPES: These new instruments are described and illustrated in pamphlet available from *Bausch & Lomb Optical Co.* They feature a low position, fine adjustment and mechanical stage with low controls. A ball bearing on the horizontal shaft of the low position fine adjustment absorbs thrust and assures effortless turning of the focusing knob. A substage illuminator is available that can be used integrally with the Labroscope in place of the mirror or separately.

35—DIE PRESSED FORGINGS: Publication of a revised edition of a reference booklet on copper and copper-alloy die pressed forgings has been announced by *Anaconda Copper Mining Co.* The booklet contains tabulation of physical properties of copper and copper alloys suitable for forgings. Also included are illustrations that show what these forgings are, what they can do, and what they have done.

36—ENGINEERING IRON SELECTION: A guide to the selection of engineering irons has been published by *International Nickel Co., Inc.* Illustrations, tables, charts, and photomicrographs show how through the use of nickel, engineering properties of cast iron can be controlled to meet almost any reasonable combination of service requirements. Nickel cast irons offer greatly improved physical and mechanical properties and can be produced by any foundry having reasonable control and in any size or shape in which ordinary gray iron is available.

— Personnel Service —

THE following employment items are made available to AIME members on a non-profit basis by the Engineering Societies Personnel Service, Inc., operating in cooperation with the Four Founder Societies. Local offices of the Personnel Service are at 6 W. 49th St., New York 18; 100 Farnsworth Ave., Detroit; 57 Post St., San Francisco; 84 E. Randolph St., Chicago 1. Applicants should address all mail to the proper key numbers in care of the New York office and include 6c in stamps for forwarding and returning application. The applicant agrees, if placed in a position by means of the Service, to pay the placement fee listed by the Service. AIME members may secure a weekly bulletin of positions available for $1.50 a quarter, $12 a year.

POSITIONS OPEN

Production Engineer to make surveys of metal fabricating plants and equipment, analyze machining, stamping and assembly operations of ordnance material, prepare estimates, etc. Salary, $5400 a year. Location, New York, N. Y. Y5840.

Metallurgical Product Engineer, recent graduate, B.S. in metallurgy, for product engineering work on rod and wire. Excellent living conditions; housing available. Reply giving training, experience, age, salary desired, etc. Location, northern Pennsylvania. Y5832.

Jr. Chemical or Metallurgical Engineer to make analytical check on ferrous materials. One or two years' experience desirable. Salary, $3900 to $5200 a year. Location, New York, N. Y. Y5831.

Instructor, B.S. or M.S. in metallurgical engineering, to teach metallurgical courses and do research work. Location, South. Y5827.

Engineers. (a) Metal Processing Engineer familiar with metal processing equipment for melting, forging and rolling. Liaison between research laboratory and production personnel. Emphasis is on the equipment aspects of processing, but an appreciation of metallurgical factors involved is important. (b) Junior Research Physical Metallurgist, recent graduate, to work in research lab assisting experienced metallurgist in the physical metallurgy research of a series of new alloys. Liking and aptitude for laboratory work essential and experimental resourcefulness desirable. (c) Senior Research Physical Metallurgist, to conduct alloy research on a new series of materials. Advanced degree in physical metallurgy or its equivalent in metallurgical research necessary. Location, Midwest. Y5826.

Area Sales Managers for sale of metal heat exchange equipment such as pipes, valves, etc. Salaries, $8000 to $10,000 a year. Territories, East and West. Y5824.

Laboratory Staff Engineer with training in metallurgical, mechanical or electrical engineering; experienced in metallurgy and chemistry in a manufacturing industry doing both production and development laboratory work. Must have supervisory experience or graduate administrative training. Location, upstate New York. Y5803.

Concentrator Superintendent for mill with 100 tons per hr iron ore capacity. Must have previous experience and be familiar with magnetic separators and tables, etc. Salary open. Location, eastern United States. Y5754.

Engineers. (a) Chemical Engineer or Metallurgist to take charge of process control of nonferrous metal, and do limited amount of research for company engaged in the manufacture of lime and magnesium. (b) Master Mechanic with minimum of five years' experience in heavy nonferrous metal industry. (c) Plant Superintendent with experience in lime, cement or gypsum for production and maintenance. (d) Foundry Superintendent with experience in melting and alloying light metals and permanent mold castings. Salary, $6000 to $7000 a year. Location, Connecticut. Y5733.

MULTIPLE SAVINGS IN ELECTROLYTIC TINNING

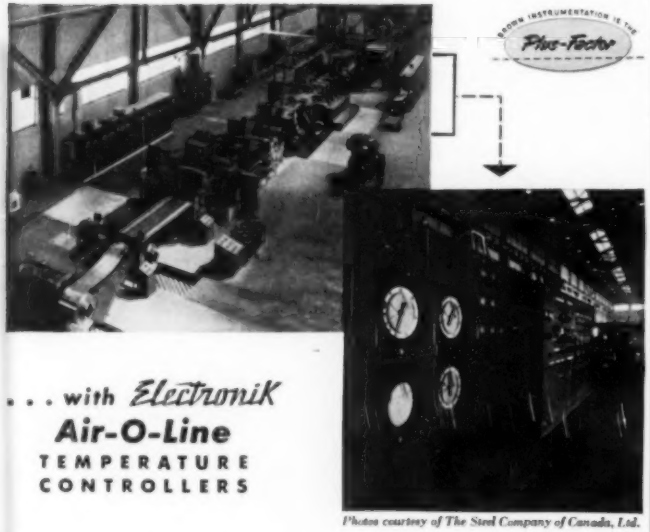

Photos courtesy of The Steel Company of Canada, Ltd.

. . . with *ElectroniK* *Air-O-Line* TEMPERATURE CONTROLLERS

COMPLETE and integrated tin line control makes possible the attainment of greater production, with greater uniformity, at greater economy.

And the use of *ElectroniK* Potentiometers, with *Air-O-Line* Control, is your best insurance for constant and continuous achievement of all three goals.

Typical is the installation pictured above, where multiple savings are effected day after day . . . through nonporous and even spread of metal, high operating speeds, less expenditure of power, and reduction in use of caustic.

Accurate, precise control is afforded for the temperature of electrolyte, alkali, acid and quench . . . plus the level of the electrolyte in the main circulating tank.

A similar control system can be engineered to your tin line requirements. Call in our local representative for a detailed discussion today.

MINNEAPOLIS-HONEYWELL REGULATOR CO., *Industrial Division*, 4573 Wayne Ave., Philadelphia 44, Pa. Offices in more than 80 principal cities of the United States, Canada and throughout the world.

MINNEAPOLIS **Honeywell**

Brown Instruments

CARBON and SULFUR ANALYSIS with Speed! Ease! Accuracy!

TWO MINUTE CARBON DETERMINATOR

High degree of accuracy assured by: fan cooling gases, leveling to meniscus line, automatically maintaining atmospheric pressure, wide selection of carbon percentage scales. Accurate within 0.002% on low range Burette.

THREE MINUTE SULFUR DETERMINATOR

Determination in accordance with A.S.T.M. specification accuracy within 0.002% inorganic or organic materials. Simple procedure.

HIGH-TEMPERATURE FURNACE

Sturdy construction with HIGHEST QUALITY insulation.

Use 3031D Boats and Zircotubes to reduce operating cost of analysis.

Use Dietert-Detroit Carbon and Sulfur Determinators for Economical Analyses

Write to Dept. C-5 for descriptive literature

CONTROL EQUIPMENT

HARRY W. DIETERT COMPANY

9330 ROSELAWN • DETROIT 4, MICH.

Assistant Professor, Ph.D. in metallurgy, with good physical metallurgy background with emphasis on engineering mechanics and mechanical metallurgy, to teach undergraduate class in physical metallurgy, graduate class in mechanics. Position starts Sept. 1, 1951. Salary, $5000. Location, Pennsylvania. Y5708.

Engineers. (a) Assistant to General Manager, graduate, with considerable experience in mine operation and some experience in management. Knowledge of Spanish desirable. (b) Metallurgical Engineer, graduate, with considerable experience in milling and research, capable of directing the operations of the heavy medium and gravity plants, and in advisory capacity at other mills. Should be able to direct and carry on research in the beneficiation of tin ores in the experimental laboratory. (c) Superintendent of Sink and Float plant, graduate, with five or more years' experience in milling. Should be mechanically inclined, and have some experience as mill superintendent elsewhere. Should have working knowledge of Spanish and be able to handle Latin American labor. (d) Junior Metallurgists, graduates, with some experience in milling practice as well as laboratory research. Location, South America. Y5549.

WANTED
MELTING DEPARTMENT SUPERINTENDENT

Immediate opening for person having experience in electric arc furnace melting of tool, high speed, stainless, and specialty steels in long-established mill in Pittsburgh district. Should have considerable practical experience, technical background, and ability for handling men. Reply giving complete record of experience, qualifications, age, references. Box H-13 JOURNAL OF METALS

MEN AVAILABLE

Metallurgical Engineer, age 32, B. Met. E. Five years' experience heat treating, brass and gray iron foundry process control, nonferrous rolling and extruding, corrosion research, metallography and routine chemical analysis. Prefer Japan or other foreign location; will also consider any location in United States. M-638.

Jr. Foundry Metallurgist, 28, single, B.S. Met. Engrg. Journeyman molder, coremaker and coreroom foreman. Familiar with brass, gray iron and steel jobbing and production work. Now employed as laboratory metallurgist large automotive foundry. Desire similar position Southwest or Mexico. M - 639 - 517 - E - 7 - San Francisco.

Just Published —

An analysis of theories and experimental facts

PHASE TRANSFORMATIONS IN SOLIDS

Symposium held at Cornell University; Sponsored by NRC Committee on Solids. Editorial Committee: R. SMOLUCHOWSKI, Chairman; J. E. MAYER, W. A. WEYL.

A collection of significant papers presented at the Cornell Symposium, plus the discussion of these papers. The Symposium and this book were based on this idea: that scientists interested in the solid state could profit by learning of the advances in other fields, and that a more complete understanding of the solid state would result from such an interchange of information.

Nearly all of the seventeen papers contain a large amount of new results. There is almost no overlapping of subject material. Each paper forms a complete unit.

CONTENTS:

1. On the General Theory of Phase Transitions, *by* LASZLO TISZA
2. A General Method for Imperfect Crystals and Phase Transitions, *by* JOSEPH E. MAYER
3. Crystallization as a Cooperative Phenomenon, *by* JOHN G. KIRKWOOD
4. Fundamental Aspects of Diffusion in Solids, *by* FREDERICK SEITZ
5. Nucleation Theory, *by* R. SMOLUCHOWSKI
6. Crystallographic Aspects of Phase Transformations, *by* M. J. BUERGER
7. The Solid-Liquid Transition in Argon, *by* O. K. RICE
8. Transitions in Silver Halides, *by* M. L. HUGGINS
9. Phase Transformations in One-Component Silicate Systems, *by* F. C. KRACEK
10. Phase Transformations in Polycomponent Silicate Systems, *by* J. F. SCHAIRER
11. Transitions in Glass, *by* WOLDEMAR A. WEYL
12. Phase Transitions in Ferroelectrics, *by* BERND MATTHIAS
13. Transformations in Pure Metals, *by* CHARLES S. BARRETT
14. Order-Disorder Transitions in Metal Alloys, *by* SIDNEY SIEGEL
15. Precipitation of Solid Solutions of Metals, *by* A. H. GEISLER
16. The Eutectoid Reaction, *by* ROBERT F. MEHL *and* ARTHUR DUBE
17. The Martensite Transformation, *by* MORRIS COHEN

1951 660 pages $9.50

Send coupon now for 10-day free examination.

APPROVAL COUPON

JOHN WILEY & SONS, INC., Dept. JM-951
440 Fourth Ave., New York 16, N. Y.

On 10 days' approval send *Phase Transformations in Solids*, edited by Smoluchowski. I will remit $9.50 plus postage or return book postpaid. (Offer not valid outside U. S.)

Name

Address

City, Zone, State

Employed by

SAVE POSTAGE We pay postage if you enclose $9.50.
Money back on same return privilege.

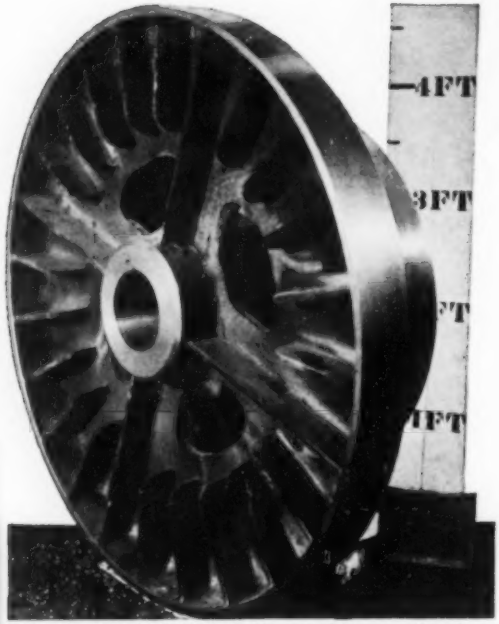

STAVER FOUNDRY COMPANY, Virginia, Minn., produced this large hoist drum in ductile iron to meet requirements of toughness with strength, and wear resistance with good machinability.

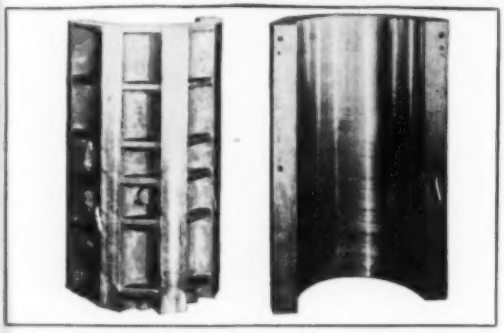

PYOTT FOUNDRY & MACHINE CO., Chicago 7, Ill., produced these ductile iron castings for dies for forming 24" to 36" diameter pipe from steel plate of ¼" to ½" thicknesses. The finished tooling was done by the Vernon Allsteel Press Co. of Chicago. The dies are to be used in large presses that exert 18,000 tons pressure.

The International Nickel Company, Inc.
Dept. J.M., 67 Wall Street, New York 5, N. Y.

Please send me a list of publications on: **DUCTILE IRON**

Name..... Title.....

Company.....

Address.....

City..... State.....

INTRICATE LARGE CASTINGS ...readily produced in DUCTILE IRON

DUCTILE IRON is a cast ferrous product that combines the *process advantages* of cast iron with many of the *product advantages* of cast steel.

In less than two years, ductile iron has attained wide acceptance because it offers excellent castability, high mechanical properties, and good machinability. Parts cast in ductile iron show superior pressure tightness, high modulus and resistance to shock.

Typical current applications include chemical pots, compressor shells, cylinders for hydraulic presses, fly wheels, housing for electric power driven tools, large gears for coal mine equipment, vise jaws, and many other parts.

AVAILABILITY

Send us details of your prospective uses, so that we may suggest a source of supply from some 100 authorized foundries now producing ductile iron under patent licenses. Request a list of available publications on ductile iron... mail the coupon now.

ST. PAUL FOUNDRY & MANUFACTURING CO., St. Paul 3, Minn., cast this hydraulic head for a billet conditioner in ductile iron having 92,000 p.s.i. tensile strength, 67,000 p.s.i. yield point and 7.8% elongation.

THE INTERNATIONAL NICKEL COMPANY, INC. 67 WALL STREET NEW YORK 5, N.Y.

Hudson Bay Mining & Smelting Co. has one furnace in its zinc fuming plant in steady operation and a second about to go into production. When operating at capacity, the 900,000 ton pile of residues will be used, along with a daily mine output of 4000 to 5000 tons. Annual production will be increased by 30 million lb to approximately 130 million lb.

ML aluminum alloy developed by the Air Forces for use in high temperature operation will permit design of casings, supports and other aircraft parts to operate at temperatures between 500° and 600°F instead of the 200° to 300°F range. Containing small amounts of Cu, Ni, Mg, Mn, Cr, V, and Ti, this ML alloy will support a 6600 psi load at 600°F for 1000 hr. Maximum tensile strength is 17,300 psi.

Koppers Co., Inc., through its Freyn Engineering Dept., will design, engineer and build Rossi continuous casting machines for ferrous and nonferrous metal casting through a deal involving purchase of interest in Continuous Metalcast Co., Inc.

A new ceramic coating, varying from 0.0005 to 0.003 in. thick, has been developed by Solar Aircraft for use in high temperature engine parts. Experimental work has been done on coating combustion chambers, diffuser cones, tailpipes, and exhaust manifolds of jet engines.

Norway will double its aluminum capacity by 1954 through the addition of a $50 million plant at Sundalsora. Capacity will be 40,000 tons per year. Counterpart Funds in Norway, Denmark, West Germany and France will be used, with these countries furnishing equipment. It is the biggest transaction thus far under American Aid to Norway and the largest loan made in support of increased raw materials.

U. S. Steel's Irvin Works, Pittsburgh, is installing facilities to neutralize waste pickle-liquor faster and more efficiently. The new system is being constructed by Rust Engineering Co., and when completed in the Fall of 1951 will handle 100,000 gal per day of raw product.

A white brass alloy, 80 pct Zn and 20 pct Cu, has been developed by du Pont. It is a substitute for nickel in chromium plating. Electrodeposited from a cyanide bath using special brightening agents, the new alloy forms an excellent base for subsequent electrodeposition of chromium.

As a substitute for high nickel alloys in certain heat and corrosion resistant uses, International Nickel Co.'s new Incoloy contains only 35 pct Ni, 20 pct Cr, and Fe.

Third quarter steel goal, 20,800,000 tons. Third quarter uses, 1,760,000 tons direct military; 15,660,000 tons defense-supporting and products used by both military and civilian under CMP; 3,380,000 tons for "free area" use not covered by CMP or other priorities. Structural steel demand for fourth quarter, 2,400,000 tons, twice the expected production.

Heavy gas cylinders on shipboard may be eliminated by a small oxygen-nitrogen plant developed by the Navy. The plant compresses, cools, liquifies, and fractionates air into oxygen and nitrogen. Oxygen is pure enough for breathing and nitrogen can be used to inert gasoline lines aboard ship. An acetylene plant is under test, and a CO_2 plant will soon be tested.

bringing a giant down to size

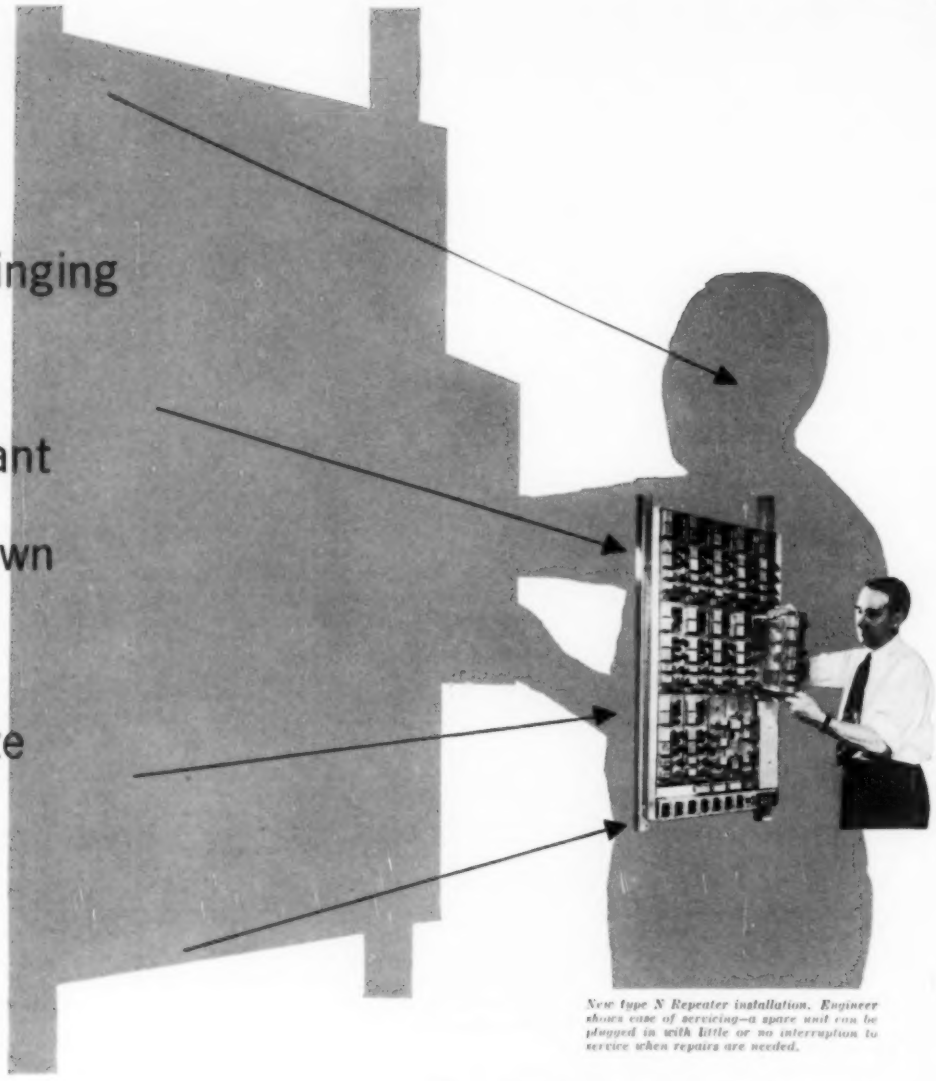

New type N Repeater installation. Engineer shows ease of servicing—a spare unit can be plugged in with little or no interruption to service when repairs are needed.

"CARRIER SYSTEM" telephony is economical, because many voices use the same pair of wires. But the extra equipment needed formerly limited it to the longer distances.

Now Bell Laboratories have developed new short-haul carrier, economical down to 25 miles, sending 12 conversations on two pairs of wires in a cable.

Keys to the new system are new circuits, miniature tubes, pocket-size wave filters and Permalloy "wedding ring" transformer cores that will barely slip over a man's finger. New manufacturing processes were developed in co-operation with the Western Electric Company. Components are pressed into a plastic mounting strip with heat, a score at a time, instead of being mounted separately.

With this new carrier system more service can be provided without laying more cables. Tons of copper and lead can be conserved for other uses. It's another example of how science takes a practical turn at Bell Telephone Laboratories, to improve service and to keep its cost down.

BELL TELEPHONE LABORATORIES

WORKING CONTINUALLY TO KEEP YOUR TELEPHONE SERVICE ONE OF TODAY'S GREATEST VALUES

Titanium Capacity To Be Increased 800 Pct by New Plant at Henderson, Nev.

Titanium Metals Corp. of America, owned jointly by National Lead Co. and Allegheny-Ludlum Steel Corp., has started operations at the first large-scale titanium producing plant at Henderson, Nev. The plant will increase titanium output in this country (and the world) from about 500 tons a year to 4100 tons a year. A contract to engineer and construct the plant has been awarded to H. K. Ferguson Co.

The basis for the new operation is the acquirement of the $150 million plant formerly owned by Basic Magnesium, Inc., an installation built during the past war by the Government. Leases have been obtained for required sections of Basic Magnesium, and an additional $15,000,000 will be spent in equipping the property for titanium production. Hoover (Boulder) and Davis Dams will supply power to the plant, chlorinators already in the plant will be used, and the magnesium cells will be used to produce magnesium chloride. The plant actually started production in July, but capacity operation of 3600 tons of titanium metal a year is not anticipated until late 1952.

Other producers of titanium likewise are looking to expansion of metal producing facilities beyond the present 500 ton a year industry capacity. With the Henderson, Nev., operation of Titanium Metals Corp. of America, it is possible that by the end of 1952 titanium metal producing capacity will hit about 10,000 tons a year.

Titanium Metals Corp. of America is the principal single supplier of titanium, with sponge coming from National Lead. This is melted into ingot by Allegheny-Ludlum Steel Corp. at Watervliet, and finished into wrought products. The Watervliet, N. Y., Brackenridge, Pa., West Leechburg, Pa., and Dunkirk, N. Y., plants of Allegheny-Ludlum, which presently produce these products, will finish 1000 to 2000 lb ingots from Henderson. Much larger ingots are expected at a later date. One of the expected results of the Henderson plant will be the reduction of costs—and also price—of titanium.

Koppers To Build Casting Machines

Koppers Co., Inc., Pittsburgh, has obtained an interest in Continuous Metalcast Co., Inc., which owns and controls the Rossi process for continuously casting metals (see JOURNAL OF METALS, March 1951, p. 227). Continuous Metalcast Co., Inc., is owned jointly by Allegheny-Ludlum Steel Corp., Scovill Mfg. Co., American Metals Co., Ltd., and Irving Rossi, president of the company and inventor of the process. Koppers acquired part of Mr. Rossi's interest.

Koppers will engineer, fabricate, erect and sell the continuous casting equipment licensed by Continuous Metalcast Co., the work coming under the Freyn Engineering Dept. of Koppers.

1952-53 Fulbright Exchange Program Announced for Europe and Near East

The 1952–1953 program for University Lecturing and Post Doctoral Research Awards under the Fulbright Act is now available. The Fulbright Exchange Program was planned to further goodwill and understanding between the United States and other countries through the exchange of students, teachers, lecturers, research scholars, and specialists, with funds derived from foreign credits acquired by the United States from the sale of surplus properties left in the participating countries at the close of the war. There are several awards available in geology, nuclear physics, and metallurgy.

Awards for university lecturers, post-doctoral research scholars, and specialists are made in the currency of the host country and usually include round trip transportation for the grantee, a maintenance allowance, and a small supplemental allowance for travel and books or equipment purchasable abroad. Awards for advanced research are not subject to taxation, but university lecturing awards are subject to U.S. Federal Income Tax.

Applicants for awards must be citizens of the United States. Research scholars must have a doctoral degree from a recognized institution of higher learning and should be proficient in the language of the host country. Visiting lectureships are expected to have had at least a year of college or university teaching experience, and with some exceptions, are expected to deliver lectures in English.

Applications will be accepted between May 15 and Oct. 15, 1951 for the 1952-1953 academic year for countries of Europe and the Near East. Additional information and forms can be obtained from The Executive Secretary, Conference Board of Associated Research Councils, Committee on International Exchange of Persons, 2101 Constitution Ave., Washington 6, D.C.

Estimated Research and Development Requirements Hit Staggering Totals

The importance and magnitude of the expenditures and manpower involved in research and development work in progress in this country were highlighted in a speech before the Engineering College Research Council by Eric A. Walker, executive secretary, research and development board, Dept. of Defense.

The price of research in dollars is summarized in Table I. Scientific and technical manpower resources now total 575,000 persons, far short of the number needed. Of this total, about 130,000 are trained for research, with 25,000 employed by the government, 70,000 by industry, and 35,000 by colleges and universities. The Dept. of Defense research program alone now requires 56,000 engineers and scientists. In 1952 it is expected that this requirement will reach 68,000 persons, and personnel requirements of the AEC and other agencies engaged in defense research would bring this total to 84,000 persons, or 65 pct of available talent.

Table I. National Expenditures for Research and Development

Year	National Expenditure Non Military	Military Expenditure Non AEC
1940	$ 350,000,000	$ 22,000,000
1945	$1,100,000,000	$ 600,000,000*
1946-1950		$ 500,000,000 per year
1951	$1,750,000,000**	$ 300,000,000 Government Labs
	$2,300,000,000**	$ 650,000,000 Industrial Cos.
		$ 100,000,000 Colleges & Univ.
		$1,100,000,000
1952		$1,300,000,000

* Including work of Office of Scientific Research & Development.
** Estimates from two sources.

Engineering Manpower Meeting

An engineering manpower convocation, under the sponsorship of the Engineering Manpower Commission of Engineers Joint Council, is scheduled for Sept. 28, at the Stephen Foster Memorial Hall in Pittsburgh. The purpose of the convocation is to inform the engineering profession about the critical shortage of engineers and to invoke cooperation in remedying the situation. Industry as well as the profession will be represented. All Local Sections of the AIME and other parent EJC societies are invited to send one or more representatives to the convocation.

Electrolytic Probe

For Underground Corrosion Studies

by W. Beck

The electrolytic probe technique is applied to determine the density of corrosive currents on buried metallic structures. The probe consists of a hollow half cylinder, placed on the outside surface of a line, connected to the installation through a current meter of low internal resistance.

INFORMATION published on corrosion usually has been concerned with cases of metal attack occurring in various aqueous solutions, air, and especially in different aggressive atmospheres at high temperatures. However, large quantities of cast iron, steel, and lead installed underground are exposed to corrosion. At the United Nations' Sectional Meeting, Mineral Resources 6(a) on Conservation by Corrosion Control, held in Lake Success on Sept. 1, 1949, it was disclosed that the United States alone suffers an annual loss of more than $500 million, because of maintenance and replacement of underground pipe lines damaged by corrosion. There is an additional loss, brought about by corrosion of the lead sheath of underground telephone and power cables. Moreover, the depletion of such resources as iron ore and lead calls for a drastic reduction of the corrosion loss.

There are different causes of pipe wall and lead sheath corrosion. Only those types of corrosion produced by the action of measurable electric currents will be considered here. Such currents can be generated by grounded dc electrical installations, by galvanic action, and by variations in the earth's magnetic field strength. The electric currents produced by grounded installations almost exclusively are stray currents flowing into the soil from the tracks of dc railroads or trolley lines. Galvanic currents are of two types, those flowing locally on metal surface and the so-called long line currents. The first type can be originated by a contact between dissimilar metals, but usually are brought about by differential aeration. The formation of such aeration cells is tied up largely with local differences in the texture of the soil surrounding the line, leading to local differences in the air permeability. Points on metal surface with a practically unlimited oxygen supply are cathodic against those suffering under air deficiency. These latter spots are anodic in such a differential aeration couple and the metal on these points is corroded. If the anodic current density is high enough, pitting and even perforation of the pipe wall results. Electrolytic cell potentials can be induced by local differences in the electrochemical behavior of adjacent soil sections (reaction, conductance, nature, and concentration of dissolved electrolytes). Also, local differences in the permeability of decayed protective coatings on underground lines or on cable ducts can set up oxygen concentration cells.

In contrast to these local galvanic cells, the so-called long line currents are generated by differences in the characteristics of soils, surrounding the line over long distances. Magnetic storms under specific circumstances can lead to local variations in the strength of the earth magnetic field, inducing the flow of strong equalization currents through the soil and particularly the buried metallic structures. Serious metal attack was produced on sections where such currents were discharged to the ground.

Anodic current flow is detrimental to the metal. However, by making iron or lead cathodic, the unfavorable influence of the current can be converted into a beneficial one. By applying a suitable current density, a buried metallic structure can be protected for practically an unlimited period. Hundreds of miles of pipe and cable lines are made completely resistant against any kind of underground corrosion by combined application of cathodic protection and surface insulation, achieved by bituminous coatings.

It is obvious that the current density on line surface controls the corrosion rate of the metal or

Fig. 1—Diagram of an electrolytic probe installed on pipe.

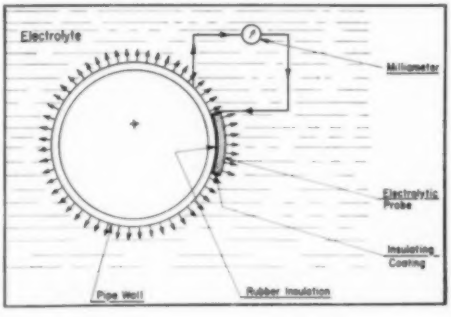

W. BECK obtained the material for this paper while Associate Professor of Metallurgy and Director of Corrosion Research Laboratory, Lehigh University, Bethlehem, Pa. He is now affiliated with American Electro Metal Corp., Yonkers, N. Y.

determines to what extent cathodic protection is achieved.

There are few methods that permit measuring current discharged to the ground by a line section. Just the knowledge of the density of the current emitted to the soil is of interest in testing and mitigation of underground corrosion. The application of special types of instruments, such as earth ammeters, unpolarizable exploring electrodes, and earth current meters, make it possible to determine the current density at any point on the circumference of a buried cylindrical conductor.[1, 2] Application of these instruments is not an easy operation and efforts were made to develop less complicated and more flexible methods. Use of a small metallic electrode to be placed on the surface of the buried metallic structure has been recommended.[3, 4] If such an auxiliary electrode is short-circuited with the pipe and consists of the same metal as the structure, it can be assumed that the potential difference between the probe and ground will be controlled by the potential of the line to ground. Inserting a low resistance current recorder in the short circuit between the pipe and electrolytic probe and insulating the latter from the pipe wall, stray currents emitted or picked up by the line section can be measured on the test electrode. If the area of the electrode is known, current density can be calculated.

When currents from small iron or lead electrodes are flowing into an electrolytic solution, polarization processes will occur on metal surface. Electrolytic probes are used exclusively for measurements on cable lines, but a disclosure of polarization processes requires the performance of elaborate measurements in the laboratory. The reliability of the probe as a reference electrode should be influenced by such processes; and a clarification of this question is required for a more critical application of the electrolytic probe technique to measurements underground.

The electrodes used in tests were made by cutting small cylindrical segments from steel pipes of slightly larger diameter than the pipe to which they were connected. Lead electrodes were cut from cable sheaths. The inside surface of the probe was lined with soft rubber so that the edge of the pad protruded over the edge of the electrode. The rubber layer was glued to the pipe and electrode by a rubber solution or asphalt, and the edges of the electrode were insulated with rubber or plastic. Leads were welded in small holes drilled in one edge of the metal segment. A glass tube was cemented watertight to the edge on the spot of welding. This tube encased the wire, connecting the electrode to one binding post of a switch. The probe surfaces were cleaned, polished with emery paper and carefully degreased. The area of the auxiliary electrodes was at least 10 sq cm because electrodes with a smaller area showed irregular performance. The test electrodes were coupled with short sections of steel or lead pipes and immersed into large cylindrical tanks with insulated walls, filled with tap water. Both ends of the cylindrical specimens were sealed by plugs of insulating material. The surfaces of iron pipes or lead cables, when exposed to the soil for a longer period, are covered with layers of corrosion products. To simulate these conditions the pipe sections before being coupled with the probes were kept at room temperature in humid soil. After 10 days the corroded specimens were removed from the soil, rinsed with cold tap water, dried, cleaned, and the

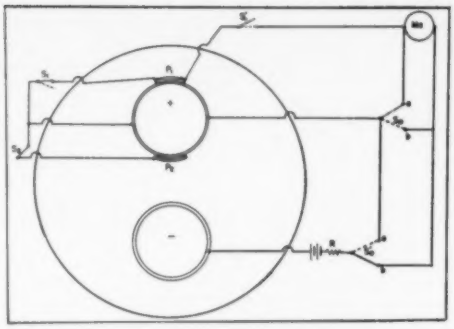

Fig. 2—Wiring diagram for measuring total current flow between pipes. Dotted lines show circuit for measuring partial current flowing through probe P_1.

probe electrodes installed. The pipe, 5 cm diam, coupled with the probe, 10 sq cm in area, was made the anode, while the cathode, a rectangular metal sheet, was placed a short distance away. Both electrodes were totally immersed in the solution.

All runs were made at a temperature of about 25°C. The insulating resistance of the rubber layer between pipe surface and electrode was checked frequently, but no decrease in resistance could be found. The tank containing the specimens was flushed occasionally with fresh tap water (pH = 6.5).

Fig. 1 shows how the probe works. Fig. 2 shows the wiring for the measurement of the total cell current and partial current flowing through P_1. With this wiring the short circuit between P_1 and P_2 and the pipe is not interrupted. The partial current flowing through P_1 is measured, while the probe P_2 is short circuited with the cylinder as shown by the broken-line connections. With this wiring, the probes remain short circuited with the anode practically throughout the total exposure time. R is an adjustable resistor. By using appropriate shunt resistors, the range of the milliameter applied (sensitivity 0.05 ma per scale division, internal resistance 2 ohm) could be varied over a broad range. The anodic current density applied was between 1 and 3 ma per sq dm, values[5] that can be considered as critical with respect to the accomplishment of electrolytic corrosion underground.

The auxiliary electrodes were placed in diametrically opposite positions because the electric field is not distributed symmetrically around the circumference of the cylinder. The current density will have its highest value at points located on the vertical line on the cylinder surface with the shortest perpendicular distance from the cathode (i_{max}). The points on that line, located diametrically opposite to the other are under the lowest current load (i_{min}). The cell current measured between the anodic pipe and the cathode is an average value, hence the current density based on this value I_{avg} must be an average value too. In general, I_{avg} cannot be calculated as the arithmetic mean value from the values for i_{max} and i_{min}. However, under the experimental conditions prevailing in these laboratory runs it is feasible to compute the value for I_{avg} from probe measurements with some degree of accuracy. The rate of agreement between the average current density, I_{avg}, determined experimentally from total cell current and that computed from measurements

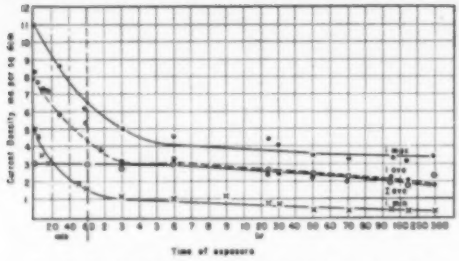

Fig. 3—Steel cylinder and plate immersed in tap water. Potential difference applied, 3 v.

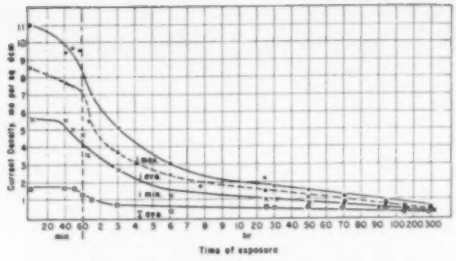

Fig. 4—Lead cylinder and plate immersed in tap water. Potential difference applied was 3 v.

Current density related to probe facing the plate is i_{max}; current density related to probe installed diametrically opposite is i_{min}; current density averaged over i_{max} and i_{min} is i_{avg}; and I_{avg} is average current density related to total surface of cylinder.

on two probes i_{avg}, placed diametrically opposite to each other on the pipe surface, indicates, at least theoretically, to what extent the average current density on the pipe surface can be characterized by probe measurements.

Runs were made with a number of auxiliary electrodes fastened one over another to different points on the pipe circumference. The differences between the values determined on a number of electrodes installed at the same vertical line were small. In the following runs only two electrodes were used, installed as shown in Fig. 2, having the same distance from the bottom of the tank and the water level respectively.

Fig. 3 illustrates the change of probe and pipe current with time of exposure. The object under investigation was a steel pipe coupled with a probe of the same metal. The auxiliary electrodes remained short-circuited with the cylinder. The currents taken in the secondary circuit, up to about 1 hr, were instantaneous values. Throughout an initial period the partial currents on both probes were dropping rapidly with time. In contrast to this, the decrease of total cell current was extremely slow. It is only after exceeding this initial period that the average current density on the pipe surface can be measured by the averaged density of currents taken on the two probes.

The rapid current drop can be explained by the formation of oxide layers, a process leading to a continual increase of contact resistance on the anodically polarized probe surface. Finally, the conditions practically become stationary. In all cases the formation of dark layers could be observed on the surface of the electrodes. By keeping the probes continually short-circuited with the pipe under-current flow, the time necessary to bring about this steady state can be shortened, at least under the current load applied to these runs. A calculation of the average current density from probe measurements made, by applying the short-circuit only for the moment of a current reading, gives values which are too high. In Fig. 4, typical current density vs time of exposure data are plotted. The measurements were taken on lead immersed in tap water. In contrast to the oxidation products formed on iron surfaces, the ones deposited on lead in tap water are more impervious and adhere firmly to the metal.[5] This explains why the currents on the lead pipes and probes finally become very small and the curves converge. The value of the current density given is fictive. The real current density on probes or on the pipe section is unknown, because only a certain (unknown) part of the total area of the metal is *not* covered by more or less insulating corrosion products. Agreement between I_{avg} and i_{avg} is accomplished so that the relatively small (not pre-corroded) probe surface anodically is polarized until a kind of equilibrium is reached between the current permeability of the rapidly growing oxide layer on probes and that present on the total pipe surface. Because of this, the currents corresponding to i_{avg}, after reaching a steady value, characterize qualitatively the currents exchanged between a pipe line and ground, through the weak spots in the corrosion layer on the metal surface.

More information pertaining to the galvanic behavior of the couple probe-pipe was needed. For this purpose a lead pipe equipped with a lead auxiliary electrode, facing the cathode, was immersed into tap water and connected to a current source. The polarizing voltage was increased and the corresponding

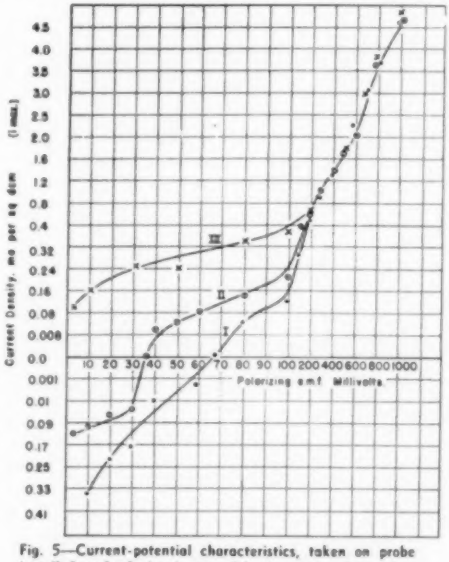

Fig. 5—Current-potential characteristics, taken on probe installed on lead pipe immersed in tap water. I is polarized on immersion; II, polarized after short-circuiting probe with pipe for 3 hr; and III, polarized after short-circuiting probe with pipe for 15 hr.

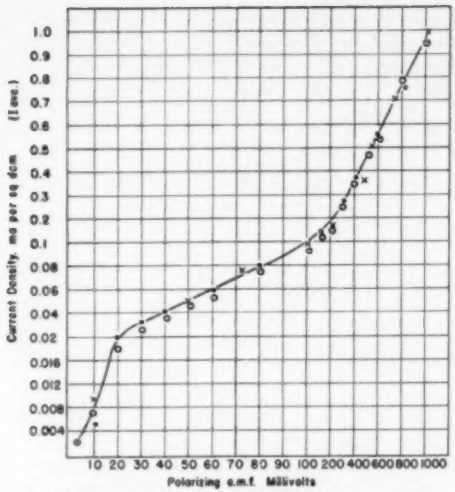

Fig. 6—Current-potential characteristics taken on lead pipe immersed in tap water.

current measured on probe and pipe respectively. Numerous runs were made and typical polarization curves are given in Fig. 5 where the max current density on probe is plotted against the polarizing emf, recorded between pipe and cathode. Curve I, for a specimen anodically polarized on immersion reveals that a considerable galvanic current is flowing between cylinder and test electrode. Up to a polarizing voltage of around 65 mv, the probe is cathodic against the pipe and is picking up currents. Short-circuiting for 3 hr, Curve II brings about a considerable decrease of the galvanic action. In order to compensate for the slight residual voltage, an emf of 35 mv has to be applied. Short-circuiting for 15 hr, Curve III achieves a practically complete equalization of the potential difference between reference electrode and pipe. No appreciable change of the galvanic behavior was achieved, by extending the short circuit up to 75 hr. Fig. 6 shows the dependency of the current density on polarizing emf. In this case the total cell current was recorded and it was polarized with increasing voltage. A galvanic current also could be observed on couples consisting of steel, but much less marked than on lead.

Experiments were carried out with coated steel pipes imbedded in humid soil. The specimens were buried in large square boxes made of insulating material and filled with soil. The humidity of the soil was checked and evaporated water was replaced. The cathode was a steel sheet, and the two anodes, consisting of a bare pipe A and a protected one B, were placed one above the other. Two electrolytic probes were fixed in a diametrically opposite direction close to the ends of both pipes. Pipe B was covered with a bitumen that had poor protection properties and the formation of cracks and crevices was expected shortly after applying the coating.

The dependency of the density and intensity of current on the time of exposure, related to the measurements, made on the reference electrodes and on the pipes as well, is illustrated in Figs. 7a and 7b. The curve B in Fig. 7a shows that, because of its decay, the coating with time becomes more permeable for the current. Fig. 7b reveals that the current on the probes, placed on the coated pipe (i'_{ave} and i''_{ave}), is dropping more rapidly than one measured on the electrodes fixed to the bare pipe (i'''_{ave} and i^{IV}_{ave}). The probes fastened to the bare pipe A show a similar behavior as could be observed in tap water, but the fluctuations are typical for the runs made in soil. Fig. 7b discloses further that the current density resulting on the probes, fastened to the protected pipe, particularly throughout an initial period, is much higher than that determined on electrodes, coupled with the bare cylinder. This phenomenon can be interpreted as follows: As long as the coating maintains its insulating properties, the probe acts like a hole in an impervious layer and the total anodic current is concentrated on the relatively small surface of the auxiliary electrode. As long as the contact resistance on the coated steel surface is high, the current density on the probe must remain high. Because of the formation of breakdowns in the coating bare spots appear on the metal surface, which, in addition to the currents discharged by the probes, also emit currents. With increasing number of breakdowns, more and more metallic spots gradually are

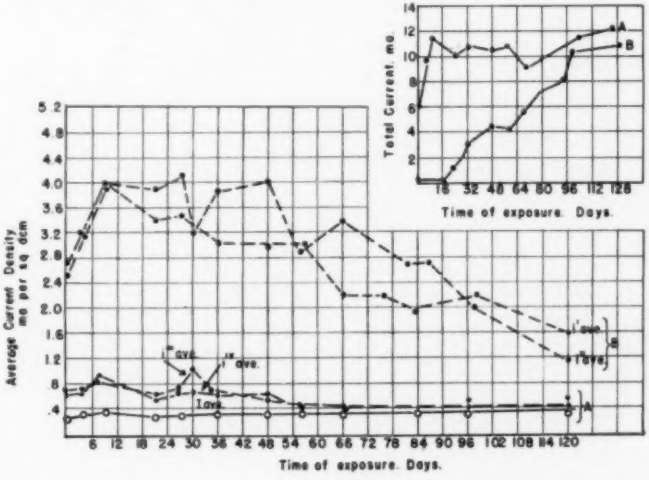

Fig. 7—Two steel pipes and plate imbedded in humid soil. Potential difference applied, 3 v. A is uncoated pipe, and B, coated pipe. Symbols i'_{ave} and i''_{ave} are average current density related to probes fixed on two different points to both halves of coated pipe; i'''_{ave} and i^{IV}_{ave} refer to the coated pipe; and I_{ave} is average current density related to total surface of uncoated pipe.

switched in series to the auxiliary electrode. In proportion to the given ratio of the current carrying area on the pipe surface to the active area on the probe, the current is distributed between these two conductors. With growing deterioration of the coating, the points not insulated on the pipe wall are continually increasing and the current on the probes is dropping accordingly. This explains why in Fig. 7b the curves for i'_{xx} and i''_{xx} approach those for i'''_{xx} and i^{IV}_{xx}.

The results of the measurements made under laboratory conditions can be summarized as follows: 1—The probe currents throughout an initial period drop rapidly with time, and finally become practically stationary; 2—The averaged current density with respect to the currents taken on two probes placed on the pipe wall in a diametrically opposite direction, to a certain extent characterizes the average current density on the pipe surface after steady values are reached; and 3—A practically steady state can be reached after a relatively short exposure period by keeping the probes short-circuited permanently with the pipe under-current flow.

The interpretation of the measurements made on probes fixed to coated pipes requires special consideration of the contact resistance on the metal surface.

An unprotected steel branch pipe, 4 cm diam, installed in a concrete wall in the basement of a building was investigated. After a hole had been made in the wall, a steel probe equipped with lead was fixed to the pipe and the gap closed with concrete. The test electrode faced the tracks of an electric railroad, located not far from the building. The concrete was dried after about one week, and then the probe was short-circuited with the line. For recording the currents picked up or emitted by the reference electrode, a special oscillographic procedure was employed. The recorder used consisted of an extremely thin aluminum foil suspended between the poles of two permanent magnets. The foil was sealed in a glass cell and shaped into a loop, and the instrument was considered as a loop galvanometer.[6,7] The apparatus had special optics and the aperiodic deflections of the loop, achieved by the corrosive currents, could be photographically recorded. One of the advantages of this type of galvanometer lies in the fact that it combines small internal resistance (< 1 ohm) with high current sensitivity (10^{-5} amp).

In Fig. 8 some values of the current density on the probe, taken from a 12 hr record and referred to an arbitrary zero point of time, are reproduced. The probe predominantly is emitting currents into the wall and peak values of +1.4 ma per sq dm are reached. Shaded sections mark the interval when a car started driving in a nearby railroad station. In general the peak values of the current density fall exactly into the short period when the load on the negative return feeder is heavy, indicating that the probe currents are stray currents, generated by the driving current of the railroad. By graphically integrating the records, the current can be averaged over the total period of recording. The current density averaged over a 12 hr period was in this case +1.2 ma per sq dm. For a certain period, following short-circuiting probe with pipe, relatively high current values resulted; however, after 75 hr, lower and more steady averaged values could be determined. The component of stray current flowing in the pipe wall was considerable and was 1.1 amps, averaged over the same period of 12 hr and flowing in one definite direction.

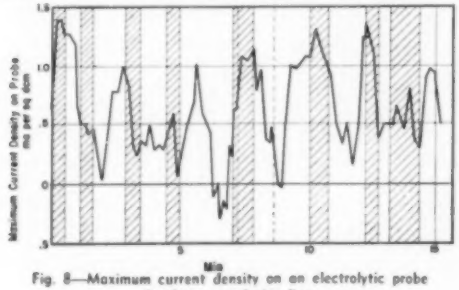

Fig. 8—Maximum current density on an electrolytic probe fixed to a steel pipe line.

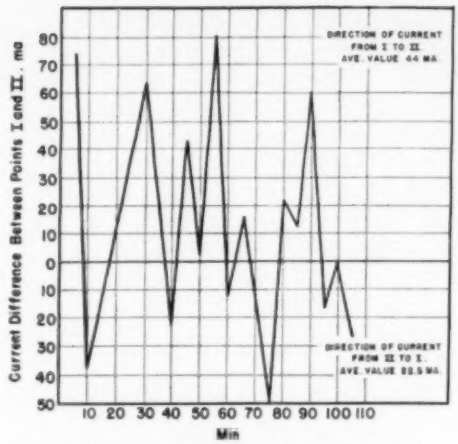

Fig. 9—Differences in sheath currents measured simultaneously at points I and II.

An average current density on the pipe surface larger than about 0.5 ma per sq dm has to be considered as critical[2] with respect to the accomplishment of electrolytic corrosion underground. This critical value being considerably exceeded in this case, attack of the metal had to be expected. An inspection of the pipe confirmed this and revealed numerous badly corroded sections on the metal surface.

The lead sheath of a telephone cable, 6 cm diam, was covered with an asphalt jute wrapping and armored by iron tape. After removal of a piece of the tape a lead probe of rectangular sheet 3x12 cm shaped in a half cylinder was fastened with asphalt to the coated cable. The electrode faced the tracks of a trolley line running parallel to the cable. Numerous electric tests were made[5] on the auxiliary electrode and of the currents flowing in the lead coat. The sheath currents were taken by interrupting the metallic continuity of the cable coat on two points 223 ft apart, and bridging the small gaps by recording instruments. All records were made after the cable was re-buried. Fig. 9 illustrates that the differences between the currents, taken simultaneously at the two points can become appreciable and the direction of the currents is changing rapidly. Values plotted were taken from a 12 hr record and belong to a period of the trolley service when the line was heavily loaded.

The differences between the averaged intensities

of the currents flowing at the same time through recorders with identical resistances, are considerable in both directions, and cannot be explained as caused by the resistance of the cable section switched between points. The lead coat was predominantly anodic against the trolley tracks (voltage, averaged over 12 hr was +1.5 v) and the reason for the current drop over the short cable section was that a part of the sheath current was lost to the ground as stray current. The average current loss can be expressed by the arithmetic mean value of the differences of the averaged currents, flowing simultaneously through the two recorders, with regard to the two directions of current flow. Based on 12 hr records, the averaged density of the current discharged to ground and referred to the total area of the lead sheath, belonging to a cable length of 223 ft (area 2.2×10^3 sq dm) was computed to 0.05 ma per sq dm.

The diameters of cable and track (approximated as a cylinder with circular cross section) and the perpendicular distance between the cable and the projection of the track being known, the maximum current density on cable was calculated by application of Kirchoff's Laws[8] and found to be 0.056 ma per sq dm. To simplify the calculation, it had to be neglected that the trolley tracks only partly are imbedded in the soil. Because of this, the value of the calculated maximum current density becomes somewhat high. The diameter of cable and current load being relatively small, the difference between the average and maximum current densities is not appreciable. On pipe lines with a large diameter, particularly when the average current density is higher than in this case, the difference between i_{max} and $i_{av.}$ can become appreciable. It should be borne in mind that rate is determined only by the maximum current density on metal surface.

The currents on the probe were taken simultaneously with the sheath currents. Recording was started after the probe was short-circuited with the cable for 4 days. Special runs were made to see if interrupting the short circuit between probe and cable had an influence on the sheath currents, but no measurable effect could be detected. Currents predominantly were emitted into the soil. The maximum current density on probe, averaged over two 12-hr records, taken on two days was computed and found to be +0.17 ma per sq dm.

The computation of the maximum density of the emitted current from the current drop over the short cable section, was based on the assumption that the insulating resistance of the coating on the lead sheath was broken down completely at any point on the metal surface. However, the measured resistivity hardly can be considered a confirmation of this assumption. The *active* area will be smaller than the total one of the cable section and hence the *real* value of the average current density is higher than the calculated one. On account of this, it is not surprising that the current density derived from probe measurements is higher than that based on measurements of the current drop, while disregarding completely the contact resistance on the surface of the coated lead sheath.

L. J. Gorman and L. F. Greve, who have made numerous corrosion investigations on the network of the power cables of the Consolidated Edison Co. of New York and Chicago, also used an electrolytic probe technique.[10, 11] Along with the probe current, the resistance of the ducts which encased the cables was determined. By application of appropriate statistical methods, Gorman succeeded in correlating the life of a cable sheath to probe current and contact resistance. Using a diagram he developed,[10] the life of the cable section between the points I and II under the prevailing electrolytic conditions definitely must be longer than 17 years. As a matter of fact, no serious attack could be detected on the cable line under investigation, which was installed 30 years before this survey was carried out.

The usability of electrolytic probes could be proved by numerous other measurements of corrosive currents, generated by galvanic action or magnetic storms. According to a personal communication of L. J. Gorman, auxiliary electrodes, similar to those described, presently are used to determine the current density on underground installations protected by cathodic currents in conjunction with insulating surface coatings.

Experience with auxiliary electrodes used for measurements on underground installations has shown that a critical application of the electrolytic probe technique makes it possible to determine the current density on underground pipe and cable lines with an exactitude sufficient for many practical requirements.

The determination of the current density on probe along with the contact resistance on the surface of a sub-soil structure with coated surface, can give useful information about the corrosion hazard of the buried metal, under the prevailing electrolytic conditions. The application of the electrolytic probe technique has the advantage that: 1—Records can be made simultaneously on a number of probes which easily can be installed at different points, distributed over line sections of any given length; and 2—The usability of an auxiliary electrode is not influenced by keeping the same, for a long period, short-circuited with the installation in the underground.

However, it must be taken into consideration that the exactitude of the measurements obtained by using unpolarizable earth current meters appreciably is higher than of those made with electrolytic probes.

Information gained from measurements with auxiliary electrodes, in many cases, will determine whether the utilization of more complicated and costly procedures is indicated.

References

[1] F. Haber, F. Goldschmidt and K. Liese: *Zeitschrift Elektrochemie*, **12**, p. 49 and p. 829 (1906).

[2] B. McCollum and K. H. Logan: Technologic Papers, Bureau of Standards, No. 351 (1927).

[3] F. Messmer: Z. *Telegraphen and Fernsprechtechnik*, **10**, p. 117, and p. 141 (1921).

[4] O. Haehnel: *Z. Fernmeldetechnik*, **4**, p. 35, and p. 49 (1923).

[5] U. R. Evans: Metallic Corrosion, p. 396 (1945).

[6] W. Beck: *Bulletin of the Swiss Assn. of Electrical Engineers*, **14**, p. 19 (1936).

[7] W. G. Radley and C. E. Richards: *Journal of the Institute of Electrical Engineers*, **85**, p. 695 (1939).

[8] W. Beck: *Electrical Engineering* (Amsterdam), **18**, pp. 139-148 (1940).

[9] M. R. Gibrat: *Revue Générale d'Électricité*, (1934), Feb. 17 and Feb. 24, pp. 203-225, and 229-253.

[10] L. J. Gorman: American Institute of Electrical Engineers, Technical Paper No. 45-59, January (1945); *Corrosion*, **1**, p. 163 (1945); Cathodic Protection, A Symposium by the Electrochemical Society and the Nat. Assn. of Corrosion Engineers, p. 175 (1947).

[11] L. F. Greve: *Corrosion*, **4**, p. 530 (1948).

Nickel

SCHEDULE $28 MILLION PROGRAM FOR SHERRITT'S LYNN LAKE

Major Portion of Fin... stantial Part of Anti... Deliveries to Start in

HIKE NICKEL PRICE 6c (U.S.) PER LB.

New Scale Effective June —Follows Revision in ... Contract With Employees

An increase of 6¢ (U.S.) per lb. in ...kel, effective ... by The ... This brin... ckel, includ... 50¢ (U.S. ... tario) refi... nadian co... cy.

...ent follo... ...tuesday. ...ne-year ... week ...hourly ...antial)

...gnished

INCO OF... GOES FA...

Parties in ... ada and Twe... in Sudbury

Twenty diam... nickeliferous nc... feature the ...

INCO PROFITS HOI... AT RECORD LEVEL...

Earnings in Last Two Quarte... Best in Company's History ... Working Capital Gains

Net earnings of International Nick... any of Canada ... and subsidiaries ... first quarter of ... U.S. funds after ... dend, were the ... in the company ... was equivalent ... stock, compared ... 1950, 90¢ for th... 54¢ for the firs... ings establishe... above the pre... quarter of 193...

Net sales fo... from the pre... expenses were ... came received ...

FURTHER CUTBACK ON NICKEL IS SEEN

National ... Admini... 'Our ...

FALCONBRIDGE AIMS AT HIGHER OUTPUT

(Continued from Page Seventeen)

...e still sold outside of Canada and the United ... CHIC States. Until the company is producing sufficient ... matte for two refineries there is no economic ... in building a refinery here, Mr. Fraser said. ... that government pressure had been ... on the company to establish ... not be subject to the risk ...

NICKEL OF CA... TO EXPAND ...

Head of Internation... Says Supply Far ... Iron Curtain Pr...

By J. V. BEALL, Editor
MINING ENGINEERING

IT was no surprise when an important NPA official harried by distribution problems remarked that "four times the current supply of nickel is needed to sustain the defense program". True as this statement is, much of the additional nickel supply in question would go begging unless supplies of other basic raw materials and production capacity were increased similarly. Nevertheless, since the discovery that nickel added to steel made good armor plate, nickel has been essential to defense. In the interim between World War I, when this important property of nickel was battle-tested, and the Korean-prompted national emergency, the myriads of nickel alloys developed made that metal as basic in the variety and number of its uses as plastics. From the kitchen to rockets, nickel is universal in its applications.

Nickel supplies are now being stretched by *use limitation* orders and substitutes. And nickel producers are delivering only to the extent of allocations made each month by the National Production Authority. Large markets for nickel have been built up in non-military uses, and the nickel is being diverted from these to the defense effort. Amended NPA order M14 issued on Feb. 28, 1951 contained a list of 380 items from motor cars to kitchen utensils in which nickel is prohibited. Another cushion for the nickel pinch is the large mothballed fleet, which will reduce nickel consumption considerably in the marine field. All of the 7200 tons of nickel available monthly is earmarked for defense; but an allotment of 15 pct of the monthly average consumption during the first six months of 1950 is allowed for some consumer businesses which are stringency cases. How long this allotment can be maintained is not known. Defense orders are being skimped since suppliers have been directed not to deliver over 60 pct of the nickel called for by rated orders.

Faced with the tight nickel supply situation, Washington officials dubiously are contemplating Sudbury, Ontario, the nickel basket of the world. Although ubiquitous to metal products, nickel in economic ore deposits is exceedingly rare. Sudbury is the notable exception. The area has produced for over 50 years, yet it has been supplying 80 pct of world consumption since 1942.

Approximately 90 pct of the nickel mined at Sudbury is by the International Nickel Co. of Canada—familiarly known as Inco—and the remainder by Falconbridge Nickel Mines, Ltd.

As nickel deposits go, the Sudbury ores are considered lavish—copper, nickel, and platinum metals,

A JOURNAL OF METALS Industry Report on Strategic Metals.

For a Similar Report on Cobalt, see JOURNAL OF METALS, January, 1951.

gold, silver, selenium, and tellurium—there is nothing comparable known in the world. However, Inco does not regard this opulence with embarrassment for the original discovery at Sudbury in 1856 was hailed as a copper bonanza. Exuberance over the discovery was shortlived, for the first shipments of copper concentrates to Orford Copper Co. refinery at Bayonne, N. J., disclosed the hitherto unsuspected presence of nickel. As the miners of Saxony had learned over 100 years earlier, the white metal produced was brittle and unworkable. The Saxons named it *Old Nick's copper* and went on to other things, whereas their sturdier successors devised the Orford process, which causes the sulphides of nickel and copper to separate by the addition of sodium sulphate to the melt. By 1900, business was fair but the market for nickel was small, about 10,000 tons annually. Its use was restricted to coinage, electroplating, and German silver. More uses for nickel were needed if the full potentialities of the discovery were to be exploited, because there was nearly 2 lb of nickel for every 1 lb of copper.

The race for naval power at the beginning of the century, coupled with a discovery by a Frenchman that the addition of nickel to steel increased its toughness, was the combination that boomed the nickel market. The United States Navy became the No. 1 consumer of nickel for armorplate for warships. Armament consumed 90 pct of the nickel during World War I and the Sudbury mines expanded phenomenally—44,000 tons per year. So it was that, suckled in war, the infant nickel suffered childhood diseases from the postwar slump in nickel demand. These diseases left their mark for never afterward was nickel, even in maturity, prone to overexpand the Sudbury basket. Fortuitously, the United States turning from war entered a decade of industrial expansion—the automotive age—which brought a new demand for nickel. These many new uses for nickel did not emerge full grown, but instead were in large part the hard, diligent work of Inco's research organization, built up by Robert Crooks Stanley.

Quite properly the growth of world nickel consumption to 158,700 short tons in 1950 can be considered a monument to the work of Mr. Stanley. Of this amount, 77 pct comes from Sudbury. The statistical story of world nickel production for the past 10 years, Table I, emphasizes the fact that capricious Nature gave such an advantage to the Sudbury ores that production elsewhere is insignificant. Russian production is significant, of course, in direct ratio to the likelihood that it will be thrown back at us in high velocity projectiles.

It is customary to refer to past records when seeking a solution to current problems and so Table II provides a study of United States' imports from the various countries of the world during the critical decade 1940 to 1949. Imports from Canada averaged about 74 pct. The results of United States efforts to stimulate nickel from Cuba and other countries to meet the demands of the war years seems small in comparison to the total need. Current United States nickel consumption at the annual rate of 86,400 tons is roughly 10,000 tons less than World War II average total imports.

There is pressure to bring nickel deliveries to the average for the war years, but even this will leave consumer business dormant. Defense production plus business as usual is not in the cards for nickel.

Nickel forms with many metals alloys of varying physical properties which have innumerable applications in manufacturing. Mention of some of these uses explains the high rate of nickel consumption in defense production. Table III briefs the record of the consumption, composition, properties, and uses of nickel and its alloys. The chief consumers of nickel are the austenitic chromium-nickel steels, which are known for their resistance to corrosion. Chromium is responsible for the corrosion resistance and nickel acts as an austenitic stabilizer. The 18 Cr 8 Ni steels and the modifications of this basic composition constitute two thirds of all the production of stainless steel. The volume of nickel going into stainless steels places them under careful scrutiny by NPA for conservation. For steels requiring extra resistance to atmospheric corrosion but not requiring deep drawing properties, nickel can be eliminated by increasing the chromium. For all other purposes, downgrading to a lower nickel content and prohibition of the uses of stainless steel in the manufacture of many nonessential articles offer the best opportunities for conservation. Enamel-coated carbon steel might be substituted for stainless in ex-

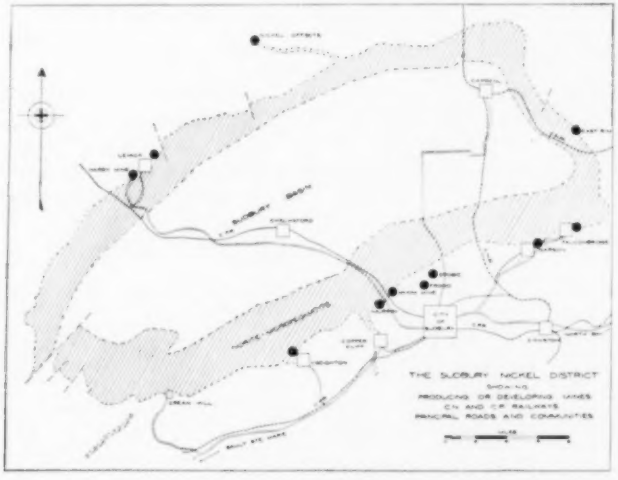

Black dots indicate the mines of the famous Sudbury basin, source of 80 pct of the world's nickel. The squares are the various towns.

Table I. World Nickel Production 1941-1950 Net Tons*

	1941	42	43	44	45	46	47	48	49	50
World	178,600	174,200	184,100	173,100	159,800	135,600	154,300	166,500	160,900	158,700
Canada	141,126	142,603	144,007	137,297	122,564	96,061	118,625	131,738	128,688	123,055
USA	660	612	642	988	1155	352	646	883	780	913
Cuba			2679	5158	13,015	12,391	2220			
Brazil		1		7	66					
French Morocco			50	52						
Rhodesia										
South Africa	558	593	544	583	554	548	583	805	623	939
Finland	167	1797	9888	245	992	686	595			
Germany	743	636	1048							
Greece	204	778	546							
Italy	160	82	47	15	13					
Norway	1000	1004	636	563	569	61				
Sweden	111	416	774	769	430					
USSR	15,000	12,130	12,330	14,330	14,770	22,000	27,550	27,550	27,550	27,550
Burma	519									
Japan	2547	1380	1778	1896	716					
Australia										
Indonesia	1323	1323	1323							
New Caledonia	11,458	10,378	8128	8945	4771	3063	3687	5381	3716	6945

* Table taken from *Materials Survey on Nickel* by Perry N. Moore, U.S. Bureau of Mines.

haust pipes of some internal combustion engines at moderate temperatures and under conditions of low stress.

Where corrosion is the chief problem, rather than resistance to heat, the stainless clad steels may be substituted for stainless. This product is applicable in many food processing and chemical industries requiring tanks and heavy equipment, but might not be useful where light sheets form the bulk of such articles.

The addition of nickel (up to 9 pct) to plain carbon steels adds greatly to strength, hardness, and toughness, as evidenced by the classic experiments in penetration of battleship armor by projectiles. Such steels contain 0.15 to 0.45 pct carbon and manganese in varying amounts.

For conservation purposes, nickel can be eliminated from cast armor. Metallurgists have had plenty of experience substituting the National Emergency steels for standard compositions. The so-called NE steels curtailed consumption of strategic metals in the alloy steels or those containing a maximum of 5.25 pct Ni and up to 1.50 pct Cr as chief alloying metals. For example, the NE 8000 series listed by AISI had the following ranges: 0.15 to 0.52 pct C; 0.70 to 1.00 pct Mn; 0.15 to 0.40 pct Mo; 0.40 to 0.60 pct Ni; and 0.40 to 0.60 pct Cr. This change from high to low alloy steels is predicated on making the best possible use of the available alloying elements in small quantities and on the utilization of alloy steel scrap to best conserve these elements. The program in World War II saved 40 pct of the primary nickel consumed for this use. During World War II segregation of alloy steel scrap became the most important source of Ni and Cr in the NE steels, reducing the amount of primary nickel consumed. Scrap generated by the production of war materials was increasing the nickel content so that the upper limit of Ni was set at 0.70 pct. The changeover to NE alloys was not made without overcoming consumer conservatism. Metallurgical complications were created by the variety of alloying elements turning up in scrap, which caused difficulty in melting single-alloy batches. Recent information on the use of intensifiers or addition agents indicates that boron can effectively replace nickel in the low alloy steels to the extent of 0.003 to 0.005 pct B for 1 pct Ni.

Second only to steels, the nonferrous alloys are a big consumer of nickel and in this era of jet engines, gas turbines, and rockets, this use will grow. In normal times the use of nickel for plating is usually right on the heels of nonferrous alloys consumptionwise. Mr. Wilson has called for 18,000 jet engines per month by 1953, which means some tall substituting for nickel will have to be worked out if this objective is to be reached. Some substitutions that have been worked out for the nonferrous group include that of stainless steel for Inconel in certain uses; and carbon steel clad with nickel, Monel, or Inconel for food and chemical processing equipment.

Starting June 1 all melting schedules must be approved by the Ferroalloys Branch of National Production Authority. Approximately 3000 rolled steel and foundry companies are reporting melting schedules about one month in advance of working

Table II. United States Imports of Nickel, by Country of Origin, 1940 to 1949*
(Nickel content in net tons estimated)

Year	Canada Amount	Canada Pct of Total Exports	U.K.	Norway	Netherlands	USSR	Union of South Africa	Cuba	Sweden	New Caledonia	Mexico	Other	Total
1940	83,478.4	67.0	227.3	53.8									83,759.5
1941	99,493.2	72.4	269.7							6,418.6			106,181.5
1942	106,521.3	76.8	236.7							7,496.9	20.1		114,275.0
1943	116,865.8	86.1	65.2							5,560.5			122,491.5
1944	107,520.0	80.5	793.8					2,956.9		7,022.3			118,293.0
1945	87,042.2	80.5	3,205.9					12,785.4		4,399.5			107,433.0
1946	81,392.8	73.1	440.7	5.0				10,660.6				0.9	92,500.0
1947	73,389.5	62.7	371.1	1,754.5		55.1		5,113.8	31.4			2.1	80,717.5
1948	92,332.7	70.0	833.4	3,112.6	9.2	57.4	28.4					26.3	96,400.0
1949	86,347.6	67.9	1,221.5	3,786.2	96.0							17.7	91,471.0
Total	934,383.5	73.9	7,665.3	8,712.1	107.2	112.5	28.4	31,516.7	31.4	30,897.8	20.1	47.0	1,013,522.0

* Table taken from *Materials Survey on Nickel* by Perry N. Moore, U.S. Bureau of Mines.

so that the NPA staff can check the composition of melts to maintain minimum consumption of strategic metals. The end-use of each melt is listed so that NPA can evaluate the specification. In the case of Munitions Board Specifications, NPA has the authority to recommend downgrading, which the Board can only countermand by proving necessity. Inspecting melting schedules enables NPA to make sure industry is not working in advance of schedule, which might cause shortages on orders requiring immediate delivery.

In addition to rigid control of the available nickel supply, the Government is closely scrutinizing world resources of the metal in the hope of finding a new producer. Nickel deposits of the world occur in association with basic intrusives. Three types of deposits are known; nickel-copper-sulphide deposits accounting for over 95 pct of the world's production, nickel silicate ores which are commercially important in New Caledonia, and nickeliferous iron ores like those from Nicaro, Cuba. The world's reserves of commercial sulphide ore are substantial—about 30 years known—but they are limited. The sulphide ores are being mined in significant amounts in Sudbury district, Canada; and by USSR in Petsamo, Finland. Sulphide deposits exist also in the Transvaal and Griqualand, South Africa; and Yakobi Island, Alaska; but these deposits have not been worked commercially.

Before the turn of the century the silicate ores were the chief source of nickel. Besides New Calidonia there are significant occurrences in Minas Gerais, Brazil; the Celebes, Indonesia; Loma de Hierro, Venezuela; and Riddle, Ore.

Table III. Consumption and Properties of Nickel by Commodities in 1949

Commodity	Consumption Tons	Pct of Total	Composition Pct	Properties	Uses
Ferrous:					
Stainless steel	11,908.6	17.4	18% Cr, 8% Ni	strength and corrosion resistance	automobile body & engine parts, food handling & chemical equipment, construction materials, kitchen appliances
Other steels	13,474.2	19.7	Up to 5.25% Ni; C, Mn, Mo, Ni, Cr	toughness, strength	armorplate, structural & engineering purposes, gears, transmissions, rock drills, basic in military equipment
Cast irons	3396.2	5.0	Up to 5% Ni	toughness, strength, uniformity, machinability, corrosion resistance	pump parts
Nonferrous:					
Malleable nickel	18,971.4	27.8	94% Ni	toughness, hardness, strength, corrosion	food processing & chem. equip., cyanide fusion pots, television, radio, coinage, boilers, furnaces
Duranickel			94% Ni, 4.3% Al	same as malleable nickel	coil springs, hand tools, flexible diaphragms, pump parts, extrusion dies for plastics
Permanickel			94% Ni, .33% Ti, .30% Mg		
Monel			67% Ni, 30% Cu, Mn, Fe	noted for corrosion resistance, strength, hardness	food, chem., petroleum, & pharmaceutical industries; laundry, hospital & kitchen equipment; marine service; household and architectural, ornamentation
Cupro-nickel			70% Cu, 30% Ni	corrosion resistance	heat exchanger tubes, steam turbine blades, coinage
German-silver			10-30%, 5-30% Zn, 1-10% Pb, balance Cu	beauty, workability, corrosion resistance	ornamentation, flatware, jewelry, food equipment, marine fittings, musical & dental instruments
Inconel			80% Ni, 13% Cr 7% Fe	resistance to corrosion at high temperatures. Will withstand repeated h.ating and working without embrittlement	petroleum refining, dairy, wine, fruit juice, caustic alkali, fatty acid, dyestuff, edible oil industries
High temperature and electrical resistance alloys	4053.9	5.9	See Table V	strength and corrosion resistance at high temperatures	furnace construction, carburizing boxes, high speed tools, gas turbine & jet engine high-temp. parts
			35-85% Ni, Cr, Fe	electrical resistance	wire in stove, heaters, household and industrial uses
			15-30% Ni, Al, Co	good magnetic properties	alnico magnets
			25% Ni, Fe	nonmagnetic	transformers, motors
			45-80% Ni, Fe	highly magnetic	generator parts, electrical sheathing for submarine cable, radio, transformers, telephone & telegraph relay parts
			36% Ni, Fe	low thermal expansion	measuring tapes, precision instruments, matches, auto engine pistons, wire for wire glass
Electroplating:					
Anodes	13,810.4	20.2		resistance to atmospheric corrosion	decorative trim & industrial protection
Solutions	724.3	1.1			
Catalysts	497.1	0.7	Raney nickel prepared by leaching aluminum out of a granular Ni-Alloy	catalyzes the hydrogenation of unsaturated hydrocarbons and other organic compounds to saturated ones	catalyst for artificial aging of liquors, drying oils, bleaching, waste water, purification, dehydrogenization and polymerization of organic compounds, the removal of organic sulphur compounds from coal, gas
Ceramics	149.6	0.2			
Other	1340.4	2.0			
Total	68,326.1				

The largest potential reserves are those of nickeliferous iron deposits, which contain about 1 pct Ni. These are highly disseminated in iron-rich material and are costly to recover. These ores have been exploited in Cuba by a United States Government sponsored project during World War II, but other unexploited deposits are in the Celebes, Greece, Japan, Philippines, and Russia. Tables IV and V show the reserves of world nickel resources.

At Sudbury, a basic intrusive called norite occurs in the form of a basket-shaped body 36 miles long by 26 miles wide. The nickel deposits occur along the margins of this eruptive and as offset deposits associated with small necks of basic intrusion away from the margins. The nickel is in the form of pentlandite (Fe, Ni) S associated with pyrrhotite.

Copper occurs in the form of chalcopyrite with a subordinate amount of platinoids. The tenor of the larger deposits ranges from 0.8 to 2 pct each of nickel and copper in varying proportions. Reserves of the two major companies operating here are sufficient for about 20 or 30 years at present rate of production, but it is doubtful if further discoveries would increase the annual output of the district.

Inco is operating the Levack on the north margin, and the Creighton, Murray, and Garson mines on the south rim of the basin. The Frood-Stobie, the biggest of them all, is an offset orebody occupying a norite dike south of the main norite intrusion. To meet the demands of World War II, the Frood-Stobie open pits were brought in at an accelerated rate and production quickly boosted from 6000 to 20,000 tons per day, 40 pct of total ore produced by the company. As a consequence of the heavy war drain on the pits it is estimated that they will be exhausted by 1953. The current inflated demand for nickel has come when the open-pit ores are nearly exhausted and no new orebodies capable of being brought into quick production by open-pit methods are available. However, underground ores are being developed to replace the open-pit tonnage, and by 1953 the transition will be completed without interrupting current production during the transition period. Indeed 13 million tons will then be produced from the underground mines, a greater tonnage than ever came from the combined underground mines and open-pit operations. It will be necessary to mine lower grade ores and to accomplish this, cheaper mining methods had to be adopted. Blasthole mining with long drill holes and block caving are being studied; the former method for the Stobie and Murray mines and the latter at the Creighton.

Converters are used for both nickel and copper smelting at Copper Cliff, Ont., by Inco.

An increase in nickel output of about 5 pct, or 6000 tons annually has been reached. In 1950 the company delivered 256,410,543 lb of nickel, as compared to 209,292,257 lb in 1949. This was a record for any previous peacetime year. The record deliveries for all time were made in 1943 and amounted to 265,389,323 lb. Inco's reserves have remained at 250 million tons for several years in spite of mining at the rate of 12 million tons annually. To retain these reserves, the company is doing extensive exploration at Sudbury and elsewhere. Exploration is being pushed at Shebandowan Lake, Ont., about 60 miles west of Port Arthur where about 1 million tons averaging less than 2 pct Ni have been found. The company has holdings at Loma de Hierro, Venezuela, which have favorable mining and transportation conditions although the deposit being a silicate, presents metallurgical difficulties. A tract 10 to 12 miles long and ½ mile wide underlain by serpentine is reported to have 30 million tons of 1.75 pct Ni. No work is in progress at this location.

Falconbridge is now producing from two properties, in the Sudbury area, the Falconbridge and the McKim mines on the south rim of the norite mass; and is making plans to produce from the Hardy mine on the north rim adjoining to the Levack mine of International Nickel. The McKim only recently has become a producer, whereas the Falconbridge has been productive for about 20 years. Recent diamond drilling shows ore to persist to 5700 ft, over twice the depth of present mining. The latter mine is being developed at lower levels. For some years refining capacity, which is in Norway, has

Table IV. Estimated Nickel Reserves of Sulphide Ores of the World as of Jan. 1950, in net tons[4]

Place	Equipped		Unequipped	
	Ore	Nickel Content	Ore	Nickel Content
Canada				
Falconbridge	14,791,000	254,500		
Inco	251,805,000			
Lynn Lake area			10,365,000	149,600
Union of South Africa				
Rustenburg				
Vlackfontein	[1]	[1]	150,000	4500
Insizwa			[1]	[1]
United States				
Alaska			22,000,000	70,000
U.S.			14,000,000	70,000
USSR				
Petsamo	4,000,000[2]	64,000[3]	[1]	[1]
Kola & Novilsk region	[1]	[1]	[1]	[1]

[1] Data not available.
[2] 7,630,000 tons Ni-Cu, ratio of Ni-Cu not available.
[3] Data prior to operation by USSR, in round numbers.
[4] Materials Survey-Minerals *Nickel Reserves of the World* by H. R. Cornwall & W. S. Burbank, USGS.

lagged matte production in Canada but by October 1951 enough additional capacity will be in service to increase output from the 1950 rate of about 12,000 tons to 15,000 tons. Concentrating and smelting facilities are being added to coincide with expanded refinery capacity. However, the company is embarking on a further expansion program, which will bring production up to 20,000 tons per year in three years after the program commences—say 1954. Additional mill and smelter capacity will be needed and the refinery, with slight additions will be able to handle 17,500 tons. The remaining matte will go elsewhere for refining.

Refining has been done in Norway because of the advantageous electric power rates, but strategic considerations are causing pressure for a refinery in Canada. Thayer Lindsley, president of Falconbridge, thinks that if this becomes a necessity, the company should not bear the full expense. Reserves for the Falconbridge and McKim mines are 9,369,000 tons of 1.60 pct Ni and 0.86 pct copper, and indicated reserves of close to 6 million tons of 1.86 pct Ni and 1.03 Cu for the company's Sudbury holdings. Falconbridge holds additional parcels of land in the Sudbury district and drilling shows favorable mining areas; but an increase in price would be helpful to further expansion. There are a number of nonproducing properties in the area owned by these two companies and by other companies, including the Nickel Offset, Junior Frood, East Rim, Sudbury Shepherd, and the Crean Hill, some of which are under development.

A major discovery of sulphide ores made in recent years is the Lynn Lake deposits of northern Manitoba, about 200 miles north of Flin Flon by Sherritt Gordon Mines, Ltd. Nickel-copper ore reserves of about 14 million tons were delimited but more would have been found by continued exploration. An estimated $28 million will be spent to bring the deposit into production by 1954 at the rate of 2000 tons per day from the two highest grade deposits. The ore averages 1.44 pct Ni and 0.68 pct Cu. Production plans call for an objective of 8500 tons of Ni, 4500 tons of Cu, 150,000 lb of cobalt, and 70,000 tons of ammonium sulphate fertilizer per year. The concentrator, mine plant, and housing will be taken from Sherridon to the new project at Lynn Lake. Copper concentrates will be shipped to the smelter at Flin Flon, but a nickel refinery will be constructed in Alberta and will be completed by the latter half of 1953. A 150-mile railroad is required for full scale mining and the Canadian National Railroad already has commenced the survey for it. A substantial portion of the nickel, copper, and cobalt is under a 5-year contract with the U. S. stockpiling agency with deliveries to start in 1954.

Other nickel deposits of unknown reserves occur in Ontario, the Bird River district of Southern Manitoba, and British Columbia. Most promising is a nickeliferous deposit near Choate, B. C., where diamond drills have disclosed 1 million tons that contain 1.3 pct Ni and 0.4 pct Cu.

The only known sulphide deposits in the world comparable in size to a small Sudbury deposit are in northern Finland at Petsamo. International Nickel did all the pioneer mine development and equipped the property with smelter and refinery capable of producing 15 million lb of nickel annually. How-

Table V. Estimated Nickel Reserves of Silicate and Nickeliferous Iron Ores of the World as of Jan. 1950, in net tons[c]

Place	Equipped		Unequipped	
	Ore	Ni	Ore	Ni
Silicate & nickeliferous iron ores				
Brazil (silicate)				
Tocantins, Goias			10-18,000,000	200-360,000
Livramento & Ipanema Minas Gerais			4,000,000	40,000
Cuba				
Levisa, Oriente (Fe-Ni)	27,700,000	401,600		
Mayari, Moa, Oriente (Fe-Ni)			3,000,000,000	24,000,000
San Felipe, Camagey (Fe-Ni)				
Greece				
Atlante-Larymna (silicate & Fe-Ni)			10,000,000	50-100,000
Idonesia				
Bornea (Fe-Ni)			200-500,000,000	1-3,000,000
Celebes				
Pomalea-Kolaka (silicate)			2,000,000	60,000
Lakes Region (silicate)			1,000,000	20,000
Lakes Region (Fe-Ni)			370-500,000,000	3-4,500,000
Japan (Fe-Ni)			63,000,000	315,000
Madagascar				
Nickelville (silicate)			900,000	3,280[a]-45,000
Nickeliferous iron ores			[a]	[a]
New Caledonia (silicate)	[d]	[d]		
Philippine Islands				
Surigao (Fe-Ni)			550,000,000	4,400,000
U. S. (silicate & Fe-Ni)			40-45,000,000	400,000
USSR (silicate & Fe-Ni)	[a]	[a]	[a]	[a]
Venezuela (silicate)			30-50,000,000[b]	450-875,000[b]

[1] Including "serpentine" ores.
[2] Estimated recoverable nickel in garnierite ore only.
[3] Data not available.
[4] Sufficient to maintain production 12,000 metric tons of Ni per year for 80 years.
[5] Data from *Northern Mine*.
[6] Materials Survey-Minerals *Nickel Reserves of the World* by H. R. Cornwall and W. S. Burbank, USGS.

ever, the Russians annexed the area in 1944 and agreed to compensate Inco to the extent of $20 million. The reserves of this district are reported at 64,000 tons of nickel but are probably much greater. Other deposits of importance are at Nivala in southwestern Finland, Norilsk area of Northwest Siberia, and at Monechegorsk on the Kola peninsula. There are also silicate and nickeliferous ores in the central and southern Urals at Ujoli, Revda, Orsk and other places, which average 2 pct Ni. Soviet nickel is controlled by a state monopoly, Glavnickelkobalt, which can probably produce nickel from ores not considered economical by western standards. Soviet nickel production should not exceed 19,000 tons annually.

In 1949, La Societe le Nickel, a French controlled company, produced ore containing 3700 tons of nickel from the nickel silicate deposits of New Caledonia. In recent years, New Caledonia ores have dropped to the position of producing about 2½ pct of the world's nickel. The decline in importance has been the result of the exhaustion of high grade ores and the increased costs of production by primitive methods. In addition, coal for the smelter must be imported from Australia. La Societe le Nickel expects to receive $965,000 from ECA for purchase of heavy mining and conveying equipment, which should bring production to 11,000 tons. Part of this would come to the U. S. in payment of the loan. Reserves are estimated to be sufficient to maintain a production rate of 13,000 tons annually of nickel for 80 years.

The existence of low grade nickel deposits in large quantities at the eastern end of Cuba has been known for many years, but prior to World War II no economic process had been developed for extracting nickel from such ores. These deposits are nickeliferous iron ores, carrying minor amounts of chromium and cobalt in addition to nickel.

However, with war impetus over 32,500 tons of nickel were extracted from these deposits at the peak rate of over 12,500 tons annually. Before mining began, reserves were estimated at 24 million tons of 1.45 pct Ni and between 35 and 40 pct Fe. However, 3 million tons were mined from 1942 to early 1947 when the operation was shut down. Practically the whole of Oriente province is underlain by the laterite formation containing nickel in varying amounts. One estimate is 3 billion tons of nickeliferous iron ore reserves averaging 0.8 pct nickel.

The Freeport Sulphur Co., having rights to some of the better grade deposits in 1942 when OPM put nickel under allocation order, formed the Nicaro Nickel Co. A plant was constructed after clearing the jungle on the coast using $32 million of RFC money. It was necessary to bring in labor from the populated areas and construct living accommodations.

Selective mining of ore by open pit methods yielded a plant feed of 1.45 pct Ni content. At the plant, the ore was crushed and dried and then ground to a fine mesh in hammer and ball mills. The fine, dry ore so obtained was reduced by producer gas in 16-hearth, oil-fired Herreshoff furnaces, the product being leached in an ammonia solution from which the nickel is precipitated in the form of nickel carbonate. This was calcined to nickel oxide and was at first shipped to a refinery in Wilmington, Del., where it was briquetted with reducing and fluxing agents and converted to nickel metal in electric furnaces. By great effort the company was able to get consumer acceptance of the oxide particularly for electric furnace steels. The speed with which this operation was brought into production was a tremendous feat and Nicaro nickel supplied relatively small but important amounts of nickel for the war effort.

The orebodies are still owned by Freeport and the plant is again being rushed into production, but this time by the Mining Equipment Corp.-Billiton interests, on behalf of the General Service Administration. It is hoped to bring the plant to 16,000 tons of nickel annual production rate. At the outset, the same metallurgical treatment will be used but metallurgical studies are in progress for the recovery of cobalt from the pregnant liquor of the ammonium leaching system, probably by fractional crystallization. The mine will produce 5000 wet tons per day, which is dryed to produce 3600 tons of plant feed. The first production is expected by 1952.

Probably the largest basic intrusion in the world, the Bushveld Complex, is located in the Union of South Africa at the north end of the Transvaal. Nickel occurs in small amounts at the Merensky reef, from which it is being recovered as a by-product of platinum mining by the Rustenburg Platinum Mines, Ltd., and the Vlackfontein deposits about 38 miles northwest of Rustenburg from which there is no production. Both orebodies are sulphide and the former produced 618 metric tons of contained nickel in matte. Also at Insizwa, Griqualand, in the Union of South Africa, there is a basic intrusion with considerable pyrrhotite. Several adits have been run in this deposit but the nickel content was too low to justify development.

In a 14-square mile area in the state of Goias, Brazil, there are about 50 near-surface deposits of nickel silicate, which aggregate 22 million tons of 1 to 4.5 pct nickel. The area is about 1000 miles from Santos, the nearest port, and neither labor, fuel, nor water power is available. Some nickel is mined by a Brazilian firm and it is reported that a Canadian company has a concession.

There are large reserves of silicate and nickeliferous iron ores in the Celebes, Netherlands East Indies, from which some small production has come. About 10 million tons of 1 to 3 pct nickel silicate ores are known in the Pomalea district. The lakes region has about ½ a billion tons of nickeliferous iron ore running 49 pct Fe and 0.9 pct Ni.

A small amount of nickel comes from Norway, Germany, Finland, Greece, Burma, India, and Japan, in addition to the producing bodies and occurrence of nickel named.

At present there are no economical nickel deposits in the United States. Somewhat less than 1000 tons has been produced annually, varying in amount from year to year, as a by-product from copper refining and also from talc production. The Riddle nickel silicate deposit in Douglas county, Ore., has been drilled by the USGS and was under consideration by the Freeport Sulphur Co. during the last war. The M. A. Hanna Co. is now exploring the property and is conducting a metallurgical investigation on a laboratory scale to determine the possibility of an eventual production of several million lb of nickel per year from the property. The deposit is favorably situated for low cost mining being near surface on the slopes of Nickel Mountain. Reserves have been roughly estimated from 40 million tons containing 1 to 2 pct Ni.

Nickel Processing Facilities of the World*

Processing Plant	Location	Capacity and Comments
Inco	Copper Cliff, Ont.	Produce salts, chem. & matte. Smelter
	Port Colborne, Ont.	200 million lb capacity electrolytic nickel per yr
	Coniston, Ont.	Smelter only
	Clydach, Wales	Refinery 50 million lb cap. Salts, chem. and Ni metal
	Huntington, W. Va.	Refinery, operates in conjunction with fabricating plant at same location. Processes New Caledonia matte
Falconbridge	Sudbury, Ont.	Smelter 23,000 tons matte capacity, 1950
	Kristiansand, Norway	Refinery—capacity being increased. Prewar 11,000 tons Ni
USSR	Norilsk	2,000 tons per yr Ni
	Orsk, Urals	Smelter & refinery, 1939 reported at 10,000 tons pr yr Ni
	Ujaloi	Refinery. Capacity 1939—2500 tons per yr Ni
	Rielj	36,000 tons Portable Knock-down type smelter
	Petsamo, Finland	Smelter. 600 tons per day capacity when operated by Germans
Nord Deutsche Affinerie	Hamburg, Germany	66,000 tons per yr capacity smelter
Finnish Govt.	Pori, Finland	Smelters. 500 to 600 tons per yr
	Frankenstein, Germany	An old smelter which processed the ore from Lokris, Greece
Krupp-Renn	Magdeburg, Germany	Produces Ni-Fe in pellet form in a rotary tube furnace
I. G. Farben	Oppau, Germany	Ni powder from matte by Mond process where nickel is separated from matte in form of carbonyl ($Ni(CO)_4$). Produced 17,000 tons per yr of Ni powder during World War II
Societe Le Nickel	Noumea	Smelter about 9000 tons per yr matte cap.
	New Caledonia	Plans under way to increase capacity to 15,000 tons of matte containing 11,000 tons Ni by four KVA furnaces.
	Le Havre, France	Prewar refinery-treated matte from New Caledonia
Societe Caledonia	Duffel, Belgium	Prewar refinery-treating matte from New Caledonia
Burma Corp.	Northern Shan States Burma	Smelter producing speiss containing 100 tons Ni per yr which was sent to German refinery
	Japan	Prewar smelter & refinery which treated New Caledonia ore plus low grade local deposits. Estimated 700 tons per yr Ni capacity

* Table taken from *Materials Survey on Nickel* by Perry N. Moore, U.S. Bureau of Mines.

Other occurrences of nickel are reported at Stillwater county, Mont., where about 1 million tons of a nickel-copper sulphide ore are favorably situated for mining; and also near Webster, Jackson county, N. C., there are discontinuous veinlets of nickel silicate bearing material amounting to 1 million tons of 1 pct or less nickel content. There is by-product nickel with the complex lead-zinc-copper-cobalt ores of Fredericktown, Mo., worked by the St. Louis Smelting & Refining Co. The cobalt-nickel concentrates are stockpiled but treatment of these has not begun. Only small amounts would be recovered in comparison to national consumption.

There are also nickel deposits in Skagit county, Wash., and in Alaska. An extremely low grade sulphide orebody associated with a basin shaped norite intrusive has been drilled by the Bureau of Mines and the USGS on Ya'kobi Island, Alaska, about 139 miles west of Juneau. Estimates are 10 million tons of 0.36 pct Ni and 0.27 pct Cu.

Development of silicate ores or the vast reserves of nickeliferous deposits in different parts of the world awaits depletion of Sudbury ores or an increased price for the metal. Previous experience with Nicaro proved this. The nickel oxide of Nicaro was produced at a small profit when only direct operating expenses were charged against production costs. Unless there are metallurgical improvements these deposits will not be competitive.

Inco is making the arduous changeover from accessible open-pit ore to underground mining and has added 5 pct capacity. Already $100 million have been spent in the past few years in changeover and further additions to capacity would require more millions, which are not warranted from a sound business viewpoint. With the dollar worth 48c of preWorld War II value, such expenditures would be burdensome should the defense effort collapse. For comparative purposes, Falconbridge built 10 million lb of nickel capacity for an expenditure of $3 million in the late 30's. A similar program today would cost three or four times that amount. The question of additional refinery capacity this side of the Atlantic has been examined thoroughly in Washington. The refinery is not likely as the United States will not construct one in Canada, and that nation frowns on the export of nickel matte to the U. S. for the excellent reason that nickel metal brings more dollars than matte. The U. S. reasoning is more obscure because this country is already spending vast sums through ECA abroad. If Mond refinery in Wales and the Norwegian refinery were destroyed or lost to an enemy, Inco would be stretched to the limit to handle the refining of this matte in Canada.

Sherritt-Gordon is going into the nickel business with both feet and without benefit of platinum values. Those close to the company say that their process for nickel recovery which is to be used will give them low cost operation and a competitive product.

The world has more sources of nickel than probably will ever be exploited. During the interim years of war, the International Nickel Co. and the few small producers are able to meet the world demand. During emergency periods, like the present there is a tremendous shortage of nickel but there are few sources that can be developed to meet this demand even with Government subsidization because they are vulnerable to wartime shipping hazards. Private development of some of the undeveloped sources is subject to meeting the competition of Inco once the emergency is relieved. Finally, subsidization of marginal deposits has not been done on a scale that would furnish relief under present conditions because of the large capital expenditure needed and the fact that the operation would not be economical in normal times. The pressure on nickel is not likely to abate until the defense buildup has been achieved.

International Research Project Studies

Low Shaft Blast Furnace

THE International Cooperative Research Project on the low-shaft blast furnace is expected to provide metallurgical information on the departure from thermodynamic equilibrium in a rapidly moving burden; redistribution of the various reaction zones in a greater thermal gradient than has been observed heretofore; the effect of various controlled variables on the proportion of direct reduction; the nature and kinetics of desulphurization by silicon disulphide formation; and the nature of intermediate slag-forming reactions.

Because the low-shaft furnace permits the use of high oxygen concentrations, high hearth temperatures can be obtained. Blast furnace operators therefore will be able to learn from the project: 1—if obtainable temperatures and rates of heat exchange are sufficient for the large volumes of slag produced in the reduction of low grade or acid ores; 2—if substantial improvements can be obtained in such a furnace when it is used for the preparation of ferroalloys; 3—if mechanically weaker or leaner fuels than coke can be used successfully in iron making; 4—if high sulphur cokes and silicious ores can be used to produce normal iron under conditions favoring the silicon disulphide reaction; 5—the oxygen concentration of the blast leading to the minimum coke rate; 6—the degree of stability and the degree of flexibility obtainable with oxygen practice; and 7—the rate of production obtainable in a low-shaft furnace.

Data on the behavior of briquetted fuels, ores, or mixtures of ores and fuels will be of considerable interest to the fuel industry. Information on the behavior of the furnace refractories under extreme conditions met in the low-shaft furnace will be important to the refractories industry. The possibility of producing acid slags suitable for cement manufacture also will be investigated.

Of the two low-shaft blast furnaces to be constructed, the one at Liege, Belgium, will have a rectangular cross section, 4x8 ft, with the corners rounded. It will have no inwall batter, and will have at least six adjustable tuyeres distributed along the long sides. The other furnace at Oberhausen, Germany, will be cylindrical and about 6½ ft diam. The height of the furnace will be about 16½ ft, although it was thought that better elimination of sulphur as silicon disulphide would be obtained in a shorter furnace working with a high top-gas temperature. The difficulty in this connection is that the side-hopper top construction contemplated for the furnace does not permit any stockline variation. It was decided to place the desulphurization problems late in the program when further information will be available upon the shaft height question. The furnaces were designed by the firm of Glockner-Humboldt Deutz together with engineers of the firm Ougree-Marihaye and the Centre National de Recherches Metallurgiques.

Among the first trials on the program are those concerned with the preparation of the burden. Since it was decided to experiment with fines and low grade ores and fuels, it will be necessary to prepare the burden into briquettes or other forms of agglomerate. The experiences of the French zinc industry, of the Glockner firm, and of Canadian and American blast furnace operators were reviewed. It was concluded that a considerable part of the research program should be devoted to the development of methods of burden preparation. The results obtained will be applicable also to the preparation of normal blast furnace burdens. The materials to be tried first on the program are Minette ores and either Belgian lean coal or French semi-coke. Wind containing oxygen concentrations up to about 70 pct will be used to determine the optimum enrichment. Top pressure operation is contemplated in a later phase of the project.

The project is being undertaken jointly by Governmental and industrial organizations in several European countries. The contracting parties are: Oesterreichische Alpine Montan Gesellschaft, Vienna, Austria; Institut pour l'Encouragement de la Recherche Scientifique dans l'Industrie et l'Agriculture, Brussels, Belgium; Institut de Recherches de la Siderurgie, St. Germain, France; Ministry of Coordination, Athens, Greece; Associazione Industrie Siderurgiche Italiano, Milan, Italy; Groupement des Industries Siderurgiques Luxembourgeoises, Luxembourg; Nederlandse Centrale Organisatie voor Toegepast Natuurwetenschappelyk Ondersoek, The Hague, Holland. Interested German parties have not yet signed up, but the firm of Oberhausen is proceeding with its share of the project. The British Iron and Steel Institute has contributed a small sum, but will have no patent rights. The contracting parties to which the project is of greatest interest are contributing sums of the order of $150,000. Other participants are contributing from $40,000 to $60,000. Austria is represented by a single firm, which is contributing $6000.

Grain Structure of Aluminum-Killed, Low Carbon Steel Sheets

by R. L. Solter and C. W. Beattie

ALUMINUM-KILLED, low carbon steel sheets are used extensively for severe deep drawing and other difficult forming operations. They usually, but not always, have a characteristic grain structure in which the grains are elongated both in the lengthwise and in the transverse direction. As described by Burns and McCabe,[1] a typical grain in the plane of the sheet has its two axes in that plane from 1½ to 4 times as long as the axis normal to the plane of the sheet. Rickett, Kalin, and MacKenzie[2] have also reported on the recrystallization behavior of such steel. The contrast in grain structures of fully processed sheets of aluminum-killed and rimmed steel is illustrated by Figs. 1 and 2. The elongated grain structure of the aluminum-killed sheet is not developed on all heats or lots of this metal, and studies of the factors controlling and influencing its formation are reported in this paper.

Jeffries and Archer[3] state that unstrained grains are normally equiaxed, but exceptions are common. For example, if a metal containing a material mechanically obstructing grain growth is subjected to considerable working followed by thorough annealing, it may exhibit grains consistently elongated in the direction of working. Our experiments demonstrate that aluminum-killed, low carbon steel is such a metal, and that the substance mechanically obstructing grain growth is aluminum nitride. The effectiveness of aluminum nitride in inhibiting grain growth has been found to be influenced by the degree of cold reduction, the rate of heating in annealing, the thermal history of the sample before cold reduction, and the residual aluminum content. A correlation between grain shape and austenitic grain coarsening temperature also was indicated and additional experiments demonstrated that aluminum nitride is also the principal cause for the fine grain characteristic of aluminum-killed steels.

Manufacture

In conventional practice, aluminum-killed sheet steel is manufactured from a low carbon steel containing approximately 0.02 to 0.07 pct residual (HCl soluble) Al. With the exception of certain samples containing greater or lesser amounts of aluminum, the steels used in these investigations were within the following composition range: C, 0.03 to 0.06 pct; Mn, 0.28 to 0.38; S, 0.017 to 0.032; Al, 0.03 to 0.06; P, <0.01; and Si, <0.01.

Properly heated ingots are rolled to slabs about 4 in. thick. After surface conditioning, the slabs are reheated to about 2300°F and hot rolled continuously to strip about 1/10 in. thick. The strip rolling is completed at a temperature of 1550°F or higher, and the strip is coiled, usually at a temperature near the lower critical transformation. After cooling, the strip is pickled to remove oxide, cold reduced 40 to 70 pct to final thickness, then annealed to 1250° to 1350°F in 20 to 80 ton charges, the size of which results in slow heating and cooling rates.

R. L. SOLTER is Supervising Research Engineer and C. W. BEATTIE is Senior Research Engineer, Research Division, Armco Steel Corp., Middletown, Ohio.

Discussion on this paper, TP 3119E, may be sent, 2 copies, to AIME by Dec. 1, 1951. Manuscript, April 18, 1951. Detroit Meeting, October 1951.

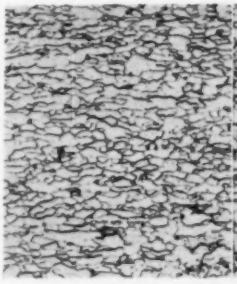

Fig. 1 — Grain structure of aluminum-killed drawing sheet. X100.

Fig. 2 — Grain structure of rimmed steel drawing sheet. X100.

Effect of Cold Reduction

According to Sachs and Van Horn,[4] the deformations of the individual grains in rolling are similar to those of the total volume. Thus individual grains would elongate in rolling according to the amount of cold reduction imposed. This is true theoretically, but as cold reduction increases the individual grains tend to fragment, and measured grain elongations become less than theoretical. The amount of grain elongation may be described by a numerical rating based on grain counts made by the intercept method. Specimens are polished normal to the plane of the sheet, with the polished surface extending parallel to the rolling direction.

After etching, grain intercepts are counted along a 50 mm line on a micrograph of suitable magnification. In random locations parallel to the plane of the sample 20 counts are made and 20 are made in the thickness direction of the sample. The average count in the thickness direction divided by the average count parallel to the plane of the sample gives a numerical rating of the grain shape called grain elongation. For example, a grain elongation of 2.00 means that the average grain is twice as long as it is thick. The average of both counts may be converted to grains per sq mm by a nomograph relating intercept counts and grain count. By the same procedure the grain elongation in the plane of the sheet but transverse to the rolling direction may be determined, using transverse metallographic samples.

A comparison of theoretical and measured grain elongation was obtained on an aluminum-killed

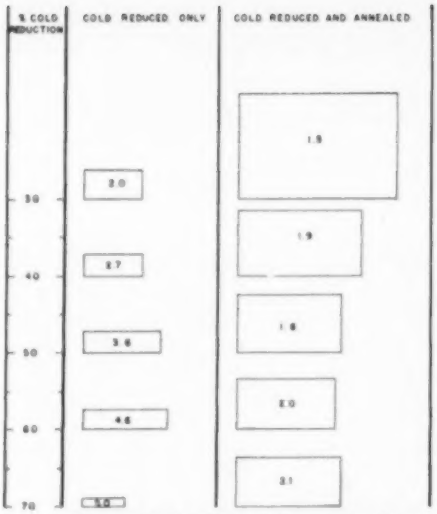

Fig. 3 — Relative grain dimensions and shape in the plane of a material cold reduced only and of a duplicate material cold reduced and annealed at 1340°F. Samples were polished parallel to the rolling direction. Numbers within rectangles are grain elongation rating.

steel that had been hot rolled and then cold reduced various amounts. This steel contained 0.046 pct C, 0.33 pct Mn, 0.026 pct S, and 0.034 pct residual Al. Cold-reduced specimens were annealed at 1340°F and grain elongations were measured on the annealed materials. This comparison is given in Table I. Measurements were impossible on specimens cold reduced 80 and 90 pct because of the extreme distortion, but it seems probable that grain elongations were considerably less than the theoretical value.

Values in Table I show that, as cold reduction increased, fragmentation of individual grains occurred and the measured elongation was considerably less than was calculated. The amount of grain elongation measured after annealing was less than after cold reduction, consequently the elongation imposed by cold work was only partially retained after annealing, indicating that any mechanical obstruction to grain growth was not completely effective. Relative grain sizes and shapes of an individual material in the cold-reduced and the cold-reduced and annealed condition are shown by appropriately dimensioned rectangles in Fig. 3. The larger grain size of annealed specimens of this material is further evidence that mechanical obstruction did not completely inhibit grain growth.

This illustration is an individual case representative of one material. Measurements of 14 other samples gave a diversity of results. No two reacted exactly alike to the influence of cold reduction. Such inconsistency indicated that factors other than the amount of cold reduction influenced grain size and shape. However, the average values of grain elongation and grain count show that a definite relationship exists with variations in cold reduction, as illustrated in Fig. 4. Both grain elongation and grain count increased with increasing cold reduction with a noticeable change in rate of increase above 60 pct. Grain elongation and grain size also appear to be related when compared at a given cold reduction. A group of 124 materials was cold reduced 60 pct and annealed at 1340°F. Grain counts and grain elongations were determined. These data were listed in order of decreasing grain elongations and grouped in ten approximately equal groups. The average grain elongation and grain count was determined for each group and plotted in Fig. 5. This curve demonstrates that for a given amount of cold reduction a sample with a larger grain count was likely to have less grain elongation than one with a smaller grain count. Thus, the final grain structure becomes finer and more elongated as cold reduction increases, but the amount of grain elongation developed by a given amount of cold reduction is more if the grain size is larger.

Table I. Comparison of Grain Elongations Calculated for Cold-Reduced Specimens with Grain Elongations Measured on Cold-Reduced Only and Cold-Reduced and Annealed Specimens

Cold Reduction, Pct	Calculated	Measured on Cold-Reduced Specimens	Measured on Annealed Specimens
30	2.0	2.0	1.5
40	2.6	2.7	1.9
50	4.0	3.6	1.8
60	6.2	4.6	2.0
70	11.2	5.0	2.1
80	25.1		2.6
90	100.0		3.0

Effect of Variations in Heating to the Annealing Temperature

Three hot-rolled strip materials were secured, each from a different heat, as given in Table II. These materials were cold reduced 60 pct and annealed with two variations in heating rate. Variation 1 consisted of heating the samples to 1340°F in ½ hr. Variation 2 consisted of heating the samples to 1340°F in 22 hr using a uniform rate of 25°F per hr above 800°F. In both instances samples were held at temperature 4 hr and cooled 25°F per hr to about 500°F before removing from the furnace. Grain elongation and grain counts resulting from these treatments are shown in Table III. Grain structures of Material 2 are shown in Fig. 6. These data show that fast heating resulted in a finer grain with less elongation than slow heating.

Table II. Composition of Materials, Pct

Element	Material 1	Material 2	Material 3
C	0.041	0.040	0.039
Mn	0.33	0.26	0.32
S	0.019	0.020	0.020
Residual Al	0.043	0.038	0.042

The same three materials were given a 2 hr heat treatment at temperatures of 300° to 1100°F prior to annealing with heating Variation 1. Heating for 2 hr at 700° to 1100°F caused the final grain structure to be coarser and more elongated than would normally have been expected from heating Variation 1. This is illustrated in Fig. 7.

Determination of Aluminum Nitride

These and other studies led to the belief that the observed recrystallization behavior of aluminum-killed steel is influenced principally by the precipitation of a constituent during the heating portion of the annealing cycle. It was long suspected that this constituent was aluminum nitride. H. F. Beeghly[5] recently reported a sound and reproducible method for determining this compound, and demonstrated that the amount present varied with the heat treatment received by the sample before analysis. Hot-rolled, aluminum-killed steel samples were shown to contain different amounts of nitrogen as alu-

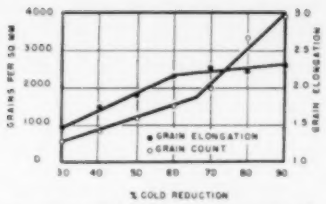

Fig. 4—Relationship of grain count and grain elongation of samples cold reduced and annealed at 1340°F.

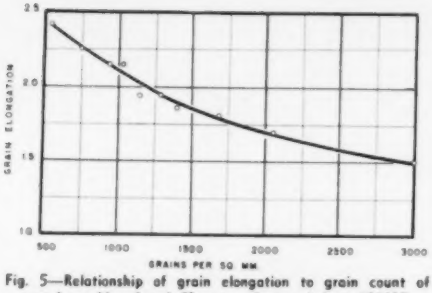

Fig. 5—Relationship of grain elongation to grain count of samples cold reduced 60 pct and annealed at 1340°F.

minum nitride if reheated 1 hr at various temperatures. His data are plotted in Fig. 8. As hot-rolled, the amount of nitrogen combined as aluminum nitride is low, but as the annealing temperature increased, the amount increased to a maximum in a temperature range from about 1300° to 1800°F. At temperatures above 1800°F, the amount decreased until at about 2350°F no more was present than in the original hot-rolled bar. This indicates that aluminum nitride is held in supersaturated solution in hot-rolled samples. If the samples are reheated the aluminum nitride precipitates up to a maximum amount at 1300° to 1800°F and at higher temperatures it redissolves.

This precipitation and re-solution of aluminum nitride is believed to be responsible for the behavior of aluminum-killed steels both with respect to the grain shape of the cold-reduced and annealed sheets and to the austenitic grain refining characteristic of such steels, and has been demonstrated by the following experimental procedures.

Effect of Thermal History before Cold Reduction

In considering the effect of thermal history on grain shape it should be understood that the grain shape referred to in the following discussion is that of the final cold-reduced and annealed product, even though the heat treatments described may have been performed before cold reduction and final annealing. Twelve samples of hot-rolled strip with the normal chemistry range were secured and reheated; one group to 1800°F and air cooled, a duplicate group to 1800°F and furnace cooled, a third group to 2100°F and air cooled, and a fourth group to 2100°F and furnace cooled. Following heat treatment the samples were cold reduced 60 pct and annealed at 1340°F. After annealing the structures were as shown in Fig. 9. All had equiaxed grain structures except those heated to 2100°F and air cooled before cold reduction. This group had the elongated grain shape as would be expected for this type of steel. The grain structures of samples heated to 2100°F were coarse as compared to those heated to 1800°F, showing that the coarsening temperature was reached or exceeded by the 2100°F treatment.

Heating to 2100°F and air cooling is believed to have caused a re-solution of aluminum nitride and a retention of the compound in supersaturated solid solution. In the final anneal after cold reduction, the aluminum nitride precipitated in the normal manner and resulted in an elongated grain structure. In the other heat treatments, precipitation of aluminum nitride occurred in the strip before cold reduction. This behavior was demonstrated in a slightly different manner by heat treatments performed on hot-rolled strip. Five different hot-rolled strip materials were used. The nitrogen content as aluminum nitride and the total nitrogen content (includes iron nitride, etc.) were determined on the hot-rolled strip: 1—as hot rolled, 2—as hot rolled, cold reduced, and annealed at 1340°F, 3—as air cooled from 2100°F, and 4—as furnace cooled from 2100°F. Nitrogen contents as aluminum nitride were determined by the Beeghly method[3] and total nitrogen contents by another Beeghly method.[4] The results are listed in Table IV.

Table III. Grain Count and Elongation of Materials Heated Slow or Fast to 1340°F

Variation	Approx. Heat-Up Time, Hr	Material 1 Grains per Sq Mm	Material 1 Elong.	Material 2 Grains per Sq Mm	Material 2 Elong.	Material 3 Grains per Sq Mm	Material 3 Elong.
1 Fast	½	5800	1.6	6300	1.3	8000	1.3
2 Slow	22	2400	1.8	950	2.6	2400	1.9

The nitrogen determinations of Group 1 for the "as hot-rolled" condition show the low nitrogen as

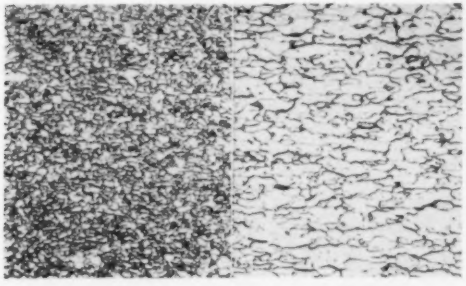

a—Fast heating. b—Slow heating.

Fig. 6—Effect of heating rate during annealing of cold-reduced samples. X100.

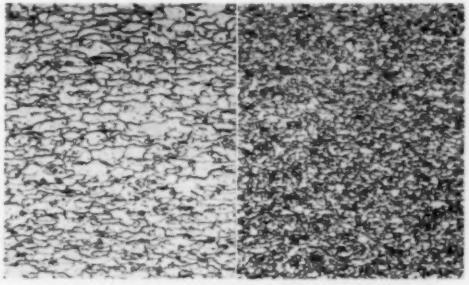

a—With preliminary heat treatment at 900°F for 2 hr. b—Without preliminary heat treatment.

Fig. 7—Grain structures resulting from annealing samples with fast heating. X100.

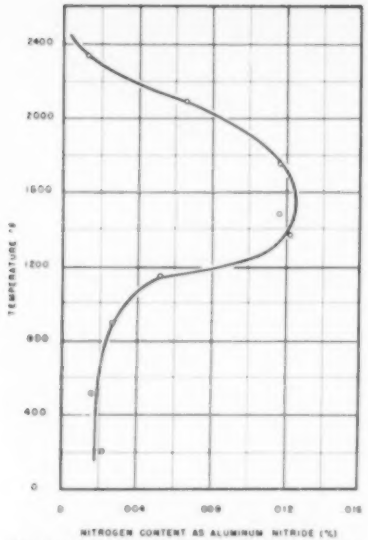

Fig. 8—Aluminum-killed steel hot rolled and reheated 1 hr at various temperatures (after Beeghly).

aluminum-nitride values which are characteristic of rapid cooling from above the critical temperature range. Group 2 for the cold-reduced and annealed condition shows that practically all of the nitrogen present has precipitated as aluminum-nitride during annealing after cold reduction. Group 3 shows that air cooling from above the coarsening temperature results in even less nitrogen as aluminum-nitride than in the hot-rolled condition. On the other hand, furnace cooling from above the coarsening temperature, Group 4, resulted in considerable pick-up of total nitrogen from the air atmosphere and the precipitation of most of it as aluminum-nitride. Samples were wrapped in soft steel sheets to minimize this but aluminum-bearing steels display a great affinity for nitrogen.

In another experiment two specimens of roughing mill stock ¾ in. thick were heated to 2100°F; one was air cooled to room temperature, the other was furnace cooled. Both were cold reduced 45 pct and annealed at 1340°F. This gave two kinds of material; the air-cooled sample in which precipitation took place during annealing after cold reduction and the furnace-cooled sample in which precipitation occurred before cold reduction. Charpy impact specimens cut parallel to the rolling direction and notched at one surface were broken at a series of temperatures with results listed in Table V. Material with the elongated grain shape had considerably less impact resistance than the same material with equiaxed grain shape. Precipitation of aluminum nitride at the boundaries of the elongated grains in the air-cooled sample, creating planes of weakness, could account for the reduced impact resistance. An equal amount of precipitate in the boundaries of the equiaxed grains of the furnace-cooled sample would not have the same effect on the impact resistance.

Effect of Cooling Rate and Heat Treatment

The effect of retarding the cooling rate after finishing the hot-rolled strip at 1550°F was studied, together with the effect of reheating such strip after air cooling or coil cooling. Strip hot rolled and held, or reheated and held at constant temperature for a certain minimum time was no longer capable of producing the elongated grain shape after cold reduction and box annealing, but yielded equiaxed grain structures. The higher the holding temperature, the less was the time required to effect the change. The minimum times required to change grain shape from elongated to equiaxed as determined on one lot of material are shown in Fig. 10. The reheating time was least for mill-rolled and coiled strip, indicating that precipitation was partially completed during coil cooling.

The effect of reheating hot-rolled strip on the nitrogen content as aluminum nitride was determined on the same five materials shown in Table IV. These materials were subjected to reheating times of 30, 60, and 100 min at 1250°F. Results of chemical analyses before cold reduction and annealing and the microstructure after cold reduction and annealing are listed in Table VI. Tests on hot-rolled only (no reheating) samples are included for comparison. The data illustrate progressive precipitation of aluminum nitride with increase in holding time. It appears that after a sufficient length of time the amount of aluminum nitride remaining in solid solution was no longer influential in obstructing development of equiaxed grains after cold reduction and annealing.

Grain Shape Related to Grain Coarsening Temperature

Two groups of six samples each were selected on the basis of their cold-reduced and annealed grain structure. The Group 1 samples had a grain size of A.S.T.M. 6 and grain elongations varying from 2.4 to 3.1. The Group 2 samples had a grain size of A.S.T.M. 8 and grain elongations of 1.3 to 2.0. Both groups were within the following composition

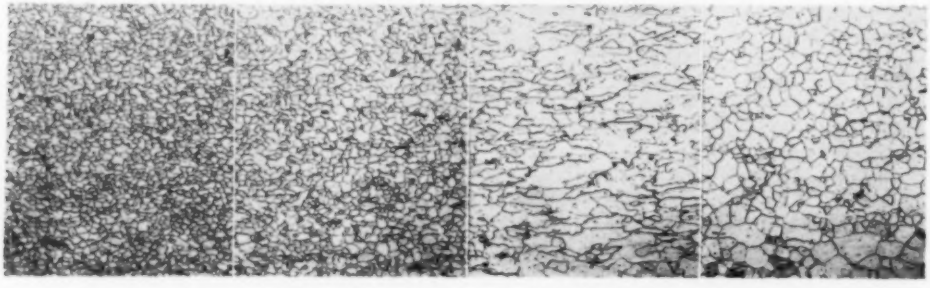

a—1800°F and air cooled. b—1800°F and furnace cooled. c—2100°F and air cooled. d—2100°F and furnace cooled.

Fig. 9—Grain structures of cold-reduced annealed samples heated before cold reduction.

Table IV. Effect of Heat Treatment of Hot-Rolled Strip on the Nitrogen Content as Aluminum Nitride as Compared to the Total Nitrogen Content

Material	Chemical Composition, Pct				(1) As Hot-Rolled, Pct		(2) Cold-Reduced and Annealed, 1340°F, Pct		(3) Air-Cooled from 2100°F, Pct		(4) Furnace-Cooled from 2100°F, Pct	
	C	Mn	S	Residual Al	Total N	As AlN	Total N	As AlN	Total N	As AlN	Total N	As AlN
1	0.033	0.33	0.021	0.038	0.0042	0.0003	0.0041	0.0034	0.0053	0.0002	0.014	0.009
2	0.042	0.33	0.025	0.044	0.0056	0.0007	0.0058	0.0031	0.0062	0.0006	0.016	0.014
3	0.047	0.32	0.020	0.065	0.0047	0.0015	0.0051	0.0041	0.0053	0.0007	0.017	0.015
4	0.044	0.30	0.024	0.059	0.0045	0.0003	0.0060	0.0043	0.0043	0.0003	0.021	0.016
5	0.042	0.33	0.020	0.043	0.0053	0.0007	0.0056	0.0051	0.0046	0.0002	0.016	0.014

ranges: 0.031 to 0.057 pct C, 0.29 to 0.38 pct Mn, 0.017 to 0.028 pct S, and 0.037 to 0.061 pct residual (HCl soluble) Al.

When samples of the hot-rolled strip from which the 12 sheet samples had been processed were heated to 1800°F for 20 min and air cooled, all were fine grained. When heated to 1950°F for 20 min and air cooled only the six Group 2 samples were uniformly fine grained. Group 1 samples had mixed grain structures containing both coarse and fine grains. After heating to 2100°F for 20 min and air cooling, all Group 1 and 2 samples were uniformly coarse grained. The samples having larger, more elongated grains in the cold-reduced and annealed condition also coarsened at a lower temperature on heating in the austenite range.

Nitrogen Content Related to Grain Coarsening

The relationship of nitrogen content as aluminum nitride to grain coarsening was studied using the five hot-rolled strip materials shown in Tables IV and V. These were heated to 1700°, 1800°, 1900°, 2000°, and 2100°F and air-cooled. Microstructure and nitrogen content as aluminum nitride are given in Table VII. These data show that there is a relationship between nitrogen content as aluminum nitride and grain coarsening. Aluminum-killed steels coarsen rapidly above a certain minimum temperature, unlike rimmed steels which coarsen progressively as temperature is raised above the transformation range. Coincident with the grain growth, which takes place between 1900° and 2000°F, there is a drop in nitrogen content as aluminum nitride indicating that the precipitate is redissolved, removing the obstruction to grain growth. At 2100°F the undissolved aluminum nitride is extremely low and the materials are fully coarsened.

Effect of Variation in Aluminum Content

Ingots from two heats of low carbon, aluminum-killed steel were alloyed to provide a range of from 0.015 to 0.20 pct residual (HCl soluble) Al. Samples of the hot-rolled strip were cold reduced 60 pct and annealed at 1340°F. Final grain shape, residual aluminum, and nitrogen contents as aluminum nitride are shown in Table VIII. These data show that within the range 0.034 to 0.066 pct residual Al (1B, 2A, 2B, 2C) elongated grain structure resulted after cold reducing and box annealing. The behavior of samples outside this range of residual aluminum content resulted in intermediate or equiaxed grain structures. Samples 1C, 1D, and 1E had equiaxed grains. Note that the available aluminum nitride was precipitated before cold reduction, thus leaving none available to precipitate during annealing.

However, samples 2D and 2E, with final grain structures respectively intermediate and equiaxed, did not precipitate aluminum nitride before cold reduction despite their high residual aluminum content. Reasons for this behavior contrasted to that of samples 1C, 1D, and 1E are not certain, but there are two probabilities. The coiling temperature of the hot-rolled strip may have been lower on Heat 2 than Heat 1, thereby affording less chance for the AlN to come out of solution during cooling. Second, samples 2D and 2E as well as others from Heat 2 had unusually low nitrogen content as aluminum nitride after cold reduction and annealing. The small amount precipitated during annealing in the presence of the higher aluminum content may have been ineffective in controlling grain shape. Sample 1A had a low aluminum content and a normal nitrogen content as aluminum nitride. The grain structure was intermediate between elongated and equiaxed shape, indicating that too low an aluminum content also tended to make the precipitate less effective in controlling grain shape.

Thus the optimum range for producing elongated grain structures was from somewhat above 0.015 to about 0.066 pct residual Al. This range of aluminum content is also of interest in austenite grain coarsening studies because, as shown by Washburn,[7] the propensity for aluminum-killed steels to be fine grained is maximum within this same range and diminishes with increased aluminum. This further indicates that the two phenomena are related, be-

Table V. Grain Size, Grain Elongation, and Charpy Values* of Air-cooled, Cold-Reduced and Annealed Vs. Furnace-Cooled, Cold-Reduced and Annealed Aluminum-Killed Steel

Sample	A.S.T.M. Grain Size	Grain Elongation	Charpy, Ft-Lb			
			80°F	50°F	32°F	15°F
Air-cooled from 2100°F, cold-reduced and annealed	6	1.7	36	11	6	8
Furnace-cooled from 2100°F, cold-reduced and annealed	5-6	1.0	83	35	26	20

* Simple beam V-notched Charpy impact test specimen as shown in Fig. 4, p. 113, A.S.M. *Metals Handbook*, 1948 Edition.

Table VI. Nitrogen Content as Aluminum Nitride of Five Hot-Rolled Materials Reheated at 1250°F and Grain Shape after 60 pct Cold Reduction and Annealing

Material	As Hot-Rolled, Pct	Reheating Time at 1250°F, Min		
		30	60	100
1	0.0003 *E**	0.0012 *E*	0.0020 *X*	0.0029 *R*
2	0.0007 *E*	0.0025 *E*	0.0040 *X*	0.0040 *R*
3	0.0015 *X*	0.0036 *X*	0.0039 *R*	0.0037 *R*
4	0.0003 *E*	0.0021 *E*	0.0033 *R*	0.0035 *R*
5	0.0007 *E*	0.0012 *E*	0.0030 *X*	0.0044 *R*

* Letters indicate grain shape after cold reduction and box annealing: *E* = elongated; *X* = intermediate; *R* = round or equiaxed.

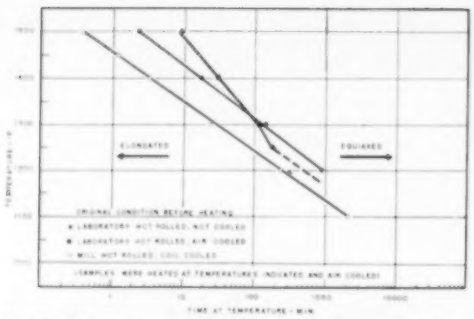

Fig. 10—Minimum time to change grain shape from elongated to equiaxed by heating hot strip before cold reduction.

cause both fine grain behavior and grain elongation characteristics diminish outside this range of aluminum content.

Conclusions

The preceding experiments demonstrate that all sheets of low carbon, aluminum-killed steel composition did not react uniformly to the conditions imposed. However, certain conditions were more conducive to the elongated grain shape than others. These were the conditions:

1—A residual aluminum content somewhat above 0.015 to about 0.066 pct.

2—Heating the hot-rolled strip to above the coarsening temperature and cooling relatively fast.

3—Coiling the hot-rolled strip near the lower critical temperature.

4—Cold reducing the hot-rolled strip without preliminary reheating.

5—Cold reducing the hot-rolled strip more than 30 pct.

6—Annealing after cold reduction using: a—A relatively slow heating rate, or b—A heat treatment at 700° to 1100°F preliminary to the final anneal.

This behavior can be explained by the following hypothesis: A supersaturated solid solution of aluminum nitride in steel is created by heating the material above the coarsening temperature and rapidly cooling to room temperature. This supersaturated solid is cold reduced. During the heating portion of the conventional annealing cycle, precipitation of aluminum nitride occurs to a major extent before the recrystallization temperature is reached. The development of more equiaxed grain structures by fast heating indicates that in this case recrystallization and grain growth takes place before precipitation.

This precipitation during slow heating takes place principally at preferred locations such as boundaries of grains elongated by cold reduction. The precipitate forms a mechanical obstruction to normal recrystallization and results in an elongated grain shape retaining part of the elongation imposed by cold reduction. When the supersaturated solid solution is heated before cold reduction, the nitride is believed to precipitate in a manner which does not influence the final grain shape. After such heating the precipitate resides in the hot-rolled strip grain boundaries and remains out of solution during cold reduction and annealing. After such material has been cold reduced, recrystallization during annealing results in an equiaxed grain structure.

The effectiveness of the compound in controlling grain shape is most pronounced in the same limited range of residual aluminum content most favorable for promoting fine grained behavior of the austenite. When heated, a re-solution of the compound takes place only at or above the austenite grain coarsening temperature. It appears that aluminum nitride not only inhibits development of equiaxed grain structure of cold-reduced ferrite, but is also largely responsible for the fine grained behavior of aluminum-killed steel in the austenite range; in the former case when the steel is supersaturated with respect to aluminum nitride prior to cold reduction and heated slowly for annealing, and in the latter case when the aluminum nitride is precipitated during heating to the austenitizing temperature.

Table VII. Correlation of Nitrogen Content as Aluminum Nitride with Grain Size after Heating to Temperatures of 1700° to 2100°F

Sample	Nitrogen Content as Aluminum Nitride, Pct				
	1700°F	1800°F	1900°F	2000°F	2100°F
1	0.0032 F*	0.0032 F	0.0024 F	0.0006 C	0.0002 C
2	0.0048 F	0.0047 F	0.0043 F	0.0027 M	0.0006 C
3	0.0040 F	0.0041 F	0.0043 F	0.0023 M	0.0007 C
4	0.0039 F	0.0038 F	0.0041 F	0.0018 C	0.0003 C
5	0.0046 F	0.0038 F	0.0041 F	0.0012 M	0.0002 C

* F = fine grain; M = mixed grain; C = coarse grain.

Table VIII. Residual Aluminum, Nitrogen Content as Aluminum Nitride, and Grain Shape of Samples Containing Variations in Residual Aluminum Content

Heat, Sample	Residual Aluminum, Pct	Nitrogen Content as Aluminum Nitride, Pct		Grain Shape As Cold-Reduced and Annealed*
		As Hot-Rolled	As Cold-Reduced and Annealed	
1A	0.015	0.0002	0.0044	*X*
B	0.043	0.0008	0.0046	*E*
C	0.108	0.0044	0.0047	*R*
D	0.146	0.0044	0.0049	*R*
E	0.197	0.0045	0.0053	*R*
2A	0.034	0.0001	0.0027	*E*
B	0.058	0.0002	0.0027	*E*
C	0.066	0.0003	0.0034	*E*
D	0.094	0.0006	0.0029	*X*
E	0.142	0.0008	0.0029	*R*

* *E* = elongated; *X* = intermediate; *R* = round or equiaxed.

Acknowledgment

The authors wish to express their appreciation to the Armco Steel Corp. for permission to publish this paper. They gratefully acknowledge the helpful advice and counsel of R. S. Burns and R. H. Heyer in its preparation and the contributions made by C. E. Bussert, G. E. Koeppel, and other members of the Armco Research Laboratories in carrying out some of the suggested investigations.

References

[1] Burns and McCabe: U. S. Patent 2,381,435 (Aug. 7, 1945).

[2] Rickett, Kalin, and MacKenzie: *Trans.* AIME (1949) **185**, pp. 242-251; JOURNAL OF METALS (March 1949).

[3] Jeffries and Archer: *The Science of Metals*, pp. 91, 92 (1924) New York. McGraw Hill Book Co.

[4] Sachs and Van Horn: Practical Metallurgy. A.S.M. (1940) p. 118.

[5] Beeghly: *Analytical Chemistry* (1949) **21**, pp. 1513-1519.

[6] Beeghly: *Analytical Chemistry* (1942) **14**, pp. 137-140.

[7] Washburn: *Trans.* AIME (1945) **162**, pp. 658-671.

Isothermal Formation of Martensite at Subzero Temperatures in a High Chromium Steel

by S. C. Das Gupta and B. S. Lement

Isothermal formation of martensite occurs in the range of —65° to —197°C and is always preceded by some athermal transformation. By rapid cooling the isothermal, but not the athermal, component of transformation can be suppressed. Stabilization against isothermal transformation can be induced by cycling from below M_s to room temperature.

ALTHOUGH the transformation of austenite to martensite is generally believed to occur only on cooling, recent evidence indicates that this reaction can also occur at constant temperature. Isothermal formation of martensite was observed in tool steel by Fletcher, Averbach, and Cohen.[1,2] They found that the hardening reaction that occurs during the quenching of a plain carbon or low carbon alloy tool steel does not stop immediately when room temperature is reached; instead austenite continues to transform at room temperature although at a decreasing rate. Since only a small amount of austenite transforms in this fashion, isothermal formation of martensite was considered to be merely a "tailing off" effect of the main hardening reaction.

Another point of view was advanced by Kurdjumov and Maksimova[3,4] who reported that the austenite-martensite reaction could be suppressed by rapid cooling of a 6 pct Mn-0.6 pct C steel in liquid nitrogen and that as much as 25 pct martensite could be formed by reheating to and holding at subzero temperatures above that of liquid nitrogen. These investigators came to the conclusion that martensite is thermally nucleated at certain special regions in the austenite and subsequently grows to observable dimensions.

Isothermal transformation of austenite to martensite was cited by Fisher, Hollomon, and Turnbull[5] as evidence supporting another nucleation and growth theory of martensite formation. According

S. C. DAS GUPTA is Research Fellow, Department of Metallurgy, University of Notre Dame, Notre Dame, Ind. B. S. LEMENT, Associate Member AIME, is on the Research Staff, Department of Metallurgy, Massachusetts Institute of Technology, Cambridge, Mass.

Discussion on this paper, TP 3123E, may be sent, 2 copies, to AIME by Dec. 1, 1951. Manuscript, April 16, 1951. Detroit Meeting, October 1951.

This paper represents part of a thesis by S. C. Das Gupta submitted in partial fulfillment of requirements for the degree of Doctor of Philosophy in Metallurgy to the University of Notre Dame.

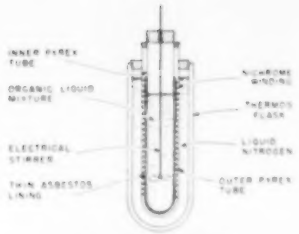

Fig. 1—Subzero furnace.

to this theory, at certain subzero temperatures the rate of growth of athermally formed martensite nuclei becomes slow enough so that isothermal transformation is measurable. This point of view was disputed by Kulin and Cohen[3] who showed that transformation of austenite to martensite is possible at a temperature as low as −266°C, where a negligible rate of growth is predicted by the nucleation and growth theory.[5]

A new mechanism involving nucleation of strain embryos has been advanced by Cohen, Machlin, and Paranjpe[2] to explain the austenite-martensite transformation. According to these investigators isothermal transformation is due to temperature fluctuations which supply sufficient energy to complete the "shearing over" to martensite of strain embryos initially below a critical "shear" angle.

The present investigation was carried out to obtain additional information with respect to isothermal transformation at subzero temperatures. In order to check whether the phenomena reported by Kurdjumov and Maksimova[4] are of general occurrence, a high chromium steel having essentially the same transformation range as reported for their manganese steel was selected for this investigation.

Experimental Details

Chemical Composition: The chemical composition of the steel investigated is as follows: C, 0.73; Mn, 0.28; Si, 0.20; S, 0.02; P, 0.02; and Cr, 14.84. This steel is from the identical heat used in the investigation of Klier and Troiano[6] to determine the effect of chromium and carbon contents on the *M*, temperature.

Austenitizing Treatment: Specimens approximately 1/16x⅛x¼ in. were sealed in an evacuated quartz tube and then austenitized for 2 hr at 1275°C ±5°C in a platinum-rhodium wound tube furnace. This treatment which resulted in a grain size of A.S.T.M. No. 1-2 was selected on the basis of obtaining complete carbide solution.

Table I. Time Required to Reach Temperature

Operation	Initial Temperature, °C	Final Temperature, °C	Medium at Final Temperature	Time Required, Sec
Subcooling	5	— 60 - —150	Organic liquid	18±3
Subcooling	5	—197	Liquid nitrogen	10±3
Up-quenching	—197	—150 - — 40	Organic liquid	15±3
Up-quenching	—197	20	Water	less than 3

Quenching Procedure: Quenching was carried out in a 10 pct brine solution maintained at a temperature of 5°C. The quartz tube containing about five specimens was quickly transferred from the austenitizing furnace to the brine quench, and the tube was broken immediately. The breaking into a vacuum resulted in an efficient quenching action since 100 pct austenite was retained at 5°C.

Subzero Cooling: After quenching the specimens were placed in a subzero furnace maintained within ±1°C of a selected temperature in the range of −60° to −150°C. The details of the subzero furnace are shown in Fig. 1. This furnace operates on the same principle as an ordinary resistance wound furnace; however, instead of room temperature at the outside of the furnace, liquid nitrogen in a thermos flask is used to provide an outside temperature of −197°C. The inner pyrex tube contains an organic liquid mixture consisting of 75 pct petroleum ether and 25 pct methylcyclohexane, which has a freezing point of just under −150°C. Temperature uniformity as well as a rapid rate of either subcooling or up-quenching is brought about by means of a stirrer. The times required for the centers of 1/16 x⅛x¼ in. specimens to reach within 1°C of selected temperatures using the subzero furnace were found to be as given in Table I. According to these results, subcooling in liquid nitrogen at −197°C is more rapid than in the organic liquid maintained as low as −150°C; and up-quenching in water at 20°C is more rapid than in the organic liquid maintained as high as −40°C.

Metallographic Analysis: Quantitative determination of the extent of transformation to martensite was carried out by the method of lineal analysis developed by Howard and Cohen.[6] The precision of measurement is estimated to be ± 1 pct martensite for the amounts of this constituent encountered in the present investigation. After a subzero treatment, specimens were mounted in bakelite, metallographically polished, and etched with a modified Vilella's reagent. Although the martensite plates are not darkened by this procedure, the boundaries between martensite plates and the austenite matrix become sufficiently sharp so that no difficulty is experienced in distinguishing between the two constituents.

It was found that the amount of martensite increases with distance below the surface of transformed specimens and reaches an approximately constant value at a depth of about 0.010 in. It is believed that this effect is due to residual stress set up on quenching from 1275° to 5°C. Since no transformation occurs during such quenching, it would be expected that due to differences in cooling rate compressive stresses are set up at the surface and tensional stresses at the interior. On subsequent cooling to subzero temperatures, the transformation is apparently hindered by the presence of compressive stresses at the surface. The amounts of martensite reported in this investigation were measured at a depth of 0.020 in. and are representative of the interiors of the specimens where tensional stresses apparently do not cause any appreciable variation.

Results

Martensite Formed on Cooling: The amount of martensite formed on cooling is shown in Fig. 2. In this experiment a specimen was kept in the subzero furnace just long enough to reach the temperature of the organic liquid bath and then up-quenched

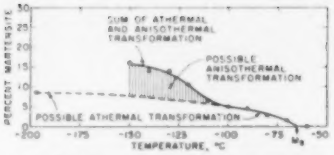

Fig. 2—Amount of martensite formed as a function of temperature in a 15 pct Cr-0.7 pct C steel austenitized 2 hr at 1275°C.

immediately to 20°C in water. The M_s temperature was found to be −65°C ±5°C. This is in agreement with the results of Klier and Troiano* who found a M_s temperature of between −38° and −77°C for ¼x ¼x¼ in. specimens heat treated in a similar fashion. However, although these investigators report that holding 1 hr at room temperature prior to subcooling lowers M_s to below −77°C, this was not confirmed. In fact, reheating as-quenched specimens to a series of temperatures as high as 500°C for 1 hr prior to subzero cooling likewise was not found to have any appreciable effect on the M_s temperature.

On cooling below the M_s temperature the amount of martensite increases progressively and apparently reaches a maximum at about −150°C, which is the lowest temperature that can be obtained with the organic liquid used. However, specimens cooled to the temperature of liquid nitrogen (−197°C) were found to contain about 7 pct less martensite than specimens cooled to −150°C. This anomaly indicates that the austenite-martensite reaction in this steel can be partially suppressed by rapid cooling in liquid nitrogen. There appears to be a limit to the extent of this suppression since decreasing the specimen thickness from 0.070 to 0.020 in., which should effectively increase the cooling rate, does not change the amount of martensite formed on subcooling in liquid nitrogen to −197°C. In fact, a thickness of 0.010 in., which is commensurate with the austenite grain size, actually results in a small increase in the amount of martensite at −197°C. Possibly, this increase is due to the greater freedom from constraints to local change of shape associated with transformation in a single crystal of austenite as compared to polycrystalline austenite.

On the basis of these experiments it appears that subcooling in the organic liquid to temperatures above −150°C does not result in purely athermal* martensite but rather a combination of athermal and anisothermal** martensite. The possible extent of anisothermal transformation is indicated by the extrapolation from −100° to −197°C in Fig. 2. By rapid subcooling it appears possible to suppress the anisothermal transformation but not the athermal transformation. Since the transformation occurs anisothermally, which means that it is time-dependent as well as temperature-dependent, isothermal† transformation would also be expected to occur.

Isothermal Martensite Formation: The amount of martensite formed as a function of time at a series of constant subzero temperatures is shown in Fig. 3. Isothermal transformation of austenite to martensite was found to occur at temperatures ranging from −70° to −197°C. The rate of isothermal transformation decreases with time and becomes very slow after about 0.05 hr at all temperatures. The observable initial rate of isothermal transformation increases with decreasing temperature, reaches a maximum at about −110°C, and progressively decreases below this temperature. If the amount of martensite is plotted against log time as in Fig. 4, the course of the reaction can apparently be represented by a straight line plot after about 0.01 hr.

Isothermal formation of martensite was found to occur as low as −197°C and as much as 14 pct martensite forms after 24 hr at this temperature. This is shown by a series of micrographs in Fig. 5. It was observed that isothermal transformation occurs

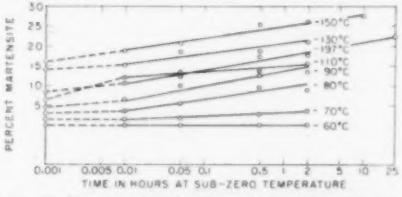

Fig. 4—Semi-log plot showing isothermal formation at various subzero temperatures in a 15 pct Cr-0.7 pct C steel austenitized 2 hr at 1275°C.

mainly by the formation of new martensite plates rather than thickening of existing plates. Except for a larger number of smaller size plates due to the partitioning effect of increased transformation, the appearance of martensite formed isothermally was found to be the same as that formed athermally.

Holding as-quenched specimens for 1 hr at 20°C prior to cooling to subzero temperatures was not found to have any appreciable effect on isothermal transformation. Here again evidence of appreciable stabilization above the M_s temperature prior to cooling below the M_s temperature is lacking.

Effect of Cycling on Isothermal Transformation: The effects of cycling between 20° and −95°C and between 20° and −150°C on isothermal transformation were studied. The treatments used are illustrated in Fig. 6 and the results are given in Table II.

In treatments A, B, and C the total time at the subzero temperature is 30 min. Up-quenching to 20°C immediately after reaching the subzero temperature (treatment A) or after holding 3 min at the subzero temperature (treatment B) results in less martensite formation than does an uninterrupted hold at the subzero temperature (treatment C). In treatments A and B virtually complete stabilization results from up-quenching to 20°C and therefore the subsequent hold at the subzero temperature is ineffective in producing additional transformation. Since in both these cases some martensite is present before up-quenching to 20°C, these results indicate that partial transformation may be required before stabilization can occur in this steel. This suggests

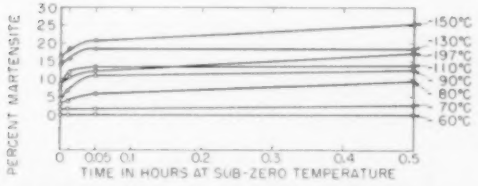

Fig. 3—Isothermal formation of martensite at various subzero temperatures in a 15 pct Cr-0.7 pct C steel austenitized 2 hr at 1275°C.

* Athermal — dependent on temperature.
** Anisothermal — dependent on cooling rate.
† Isothermal — dependent on time (for a given temperature).

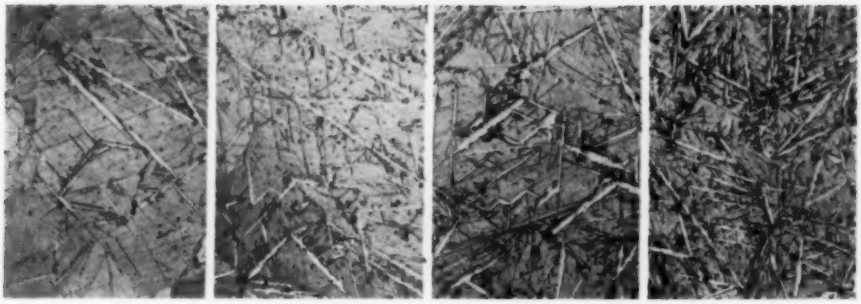

Zero time at −197°C. 3 min at −197°C. 2 hr at −197°C. 24 hr at −197°C.

Fig. 5—Micrographs showing isothermal transformation at −197°C in a 15 pct Cr-0.7 pct C steel. X150.

that partial transformation stimulates subsequent isothermal transformation and that heating to 20°C wipes out the stimulating effect.

Isothermal Transformation after Up-quenching from −197°C: The effect of cooling to −197°C followed by up-quenching to and holding at various subzero temperatures is shown in Fig. 7. These experiments were carried out in order to study the effect of a constant initial amount of martensite on subsequent isothermal transformation at various temperatures. Series A specimens were held 3 min at −197°C, which resulted in the formation of about 11 pct martensite prior to up-quenching. Series B specimens were held 2 hr at −197°C, which resulted in the formation of about 17 pct martensite prior to up-quenching. In both series up-quenching to temperatures as high as −40°C results in additional transformation prior to isothermal holding. The increases amount to about 6 pct martensite for series A and about 4 pct martensite for series B. The constancy of these amounts for a given series suggests that the additional transformation occurred during the short period of time the temperature passed through the range of −197°C to about −150°C.

At all temperatures below −70°C, series A specimens show a higher initial rate of isothermal transformation than do series B specimens. This indicates that an increase in the initial amount of martensite from 17 to 21 pct results in a decrease in the rate of isothermal transformation at a given temperature. Since a larger initial amount of martensite would be expected to exert a greater stimulating effect on isothermal transformation, the observed decrease may be due to the greater influence of partitioning. Because of this effect, the larger the amount of initial transformation, the smaller the volume generated by nucleation of each martensite plate. Partitioning also may slow down transformation by increasing constraints to the local change of shape required by the formation of each new plate.

For both series the observable initial rate of isothermal transformation is apparently higher at −150° than at −197°C and very low or zero just below the M_s temperature. For series A a maximum initial rate occurs at a temperature judged to be about −140°C. Since these experiments were carried out keeping the initial amount of martensite constant, the observed temperature dependence of initial rate of transformation should be a direct consequence of the temperature dependence of rate of nucleation of martensite plates. This assumes that the generation of such plates, once nucleated, is practically instantaneous.

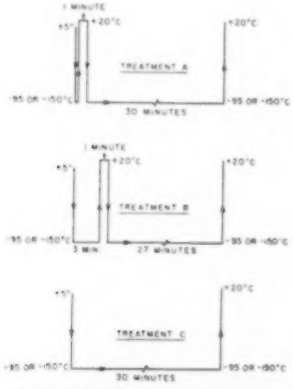

Fig. 6—Schematic representation of cyclic treatments used in investigation of stabilization effect.

Discussion of Results

The 15 pct Cr-0.7 pct C steel investigated was found to have a fairly definite M_s temperature of −65°C ±5°C corresponding to the particular austenitizing treatment of 2 hr at 1275°C employed. Isothermal formation of martensite was found to occur below this M_s temperature and is apparently always preceded by some athermal formation of martensite. Since it was not found possible to differentiate between athermal and isothermal martensite by metallographic examination, it appears that the mechanism of formation is essentially the same whether martensite forms on cooling or at constant tempera-

Table II. Effect of Cycling on Isothermal Transformation

Temperature of Subzero Isothermal Run, °C	Percent Martensite		
	Treatment A*	Treatment B*	Treatment C*
−90	4.0	8.8	10.3
−150	18.3	19.6	23.8

* See Fig. 6.

ture. The rate of the reaction seems to be governed by the rate of nucleation of martensite plates rather than their rate of "growth" which appears practically instantaneous at all temperatures studied.

The isothermal behavior of the chromium steel was found to be similar to that of the manganese steel investigated by Kurdjumov and Maksimova.[3] The following points of similarity were observed. Isothermal transformation of austenite to martensite was found to occur at subzero temperatures below −65°C. Such transformation occurs either after cooling directly to a subzero temperature below −65°C, or after first subcooling to the temperature of liquid nitrogen (−197°C) and then up-quenching to the selected subzero temperature. The observable initial rate of isothermal transformation goes through a maximum with decrease in temperature below −65°C.

It was not found possible to suppress completely the austenite-martensite reaction in the chromium steel by cooling to the temperature of liquid nitrogen (−197°C) as claimed by Kurdjumov and Maksimova[3] for their manganese steel. Confirmation of the results of Kurdjumov and Maksimova by other investigators is necessary in order to establish whether complete suppression can actually be attained. Thus far, attempts to accomplish this have proved unsuccessful[6] and it is probable that the reported chemical composition of the manganese steel[3] is erroneous.

The phenomenon of stabilization which plays an important role in isothermal transformation was not investigated by Kurdjumov and Maksimova.[3] This phenomenon apparently is a result of removing the stimulating effect of partial transformation by thermal means. Stabilization is nicely explained by the strain embryo theory[7] according to which transformation to martensite generates strain embryos that can be relaxed by stress relief even at relatively low temperatures. That partial transformation is necessary before austenite can be stabilized against further transformation on cooling was pointed out by Harris and Cohen.[10] The occurrence of extremely rapid stabilization resulting from interrupting the quench at room temperature prior to cooling below M_s as claimed by Klier and Troiano[5] was not investigated in the present work. The possible relationship of such a phenomenon to isothermal transformation merits further study.

As indicated by the results of this investigation, isothermal transformation of martensite is influenced by the temperature dependence of rate of nucleation of martensite plates, the stimulating effect of partial transformation, the geometrical effect of partitioning, and the previous history with respect to stabilization. A more detailed knowledge of these factors is required in order to judge the validity of the current theories of the mechanism of the austenite-martensite transformation.

Summary

The following characteristics of the austenite-martensite transformation have been observed in a 15 pct Cr-0.7 pct C steel:

1—Partial but not complete suppression of martensite is attainable by quenching to −197° in liquid nitrogen. The part of the transformation that is suppressible probably corresponds to the isothermal rather than the athermal component of the transformation.

2—Isothermal transformation occurs at subzero temperatures below −65°C which is the M_s point corresponding to an austenitizing treatment of 2 hr at 1275°C followed by water quenching to 5°C and then subcooling in an organic liquid.

3—Isothermal transformation is always preceded by some athermal transformation and occurs mainly by the formation of new plates rather than the growth of existing plates.

4—The observable initial rate of isothermal transformation goes through a maximum with decrease in temperature below the M_s point.

5—Stabilization against isothermal transformation at a given subzero temperature results from cycling between that temperature and room temperature.

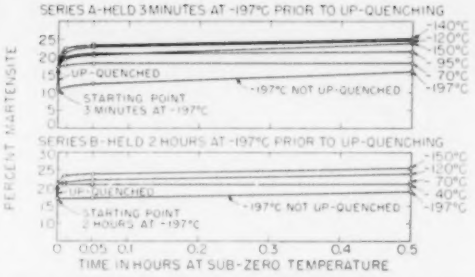

Fig. 7—Isothermal formation of martensite following up-quenching a 15 pct Cr-0.7 pct C steel from −197°C and holding at various subzero temperatures. Austenitizing treatment consisted of 2 hr at 1275°C.

Acknowledgments

The authors wish to thank the Union Carbide and Carbon Corp. for the pre-doctoral fellowship and the Studebaker Corp. for the financial aid which made this work possible.

References

[1] B. L. Averbach, M. Cohen, and S. G. Fletcher: The Dimensional Stability of Steel. Part III—Decomposition of Martensite and Austenite at Room Temperature. *Trans.* ASM (1948) **40**, p. 728.

[2] B. L. Averbach and M. Cohen: The Isothermal Decomposition of Martensite and Retained Austenite. *Trans.* ASM (1949) **41**, p. 1024.

[3] G. V. Kurdjumov and O. P. Maksimova: Kinetics of the Transformation of Austenite to Martensite at Low Temperatures. *Doklady Akad. Nauk, SSSR* (1948) **61**, p. 83.

[4] G. V. Kurdjumov and O. P. Maksimova: On the Energy of Formation of Martensite Nuclei. *Doklady Akad. Nauk, SSSR* (1950) **73**, p. 95.

[5] J. C. Fisher, J. H. Hollomon, and D. Turnbull: Kinetics of the Austenite-Martensite Transformation. *Trans.* AIME (1949) **185**, p. 691; JOURNAL OF METALS (October 1949).

[6] S. A. Kulin and M. Cohen: On the Martensitic Transformation at Temperatures Approaching Absolute Zero. *Trans.* AIME (1950) **188**, p. 1139; JOURNAL OF METALS (September 1950).

[7] M. Cohen, E. S. Machlin, and V. J. Paranjpe: Thermodynamics of the Martensite Transformation. ASM Seminar on Thermodynamics in Physical Metallurgy (1950) p. 242.

[8] E. P. Klier and A. R. Troiano: Ar" in Chromium Steels. *Trans.* AIME (1945) **162**, p. 175.

[9] R. T. Howard and M. Cohen: Quantitative Metallography by Point-Counting and Lineal Analysis. *Trans.* AIME (1947) **172**, p. 413; METALS TECHNOLOGY (August 1947).

[10] W. J. Harris and M. Cohen: Stabilization of the Austenite-Martensite Transformation. *Trans.* AIME (1949) **180**, p. 447; METALS TECHNOLOGY (September 1948).

Desulphurization of Pig Iron with Pulverized Lime

by Bo Kalling, C. Danielsson, and Ottar Dragge

THE desulphurizing of pig iron has been accomplished with a number of different additions. The oldest and still most commonly used agent is soda, the extensive use of which commenced about 1925, when it was used principally for cupola furnace iron. More recent experience[1] seems to show that better results can be obtained with sodium hydroxide. The well-known desulphurizing properties of lime have also been exploited in different technical processes. Another material with even more powerful effect is calcium carbide.[2] The desulphurizing ability of manganese, when added to the ladle in sufficient quantity, should also be mentioned in this connection. During recent years increasing attention has been paid to the desulphurizing properties of metallic magnesium.[3] An addition of a suitable alloy of magnesium is now in use purely for the purpose of sulphur elimination.

Of the desulphurizing agents mentioned, lime is by far the cheapest, provided that the reaction can be brought about rapidly and completely. Therefore, a method that makes full use of the desulphurizing ability of lime may be able to compete with other processes. A method developed at the Domnarfvet Iron and Steel Works (Sweden) will be described, which enables pig iron to be rapidly desulphurized to very low sulphur contents by using a burnt lime powder as the desulphurizing agent.

Lime in Older Processes

In cases where lime has been used for the desulphurization of pig iron, it has generally not been used alone, but mixed with other substances such as fluorspar, to obtain the formation of a molten slag during the process. This method has been tried by Tigerschiöld,[4] who treated the iron with a lime-fluorspar mixture, the stirring of the iron being brought about inductively with low frequency alternating current. Very good results were obtained. A process of this type has also been suggested by R. P. Heuer, U. S. A. The principles of this method, which has been tested in Great Britain by Newell, Langner, and Parsons,[5] are that a mixture of lime and fluorspar is added to the hot metal in the ladle, while a powerful stream of nitrogen gas is blown into the bath to produce the required intermixing. The results of the tests were unsatisfactory, however. A similar process has been developed at The Steel Co. of Canada, according to a statement by H. M. Griffith.[6] Here the tests were carried out in a carbon-lined ladle provided with carbon tuyeres in the side wall for blowing nitrogen into the bath. The addition consisted of about 20 lb of a mixture of burnt lime and fluorspar per ton of pig iron. Good results appear to have been achieved. The sulphur content of the pig iron is stated to have been reduced from 0.025 to 0.050 pct down to 0.006 pct.

Various methods of desulphurizing pig iron have been tried using lime powder without fluxing material for fusing. Eichholz and Behrendt[7] have experimented with blowing a powdered lime-coke mixture with air into the ladle. Their results were, however, not conclusive and the experiments do not appear to have been continued. Similar experiments have been carried out at Domnarfvet, using nitrogen instead of air in order to avoid oxidation. But these attempts were not particularly successful. It appears to be difficult to achieve the required agitation by this means. The strong cooling effect of the gas on the iron is also a serious drawback.

A method in many respects similar to that tried at Domnarfvet was tried by Eulenberg and Krus at the end of the 1930's. Here again desulphurization was carried out with lime alone, brought into contact with the molten iron in a rotary furnace. The temperature was kept at the required level, 1400° to 1500°C, by the introduction of a pulverized coal burner in one end of the furnace. The speed of rotating was not given. A paper by Bading and Krus[8] states that, in one of the first experiments, the sulphur content in 56 tons of pig iron was brought down from 0.186 to 0.035 pct in 117 min, but that a considerable shortening of the time would be possible. According to later reports by Eichholz and Behrendt,[7] it should be possible by this process to achieve a desulphurization speed of 0.35 pct S per hr for a consumption of 6 to 10 pct limestone and 2 to 3 pct coke, as fuel exclusively. The final sulphur content is, however, not stated.

Domnarfvet Method

After a number of different procedures had been investigated, the tests at Domnarfvet were directed to desulphurization with lime in a rotary furnace. Before going into the practical details of the method, the theoretical aspects will be discussed briefly.

If the pig iron does not contain alloying elements other than carbon, the reaction can be expressed most simply by the usual equation:

$$FeS + CaO + C = Fe + CaS + CO \qquad [1]$$
$$\Delta H_{\infty} \sim 34{,}000 \text{ cal}$$

That this reaction can be carried through to a very complete desulphurization of pig iron has been shown by Oelsen[9] in a discussion in connection with the Eulenberg and Krus' method. He mentions two laboratory tests, in one of which the sulphur content in the pig iron at 1400°C was reduced from 0.540 to 0.006 pct after treating with 3.35 pct lime. The pig iron had a low manganese content, but other analysis is not given.

Mention also should be made of the recently published investigations by Fischer and Cohnen[10] dealing with the influence of the carbon content of the iron on desulphurization with lime, although in this case fluorspar was added also. The tests show that efficient desulphurization is possible with lime in the steel bath, provided that the carbon content is sufficiently high. The temperature employed in these tests was considerably higher (1620°) than that normal for treatment of pig iron. The author concludes that the product S% × C% = 0.011 at the temperature in question.

B. KALLING, Member AIME, C. DANIELSSON, and O. DRAGGE are associated with the Research Department, Stora Kopparbergs Bergslags Aktiebolag, Domnarvet, Sweden.

Discussion on this paper, TP 3109C, may be sent, 2 copies, to AIME by Oct. 1, 1951. Manuscript, Feb. 27, 1951. St. Louis Meeting, February 1951.

In practice the conditions are complicated by the fact that the pig iron to be desulphurized is very seldom free of silicon. In a pig iron containing silicon above a certain level, the carbon is replaced by silicon as a reducing agent, and the reaction equation may be written:

$$2FeS + CaO + FeSi = 3Fe + 2CaS + SiO_2 \quad [2]$$

The silica reacts with the lime present to form a silicate, presumably Ca_2SiO_4 in the main, when there is an excess of lime. The reaction equation will then be:

$$2FeS + 4CaO + FeSi = 3Fe + 2CaS + Ca_2SiO_4 \quad [3]$$
$$\Delta H_{298} \sim -102{,}000 \text{ cal}$$

The formation of silicate here implies that a large part of the lime is bound to the silica, so that the consumption of lime may be much higher in this case than that with silicon-free iron.

How far reaction 3 can be carried, when desulphurizing to a certain sulphur content in the pig iron, is difficult to estimate reliably. A knowledge is required, for instance, of the intersolubility of

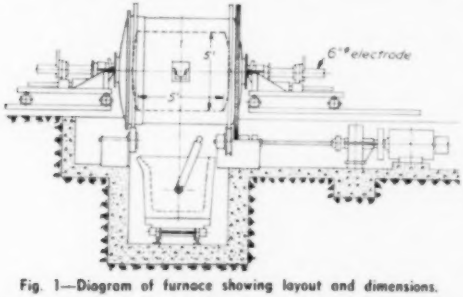

Fig. 1—Diagram of furnace showing layout and dimensions.

the different components. Their solubility is probably very limited, so the reaction should be nearly complete even in desulphurizing to a low sulphur content in the pig iron. On the assumption that transformation takes place completely according to eq 3 and that 0.1 pct S is eliminated, the following data are obtained, whatever the sulphur content in the pig iron during treatment: lime consumption, 0.35 pct of the weight of pig iron; oxidation of silicon, 0.05 pct; S and SiO_2 content of lime product, 20 and 19 pct, respectively.

Some of the test results presented in the following indicate that while the theoretical consumption of lime is roughly that stated above, in practice certain cooperative factors make it necessary to calculate with a considerably higher consumption of lime.

It should be pointed out that reduction with carbon, as above, is endothermic, while silicon reduction is exothermic. The equilibrium of the carbon reaction should therefore be displaced towards lower sulphur contents at a higher temperature, while the opposite applies to reduction with silicon. But since equilibrium for an excess of lime corresponds in both cases to an extremely low sulphur content in the iron, the temperature has no great influence on the reaction. Nor does the temperature appear particularly to affect the rate of reaction within the normal temperature range applying here. The evolution of heat in the silicon reaction is valuable, as the temperature loss in the treatment of the hot metal is thus counteracted to a large extent.

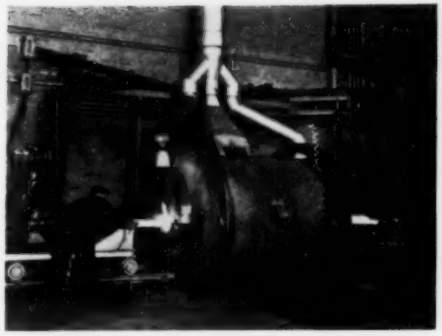

Fig. 2—Furnace as electrodes are being withdrawn.

The silicon content required within this temperature range for the reducing effect of the silicon to exceed that of the carbon, is certainly very low. Our experiments indicate that the reducing action of silicon is as great as that of saturated carbon at a silicon content of about 0.05 pct at 1300°C.

A matter of prime importance to the result of the process has proved to be that unnecessary oxidation of silicon should be avoided as far as possible. The silica formed opposes the reaction primarily by binding the lime as silicate, but also to a large extent by the silicate adhering to unused grains of lime and thus preventing the latter from intimate contact with the pig iron. The process should therefore take place under strongly reducing conditions. All oxidizing gases should be eliminated from the furnace during treatment. Therefore, the furnace should not be heated with combustion gases even if they are "reducing," i.e., contain unburnt carbon monoxide. As previously stated, even pure carbon monoxide has a strong oxidizing action on silicon in normal contents in the pig iron. The best result should be achieved then if the process is carried out in a closed furnace. Oxygen-free gases, hydrogen, and hydrocarbons, may nevertheless be supplied, which can be of advantage, as the presence of hydrogen should increase the reaction speed. But even when every possible step is taken to prevent external oxidizing gases from entering the furnace during the process, it is difficult to avoid some oxidation of silicon taking place apart from that occurring by the desulphurization reaction.

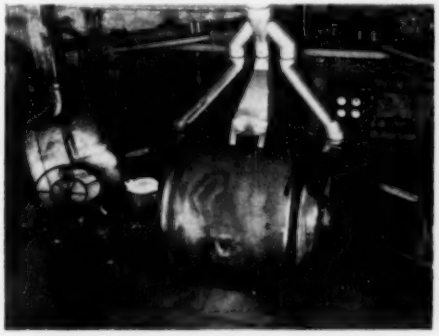

Fig. 3—Furnace during charging of pig iron.

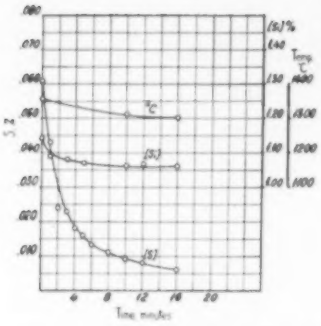

Fig. 4—(left) Heat KR8

Hot metal 2400 kg; C, 3.6 pct; 40 rpm. Lime powder, 39 kg; Mn, 1.1 pct. Coke powder, 10 kg; Si, 1.14 to 1.08 pct; P, 0.05 pct.

Fig. 5—(right) Heat A34

Hot metal, 2230 kg; C, 3.7 pct; 40 rpm. Lime powder, 45 kg; Mn, 0.5 pct. Coke powder, 45 kg; Si, 0.58 to 0.40 pct; P, 1.7 pct.

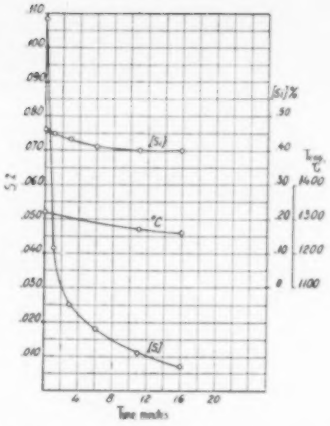

The lime must be in a very finely pulverized form if a sufficiently large contact surface is to be obtained with the hot metal. The tendency of fine grained lime to form balls must, however, be avoided. For this reason, the temperature of the hot metal must not be kept too high. A safety measure which is generally found desirable, but perhaps not always necessary, is to mix in a certain quantity of fine grained coke dust in the lime to counteract the tendency to stick.

If a rapid reaction is desired, an extremely intensive agitation of lime and hot metal is imperative. A short time of treatment is important not only for the saving in time, but also for the avoidance of an unnecessary temperature loss during the process, which, as stated above, should preferably be carried out without external heating. It has been found necessary to increase the speed of rotation of the furnace to a rate far above that employed with other rotary furnaces for metallurgical use. In this way the time of reaction can be lowered to only a few minutes.

Results

The first tests with this method were started at Domnarfvet in 1947. They were made in a semiscale, cylindrical rotary furnace with a capacity of about 3 tons. Laboratory experiments were made later to study in greater detail the factors affecting the reactions and the states of equilibrium. This work has, however, not advanced so far that definitive results can be given. During the first half of 1950 operations were started in a plant for commercial use of the method at Surahammars Bruks AB, Surahammar, Sweden. The maximum capacity of the furnaces is about 18 tons. The results obtained from this plant are reported by S. Fornander.[1] The present paper will deal only with the results obtained from tests in the 3-ton furnace at Domnarfvet.

From Fig. 1, which shows the dimensions of the furnace, it can be seen that electrical heating was employed with graphite electrodes introduced through central openings in the two ends. Fig. 2 shows the furnace at a moment when the electrodes are just being withdrawn, and Fig. 3, during the charging of the pig iron. The tapping of the hot metal and lime charge was made through the visible tap hole in the center of the furnace mantle.

In all experiments the furnace was lined with ordinary fire clay. Desulphurization can be carried through without any formation of balls or lime attack on the furnace lining, as long as the temperature of the pig iron does not exceed about 1350° to 1400°C. A more favorable result may be obtainable through the use of a basic furnace lining such as magnesite or tar-dolomite, or, perhaps even better, a carbon lining. Fire clay, however, has given such satisfactory results that there was no reason to change to another material, and in any case it appears to be the most economical.

In most experiments the pig iron was first introduced into the furnace, after which a quantity of finely ground, burnt lime in suitable proportion to the pig iron was shovelled on to the surface of the bath, usually mixed with a varying quantity of coke powder. The screen analysis of the lime used is recorded in Table I. The lime charge contained a not inconsiderable amount of CO_2 and H_2O, which caused a strong development of gas at the beginning of the treatment. After the gas evolution had ceased, the furnace was kept tightly shut. The rate of rotation was in most cases 40 rpm, which was the maximum for the furnace.

In Figs. 4 to 13 the course of desulphurization in a number of tests is shown, as is the change in the silicon content of the hot metal and the temperature loss during each treatment. The temperature of the

Table I. Grain Size of the Lime Powder Used

Mesh	A-heats, Pct	KR-heats, Pct
—3*	16.9	2.7
32-65	11.9	7.3
65-150	23.5	8.2
150-250	39.9	10.0
<250	7.8	71.8
	100.0	100.0

Table II. Chemical Analysis of the End Lime, in Percent

Heat	Fe*	MnO	CaO	CaS	SiO_2	Al_2O_3	S	C	Na_2O
KR 16	5.0	0.23	69.0	8.8	7.6	1.7	3.9	4.5	
KR 18	3.4	0.34	67.8	10.6	10.8	2.3	4.7	1.1	
KR 22	10.1	0.39	36.8	27.0	7.3	1.6	12.0	12.9	
KR 25	2.1	0.34	62.2	13.1	15.3	2.6	5.8	0.85	0.27†
KR 34	9.5	0.35	51.6	14.6	17.4	2.2	6.5	0.63	
KR 36	12.1	1.03	49.6	16.2	14.6	2.7	8.1	0.99	
KR 40	9.8	1.07	55.1	11.0	8.0	3.2	4.9	9.0	
KR 41	4.4	1.59	28.4	35.1	17.1	2.4	15.6	9.2	
KR 42	8.4	0.23	45.0	18.2	10.8	3.1	8.1	13.1	

* The main part of the Fe content is probably in the metallic state.

† The Na_2O content at the start of the heat corresponds to 4.4 pct Na_2O at the end.

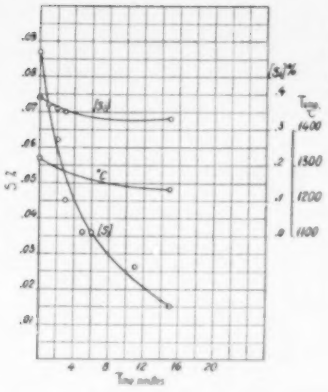

Fig. 6—(left) Heat KR36

Hot metal, 2690 kg; C, 3.0 pct; 40 rpm. Lime powder, 74 kg; Mn 0.8 pct. Coke powder, 12 kg; Si, 0.39 to 0.33 pct; P, 1.8 pct.

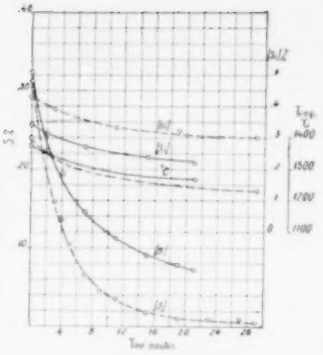

Fig. 7—(right) KR41 and KR42

KR 41 (solid line) — Hot metal, 2880 kg; C, 3.6 pct; 40 rpm. Lime powder, 49 kg; Mn, 0.4 pct. Coke powder, 74 kg; Si, 0.34 to 0.22 pct; P, 2.1 pct.

KR 42 (broken line) — Hot metal, 2640 kg; C, 3.7 pct; 40 rpm. Lime powder, 100 kg; Mn, 0.3 pct. Coke powder, 50 kg; Si, 0.43 to 0.30 pct; P, 2.2 pct.

furnace when the pig iron was introduced was normally about 1100°C.

Table II gives the analysis of the "end lime" obtained during treatment for the majority of heats. Prior to analysis, the major part of the metallic iron had been separated magnetically. The analysis applies to material having passed through a 65 mesh screen. Much of the product is admittedly coarser, but it was considered important to form a clear picture of how far the reaction could be taken with the finest material. The sulphur content has proved slightly higher in the analyses recorded than in an average sample of the end lime.

The silica content of the end lime does not originate only from the silicon oxidized in reaction 3. Some is obtained from silica in the lime and coke dust, and a varying quantity also from the lining. Generally a certain quantity of silica has been formed through the presence in the furnace of undesirable oxidizing substances, such as iron oxides and sulphates formed through oxidation of residues, in the furnace after tapping the previous charge, carbon dioxide and water vapor from the lime charge, etc. In Table III are recorded the proportions of the different sources of silica in the charges examined.

An attempt has been made to determine the "lime yield" in the different heats on the basis of the analyses, by which is meant the theoretical amount of lime required for the completion of reaction 3 in proportion to the total quantity actually used. The somewhat doubtful assumption has thus been made that all silica is bound to lime in the form of Ca_2SiO_4, and that Al_2O_3 and the insignificant MnO content need not be taken into consideration. The calculated lime yield therefore will probably be too high in some cases, which is partly shown by the fact that the free amount of CaO has been negative in one case (KR 41). Thus, all silica is not bound as Ca_2SiO_4, but is also in the form of other more acid silicates. The result of the calculations is given in Table IV.

The coke added has, like the lime, been finely pulverized. The addition of coke generally has been about half that of lime. A large part of the coke, however, has been used up through dissolving of the carbon in the pig iron, which was not previously fully saturated with carbon. This is seen by the comparatively low carbon content in the end-lime analyses. In other cases, where the pig iron is high in silicon, there has been a considerable separation of graphite during the process, which means that a smaller amount of coke is required. How much coke is needed under different conditions has not been fully worked out, but that a certain, even if small, addition is desirable has been clearly shown from the experiments.

Figs. 4 to 6 show some normal heats. In the case of heat KR-8 a pig iron fairly high in silicon, but with low phosphorus content, has been treated, while the other two diagrams show the desulphurization of a basic bessemer pig iron of normal analysis. As will be seen, the desulphurization is very rapid if the amount of lime is sufficient, and about equally so whether the pig iron is high or low in silicon. The lesser amount of lime in experiment KR-36 (Fig. 6) caused a slower and less complete reaction. The experiment shows, however, that a considerable desulphurization can be obtained with the addition of only about 1 pct lime. The yield of lime, 58 pct according to Table IV, in this case is very satisfactory.

Table III. Origin of the SiO_2 Found in the End Lime, in Percent

	CaO	SiO_2	Al_2O_3
Analysis on used materials:			
Lime	96.2	3.1	0.7
Coke		4.0	2.7
Lining		57.0	39.0

Heats	KR 16	KR 18	KR 22	KR 25	KR 34	KR 36	KR 40	KR 41	KR 42
SiO_2 by reaction 3	43	37	0	32	35	50	8	83	66
SiO_2 from the coke ash	22	16	18	11	5	10	21	7	12
SiO_2 from charged lime	35	24	27	16	13	15	28	11	19
SiO_2 from the lining*	†	8	16	10	9	13	29	10	24
SiO_2 through unwanted oxidation	†	15	39‡	31	38	12	14‡	−11§	−21§

* At continuous operation, the SiO_2 from the lining is expected to decrease to negligible values.

† The furnace is quite clean at the start of the heat.

‡ The main part of the unwanted SiO_2 content seems to originate from oxidation of products remaining in the furnace from the preceding heat.

§ Heats with both Si and C reduction during the desulphurization.

Table IV. Calculated Partition of Original CaO in End Lime, Percent

Heats	KR 22	KR 25	KR 34	KR 36	KR 40	KR 41	KR 42
CaO bound in Ca_2SiO_4	24.1	39.5	51.7	42.8	23.5	57.4	34.2
CaO transferred to CaS	37.0	14.0	11.4	21.3	13.5	49.1	24.0
Unused CaO	38.9	46.5	36.9	35.9	63.0	−6.5	41.8
Total	100.0	100.0	100.0	100.0	100.0	100.0	100.0
"Yield" of CaO	61.1	53.5	63.1	64.1	37.0	106.5	58.2

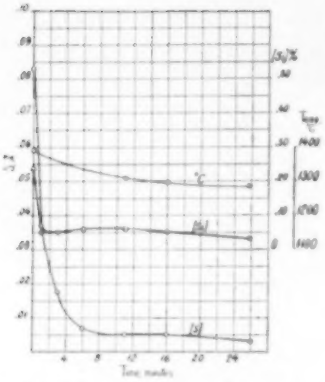

Fig. 8—(left) Heat A31

Hot metal, 2900 kg; C, 4.2 pct; 40 rpm. Lime powder, 40 kg; Mn, 0.4 pct. Coke powder, 40 kg; Si, 0.24 to 0.03 pct; P, 1.7 pct.

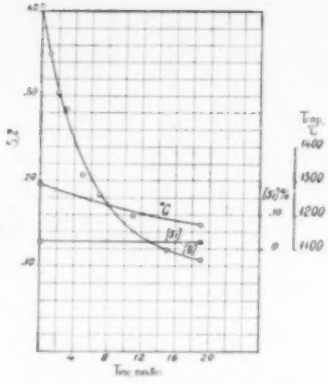

Fig. 9—(right) Heat KR22

Hot metal, 1880 kg; C, 3.4 pct; 40 rpm. Lime powder, 38 kg; Mn, 0.8 pct. Coke powder, 19 kg; Si, 0.02 pct; P, 1.7 pct.

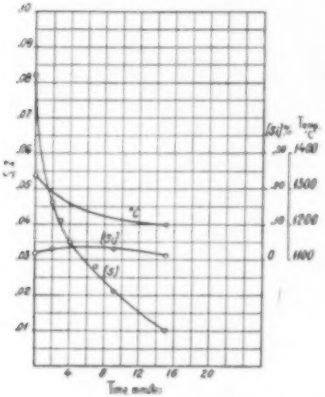

Fig. 10—(left) Heat KR40

Hot metal, 2170 kg; C, 3.7 pct; 40 rpm. Lime powder, 50 kg; Mn, 1.2 pct. Coke powder, 30 kg; Si, 0.02 to 0.01 pct; P, 1.9 pct.

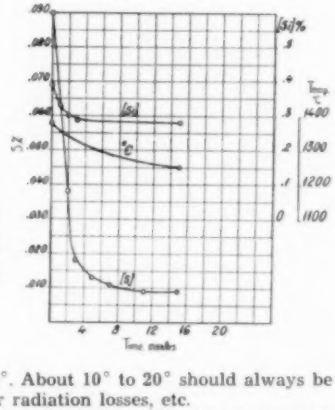

Fig. 11—(right) Heat KR25

Hot metal, 2400 kg; C, 3.4 pct; 40 rpm. Lime powder, 40 kg; Mn, 0.8 pct. Coke powder, 20 kg; Si, 0.39 to 0.28 pct; P, 1.9 pct.

The silicon content in the pig iron sinks, in all cases, by about 0.05 pct, which shows that the losses through "foreign" oxidation have been negligible.

The temperature drop during the process is about 50°C (rather more in heat KR-36), which is satisfactory considering the small size of the furnace. It can be assumed that heating 1 pct dry carbon dioxide-free lime to the reaction temperature will cool the hot metal by about 15°. The corresponding figure for coke dust is about 25°. The heat of reaction in the presence of silicon, on the other hand, corresponds to an increase in the temperature of the hot metal by about 10° for oxidation of 0.05 pct Si. The resulting temperature drop in desulphurization of a pig iron containing about 0.1 pct S with 1.5 pct lime and 0.5 pct coke is calculated from these figures to be about 25°. About 10° to 20° should always be added to cover radiation losses, etc.

Heats KR-41 and KR-42 in Fig. 7 are examples of how far desulphurization can be brought in one operation commencing with pig iron with a sulphur content of between 0.3 and 0.4 pct. In charge KR-42 the sulphur content has been brought down from 0.31 to under 0.003 pct when using 3.8 pct lime, i.e., an elimination of 99 pct. The lime yield is high notwithstanding, 58 pct according to the calculations. In heat KR-41, where the addition of lime was only half as great, 1.9 pct, the sulphur content sank only to 0.072 pct in 20 min, but at this time was still sinking. The yield of lime here, as already stated, was over 100 pct, according to the method of calculation used, but still as high as 78 pct if all silica is assumed to be in the form of $CaSiO_3$ instead of Ca_2SiO_4. A sulphur content in the end lime of 15.6 pct, as in this case, with a simultaneous silica con-

Table V. Data for Heats KR-30 to KR-34

Heats	KR-30 Before	KR-30 After	KR-31 Before	KR-31 After	KR-32 Before	KR-32 After	KR-33 Before	KR-33 After	KR-34 Before	KR-34 After
C, Pct	2.91	2.97	3.08	3.47	3.26	3.41	3.16	3.34	3.18	3.16
Si, Pct	0.30	0.28	0.43	0.37	0.40	0.34	0.61	0.55	0.73	0.68
Mn, Pct	0.65		0.67		0.72		0.96		1.01	
S, Pct	0.054	0.022	0.118	0.014	0.104	0.010	0.133	0.008	0.091	0.008
Temperature, °C	1330	1255	1320	1256	1375	1332	1310	1278	1360	1296
Hot metal, kg	2900		2470		2410		2350		2290	
Lime powder, kg	240									
Coke powder, kg	30		40							

Total lime consumption, 240 kg
Total coke consumption, 70 kg
Hot metal treated, 12,500 kg

tent of 17 pct, is an unusually high figure, which would hardly be attained in practice if the sulphur content is at the same time to be lowered to values below 0.025 pct.

At low silicon contents, the carbon as reducing agent also takes part in the reaction. At high sulphur contents an appreciable evolution of carbon monoxide can be noticed even at quite high silicon contents, such as 0.3 to 0.4 pct. This was the case, for instance, with the last described heats, KR-41 and KR-42. With lower ingoing sulphur contents, however, the silicon content must be under 0.05 pct, if the carbon is to take part in the reaction to any appreciable extent.

Figs. 8 to 10 show three heats, in which the carbon has, for the most part, taken over the role of silicon as reducing agent. It might be possible to deduce from these results that equilibrium between saturated carbon and silicon is about 0.05 pct Si at 1300°, and at 1200° about 0.02 pct.

In heat KR-40 (Fig. 10) the manganese content of the pig iron was 1.2 pct. This was maintained practically unchanged throughout the heat, which is partly shown by the low manganese content in the end lime. This reveals that the manganese content of the pig iron did not appreciably promote desulphurization, either as a reducing agent, or on account of its sulphur binding capacity.

Due to the rapid rotation of the furnace during the process, small drops of iron are formed that are mixed up in the lime charge and remain in the end lime. It is therefore advisable to allow the lime powder to pass a magnetic, dry separator after the process, by which the main part of the iron can be recovered. The grains can either be returned to the process or put back in the blast furnace, if other uses are not possible. Certain means have been found of counteracting the generation of these grains in the end lime. An addition of soda to the lime has a favorable effect in this respect. If the addition is not too great, at most about 10 pct of the amount of lime, the soda does not appear to exert any great influence on the sticking tendency of the lime charge.

In Fig. 11 the result of an experiment with an addition of soda is recorded. The rate of reaction has

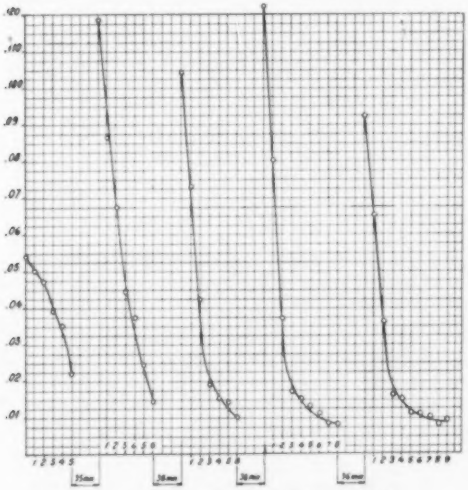

Fig. 12—Heat KR30, KR31, KR32, KR33, and KR34.

Fig. 13—Heat KR16 and KR18.

KR16 (solid line) — Hot metal, 2370 kg; C, 3.2 pct; 20 rpm. Lime powder, 38 kg; Mn, 0.5 pct. Coke powder, 19 kg; Si, 0.32 to 0.30 pct; P, 1.5 pct.
KR18 (broken line) — Hot metal, 2500 kg; C, 2.9 pct; 40 rpm. Lime powder, 40 kg; Mn, 0.5 pct. Coke powder, 20 kg; Si, 0.57 to 0.54 pct; P, 1.8 pct.

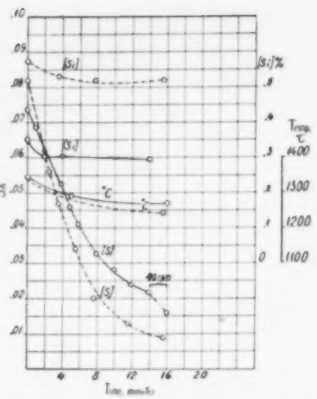

been very slightly higher than normal, which can be ascribed to a certain catalytic influence from the soda addition. As will be seen from Table II, the sodium content in the lime charge has, however, been practically completely volatilized.

It is of course desirable from many points of view that the necessary quantity of lime be as low as possible. Even if the saving in lime is in itself of no great economic significance, a lower addition of lime has, among other things, the advantage of a smaller temperature drop in the hot metal. It seems that the amount of lime required for desulphurization of a pig iron from, for instance, 0.100 to 0.010 pct need not be expected to exceed 1 pct of the weight of the pig iron. When so small an amount of lime is used, however, the lime charge will form a thin and therefore comparatively stationary layer on the iron bath during the rotation, whereby the mixing effect may deteriorate. In order to be able to maintain a sufficiently high layer of lime in the furnace, without increasing the percentage of lime, it can be arranged so that the lime is retained in the furnace, when the hot metal is discharged, and re-employed for one or several subsequent operations. The result of an experiment along these lines is found in Fig. 12 and Table V.

Altogether 12.5 tons of pig iron was introduced in five stages, i.e., about 2.5 tons at a time. The whole amount of lime, 240 kg, was introduced at the beginning, thus corresponding to practically 10 pct of the lime present in the furnace at each treatment. Apart from the first operation, which was carried out at much too low a temperature due to the cooling effect of the large quantity of lime, in all cases the desulphurization went down to low contents very rapidly. Particularly remarkable is the rapid and complete sulphur removal even in the last experiment, although the lime in this case must, from the beginning of the treatment, have had a sulphur content of about 5 pct.

The method here described of sulphur removal in stages may be found suitable especially when very large quantities of hot metal are to be handled. Admittedly there does not appear to be any technical objection to building large furnaces, e.g., up to 100 tons capacity, but it may be preferable to employ a smaller furnace and repeat treatment several times, thus putting the lime to better use. The total treatment time need not be much longer on that account, as each part of the operation would proceed more rapidly.

As the tests have shown that desulphurization can be effected in only a few minutes, it is certainly also possible to arrange for continuous treatment by passing the hot metal at a suitable speed through a long rotating drum, in which the lime has either been placed in advance or is fed simultaneously. This procedure has been tested on small scale with promising results. Possibly an even better result can be achieved, if the lime is made to pass in countercurrent to the iron by means of suitable sluice arrangements. To judge from the test results in Fig. 12, however, there does not appear to be much to be gained from employing the countercurrent principle.

The rate of rotation of the furnace can have a decisive influence on the result. In most tests 40 rpm has been used, as previously mentioned, and at this rate satisfactory results were always obtained. A few tests were made at 20 rpm, but desulphurization was not nearly so efficient.

Fig. 13 shows two heats, one at 40 rpm and the other at 20 rpm. Otherwise the treatment of the two heats was identical. At the lower rate, desulphurization proceeded far too slowly, but when the speed was increased to 40 rpm at the end of treatment, a more rapid desulphurization immediately occurred. Which rate is most suitable in different cases is hard to determine in advance, but there have been no practical difficulties whatever at the rotation speeds described. Mixing of course can be performed more efficiently by giving the furnace a form which deviates from the circular. Model experiments, for instance, have shown that the agitation effect can be greatly increased by making the furnace section slightly oval.

Finally it may be mentioned that a number of tests have been made with the addition of certain other substances to the lime charge in an attempt to improve the result still further. The addition of aluminum and calcium carbide has been tried in certain tests to increase the reducing effect. The additions resulted in a reduction of silicon to the pig iron from the furnace lining, but the desulphurization efficiency deteriorated, principally because of an increased tendency of the lime charge to form balls. Dolomite can be used as a substitute for lime, but lime is to be preferred.

The end lime obtained always has a high sulphur content, as the analyses show. The silica content has also been comparatively high in several of the tests, but if the attempt is made to avoid all unnecessary silicon oxidation and other introduction of silica, it can be kept at a low level in relation to the CaO + CaS content. The end lime should therefore be a valuable addition for sintering of iron ore, where this takes place. Most of the sulphur content then escapes in gas form.

Summary

The method described has been carried out in a 3-ton rotating furnace at Domnarfvet Iron and Steel Works. It has the following characteristic features.

The molten iron is brought into intimate contact with powdered burnt lime by treatment in a rapidly rotating furnace.

The treatment has to take place under strongly reducing conditions, which can be made in a simple way by keeping the furnace tightly closed during the process.

The lime must be maintained in the fine powdered form during the whole treatment, which is made possible both by avoiding a temperature in excess of 1350° to 1400°C and by the addition of a suitable amount of coke powder to the lime.

By carrying out the process in this way it has been found possible to desulphurize hot metal down to very low sulphur contents in a few minutes even from relatively high starting values, and with a high lime yield.

Owing to the short time of treatment and the small lime addition necessary, the drop of temperature during the process has been very small, with the consequence that external heat supply and its associated disadvantages have been avoided.

The rotation speed normally has been the maximum of the furnace, 40 rpm. Lower speeds have also been tried, but with unsatisfactory results. No inconveniences with the high speed have been encountered.

The advantages of the method can thus be summarized as follows:

1—A very rapid and complete desulphurization can be obtained. The sulphur content can in one operation be brought down to very low values even with high starting content in the iron and with high lime yield.

2—The desulphurizing material is cheap and can be obtained everywhere. After the treatment it may be used for other purposes.

3—No formation of molten slag is taking place, with the result that attack on the lining of furnace and ladle is avoided. The furnace is of a simple construction and can advantageously be lined with ordinary fire clay.

4—The iron during the tapping can be separated easily from the lime.

5—No dangerous smoke is formed during the process.

The first plant for commercial production is in operation at Surahammar Iron and Steel Works, Surahammar, Sweden.

References

[1] Best: Desulphurizing for the Bessemer Process. *Blast Furnace and Steel Plant* (March 1950).

[2] Wood, Barrett, and Holbrook: Desulphurization of Pig Iron with Calcium Carbide. *Trans.* AIME (1940) **140**, p. 87.

[3] Rehder: Magnesium Additions and Desulphurization of Cast Irons. *American Foundryman* (September 1949) p. 33.

[4] Tigerschiöld: Desulphurization of Cast Iron. U.S.A. patent 2,243,514.

[5] Newell, Langner, and Parsons: New Methods of Ladle Desulphurizing Pig Iron. *Foundry Trade Journal* (1948) p. 165.

[6] Griffith: Desulphurization of Pig Iron. AIME *Open Hearth Proceedings* (1949) **32**, p. 43.

[7] Eichholz and Behrendt: Entschwefelung von Thomasroheisen. *Stahl und Eisen* (1940) p. 677.

[8] Bading and Krus: Entschwefelung von Roheisen mit gebranntem Kalk in Stürzelberger Trommelofen. *Stahl und Eisen* (1938) p. 1457. (See also *Iron Age* (April 1942) p. 46.)

[9] Oelsen: *Stahl und Eisen* (1938) p. 1460.

[10] Fischer and Cohnen: Der Einfluss des Kohlenstoffgehaltes auf die Entschwefelung von Eisenschmelzen durch einer Kalk-Flusspat-Tiegel in Hochfrequenzofen. *Archiv f. das Eisenhüttenwesen* (1950) p. 355.

[11] Fornander: Kalling-Domnarfvet Process at Surahammar Works. This issue, p. 739.

Kalling-Domnarfvet Process at Surahammar Works

by Sven Fornander

An account is given of the way in which a new process for desulphurization of hot metal is carried out at a Swedish blast-furnace plant. In the process powdered burnt lime is used as a desulphurizing agent in a rotary furnace. Results are given.

IN a paper by Kalling et al.* the fundamentals of a new process for desulphurization of hot metal using powdered burnt lime as a desulphurizing agent were outlined. The purpose of the present paper is to give a brief account of the way in which this process is being carried out in practice by Surahammars Bruks AB, Sweden, and of the results obtained.

The hot metal from the blast furnace is tapped into a ladle of 15 tons capacity and transferred to a rotary furnace, a simplified drawing of which is given in Fig. 1. The rotary furnace has a total length of about 160 in. and an outside diameter of the rings of about 130 in. The furnace is in a horizontal position, with its rings placed on four rollers, and can be rotated by a driving mechanism at various speeds of up to 34 rpm. The rotary furnace and its driving mechanism were designed and constructed at Surahammar.

The hot metal is charged into the rotary furnace through the opening to the left in Fig. 1. See Fig. 2. An addition is then made to the furnace consisting of finely ground burnt lime amounting to 2 pct of the weight of the hot metal as well as 0.5 pct of coke breeze. After the additions are made, the furnace is sealed to the atmosphere by means of two lids and set in rotary motion at a rate of 34 rpm. The sulphur in the hot metal is rapidly absorbed by the lime added, the time of treatment needed is normally 30 min. The process is then stopped, the lid is removed, and the furnace is lifted up by a crane and used as a tilting ladle for pouring the metal into the pig-iron molds, Fig. 3.

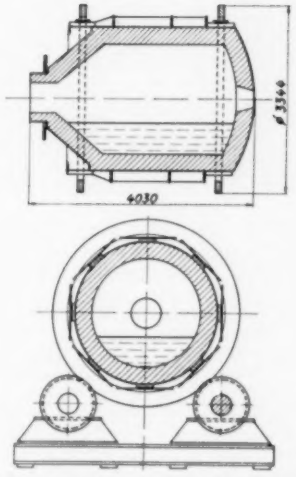

Fig. 1—Rotary furnace for desulphurization.

Process Metallurgy

The hot metal charged into the rotary furnace has a composition which usually lies within the following limits: C, 3.70 to 4.10 pct; Si, 0.80 to 1.80; Mn, 0.40 to 0.80; P, 0.025 to 0.030; and S, 0.060 to 0.200. Figs. 4 and 5 give examples of the changes in hot metal composition taking place during the treatment in the rotary furnace. As will be seen from the diagrams, the sulphur content of the metal decreases very rapidly during the first 10 min of treatment from about 0.100 to about 0.020 pct S. During the following 20 min, the sulphur content goes down slowly to about 0.005 pct S. The carbon and silicon contents of the metal decrease by about 0.10 pct each during the treatment. The manganese and phosphorus contents remain unchanged. Thus, if the process is started with an iron of the composition given above, the finishing composition of the metal usually lies within the following limits: C, 3.60 to 4.00 pct; Si, 0.70 to 1.70; Mn, 0.40 to 0.80; P, 0.025 to 0.030; and S, 0.002 to 0.020.

The chemical reaction taking place during the process can be written:

$$2\,FeS(\text{in liquid Fe}) + Si(\text{in liquid Fe}) + 2CaO(\text{solid}) = 2CaS(\text{solid}) + SiO_2(\text{solid}) + 2Fe(\text{liquid})$$

S. FORNANDER, Member AIME, is Research Manager, Surahammars Bruks Aktiebolag, Surahammar, Sweden.

Discussion on this paper, TP 3110C, may be sent, 2 copies, to AIME by Oct. 1, 1951. Manuscript, March 7, 1951. St. Louis Meeting, February 1951.

* B. Kalling, C. Danielsson, and O. Dragge: Desulphurization of Pig Iron with Pulverized Lime. This issue, p. 732.

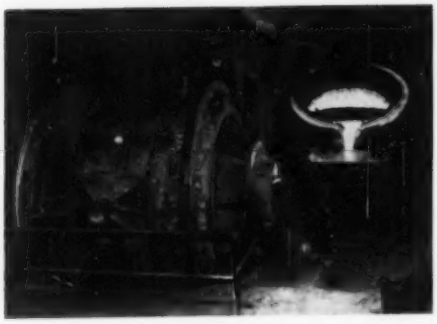

Fig. 2—Charging of the furnace.

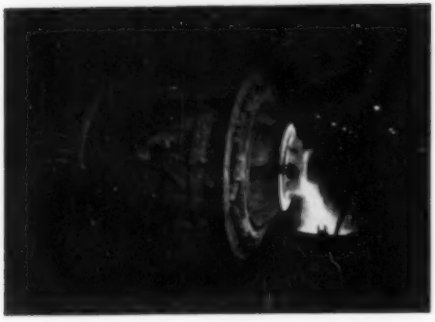

Fig. 3—Tapping of the furnace.

The sulphur in the hot metal is absorbed by the burnt lime under formation of calcium sulphide, and the oxygen liberated from the calcium oxide combines with silicon, which is in solution in the iron, forming silica. Thus silicon is the reducing agent in the process. From the reaction formula it is obvious that the process is promoted by reducing conditions. It is quite likely that during the process the silica formed combines with lime in the form of a calcium silicate.

It may probably be said that the process is a unique one in the metallurgy of iron and steel with regard to the fact that a solid phase is reacting with a liquid metal. No liquid slag is formed during the process. After finished treatment of the iron, the "lime" (the reaction product) still is in the form of a fine powder.

The fact that the reaction takes place in the surface of contact between the solid lime and the liquid metal is of practical consequences. In order that the reaction should proceed rapidly, the surface of contact must be large. This is the reason why the lime used is in the form of a powder and also, why a rotary furnace is required in the process. In the rotary furnace an intimate contact is brought about between the liquid metal and the solid lime. Within each of the two phases an efficient stirring action is produced.

Table I. Screen Analysis of Lime Powder

Sieve Opening, mm	Percent
Over 1.5	4.0
1.5-1.0	2.6
1.0-0.6	5.4
0.6-0.2	5.8
0.2-0.2	14.3
0.2-0.1	19.1
0.1-0.06	17.4
Under 0.06	31.4

Factors Affecting Desulphurization

The first trials on a commercial scale with the process described above were made in May 1950 at the blast-furnace plant of Surahammars Bruks AB. In the first trials the sulphur content of the hot metal treated was not uniform from cast to cast. Since then, however, various measures have been adopted with the result that during the last few months the process has been applied continuously and given uniform results. The following factors have been found to have an influence upon the results obtained.

Lime Character: The lime powder used should be as pure as possible, the most harmful impurities being silica, carbon dioxide, and water. Detailed investigations on the influence of the impurities upon the desulphurization have yet not been carried out, but as rule of thumb it can be said that if the silica content of the burnt lime exceeds 5 pct, the sulphur content of the metal treated will be higher than 0.010 pct S. During the last few months of operation, the lime used has been burnt at the plant in a small and simple furnace with blast-furnace gas as a fuel. The burnt lime is stored in an air-tight container before being ground. The screen analysis of the lime powder used is given in Table I.

Oxidation: If good desulphurization is to be obtained, it is of particular importance that the furnace chamber is not exposed to oxidizing conditions either during the desulphurizing treatment of the metal or during the time elapsing between the treatments. During the first few months of operation, the furnace was heated between the treatments by a gas burner, which was inserted through a central opening in one end of the furnace. During this period of time, the desulphurization was incomplete and the results varied considerably. Prob-

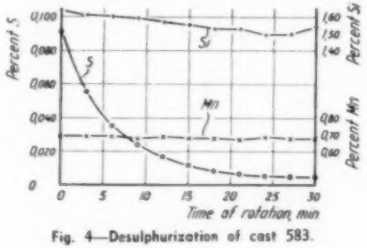

Fig. 4—Desulphurization of cast 583.

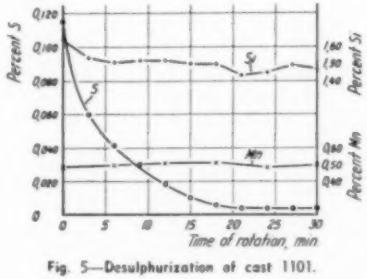

Fig. 5—Desulphurization of cast 1101.

ably this was due to the fact that small amounts of iron sticking to the furnace wall were oxidized by the combustion gases from the burner, the oxides formed decreasing the desulphurizing effect of the lime. However, when the furnace was sealed to the atmosphere both during the treatments and the time elapsing between them, the method gave fully satisfactory results.

If oxidizing conditions prevail in the furnace during the treatment, the lime powder forms balls when the furnace is in rotary motion. In unfavorable cases, these balls can be up to 8 in. diam. Balls will form also, if blast-furnace slag enters the furnace. The occurrence of balls is an indication of incomplete desulphurization. Difficulties of this kind have not appeared during the last few months of operation.

Furnace Lining: The furnace lining consists of an inside 6 in. course of ordinary fireclay bricks and two outside courses of insulating bricks having a thickness of 2½ in. each.

Table II. Results of Desulphurization of 300 Casts

Before Treatment S, Pct	No. of Heats	After Treatment S, Pct	No. of Heats
0.020-0.050	51	0.002-0.010	216
0.051-0.100	127	0.011-0.020	60
0.101-0.150	87	0.021-0.030	21
0.151-0.200	25	0.031-0.040	3
0.201 and over	10		
Average 0.095	300	0.009	300

After a treatment of a cast in the furnace, the inside wall is covered with a thin adhering layer, consisting of a mixture of lime powder, coke breeze, and solidified iron. The layer grows thicker with every cast treated, and when 50 or 60 casts have been treated, the layer is so thick that the furnace room is insufficient. The layer is removed by heating the furnace wall to a high temperature, about 1400°C, by means of an oil burner. However, the heating must be made with care in order to prevent the fireclay bricks from being damaged.

At present a new rotary furnace is under construction, and this unit will be provided with a basic lining. The unit will be used when the existing one is under relining.

Hot Metal Temperature: The temperature of the hot metal was determined at various stages of the process by means of quick-immersion thermocouples. The following figures refer to normal conditions: In blast-furnace runner, 1400°C (2550°F); in ladle when full, 1340°C (2440°F); in rotary furnace before treatment, 1320°C (2400°F); and in rotary furnace after 30 min treatment, 1250°C (2280°F).

Table III. Results of Three Days' Operation

Cast No.	Weight of Metal, Tons	S in Iron, Pct Before Treatment	S in Iron, Pct After Treatment	Desulphurization, Pct
545	11	0.068	0.005	92.7
548	8	0.068	0.003	95.6
549	12	0.068	0.005	92.7
550	12	0.068	0.011	83.8
552	9	0.091	0.009	90.1
553	11	0.082	0.009	89.0
556	11	0.105	0.007	93.4
558	12	0.100	0.005	95.0
559	12	0.100	0.006	94.0
560	13	0.086	0.005	94.2
561	11	0.086	0.008	88.4
562	11	0.086	0.004	95.3
563	11	0.077	0.004	94.8
564	11	0.077	0.004	94.8
565	10	0.070	0.004	94.3
566	11	0.059	0.008	86.5
569	10	0.100	0.006	94.0
570	11	0.100	0.005	95.0
571	12	0.086	0.005	94.2
Average	11	0.082	0.006	92.7

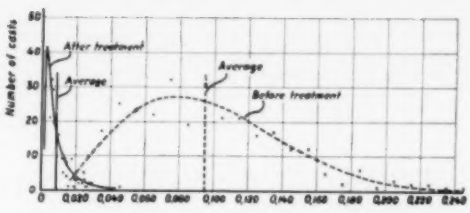

Fig. 6—Results of desulphurization of 300 casts.

Thus the temperature loss during the whole process amounts to about 150°C (270°F). A hot-metal temperature of 1250°C (2280°F) is sufficient for pouring the metal into the molds. However, at Surahammar's blast-furnace plant, the iron is partly used for the manufacture of ingot molds, and for this purpose a temperature of 1250°C is too low. In the near future, the hot metal will be tapped from the blast furnace directly into the rotary furnace. This procedure will probably reduce the temperature loss to 70° or 80°C, and it is intended to use the hot metal treated in the rotary furnace in the ingot mold foundry. Variations in the temperature of the hot metal seem to have no influence upon the desulphurization obtained.

Results Obtained

In order to illustrate the desulphurizing effect that can be expected if the process is used in practice, a collection has been made of the results obtained in the treatment of the last 300 casts from the blast furnace, Table II and Fig. 6.

As will be seen from the table the majority of the casts (249 out of 300) had a sulphur content before treatment of 0.051 pct S or more. The sulphur content in the casts treated was 0.010 pct S or less in 216 cases and 0.020 pct S or less in 276 cases.

The average sulphur content of the iron cast from the blast furnace was 0.095 pct S during the period in question. The average sulphur content of the iron treated in the rotary furnace was 0.009 pct S. This implies that on an average 90.5 pct of the sulphur in the hot metal was removed in the rotary furnace.

Table III shows results of three days' operation. The values confirm that the desulphurizing process described above is an effective one.

Summary

An account is given of the results obtained by Surahammars Bruks AB, Sweden, with a new process for desulphurization of hot metal from a blast furnace. In the process the hot metal is treated with finely ground powder of burnt lime in a rotary furnace. About 90 pct of the sulphur in the metal is removed in the process, which after some months of experience has been found simple and inexpensive in operation.

Acknowledgments

The author is indebted to Einar Ameén, Managing Director, and Yngve Törneman, Technical Director, of Surahammars Bruks AB, for their kind permission to publish the results presented in this paper.

A Corrected CO/CO_2 Ratio for Blast Furnaces

by Sid T. Killian

The utilization of the reducing power of blast-furnace gas can be estimated by applying two rectifying calculations to the gas analysis. A resulting corrected CO/CO_2 ratio varies inversely with furnace production. Directions for calculating the corrected CO/CO_2 ratio are given, and a corrected CO/CO_2 ratio is compared with actual furnace production.

THE inadequacy of the normally accepted CO/CO_2 ratio as a measure of blast-furnace performance and furnace efficiency was discussed following the presentation of the paper by H. F. Dobscha.* In this outstanding example of careful observation on large scale blast-furnace operation, the changes occurring with beneficiated ores were: 1—A net gain in tonnage of 21.2 pct. 2—A decrease in net coke of 15.3 pct. 3—A decrease of 1.9 pct in the CO/CO_2 ratio. In this great change in furnace performance, the CO/CO_2 ratio proved itself worthless.

The discussion of the inadequacy of expressing furnace performance and efficiency by the CO/CO_2 ratio led indirectly to the calculations forming the basis of this paper. At that time Dr. T. L. Joseph said: "We must consider difference in CO_2 from the stone in the two cases when we talk about the ratios of CO/CO_2." This statement is used for the second of the two CO/CO_2 ratio corrections forming the basis of this paper.

The research work in attempting to find out why the furnaces could operate so differently with practically the same CO/CO_2 ratio lead not to the answer sought but, after a shift to the gaseous phase in the research work, the proof that the normal CO/CO_2 ratio was outmoded and a new corrected ratio should replace it. To be of any value, any new corrected ratio should express approximate furnace efficiency and give an idea of practical furnace performance to be expected. This the normal CO/CO_2 ratio has failed to do. However, in the absence of anything better, some credence has been attached to the normal CO/CO_2 ratio. As far as the writer can ascertain, the present paper is the first attempt to change or improve the normally accepted index of

S. T. KILLIAN is in Johnstown, Pa.

Discussion on this paper, TP 3111C, may be sent, 2 copies, to AIME by April 1, 1952. Manuscript, Jan. 15, 1951; revision, May 24, 1951. New York Meeting, February 1952.

* H. F. Dobscha: Effect of Sized and Sintered Mesabi Iron Ores on Blast-furnace Performance. *Proc.* Blast Furnace, Coke Oven and Raw Materials Committee, AIME (1948) 7, p. 49.

Table I. Various Gas Analyses with One Corrected Ratio

Volume CO	29.50	29.00	28.50	28.00	27.50	27.00	26.50
Volume CO_2	11.00	11.50	12.00	12.50	13.00	13.50	14.00
Volume H_2	00.00	00.50	01.00	01.50	02.00	02.50	03.00
Volume N_2	57.50	57.50	57.50	57.50	57.50	57.50	57.50
Volume Total	98.00	98.50	99.00	99.50	100.00	100.50	101.00
Percent CO	30.10	29.44	28.79	28.14	27.50	26.87	26.24
Percent CO_2	11.22	11.68	12.12	12.56	13.00	13.43	13.86
Percent H_2	0.00	0.51	1.01	1.51	2.00	2.49	2.97
Percent N_2	58.67	58.38	58.08	57.79	57.50	57.21	56.93
Percent Total	99.99	100.01	100.00	100.00	100.00	100.00	100.00
CO	30.10	29.44	28.79	28.14	27.50	26.87	26.24
ratio							
CO_2	11.22	11.68	12.12	12.56	13.00	13.43	13.86
Ratio	2.683	2.521	2.375	2.240	2.115	1.994	1.893

furnace efficiency. A corrected CO/CO_2 ratio is proposed as the future criterion of the blast furnace.

Corrections Necessary

The calculations involved in figuring the corrected CO/CO_2 ratio are performed in two main steps. The first calculation involves placing the gas analysis on a hydrogen-free basis. The second calculation consists of deducting the amount of CO_2 evolved by the flux from the gas analysis.

The first correction is almost mandatory, if the CO/CO_2 ratio is to be continued as a measure of furnace efficiency, inasmuch as it can be figured so easily. The second step however should be adapted to furnace records and must be used carefully to render true service.

When the gas analysis is placed on a hydrogen-free basis, the CO/CO_2 ratio expresses the ratio of the total unused reducing power to the used reducing power with the flux CO_2 included as used reducing power. The normal CO/CO_2 ratio attempted to give a ratio of unused to used reducing power, but the resulting ratio could vary considerably due to the exclusion of the hydrogen content of the gas and the inclusion of the flux CO_2 in the ratio. However when both corrections are made, a close expression of the ratio of unused reducing power to used reducing power in the gaseous phase is obtained. Neither correction should be omitted if any resulting corrected CO/CO_2 ratio is to be used as a representation of furnace efficiency or furnace performance.

Chemical Principles of the First Correction

Gas Analysis on a Hydrogen-Free Basis: The gas-analysis correction of placing the gas analysis on a hydrogen-free basis in no way involves furnace reactions, but merely corrects the gas analysis for a variable which can change the actual gas analysis and the ratio calculated from it.

The equation:

$$CO_2 + H_2 \rightleftarrows CO + H_2O$$
$$1 \text{ vol} + 1 \text{ vol} \rightleftarrows 1 \text{ vol} + 1 \text{ vol}$$

shows how the interaction of the CO_2 and the H_2 with the CO and the H_2O can change the ratio. As the H_2 increases, the CO_2 is increased at the expense of and in the same amount as the CO is decreased. Similarly, as the H_2 decreases, the CO_2 is decreased in the same amount as the CO is increased. The variable of the hydrogen content of the gas is eliminated by changing the gas analysis so that the reaction goes to completion in the direction that eliminates the hydrogen. The two components of the CO/CO_2 ratio are then left for the calculation. Thus the correction merely involves the subtraction of the percentage of hydrogen in the gas from the percentage of carbon dioxide in the gas and the simultaneous addition of the percentage of hydrogen in the gas to the percentage of carbon monoxide in the gas. In other words, every 1 pct of H_2 in the gas analysis will drop the CO_2 percentage exactly 1 pct and simultaneously raise the CO percentage exactly 1 pct when the correction is made.

In order to show clearly how the hydrogen content of the gas changes the normal CO/CO_2 ratio, Table I has been calculated. In it all volumes are changed entirely by the reaction:

$$CO_2 + H_2 \rightleftarrows CO + H_2O$$

in steps of 0.50 volumes of each of the reacting gases. All the analyses and CO_2 ratios in Table I are identical when placed on the hydrogen-free basis. All given an identical corrected ratio of 2.683.

Second Correction

Gas Analysis with Flux CO_2 Deducted: While the CO_2 evolved from the stone is an important factor in furnace performance and furnace efficiency, from an overall viewpoint, the calcining of the stone consists of the addition of CO_2 (completely oxidized carbon) to the gaseous phase. The inclusion of this CO_2 tends to give an illusion that a greater oxidation of carbon is taking place than really occurs. In other words, the inclusion of this CO_2 tends to hide the real efficiency.

The second correction of taking the gas analysis on a hydrogen-free basis and deducting the CO_2 evolved from the flux is best accomplished by equating the total carbon input with the total carbon output. The easiest means of computing this carbon balance should be to use 24 hr as the basis with no calculations involving the wind blown. The blowing media used vary widely in efficiency and quite often the wind ordered differs markedly from the actual wind delivered. Thus complex stoichiometric calculations are avoided and practically all calculations can be made from furnace records.

Carbon Balance: The carbon input normally includes: 1—net coke carbon to furnace excluding fractions not charged, 2—carbon in stone, and 3—carbon in scrap. The carbon output normally includes: 1—CO in gas, 2—CO_2 in gas, 3—carbon in total amount of pig iron produced, 4—carbon in flue dust and sludge, 5—coke messes, 6—rolls and slips, 7—carbon in the gas as coke particles and as stone particles, and 8—hydrocarbons in the gas.

All the items should be observed and calculated before assuming them to be negligible. For a complete carbon balance, every item should be checked.

Illustration of Calculation: The corrected CO/CO_2 ratio is illustrated in the calculation of a furnace using 1.00 fuel (80 pct net carbon) with 300 lb of

Table II. Calculation of Corrected CO/CO_2 Ratio

Input	
Coke, net lb carbon per ton pig	1600.
Stone, net lb carbon per ton pig	100.
Input, net lb carbon per ton pig	1700.
Output	
Pig iron, net lb carbon (4.2 pct)	84.
Flue dust, net lb carbon	30.
Gas, net lb carbon by difference	1586.
Output, net lb carbon per ton pig	1700.

Fraction carbon in gas from flux = 100/1586 = 0.0631
In gas analysis from flux = (30.10 + 11.22) × 0.0631 = 2.61 pct
In gas analysis not from flux = 11.22 — 2.61 = 8.61 pct
In gas from furnace reactions = 8.61 pct

Table III. Blast Furnace Performance

Ores Used	Normal	Beneficiated	Difference, Pct
Iron production, net tons per day	1324	1605	+21.2
Coke, net lb per ton	1782	1510	−15.3
Flue dust and sludge, lb per ton	284	227	−20.1
Silicon in iron	0.91	0.87	
Sulphur in iron	0.030	0.030	
Wind blown, cfm at 60°F and 30 in. Hg	83,604	85,651	+ 2.4
Moisture in blast, grains per cu ft	2.3	2.3	
Analysis of top gases, pct			
CO	26.57	26.17	
CO_2	12.33	12.40	
H_2	2.30	1.60	
CH_4	0.13	0.13	
N_2	58.67	59.70	
Ratio CO/CO_2	2.15	2.11	

flue dust (10 pct carbon). Carbon in the flux is taken at 100 lb per ton of pig iron. The gas analysis equating the various CO/CO_2 ratios to a hydrogen-free basis is used for this calculation, Table II.

Thus with the gas analysis illustrated and containing 2.00 pct hydrogen, the normal CO/CO_2 ratio is 2.115. The CO/CO_2 ratio on a hydrogen-free basis is 2.683. The corrected CO/CO_2 ratio on a hydrogen-free basis with the correction for the CO_2 evolved from the flux is 3.496.

Comparison of Corrected CO/CO_2 Ratio with Furnace Performance

The method involved in calculating the corrected CO/CO_2 ratio from the Dobscha-United States Steel furnaces differs markedly from the preceding calculations, which are given as the method to be used normally. In the following calculations, the corrected CO/CO_2 ratio is calculated from the carbon distribution in the gas, since complete figures for calculating by the carbon-balance method were not included in the paper. Then the old ratio and the corrected CO/CO_2 ratio are compared with the furnace production. In other words, the old and the corrected CO/CO_2 ratios are being checked against the performance of the Dobscha-United States Steel furnaces.

For the benefit of any who have not read Dobscha's paper,* the following is taken directly from it: "A program was carried out involving two modern identical blast furnaces with a hearth diameter of 27 ft 6 in. A mixture of beneficiated ores was charged on one furnace for a continuous period of one month and normal ores charged on the other furnace. During an interim period of one month, the burdens were reversed and the test was continued for a two-month period. Coke, flux, and miscellaneous burdening materials were of the same quality on both furnaces; the quantities of the latter being identical except for deviations dictated by operating practice." Table III is taken from p. 55 of the 1948 *Proceedings* of the Blast Furnace, Coke Oven and Raw Materials Committee, AIME.

Table IV. Carbon in Top Gases per Ton Iron

	Normal Ores	Beneficiated Ores
Carbon in CO, lb	1024	838
Carbon in total CO_2, lb	475	397
Carbon in flux CO_2, lb	113	76
Fraction of total carbon in the gas evolved from the flux	113/(1024 + 475)	76/(838 + 397)
Percentage of the total carbon in the gas evolved from the flux	7.54	6.15

Table V. Percentage CO_2 from Flux

Gas Analysis, Hydrogen Free	Normal Ores	Beneficiated Ores
CO in gas, pct	28.87	27.76
CO_2 in gas, pct	+ 10.03	+ 10.80
Total CO + CO_2, pct	38.90	38.56
	× 0.0754	× 0.0615
CO_2 from flux, pct	2.93	2.37

Gas Ratio Calculated to a Hydrogen-Free Basis

The gas ratio calculated to a hydrogen-free basis follows:

Normal Ores	Beneficiated Ores
$\frac{26.57 + 2.30}{12.33 - 2.30}$	$\frac{26.17 + 1.60}{12.40 - 1.60}$
28.87 / 10.03	27.76 / 10.80
2.878	2.562

Corrections for Flux CO_2 in Gas Analysis

The second correction in calculating the corrected CO/CO_2 ratio is to deduct the CO_2 evolved by the flux from the total CO_2 in the gas analysis on a hydrogen-free basis. In this case it is performed in three steps. 1—The fraction or percentage of total gas carbon which comes from the flux carbonate is calculated. 2—This fraction or percentage then is expressed as percentage CO_2 in the gas analysis. 3—The percentage CO_2 from the flux is subtracted from the CO_2 in the gas on a hydrogen-free basis. The corrected CO/CO_2 ratio can then be calculated.

Percentage of Total Gas Carbon from Flux Carbonates: The first step in tying in the CO_2 from the flux with the CO_2 in the gas analysis is to calculate the percentage of the carbon in the gas which comes from the flux. The figures for that calculation follow.

The carbon distribution in the top gases in Dobscha's furnaces is given in Table IV.

Gas Analysis Percentage of CO_2 from Flux Carbonate: The second step in tying in the CO_2 from the flux with the CO_2 in the gas analysis is to find the percentage of CO_2 which came from the flux expressed in gas analysis percentage. This calculation

Table VI. Correction of Gas Analysis for CO_2 from Flux

Gas Analysis, Hydrogen Free	Normal Ores	Beneficiated Ores
CO_2 in gas, pct	10.03	10.80
CO_2 from flux, pct	− 2.93	− 2.37
CO_2 from furnace reactions, pct	7.10	8.43

Table VII. CO/CO_2 Ratio vs. Production

	Normal Ores	Beneficiated Ores	Comparative Ratio
Production, tons pig iron	1324	1608	0.8240
CO/CO_2 ratio, regular gas analysis	2.1546	2.1105	1.021
CO/CO_2 ratio, corrected for H_2	2.878	2.562	1.123
CO/CO_2 ratio, corrected for H_2 and flux CO_2	4.066	3.280	1.235
Inverse ratio of pig iron production			1.212

is given in Table V. These figures show the direct amount in gas analysis percentages of CO_2 evolved from the flux. In other words, these calculated percentages of CO_2 are to be deducted from the total percentage of CO_2 on a hydrogen-free basis.

Gas Analysis Correction for CO_2 Evolved from Flux: The calculations correcting the gas analysis on a hydrogen-free basis for the CO_2 evolved from the flux is given in Table VI.

The corrected CO/CO_2 ratio then is:

28.87	37.76
7.10	8.43
4.066	3.293

The above figures show the corrected CO/CO_2 ratio calculated on a hydrogen-free basis with the correction for the CO_2 evolved from the flux.

The ratios 1.235 and 1.212 in Table VII show how closely the ratio of the corrected CO/CO_2 ratios compares with the ratio of iron production in an inverse manner. Mathematically:

$$\text{Production} \times \text{Corrected Ratio} = \text{A Constant}$$

As shown in Table VIII, the product of the corrected CO/CO_2 ratio and the iron production differ by approximately 2 pct when the normal and beneficiated ores are compared. In other words, the product of the corrected CO/CO_2 ratio and the iron production should approximate a constant when similar furnaces are compared or when conditions are changed on the same furnace.

This constant might be one of the benefits of the corrected CO/CO_2 ratio as a tool of production. However, the constant might not be a straight-line function of the inverse production and checking should be done before it can be accepted as such. For normal changes on one furnace, the variation from a straight line would be negligible. At this time, the constant is used only to illustrate the close tie-in of the corrected CO/CO_2 ratio with the corresponding furnace production.

Summary and Conclusions

1—A corrected CO/CO_2 ratio is proposed as an index of blast-furnace performance. It is the CO/CO_2 ratio of the blast-furnace gas on a hydrogen-free basis with the flux CO_2 deducted from the gas analysis. On iron of similar analysis, it gives a closer expression of the efficacy of the gasified carbon of the fuel in removing the oxygen from the ore.

2—The calculations involved in figuring the corrected CO/CO_2 ratio should be as accurate as possible. Since the answer is in the form of a ratio, the methods used in obtaining all figures should be the same in all cases. They should not vary unless the same answer is obtained.

3—The corrected CO/CO_2 ratio probably will show changes in furnace performance quicker than any other method available. Given similar conditions of furnace performance, a 24-hr lapse should show whether any change is or is not beneficial. One decided advantage is that a satisfactory comparison can be made on a furnace when changing ore, fuel, flux, slag volume, moisture in the wind, products, or any variable affecting furnace performance such as filling, shape of combustion zone, or top pressure. In short, factors changing furnace performance can be correlated quicker and better due to the more accurate ratio used for comparison.

4—If large changes are made in iron analysis, additional corrections might be necessary to allow for oxygen removed from reduced elements entering the iron. A distinct possibility exists that with due allowance for heats of reaction, almost all furnace products could be placed on a comparable basis.

5—No attempt has been made to introduce too many additional corrections at this time. Subsequent evaluation of the Killian-Joseph corrections should suggest them if needed. For instance the oxygen evolved from the metalloids has not been considered. It is felt that this paper covers sufficient territory at this time.

6—Attention is again called to the fact that the basis for the second correction was first proposed by Dr. T. L. Joseph in his discussion on why the normal CO/CO_2 ratio failed.

7—The corrected CO/CO_2 ratio as here applied to the furnace performance used, deviates 1.84 pct from being an accurate ratio, compared with a deviation of 17.12 pct with the normal ratio. In the instance used, the corrected CO/CO_2 ratio shows one-ninth the divergence of the normal ratio if applied directly to furnace production. Roughly speaking it is nine times as accurate.

8—Attention is again called to the fact that the normal CO/CO_2 ratio changed from 2.15 to 2.11 in going from normal to beneficiated ores, while the corrected CO/CO_2 ratio changed from 4.066 to 3.293. Thus the normal CO/CO_2 ratio was not only worthless, but in this specific case must be considered as definitely misleading. While the normal CO/CO_2 ratio tends to hide it, the corrected CO/CO_2 ratio expresses the change in the reducing power of the gas which has been utilized by the furnace.

9—In order to have the second portion of this work presented in as clear form as possible, the 0.13 pct CH_4 in the furnace gases from the normal and beneficiated ores has been omitted from the calculations. A correction similar to, but more complicated than, placing the gas on a hydrogen-free basis would have been necessary. Thus every volume of CH_4 in the gas would require the deduction of three volumes of CO_2 and the simultaneous addition of four volumes of CO when the correction is made. With 0.13 pct CH_4 in both gases, this correction was omitted.

10—The corrected CO/CO_2 ratio is not a perfect comparison of the working of a furnace and must not be considered as such. It is presented as the simplest and most practical numerical expression of the efficiency of the blast furnace in terms of relative efficiency and relative production.

Table VIII. Comparison of Normal and Beneficiated Ores

	Normal Ores		Beneficiated Ores
Product	1324 x 4.066		1605 x 3.293
Product	5384.4		5285.3
Average		5334.9	
Difference		99.1	
Difference/Average		1.84%	

The above product of the corrected CO/CO_2 ratios and the iron production approximate a constant with a swing of 1.84 pct.

Product	1324 x 2.1549		1605 x 2.1105
Product	2853.1		3387.4
Average		3120.3	
Difference		534.3	
Difference/Average		17.12%	

The above product of the normal CO/CO_2 ratios and the iron production approximate a constant with a swing of 17.12 pct.

Burst Phenomenon in the Martensitic Transformation

by E. S. Machlin and Morris Cohen

The martensite reaction in single crystals and polycrystals of 70 pct Fe-30 pct Ni alloys is shown to be autocatalytic in nature, producing bursts of transformation during cooling. The temperature of the first burst of transformation, called M_b, occurs below M_s in these alloys. Experiments were devised to test the athermal embryo and strain embryo theories of martensite nucleation. The results indicate that internal strains, either within the virgin austenite or around existing martensitic plates, control the nucleation process in these alloys. Furthermore, the growth of martensitic plates is not limited by the attainment of an elastic balance with the austenitic matrix, but by the occurrence of plastic deformation at the martensite boundaries which interferes with the propagation mechanism.

IN an investigation of the martensitic habit in single crystals of a 69 pct Fe-31 pct Ni alloy,[1] it was observed that about 25 pct of the austenite transformed during subatmospheric cooling within the time-interval of an audible click. This event proved quite spectacular: The shock wave sent out from the specimen freely suspended on a thread in the refrigerating liquid was occasionally sufficiently intense to shatter the Dewar container and to separate the toluene column in the immersed thermometer. The present investigation was undertaken to determine the kinetics and mechanism of this "burst" type of martensitic reaction.

The analyses of the alloys studied are given in Table I. The composition of the single crystal specimens is designated by alloy A, while the polycrystalline specimens were made of alloys B and C as noted in the text. The single crystals were prepared in a vacuum furnace, using a modified Bridgman technique. Most of these crystals were homogenized by holding for 24 hr at about 1300°C just after solidification. However, it may be emphasized here that the degree of homogenization was not a controlling factor in the subsequent experiments, inasmuch as specimens having different degrees of homogenization yielded the same results. All of the single crystals were fully austenitic as slowly cooled to room temperature.

An illustration of the burst phenomenon is given in Fig. 1, which shows oscillograms of electrical resistivity and temperature vs. time during the continuous quenching of 1/16 in. wire specimens (alloy B) in a dry ice and acetone bath at −77°C. There are at least two observable bursts in this case, as indicated by the sharp decreases of resistance accompanying the sudden formation of substantial quantities of martensite. The thermal arrest during the quench probably corresponds to the larger burst. Usually the bursts are followed by more or less progressive transformation during continuous cooling.

E. S. MACHLIN, formerly with Massachusetts Institute of Technology, is now with the School of Mines, Columbia University, New York, and M. COHEN, Member AIME, is with the Department of Metallurgy, Massachusetts Institute of Technology, Cambridge, Mass.

Discussion on this paper, TP 3127E, may be sent, 2 copies to AIME by Dec. 1, 1951. Manuscript, April 10, 1951. Detroit Meeting, October 1951.

This paper is based on a thesis submitted by E. S. Machlin in partial fulfillment of the degree of Doctor of Science in Metallurgy to the Massachusetts Institute of Technology, September 1950. The investigation was sponsored by the Office of Naval Research under Contract N5-ori-07814, Task No. XIV, Designation No. NR-031-142.

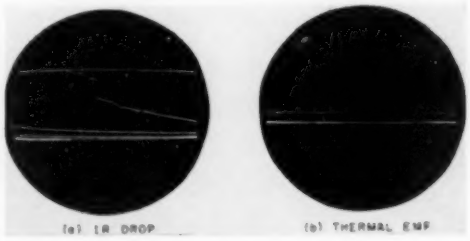

Fig. 1—Oscillographs recorded during quench of a 70.5 pct Fe-29.5 pct Ni alloy into a CO_2 and acetone bath at −77°C. Each horizontal interval corresponds to 0.1 sec. a—Change in resistivity of specimen. b—Change in temperature of specimen. In each case, top line corresponds to +25°C, bottom line corresponds to −77°C.

It will also be noted that the resistance continues to decrease after the specimen has reached the bath temperature. This isothermal change denotes the formation of martensite at constant temperature, and will be the subject of another paper.

Examination of fiducial scratches on the surface of a transformed single crystal has shown[2] that the scratches in adjoining nonparallel martensitic plates are usually bent in opposite directions, as though one plate forms in such a way as to relieve the matrix stresses set up by the adjacent plate. This, together with some of the results described in ref. 1,

Table I. Compositions of Alloys Studied, in Percent

Alloy	Ni	C	N	Mn	Si	P	S	Cr
A	31±0.3	0.048	0.027	0.003	0.56	0.007	0.002	
B	29.5±0.2	0.036	0.02	0.19	0.09	0.008	0.006	
C	19.99	0.52		0.37	0.47	0.010	0.015	0.04

led to the tentative concept that a cooperative action exists which provides the impetus for much of the transformation that appears during the burst. The following series of experiments were performed in order to test this idea.

Cooperative Nature of the Burst

Two adjacent disks, 1/8 in. thick x 3/4 in. diam, were cut from a single austenite crystal of alloy A using a jeweler's saw. One of the disks was then cut into 15 parts. Then 12 of the latter pieces and the second disk were austenitized (stress relieved) at 600°C for 30 min and water quenched to room temperature. The temperatures at which the first burst of transformation appeared were determined for

each specimen by cooling below room temperature. The temperature of the first burst of transformation has been termed M_b to distinguish it from the well-known M_s temperature, where the first plates of martensite form. The results given in Table II show that M_b varied from −54° to −78°C* and that the whole disk transformed within 2° of the highest burst temperature found for the separate parts. Furthermore, the amount of martensite produced at M_b in the disk and in each of the individual pieces was of the order of 20 to 30 pct. Before examining the significance of these findings, another series of experiments that yielded similar results will be described.

Martensite range curves were determined for bulk specimens of polycrystalline alloys B and C as well as for powders (200 mesh) comprised of filings from these alloys. The purpose of subdividing the polycrystalline specimens into powders was the same as for the single crystal experiments, namely, to eliminate the cooperative effect, if such existed, and to reveal the distribution of transformation among the individual polycrystalline particles. This principle has already been applied to a study of solidification of liquids by Turnbull.[6]

The procedure involved in obtaining the range-curve data was as follows: The specimens were sealed in evacuated Vycor tubes, then austenitized at 1200°C for 1 hr, quenched in water to room temperature (after which the tubes were broken), and finally cooled to a sequence of subzero temperatures in the martensite range. The amounts of martensite in both the massive and powdered specimens were determined by lineal analysis.[4]

Results for alloy C** are given in Fig. 2. Alloy B yielded similar effects. The range curve for the bulk polycrystalline specimens exhibits a sharp increase in transformation at M_b, followed by an increase in the amount of transformation (possibly stepwise) with decreasing temperature. The range curve for the powdered samples discloses a gradual increase in amount of transformation with decreasing temperature, without the initial sudden jump found for the bulk specimens. Thus, the subdivision effect reported in Table II for the single crystals is also displayed by the polycrystalline specimens: That is, not all the powder transformed the same amount at the same temperature, but instead there were particles that burst at different temperatures. The number of particles that burst increased with decreasing temperature, until all the particles had undergone a burst.

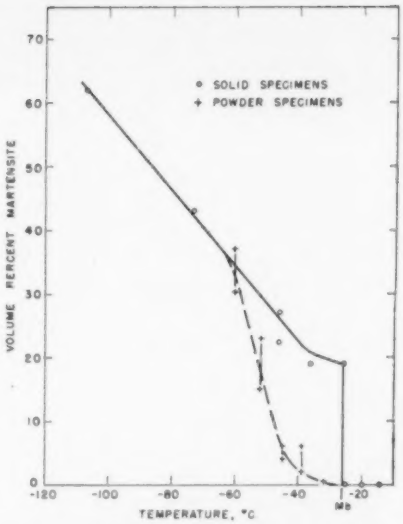

Fig. 2—Martensite range curves of bulk and powdered polycrystalline specimens of 79.5 pct Fe-20 pct Ni-0.5 pct C alloy.

It was found that the physical subdivision of the whole into parts resulted in less total transformation and a smaller number of martensitic plates, at a given temperature, than would have been obtained for the unseparated whole. The separation eliminates the elastic coupling between the isolated parts, so that no stresses are transmitted from one part to another. Hence, it may be concluded that a cooperative effect exists in the phenomenon of the burst. The formation of a small number of plates, presumably beyond some critical amount or in some critical way, appears to catalyze the further transformation which occurs cataclysmically as a burst in less than 10^{-4} sec.[6]

The burst phenomenon cannot be explained either by the existence of a large number of embryos that are slightly subcritical just above the burst temperature, in accordance with the athermal nucleation concept of Fisher, Hollomon and Turnbull,[6] or by the sudden isothermal formation of a large number of embryos at the burst temperature, in accordance with the thermal nucleation concept of Kurdjumow.[7] This is deduced from the fact that very few of the subdivided parts of the crystals or powders of polycrystals undergo the burst at the same temperature. If it should be argued that the temperature variation of the burst was caused by the samples being too small to be representative and/or that the nickel

Table II. Effect of Subdividing Single Crystals of 69 Fe-31 Ni Alloy upon Martensite Burst Temperature

All specimens were austenitized at 600°C after being cut to size.

Specimen	M_b, °C
Single crystal disk (⅛ in. thick × ⅞ in. diam)	−36
Position from Single Crystal Disk	
No. 1	−54
No. 11	−56
No. 2	−62
No. 4	−68.4
No. 8	−70
No. 15	−71.5
No. 12	−76.5
No. 7	−77.5
No. 14	−77.5
No. 3	−78
No. 6	−78
No. 9	−78

* This variation of burst temperatures was not due to segregation as shown by subsequent experiments.

** The range curve for the bulk specimens of alloy C was determined by S. A. Kulin.

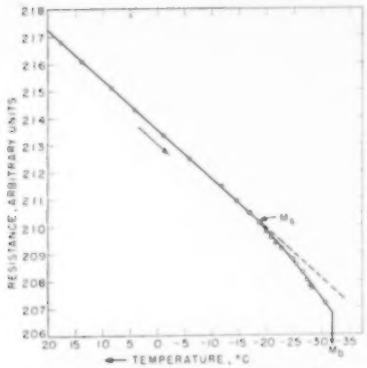

Fig. 3—Electrical resistance as a function of temperature during subcooling of polycrystalline 70.5 pct Fe-29.5 pct Ni alloy.

content of the alloy varied from part to part, these alternatives may be ruled out by the following:

1—The samples in the single crystal experiments were at least $\frac{1}{8}$x$\frac{1}{8}$x$\frac{1}{8}$ in. and hence should have been large enough to contain a representative distribution of embryos. Also the martensitic plates formed therein were not perceptibly controlled by the specimen size, judging from the fact that they were no smaller than in the $\frac{1}{8}$ in. thick x $\frac{3}{4}$ in. diam specimen.

2—The nickel content did not indicate any correlation with the burst temperature as shown by the data of Table IIIa. These results were obtained with a new set of specimens subjected to the same procedure as for the specimens corresponding to Table II.

Relation of M_s to M_d

Two properties were measured in an attempt to determine whether any transformation took place above M_s: 1—intensity of magnetization, and 2—electrical resistance. The sensitivity of these methods as used were 1 pct martensite and 0.05 pct martensite, respectively, and hence only the electrical resistance results will be presented here.

The electrical resistance specimens were 1/16 in. diam wires of alloy B. Austenitizing was carried out at 1100°C for 30 min in an atmosphere of prepurified nitrogen, followed by oil quenching to room temperature. A Kelvin double bridge was used for determining the electrical resistance, while the specimens were cooling to subatmospheric temperatures.

Measurements of electrical resistance as a function of temperature yielded curves similar to the one shown in Fig. 3. It is to be noted that the points deviate from a straight line in the temperature range just above M_s. This result provided the first definite clue that some martensite formation may take place above M_s.

It seemed worthwhile at this point to determine whether the deviation of the line above M_s represented a reversible or irreversible process. Accordingly, an electrical resistance vs. temperature curve was run on a specimen to 5° below the temperature at which the curve became nonlinear, but still above the burst temperature. There the cooling was stopped, the specimen was reheated, and resistance measured as a function of temperature. The heating curve did not retrace the nonlinear curve, but remained quite parallel to and below the linear part of the cooling curve. Thus, the deviation from linearity was not reversible. In fact, subsequent metallographic observations demonstrated conclusively that some martensite actually formed above M_s. The extent of such transformation was estimated by means of a set of curves of electrical resistance vs. percentage of martensite (each curve corresponding to a given temperature) where lineal analysis was employed for calibration purposes. Using these master curves with linear extrapolation to 0 pct martensite, it was found that the maximum amount of martensite formed above M_s was approximately 0.5 pct in the alloys under consideration. Repetition of these experiments using precision-length techniques yielded the same results.

Table III. Effect of Nickel Content and Plastic Deformation on Burst Temperature of 69 Fe-31 Ni Single Crystals

a—Austenitized at 600°C

Ni, Pct	Position in $\frac{7}{8}$ In. Diam Disk	M_b, °C
30.98	Center	−60
30.99	Periphery	−65.5
31.02	Periphery	−74.5
31.09	Periphery	−60.8
31.22	Midway	−50
31.38	Periphery	−59.5
31.39	Periphery	−64
31.43	Periphery	−70
31.43	Periphery	−60.8

b—Plastically Compressed Above 60°C

Ni, Pct	Degree of Deformation, Pct	M_b, °C
30.74	10	−48
31.02	20	−46
31.09	30	−44.5
31.12	30	−45
31.18	30	−44

With these results, it was clearly demonstrated that M_d is higher than M_s for the specific cases investigated. It is conceivable, however, that M_d may equal M_s under different experimental conditions.

Visual Study of Martensitic Plates

The martensite formed above M_s appears primarily at the surface of single austenite crystals and at the grain boundaries of polycrystals. In the former case, the martensitic plates exist entirely within the austenite crystal (except where they meet the air surface) and do not require grain boundaries or

Fig. 4—Upheaval of martensite plate on surface of single crystal of 69 pct Fe-31 pct Ni alloy that had been electropolished prior to subcooling. Note slip in austenite around plate. Oblique illumination. X1500.

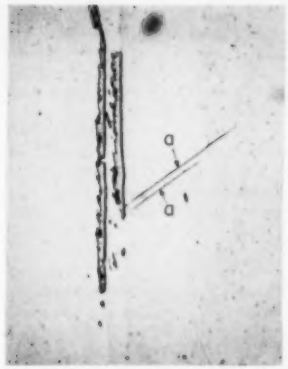

a—Plates *a* formed after electropolishing surface, etching with Marble's reagent and requenching to −50°C. Surface then electropolished and electroetched prior to taking micrograph.

b—Plate *b* formed after requenching to −50.5°C. Surface then electropolished and electroetched.

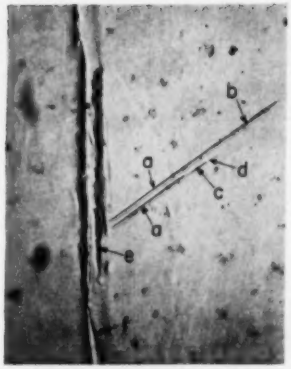

c—Plate *c* formed after requenching to −51°C. Surface then electropolished and electroetched. On requenching to −51.5°C, plates *d*, *e*, and *f* were formed. Micrographs were then taken without any further surface preparation.

Fig. 5—Martensite plates formed above M_s at surface of single crystal. Vertical plates formed on initial quench to −52°C. Oblique illumination. X750.

other plates to inhibit their growth. For example, the plate of Fig. 4 was examined not only on the surface shown but after repeated electropolishing and etching to reveal the complete three-dimensional surroundings. The plate extended below the surface for a distance roughly equivalent to its length in the plane of the surface, and there were no grain boundaries or nearby martensitic plates to prevent further growth. In addition, it was observed that subboundaries (veining) and slip lines in the single crystals did not act as noticeable barriers to the growth of martensitic plates. Fig. 4 provides an illustration of a plate that propagated through a veining boundary. These findings are contrary to the postulation that the plates should grow out to boundaries at which resisting stresses can develop.[5]

It was noted in these metallographic studies that the ends of the martensitic plates acted as favored (but not exclusive) nucleation sites for the formation of plates which came into being on further cooling (still above M_s). Sequences of this phenomenon are shown in Figs. 5 and 6. The vertical plates of martensite in Fig. 5a were formed at the surface of a single crystal of austenite during a quench to −52° ± 0.5°C. This surface was then electropolished at room temperature and lightly etched with Marble's reagent*** to disclose the etched pattern of the plates. The specimen was then quenched to −50°C, 2°C higher than previously,† and the thin plates marked "a" appeared. The micrograph in Fig. 5a was taken at this stage.

As a next step, the same specimen was quenched to −50.5°C, and the plate marked *b* appeared. This is shown in Fig. 5b which was taken after re-electropolishing and electroetching at room temperature. Despite the fact that plate *b* seems to be an extension

*** Copper sulphate 20 g, concentrated hydrochloric acid 100 ml, water 100 ml, ethyl alcohol 200 ml yields a modified Marble's reagent which is very sensitive to the presence of martensite in this alloy.

† The martensitic transformation in single crystals is quite sensitive to the state of the surface, which accounts for the increment of transformation during the second cooling.

a—Same as Fig. 5e. Micrograph taken at X375 in order to include all of plate *f*.

b—Same as Fig. 5e. Plates *g* and *h* were formed at same time as plates *d*, *e*, and *f*. Micrograph taken at top of original vertical plate. Compare with Fig. 5b. X750.

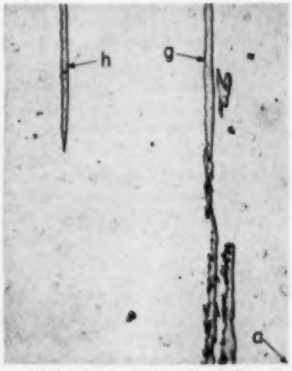

c—After taking micrograph of Fig. 6b, specimen was lightly etched with Marble's reagent to bring out transformation. Note that lines at sides of plates *g* and *h* have disappeared indicating they are slip lines. X750.

Fig. 6—Martensite plates formed above M_s at surface of single crystal. Note that, as in Fig. 5, new plates have appeared at ends of existing plates. Oblique illumination.

Fig. 7—Micrograph of a previously electropolished surface after a burst of transformation has occurred. Lines shown in micrograph are slip lines. Bending of slip lines indicates that slip occurred prior to the transformation in such regions. X500.

of plate *a*, there is actually a discontinuity between the two, and *b* must be regarded as a new plate that was nucleated at the end of the existing plate.

The micrograph in Fig. 5c was taken on the same specimen after quenching to −51°C, electropolishing, electroetching, and requenching to −51.5°C, with no further surface treatment. Plate *c*, which is etched in Fig. 5c but not present at all in Fig. 5b, formed during the quench to −51°C. Plates *d*, *e*, and *f* of Fig. 5c, plates *e* and *f* of Fig. 6a and plates *g* and *h* of Fig. 6b are visible as upheavals, and hence must have formed during the last quench to −51.5°C. The discontinuous nature of the propagation of successive plates is evident. It is also clear that the later plates may or may not have the same orientation as the existing plates, and that the ends of prior-formed plates are activated regions for the nucleation of new plates. (The different orientations merely represent various permutations of the habit ± {259}‡). These findings are in accord with the previous observation that the burst phenomenon is an autocatalytic reaction.

Examination of Figs. 4 and 6b reveals the presence of fine lines in the austenite around the martensitic plates. In order to determine whether these lines were due to slip or to upheavals of tiny martensitic platelets, the specimen of Fig. 6b was lightly etched with Marble's reagent. The resulting structure, shown in Fig. 6c, indicated no trace of the fine lines, and therefore the latter could not have been caused by martensitic platelets. It may be concluded that the lines were slip lines due to plastic deformation of the austenite. This supports the suggestion of Kurdjumow[7] that plastic flow around the martensite produces a loss of coherency and limits the size of the plates. By the same token, the plate thickness is not controlled by a balance between the driving free energy and elastic restraining energy, and calculations[2] based on such an hypothesis can have little significance, at least for Fe-base alloys in which large transformation strains occur.

Additional evidence contrary to the energy-balance hypothesis was obtained from a study of martensitic plate-thickness vs. temperature in the martensite range, which demonstrated that existing plates do not increase in thickness during cooling. According to the above hypothesis,[2] the plates should thicken by 33 to 700 pct (depending on the extremes in thermodynamic data found in the literature[5, 10]) on cooling between −20° and −90°C, but no such change was found. In a few instances, the apparent thickness increased due to the formation of platelets alongside the original plate, but this took place stepwise with decreasing temperature.

The specimen of Figs. 5 and 6 was finally cooled to −64°C where the burst occurred. A typical region of the resulting upheavals is given in Fig. 7. Clearly, the average thickness of plates formed in the burst is many times larger than that of plates formed above M_s. This signifies that during the burst the stresses developed at the side-boundaries of the transforming plates are much less for a given plate thickness (and therefore the plates can grow much thicker before plastic flow occurs) than in the case of plates forming above M_s. The foregoing conclusion seems reasonable in the light of the fact that there are at least four different permutations of the ± {259} habit‡ which tend to move the adjacent austenite in about the same direction when martensite forms cooperatively along these planes.[1]

Fig. 7 also shows numerous slip lines which are bent where they cross martensite plates. This indicates that extensive slip may take place during the burst in some regions prior to the formation of martensite there. Moreover, it means that such slip lines are not sufficiently strong barriers to prevent the propagation of martensite.

Two important questions are raised by the above results: 1—What is the criterion for the triggering of the burst? 2—What is the significance of the fact that the ends of existing plates are favored nucleation sites for new plates?

A tentative answer to the first question is obtained from consideration of some additional experiments. It has been found that room temperature alteration of the state of the surface of a single crystal after quenching to a given subatmospheric temperature may induce a burst on requenching to that same temperature. Furthermore, it has been noticed that bursts may occur isothermally in polycrystalline specimens after some time at a subzero temperature (held constant within ± 0.2°C), either with or without a measurable change in resistivity occurring prior to the burst at that temperature. It has also been observed that rapid quenching of 1/16 in. diam polycrystalline wires into a bath at −77°C can depress M_s by about 20°C as compared to slow cooling. These findings indicate that the triggering of the burst does not take place at a characteristic temperature for the alloy at hand, but is sensitive to other experimental variables.

In the light of ref. 1, a possible criterion for the onset of the burst is that a number of plates, which have the same direction of adjacent austenite motion and which bound the same region of austenite, must be nucleated almost simultaneously. Under these conditions, it appears that stresses are transferred to other austenite regions where new plates can be activated. Undoubtedly, the momentum of the process helps to increase these stresses. The activation can occur either at existing regions of strain or even in previously strain-free regions, if sufficient stress of the proper direction is developed.

This mechanism for producing the burst leads to the observed structure-sensitivity of the burst tem-

‡ In systems having the ± {225} habit, the degree of cooperation as measured by the number of austenite directions of motion within the same solid angle used for the ± {259} case, is roughly about one half that for the latter.

perature because the probability of activating an embryo is affected by the prior state of internal strain at the embryo. The mechanism also provides for autocatalytic action through the dynamic as well as static stresses developed by the cooperative displacements. Consequently, it can be predicted that bursts will not occur as markedly in other systems where the crystallography of the transformation happens to permit less cooperation than in these alloys. For example, the cooperative effect is not so great for systems with {225}$'$ habits as for systems with {259} habits. Thus, it may be expected that the burst phenomenon will not be so prominent in ordinary steels as in these Fe-Ni alloys.

Let us now consider the significance of the preferential nucleation of martensite above M_s at the ends of isolated martensite plates. It is very likely that the magnitude of the internal stress in the austenite bounding an isolated martensite plate is largest at the rim of the plate. The consequence of this situation can be interpreted in at least two ways. According to the theory of martensite nucleation via athermal[5] embryos of the martensitic phase, stress should act to decrease the critical size of the embryos, and hence stressed regions should be favored sites for nucleation. However, inasmuch as the volume of the highly stressed region about the rim of an isolated martensite plate is extremely small, either the critical size would have to be an exceptionally sensitive function of stress, or the concentration of athermal embryos would have to be very high. An alternate interpretation, according to the theory of martensite nucleation via strain embryos,[2] is that the region of internal stress at the rim becomes an embryonic region of large strain and appropriate direction of strain to nucleate additional martensite. Although there does not appear to be any way of positively distinguishing between these theories from the data obtained so far, an important conclusion can be drawn; that is, whether the new martensite is nucleated at existing martensite rims by athermal embryos or not, the nucleation there is controlled by the internal strains and not by the distribution of athermal embryos. Inasmuch as any real specimen contains many internal strains, this conclusion might be generalized to include internal strains other than those at the martensite plates. It is important to note here that the plates appearing above M_s are not nucleated exclusively by the prior-formed martensite. This applies to the plate in Fig. 4 and, of course, to the original plates in Fig. 5.

Further experimental verification of the above deduction as applied to the general transformation is given in the next section.

Athermal Nucleation

The aspect of the athermal nucleation theory that was checked was the supposed role of an equilibrium statistical-mechanical distribution of martensitic embryos at the austenitizing temperature. According to this concept, the amount of martensite produced for a given temperature in the martensitic range, and for a given grain size, is a function of the martensitic embryo distribution, and hence of the austenitizing temperature. Thus, one series of specimens was subjected to the cycle illustrated in Fig. 8a, another to the cycle of Fig. 8b, and a third to the cycle of Fig. 8c. In all instances, the heating

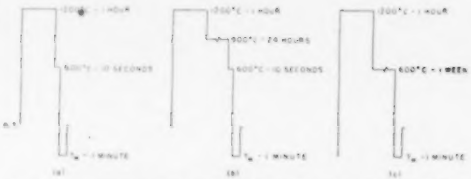

Fig. 8—Temperature-time cycle to determine effect of austenitizing temperature on martensite range curve.

for 1 hr at 1200°C "set" the grain size which did not change during the subsequent treatments. In case b, the temperature was then lowered to 900° for 24 hr to establish an embryo distribution characteristic of this temperature. In case c, the holding time at 600°C was for one week. In cases a and b, the quench to room temperature was interrupted momentarily at 600°C so that the final quenching stresses would be the same in the three series, after which the subzero transformation was determined immediately. Direct quenching was also conducted from 1200° and 900°C to room temperature, but there was no effect on the results and hence the interruption at 600°C was actually not a factor.

The results obtained from these experiments, given in Fig. 9, show that the amount of transformed phase is independent§ of the austenitizing temperature, grain size being maintained constant. It may therefore be concluded that athermal embryos of the martensitic phase, if they exist at all, do not activate the martensitic transformation in these Fe-Ni alloys. It may further be inferred, from the generality of the concept, that this negative conclusion also applies to other materials.

Experiments Relating to Strain Embryos

Having demonstrated that the possible existence of statistical distributions of martensitic embryos in the austenitic phase was irrelevant to the problem under consideration, it appeared worthwhile to investigate the alternate suggestion that the embryos for the martensitic reaction are comprised of regions of internal strain in the austenite[2] (e.g., accidental lattice disturbances or dislocations). On this basis, it would be predicted that a cold-worked sample should undergo transformation at a higher temperature than a non-cold-worked sample. Moreover, specimens as cut from a single-crystal ingot should transform at higher temperatures than similar specimens after stress relieving. Because plastic deformation of polycrystals may introduce barriers to the transformation as well as the higher energy strain embryos being sought, it was decided to per-

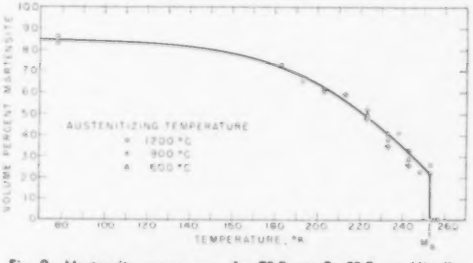

Fig. 9—Martensite range curve for 70.5 pct Fe-29.5 pct Ni alloy. Austenitizing temperature varied according to cycles in Fig. 8.

§ The exact agreement of some of the data in Fig. 9 is considered fortuitous.

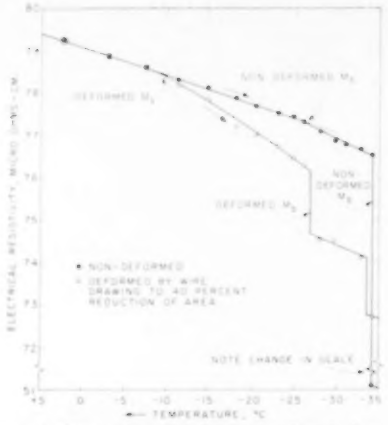

Fig. 10—Effect of plastic deformation performed above M_s (60°C) upon subsequent martensite transformation in 70.5 pct Fe-29.5 pct Ni alloy.

form these experiments first with single crystals of alloy A.

Several cube specimens, $\frac{1}{4}$ in. on a side, were cut from a single crystal of austenite, then stress relieved at 600°C, and refrigerated to ascertain the M_s temperatures. Similar stress-relieved specimens were compressed by 10 to 50 pct at a temperature above M_d†† (~ 60°C), and the M_s temperatures were determined. Two single-crystal ingots were used. The results with specimens from one ingot (Table III) showed that the average M_s temperature was raised from −63° to −46°C by the cold working, and that the inherent spread in these values was markedly reduced. For specimens from the second ingot, the average M_s temperature was raised from −55° to −47°C by cold working.

Further verification was obtained in the following way: A $\frac{1}{8}$ in. cube single crystal was cooled to as low a temperature as possible, called the reference temperature, above M_s. Then the specimen was heated above the M_d temperature, compressed 10 pct and cooled back to the reference temperature. If no burst occurred during this cooling, the specimen was heated back above M_d, compressed further, and the cycle repeated to determine whether a burst would ultimately occur on cooling to the reference temperature. The results definitely proved that plastic deformation above M_d raises the burst temperature. For example, compression in the range of 10 to 35 pct raised M_s 4.5° to 7.5°C above the reference temperature from its previous level below the reference temperature.

Another manifestation of this phenomenon was shown by comparison of the M_s values for specimens as cut from the single-crystal ingot with those for similar specimens after stress relieving at 600°C. The average M_s of the annealed crystals was 15°C lower than the average M_s of the as-cut crystals. The strain-embryo concept is consistent with all these experiments on single crystals.

Previous investigators[10, 17] have reported that plastic deformation of polycrystalline alloys usually has a stabilizing effect on the subsequent transformation. This trend is contrary to the results just described for single crystals. In order to ascertain the reason for the anomaly, experiments were performed with polycrystalline wires of alloy B in the following way. Several wires, 1/16 in. diam, were first austenitized in an evacuated Vycor tube at 1100°C for 30 min, then quenched in water to room temperature. Reductions in area of 0, 10, 20, 30, and 40 pct were achieved by drawing the wires through dies while kept above M_d (~ 60°C). Immediately after this plastic deformation, each specimen was subcooled, and the electrical resistance measured as a function of the temperature.

The results of these experiments can be summarized as follows: With increasing amounts of plastic deformation (up to 40 pct reduction in area) above M_d: 1—M_s was raised progressively (40 pct reduction in area corresponded to an increase in M_s of about 17°C). 2—M_s was first increased slightly, then decreased. 3—At temperatures somewhat below M_s of the nondeformed specimen, the amount of transformation was less, the greater the amount of deformation. These characteristics are illustrated in Fig. 10, which shows the temperature-resistivity curves for specimens having 0 and 40 pct reduction in area subsequent to austenitizing.

The above relationships clearly indicate that there are two opposing effects of prior plastic deformation on the martensite transformation during subsequent cooling. The first effect is an increase in the magnitude of the submicroscopic internal strains, and thus martensite can be nucleated at higher temperatures. This accounts for the fact that M_s increases with the extent of plastic deformation. The second effect of plastic deformation, appearing primarily in polycrystalline alloys, is to "subdivide" the grains into smaller units as a result of the inhomogeneous nature of the deformation (the formation of kink bands and deformation bands provides an effectively finer grain size). Because the average length of plate formed from a given strain embryo is smaller in the "subdivided" grains, the volume of martensite per activated embryo would be expected to decrease with increasing plastic deformation. Hence, even though there is an increase in the number of embryos activated at any given temperature, the actual amount of transformation may be less. The net result of plastic deformation is a combination of these two opposing effects. A somewhat similar conclusion has been reached by Kurdjumow[18] in his studies on the influence of prior plastic deformation on the subsequent isothermal martensite transformation.

The two opposing trends also bear directly on the M_s temperature. As M_s is raised by plastic deformation, M_s is also raised; but with increasing amounts of deformation as applied to polycrystals, the partitioning of the austenite caused by inhomogeneous deformation makes it progressively more difficult for the burst to occur. Consequently, M_s then begins to drop. This characteristic may be regarded as a grain-size effect, which is discussed in the next section.

Constraint and Grain Size Effects

The explanation of the burst phenomenon herein presented predicts that if restraint is provided at the boundaries of the single crystal then the burst temperature should be depressed, but not necessarily the M_s temperature. To test this prediction the following experiments were performed: Single crystals of alloy A, 1/16×$\frac{1}{8}$×$\frac{1}{8}$ in., which had been serrated on their faces to provide a good mechanical bonding

†† M_d is the temperature above which austenite is not converted into martensite by plastic deformation.[13]

surface and etched for 1 hr to remove the cold-worked surface layer, were stress relieved at 600°C and mounted in bakelite with a 1/16x⅛ in. polished face exposed. Control specimens from adjacent positions in the single-crystal ingot were also mounted in bakelite in exactly the same manner, then removed carefully from the bakelite by cutting the bakelite away from the sides with a jeweler's saw. The M_s temperatures of the control specimens were determined by immersing in cold baths at lower and lower temperatures until the burst took place. This was detected audibly by the "click" as well as by the visible evolution of bubbles in the bath due to the heat of transformation. Also after heating back to room temperature, the martensite could be seen by microscopic examination on the polished surface.

Before the burst temperatures of the bakelite-constrained specimens were determined, a run was conducted to establish the time required for the specimen to reach within 1° of the bath temperature. It was found that about 3 min were required. Accordingly, the bakelite-constrained specimens were kept in the bath for 6 min in order to insure that the bath temperature was reached. Exactly the same methods were used for observing the burst in the bakelite-constrained specimens as in the case of the control specimens. The results obtained are given in Table IV.

It is evident that the bakelite-constraint caused a lowering of the burst temperature. The extent of depression of M_s ranged from about 15° to 20°C. (The good reproducibility of burst temperatures for the control specimens was undoubtedly due to the fact that the mounting in bakelite introduced some strain into the specimens.)

According to the ideas presented here to account for the burst phenomenon, there should be small amounts of martensite in the constrained specimens at a temperature above their M_s and below the M_s of the control specimens. When painstaking care was taken in preparing and examining the surfaces of the specimens, such small amounts of transformation were detected.

A further prediction stemming from this picture of burst formation is that, if two different sizes of specimens are constrained, the smaller specimens should burst at the lower temperature. This follows from the fact that with a given surface constraint, more resistance to the burst transformation is generated in the smaller specimen than in the larger one, other things being equal. To test this consequence, two sizes of single crystals were mounted in bakelite. One was ¼x¼x¼ in. and the other 1/32x⅛x⅛ in. The average M_s values so obtained were: −38.5°C (free control specimen), −50.5°C (large constrained specimen), and −55°C (small constrained specimen).‡‡

Constraint may also be achieved if the crystal is surrounded by other crystals in the form of a polycrystalline aggregate. In order for the chain of transformation to continue, the austenite along the

Table IV. M_s Values for Constrained vs. Free Specimens

M_s, °C		
Free Control	Constrained	Difference, °C
−51.5	−67.5	16
−50	−70	20
−51	−70	19
−51	−72	21

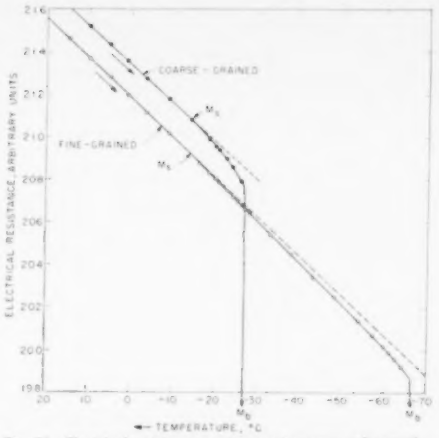

Fig. 11—Electrical resistance vs. temperature curves for specimens having A.S.T.M. No. 4-5 and A.S.T.M. No. 9 grain size. Alloy of 70.5 pct Fe-29.5 pct Ni.

side of the transforming plate must be able to move. If it is constrained by a rigid material such as bakelite, then a chain of transformation, once started, would be quickly stopped by the resistance to motion developed at the boundaries, and the temperature would have to be decreased to overcome this resistance. In a similar way, grains of different orientation at the boundaries of the crystal can act as constraints, from which it follows that the burst temperature should decrease with decreasing grain size, even though the M_s temperature may not be appreciably affected.

To check the predicted effect of grain size, electrical resistance measurements were made on 1/16 in. diam wires of alloy B having grain sizes of ASTM No. 9 and ASTM No. 4-5. The first series of specimens was austenitized at 760°C for 20 min and the second series was austenitized at 1100°C for 1 hr. All of the specimens were oil quenched to room temperature. The results of these measurements are given in Fig. 11.

Two points are immediately clear. One is that the M_s of the fine-grained material is about 40°C lower than that of the coarse-grained material. The other is that the deviation from linearity in the resistance vs. temperature curves starts at about the same temperature in both cases. Subsequent metallographic investigation showed that the deviation from linearity is associated with the formation of martensite plates above M_s.

This phenomenon was checked in still another way. Length measurements made during subcooling and reheating in a high precision linear coefficient of expansion apparatus[14] agreed unambiguously with the electrical resistance determinations in disclosing the existence of transformation above M_s in both the coarse-grained and fine-grained material. Thus, the predictions of grain size upon both M_s and the transformation above M_s were confirmed. According to these results, M_s is not sensitive to grain size, if it is defined as the temperature at which the martensitic reaction starts.

To account for the grain-size effect on M_s on the basis of the nucleation and growth theory,[5] it is

‡‡ These three M_s values happen to be higher than those given in the previous tables because of an unusually low Ni content.

necessary to assume that, with decreasing grain size, the plates become thinner in proportion to their decreasing length, and hence become more difficult to detect under the microscope. However, no such dependence of thickness on length was found. Within a very wide range of grain sizes,§§ the plates formed at M_s were comparatively constant in width, despite enormous differences in length.

It was observed that the amount of transformation involved in the burst often decreased with decreasing grain size and that the transformation sometimes occurred isothermally over a measurable period of time. This phenomenon will be discussed in another paper.

Summary and Conclusions

The first substantial (> ½ pct) amount of transformation in 70 pct Fe-30 pct Ni alloys occurs within the interval of an audible click at a temperature called M_s. This phenomenon, designated as a burst, was investigated experimentally using both single and polycrystalline specimens with the following results:

1—The reaction occurring during the burst is autocatalytic, that is, the first transformation to appear in the burst provides the impetus for the nucleation of succeeding plates and so on.

2—Martensite forms in amounts up to ½ pct above M_s, (M_s is lower than or equal to M_i) and new plates are nucleated preferentially at the rims of previously formed plates on decreasing the temperature.

3—Plastic deformation (slip) takes place locally at the martensite-austenite interface in plates formed above M_s, while substantial amounts of widely dispersed slip occur in the austenite during the burst.

4—The thickness of plates formed above M_s is very much less than that of plates formed during the burst.

5—Constraint to change-of-shape as offered by bakelite depresses M_s but not M_i, and a decrease in the size of the specimen being constrained enhances the depression of M_s.

6—Decrease in grain size depresses M_s, but does not measureably affect M_i.

7—Prior plastic deformation in single crystals raises M_i and M_s, and reduces markedly the range of scatter of M_s values. Prior plastic deformation in polycrystals raises M_i, first raises then lowers M_s, and decreases total amount of transformation measured below the M_s for zero deformation.

Additional experiments were conducted to check the validity of the nucleation and growth theory as applied to the burst phenomenon, with the following results:

1—Once formed, the martensitic plates do not thicken with decreasing temperature, as required by this theory.

2—The martensite range curve below M_s is insensitive to the austenitizing temperature for the Fe-Ni alloys, which demonstrates the independence of the transformation upon distributions of athermal martensite embryos.

3—The grain size explanation based on nucleation and growth is invalid for two reasons: (a) Plates can exist which are not bounded at the ends by existing plates, grain boundaries or other such obstructions. (b) A direct dependence of plate thickness to length is predicted by the theory, and is not found when the grain size is decreased.

4—The concept of loss of coherency due to plastic flow in limiting the size of plates, as proposed by Kurdjumow, has been found to be consistent with experiment.

It is concluded that regions of internal strain are preferential sites for nucleation of martensite in these alloys. Two such regions are the internal strains within the virgin austenite and the internal strains at existing martensite plates. It appears that the nucleation is more sensitive to the state of strain than to variations in composition.

A tentative explanation for the burst phenomenon has been presented. Use is made of the cooperative nature of the reaction in these alloys to nucleate new plates and thus generate a chain of transformation.

The possibility exists that many martensitic transformations involve bursts, to a greater or lesser extent. If this proves to be the case, the burst phenomenon may provide a new basis for understanding important features of the martensitic transformation.

§§ Starting with grain diameters somewhat larger than the average thickness of plates formed in a burst and extending up to massive single crystals.

Acknowledgments

The authors gratefully acknowledge the assistance of William R. Yankee, and the support of the Office of Naval Research. The International Nickel Co. kindly supplied alloy B for this investigation.

References

[1] E. S. Machlin and M. Cohen: The Habit Phenomenon in the Martensitic Transformation. Submitted to AIME.

[2] M. Cohen, E. S. Machlin, and V. G. Paranjpe: Thermodynamics of the Martensite Transformation. *Thermodynamics in Physical Metallurgy*. A.S.M. (1950).

[3] D. Turnbull: Principles of Solidification. *Thermodynamics in Physical Metallurgy*. A.S.M. (1950).

[4] R. T. Howard and M. Cohen: Quantitative Metallography by Point-Counting and Lineal Analysis. *Trans.* AIME (1947) **172**, p. 413; METALS TECHNOLOGY (August 1947).

[5] F. Förster and E. Scheil: Untersuchung des Zeitlichen Ablaufes von Umklappvorgangen in Metallen. *Ztsch. Metallkunde* (1940) **32**, p. 165.

[6] J. C. Fisher, J. H. Hollomon, and D. Turnbull: Nucleation of Phase Transformations. *Journal of Applied Physics* (August 1948) **19**.

[7] G. V. Kurdjumow: Diffusionless (Martensitic) Transformations in Alloys. *Journal of Technical Physics* USSR (1948) **18**, No. 8, p. 1011.

[8] J. C. Fisher, J. H. Hollomon, and D. Turnbull: Kinetics of the Austenite to Martensite Transformation. *Trans.* AIME (1949) **185**, p. 691; JOURNAL OF METALS (January 1949).

[9] F. W. Jones and W. I. Pumphrey: Free Energy and Metastable States in the Fe-Ni and Fe-Mn System. *Journal* Iron and Steel Inst. (1949) **163**, part 2.

[10] O. Kubaschewski and O. von Goldbeck: The Thermodynamics of the Iron-Nickel Alloys. *Trans.* Faraday Soc. (1949) **45**, p. 948.

[11] A. W. McReynolds: Effects of Stress and Deformation on the Martensite Transformation. *Journal of Applied Physics* (1949) **20**, p. 896.

[12] C. S. Barrett and D. F. Clifton: Transformation Characteristics of a Lithium-Magnesium Alloy. *Trans.* AIME (1950) **188**, p. 1329; JOURNAL OF METALS (November 1950).

[13] G. V. Kurdjumow, O. P. Maksimova, and T. V. Jagunova: On the Transformation of Deformed Austenite into Martensite. *Doklady Akademii Nauk* SSSR (1950) **73**, No. 2, p. 307.

[14] B. S. Lement, B. L. Averbach, and M. Cohen: The Dimensional Behavior of Invar. A.S.M. (1950) Preprint 39.

Fundamental Effects of Cold Working on the Creep Resistance of an Austenitic Alloy

by D. N. Frey and J. W. Freeman

Fundamental reasons for the improvement in creep resistance of an austenitic alloy by cold working were investigated mainly by X-ray diffraction. The creep resistance was found to be improved by the internal stresses in the lattice of the alloy induced by the cold work.

THIS investigation was concerned with the fundamental reasons for improvement in creep resistance of an austenitic alloy as a result of cold working. Also, the investigation was carried out to elucidate the conditions under which cold working could be expected to improve the creep resistance.

To achieve these ends, creep resistance and internal structure were correlated for a variety of cold-worked conditions. Since the aim of the investigation was not to obtain specific and extensive information on any one alloy, creep testing was done with a single stress at 1200°F. Structural studies were carried out primarily with X-ray diffraction characteristics. The alloy used, low carbon N-155, was selected on the basis of being representative of at least some of the alloys used in gas turbines.

Low carbon N-155 alloy in the form of ⅞-in. sq bar stock was used in this investigation. The chemical composition, in percent, was: C, 0.13; Mn, 1.43; Si, 0.34; Cr, 20.73; Ni, 18.92; Co, 19.65; Mo, 3.05; W, 1.98; Cb, 0.98; N, 0.14; and Fe, balance.

The bar stock was produced from a 13-in. sq billet, finished to ⅞ in. round cornered square between 2060° and 1910°F.

D. N. FREY and J. W. FREEMAN, Members AIME, are Assistant Professor and Associate Professor, respectively, Department of Chemical and Metallurgical Engineering, University of Michigan, Ann Arbor, Mich.

Discussion on this paper, TP 3129E, may be sent, 2 copies, to AIME by Dec. 1, 1951. Manuscript, March 28, 1951. Detroit Meeting, October 1951.

Prior to use in this particular investigation, the bar stock was solution-treated 1 hr at 2200°F and water quenched. This procedure was used in order to put the stock in a condition where effects of prior processing were minimized.

Experimental Procedure

The specific approach to the problem was twofold. First, the influence of cold working, under various conditions, on the creep rate under a single stress at 1200°F and on the internal structure was in part determined. Second, the effect of annealing at various times and temperatures on the creep rate and internal structure of the cold-worked samples was in part evaluated. The first step was basic to the investigation—creep resistance and structure were to be correlated. The second step was taken to see if the annealed samples showed some internal changes which could also be correlated with changes in creep resistance. This it was felt would facilitate solution of the basic problem.

The creep and structural studies were carried out on samples reduced approximately 5, 15, and 40 pct at room temperature and 15 pct at temperatures up to 2200°F. Annealing of various of the samples was done at 1200°, 1400°, 1600°, and 1800°F for time periods up to 1000 hr. Studies of the annealed samples were concentrated on materials rolled approximately 5, 15, and 40 pct at room temperature and 15 pct at 1400°F. The creep tests were carried out at 1200°F under 40,000 psi, the latter being approximately the 1000 hr rupture stress of the material

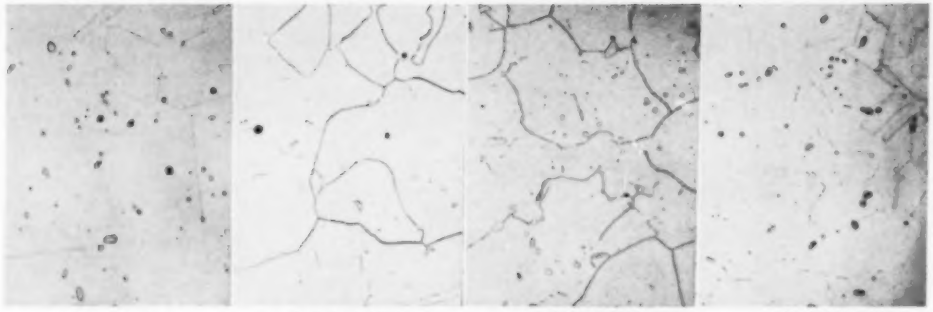

Rolled at 80°F. Rolled at 1400°F. Rolled at 1800°F. Rolled at 2200°F.

Fig. 1—Effect of rolling temperature upon microstructure of solution-treated low carbon N-155 alloy reduced 15 pct. Electrolytic chromic acid etch. X1000. Area reduced approximately 70 pct for reproduction.

cold reduced 15 pct. No transient creep was observed, and all tests were run for time periods of from 200 to 500 hr, which was sufficient time to establish the steady state creep rate. All creep data are reported in terms of this steady state rate. The estimated accuracy of these rates was ±40 pct.

The structural effects of cold working were studied primarily by X-ray diffraction, although microscopic examination, both optical and electronic, was also used. For the diffraction work, surfaces normal to the bar axis were prepared by electrolytic removal of a minimum of 0.020 in. of metal. This was done to avoid artificially cold-worked metal produced by the sample preparation process itself. Conventional metallographic methods were employed, including the use of uranium shadow-cast Formvar replicas in the electron microscope.

Previous work has shown that broadening of diffraction lines occurs as a result of cold working.[1] This has been ascribed both to particle size broadening from fragmentation of the grains and to a distribution of lattice parameters resulting from residual elastic stresses. It was felt that either effect would be important as far as creep resistance was concerned, and accordingly the width of the (220) line of the austenite was photographically recorded as a function of the various rolling and heat treatments. Chromium radiation was used to eliminate fluorescent effects, and with this radiation the (220) line was at 67° θ, where fair resolution was obtained. The specimen was mounted normal to the X-ray beam and rotated slowly about an axis parallel to, but offset from the X-ray beam. This latter was occasioned by the desire to cover the largest possible area on the sample surface (cover more grains), and thus obtain diffraction lines with uniform blackening along the diffraction cone.

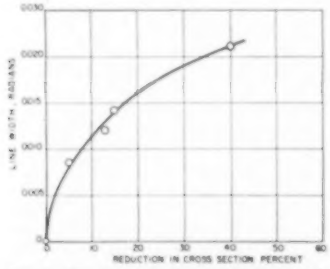

Fig. 2—Effect of reduction at 80°F on width of (220) line of solution-treated low carbon N-155 alloy.

The width of the (220) line was then taken at a density half way between that of the top and bottom of the line. Correction for instrumental broadening was done by the method of Warren[2] and by further assuming that the broadness of the (220) line from the solution-treated sample was due entirely to instrumental broadening and using it as the instrumental broadening factor in Warren's formula. All broadening data reported thus are relative to the solution-treated sample. The reproducibility of line widths was not better than ±10 pct.

As an aid to determining the basic cause of the line broadening observed, integrated intensity measurements were made on the (111) line of some of the cold-rolled and cold-rolled and annealed samples. Here it was anticipated that extinction* effects would be of major interest. Inasmuch as the lowest order line shows maximum intensity variation with variation in amount of extinction, the (111) line was used. In particular, it was necessary to determine the variation of (111) line intensity with variation of the angle between the (111) planes contributing to the intensity measurements and the rolling direction in the bar. For this, samples were mounted in a Schultz fixture[3] and placed in the Norelco spectrometer, where intensity measurements were taken at 5° or 10° intervals from 0° to 90° with respect to the rolling direction. To cover this range from 0° to 90°, two sample surfaces were used—one parallel and one normal to the rolling direction. Data were taken from each of these samples over a 50° range. This was necessitated by the fact that Schultz's method breaks down over an angular range of more than about 50°. Over the 50° range used, checks were made with randomly oriented samples to insure the applicability of Schultz's method. A standard of comparison for these intensity measurements was a randomly oriented powder compact made of low carbon N-155 filings prepared so that extinction was believed negligible.

Structural Alterations as a Result of Cold Working

From a microstructural standpoint little change was observed in samples rolled at room temperature until reductions of the order of 15 pct were reached, at which reduction a very few slip lines or bands

* Extinction is the loss of intensity of the diffracted beam due to increasing loss of energy in the primary beam as diffraction itself occurs.

could be observed in polished and rather heavily etched samples. Increasing degree of reduction resulted in greater density of such lines, at least up to reductions of 40 pct.

Increase in the rolling temperature with the degree of reduction held constant at 15 pct resulted in several microstructural changes. From 80° to 1800°F, the grains become more clearly outlined, with possibly some precipitate actually formed at the boundaries at the higher temperatures, see Fig. 1. The change was similar to that obtained when solution-treated material is simply heated at the various rolling temperatures for about 1 hr. After rolling at 2200°F, recrystallization was evident, see Fig. 1. A check on material rolled at 2050°F revealed no recrystallization; it appeared much the same as material rolled at 1800°F. The simultaneous recrystallization temperature† of low carbon N-155 for reductions of 15 pct may thus be placed between 2050° and 2200°F. Greater reductions would probably lower this temperature.

For an interpretation of the widening of the (220) line after rolling, see Fig. 2, reference should again be made to the two possible causes of line broadening due to "cold" work. They are fragmentation of the matrix into crystallites which must have thicknesses less than 1000A to cause broadening, or the introduction of a range of interplanar spacings, (100) spacings in this case, in turn due to the presence of residual elastic stresses.

In order to separate these two causes of line broadening, use was made of the fact that if the observed broadening were due to crystallites, the crystallites would have to be so small as to preclude any extinction being present. Accordingly the first step in the separation of the two causes of line broadening was to make measurements of the (111) line integrated intensity in order to determine the extinction coefficients‡ of cold-rolled material.

However, before these intensities could be interpreted in terms of extinction coefficients a further complication had to be considered. An intensity increase could be due not only to reduction in extinction, but also to preferred orientation of the crystallites. This latter would act to increase the intensity of various diffraction lines in certain directions relative to the bar axis, such increase not having any relation to a decrease in extinction.

Fig. 3 shows a more detailed study of the intensity of the (111) line at various angles to the rolling direction of materials reduced 15 and 40 pct at 80°F. The curves of Fig. 3 may be taken as representing the relative number of crystallites having the various indicated orientations with respect to the bar (rolling) axis. Further study showed that the preferred orientation was of the "fibered" type with two components (111) and (100). The crystallite distribution about any axis parallel with the bar axis was found to be random. In order to obtain the change in (111) line intensity due to rolling and corrected for the preferred crystallite orientation, use was made of an important feature of Fig. 3. With no change in extinction, the areas of the curves from 0° to 90°, relative to the rolling direction, would remain constant to a very close degree, irrespective of whether the fibered orientation is present or not. Thus, any change in this area is due to extinction effects. For the particular curves of Fig. 3 the height of a rectangle running from 0° to 90° equalling the above-mentioned area would give the (111) line intensity, relative to the extinctionless low carbon N-155 powder compact, of a material having the same crystallite size as the rolled bars but with the crystallites completely random.

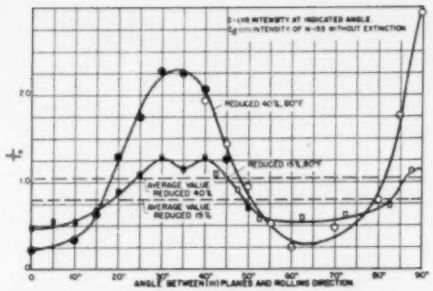
REDUCED 40%, 80°F
REDUCED 15%, 80°F
AVERAGE VALUE REDUCED 40%
AVERAGE VALUE REDUCED 15%
ANGLE BETWEEN INTERPLANES AND ROLLING DIRECTION

Fig. 3—Effect of rolling at 80°F on (111) intensity at indicated angles with the rolling direction of solution-treated low carbon N-155 alloy.

Construction of such rectangles was carried out on Fig. 3. For the material rolled 15 pct at 80°F, the resulting (111) intensity relative to the standard was 0.80 and for the material rolled 40 pct, 1.05. The same figure for the plain solution-treated, low carbon N-155 was 0.77. The estimated accuracy for all of these figures was ±5 pct.

Since the standard of comparison for the intensity measurements on Fig. 3 was powdered low carbon N-155 with no extinction, the above figures represent extinction coefficients. It is obvious therefore, that rolling 15 pct hardly reduced extinction in low carbon N-155 over what it was without rolling, while rolling 40 pct eliminated extinction at least to within the experimental error.

If these values at the extinction coefficients are entered into the Darwin formula for extinction as a function of crystallite size, it is found that the as-solution-treated low carbon N-155 and the stock rolled 15 pct had crystallite sizes of the order of 10^{-4} cm, while all that can be said for the stock rolled 40 pct is that its average crystallite size was probably less than 10^{-5} cm.

Going back to the original problem of separating particle size broadening from residual strain broad-

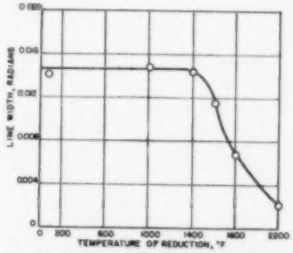

Fig. 4—Effect of rolling temperature on width of (220) line of solution-treated low carbon N-155 alloy reduced 15 pct.

† The simultaneous recrystallization temperature is defined as the temperature of rolling or forging, where recrystallization takes place during or just after working, as evidenced by a finer grain size after cool down than was present prior to working.

‡ The extinction coefficient is here defined as the ratio of the observed (111) integrated intensity to the (111) integrated intensity from a powdered sample of low carbon N-155 believed to have no extinction.

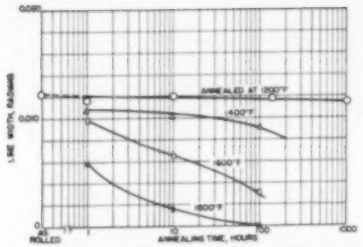

Fig. 5—Effect of annealing on width of (220) line of solution-treated low carbon N-155 alloy reduced 13 pct at 80°F.

ening, the Scherrer formula shows that small particle line broadening is negligible with particles greater than 10^{-5} cm, and so particle broadening was certainly absent in solution-treated low carbon N-155 cold reduced up to 15 pct and of unknown proportions in the material reduced 40 pct. It can thus be concluded that for a cold reduction of 15 pct, the line broadening which occurred was due entirely to residual elastic strains, while the line broadening in samples reduced 40 pct could be due in part to small particle size but not very probably. Accordingly, line widths shown in Figs. 2 and 4 may be considered as indicating some average value of the internal "locked up" stresses present after the various treatments indicated.

Fig. 2 indicates that the internal stresses did not increase uniformly with degree of reduction, but rather that the internal stresses apparently would reach a maximum value independent of further reduction. Such results have been noted before by many investigators.

Fig. 4 shows that rolling 15 pct up to temperatures of approximately 1500°F resulted in the same average internal stress. Increasing the temperature of reduction past this point reduced the internal stresses, and rolling at temperatures of about 2200°F resulted in practically no residual internal stresses. It appears that the amount of relaxation of the internal stresses occurring during or just after the rolling operation (during cool down) is the factor which limits the line widths obtainable at the higher rolling temperatures.

Microstructural examination of all the various annealed samples revealed that only the material reduced 40 pct at 80°F recrystallized. This recrystallization started after about 10 hr at 1600°F and was

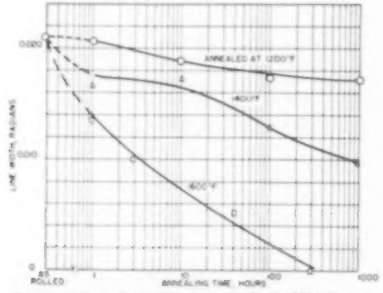

Fig. 6—Effect of annealing on width of (220) line of solution-treated low carbon N-155 alloy reduced 40 pct at 80°F.

complete after 1000 hr at 1600°F. It was completed at 1800°F in less than 10 hr. The recrystallized texture was of the same general type as existed before recrystallization.

Fig. 5 is typical of the effects of annealing on the (220) line width of all stock reduced 15 pct at temperatures from 80° to 1400°F. Similar results were had for the stock rolled 5 pct at 80°F—line widths of course being at correspondingly lower values, for the same annealing times and temperatures. Reduction of the (220) line widths may be interpreted as the result of internal stress relaxation during the annealing process. It should also be emphasized that this reduction is a recovery phenomenon occurring before recrystallization as the microstructural examination of annealed samples showed.

Comparison of Fig. 6, indicating the effects of annealing on the (220) line of the material rolled 40 pct at 80°F with Fig. 5 shows that 40 pct reduction resulted in significant line sharpening at 1200°F while 15 pct reduction did not. Apparently, the greater the magnitude of the internal stress, the

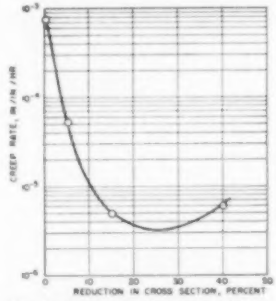

Fig. 7—Effect of reduction at 80°F on creep rates of solution-treated low carbon N-155 alloy under 50,000 psi at 1200°F.

lower the temperature at which effective relaxation occurs. This reduction of stability of the cold-worked structure with greater degree of cold working seems well substantiated by other investigators of recrystallization phenomena.

Effects of Cold Working on Creep Resistance

Fig. 7 shows a maximum amount of creep resistance with reduction of the order of 25 pct and that further reduction resulted in either no further improvement of creep resistance or possibly an actual reduction. These results probably hold only for temperatures near 1200°F and in all probability would change for other temperatures of creep testing.[4] While this maximum effect of rolling on creep resistance was present, Fig. 2 indicates essentially that the internal stresses continued to increase with amount of rolling to at least 40 pct reduction.

Fig. 8 shows that the temperature of reduction had small effect on creep resistance under the conditions of testing at 1200°F, unless rolling temperatures greater than about 1500°F were used. For rolling temperatures greater than this, the creep resistance dropped off sharply. Fig. 4 indicates that this drop in creep resistance corresponded closely with the drop in line width.

Fig. 9 shows a typical relationship between creep resistance and annealing. Practically identical results were obtained for material rolled 15 pct at

1400°F. Creep rates for any given anneal after 5 pct reduction at 80°F were somewhat higher than those shown on Fig. 9, while creep rates for the material reduced 40 pct at 80°F were roughly similar for any given anneal to those on Fig. 9.

When comparison of the creep data obtained from the annealed samples was made with the line width data obtained from samples given the same anneal, it was apparent that a correlation between creep rate and line width might exist, but with the creep rate decreasing very rapidly with decreasing line width. This was also evident from comparison of the data on Figs. 3 and 4.

With this in mind, a correlation of the logarithm of the creep rate and the line width for both rolled, and rolled and annealed samples was tried with the result shown on Fig. 10. Considering the possible errors in measuring creep rates and line widths, most points fall no further off the mean line than could be accounted for by experimental error.

Some comment on the significance of this correlation can be made. If the Eyring reaction rate theory for creep is extended to include some average in-

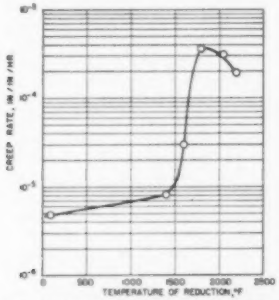

Fig. 8—Effect of rolling temperature on creep rate under 50,000 psi at 1200°F of solution-treated low carbon N-155 alloy reduced 15 pct.

ternal stress, the correlation shown on Fig. 10 can be predicted.

The appropriate expression from the theory for metallic creep appears to be:

$$\dot{\epsilon} = \text{constant}_1 \times T \times e^{-\frac{\Delta F}{RT}} \sin h \frac{\text{constant}_2 \sigma}{RT} \quad [1]$$

where $\dot{\epsilon}$ is the creep rate at temperature T and stress σ, ΔF the free energy for activation of the fundamental unit of creep, and R the gas constant. When considering materials with internal stresses, satisfaction of equilibrium conditions results in the stresses appearing in regions of positive and negative sense. Thus in alternating regions the sense of the internal stress will be opposite to the sense of the applied stress and in the remaining regions it will be the same. However, if one assumes that the periodicity of these alternating stresses meets certain requirements,[3] the regions of internal stress opposite to the sense of the applied stress will control the creep rate. For these regions eq 1 becomes:

$$\dot{\epsilon} = \text{constant}_1 \times T \times e^{-\frac{\Delta F}{RT}} \sin h \, \text{constant}_2 \left(\frac{\sigma - \bar{\sigma}_i}{RT} \right) \quad [2]$$

when $\bar{\sigma}_i$ is the effective internal stress. For a series

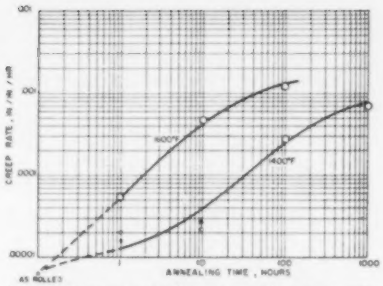

Fig. 9—Effect of annealing on secondary creep rate at 50,000 psi and 1200°F of solution-treated low carbon N-155 bar stock reduced 15 pct at 80°F.

of tests at constant T and σ, but with varying $\bar{\sigma}_i$, eq 2 can be rewritten:

$$\log \dot{\epsilon} = \text{constant}_3 - \text{constant}_4 \times \bar{\sigma}_i \quad [3]$$

Assuming a linear relation between $\bar{\sigma}_i$ and the line width as measured herein, this is the relationship appearing on Fig. 10.

There are difficulties, however, in selecting from line broadening data an average internal strain and in turn converting this to an average internal stress. What half-height width of a line represents in terms of some average internal stress is not known, without further analysis of the broadened lines and other assumptions.[1] Even the correction for instrumental broadening using Warren's method is dependent upon an assumption as to the shape of the broadened lines, which assumption imperfectly represents the facts in this case. One is forced therefore, to conclude that the quantitative theoretical significance of Fig. 10 is limited at the present time, although qualitatively it indicates the relationship between internal stress and creep resistance.

The point (3) for the material reduced 40 pct at room temperature fell far off the correlation of Fig. 10. The observed creep rate of this material was too high for the measured line width. Further, the data of Fig. 6 showed that the (220) line width of this material (and this material only) was reduced appreciably during annealing at 1200°F. The conclusion is that reductions of the order of 40 pct on low carbon N-155 in the cold-working range resulted in appreciable relaxation of internal stresses at temperatures as low as 1200°F, such relaxation occurring during the creep test at this temperature. This limits the amount of reduction, and internal stress formation, that is useful for service at 1200°F, as shown in Fig. 7. Further, the line width that should have been entered on the correlation of Fig. 10 was some average line width which existed during the creep test at 1200°F. All other samples for which the data lie on the correlation of Fig. 10 had structures stable enough at 1200°F after rolling and/or annealing that the line widths measured before testing were substantially those existing during the creep test at 1200°F.

The factors explained above, which limited the amount of cold reduction that was useful in improving creep resistance of low carbon N-155 at 1200°F to about 40 pct, can be generalized somewhat with the aid of data published by Zschokke.[4] Zschokke found on another austenitic steel that there was a maximum benefit from cold working similar in na-

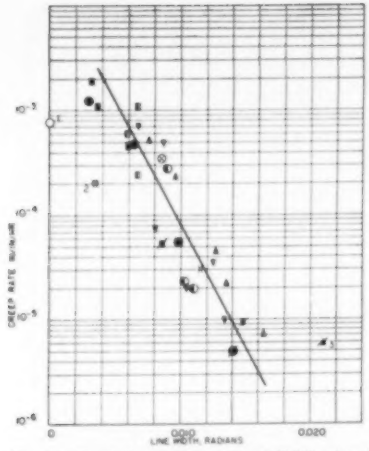

Fig. 10—Correlation of creep rate at 50,000 psi and 1200°F with (220) width of solution-treated, "cold" worked and annealed low carbon N-155 alloy.

ture to the results shown in Fig. 7. There appears to exist therefore, a critical amount of cold work beyond which relaxation of the internal stresses will occur to such an extent at the temperature of test or service considered that a maximum value for internal stresses effectively exists at each such temperature. Further, Zschokke found that the amount of cold work which gave the maximum effect decreased with increasing creep test temperature. This may be explained by saying that the temperature at which relaxation occurs to any appreciable extent is reduced as the amount of cold working is increased.

The materials reduced 15 pct at either room temperature or 1400°F were similar in every respect in regards to the interrelation between line width or internal stress and creep resistance either before or after annealing. Further, the results shown on Fig. 4 indicate that internal stresses after reductions of 15 pct are also the same up to temperatures of reduction of the order of 1500°F. Beyond this point relaxation during the rolling operation occurs. Since it is the internal stresses which improve creep resistance, it can be said that the temperature of "cold work" is immaterial as far as creep resistance is concerned over the temperature range, 80° to 1500°F.

The data for material rolled at 2200°F and the as-solution-treated material also did not fall on the correlation of Fig. 10 (points 1 and 2). Further, Fig. 8 showed that within the temperature range 1800° to 2200°F a rather curious reversal in creep resistance occurred. In view of the above, it seems that the creep resistance for material rolled in the vicinity of 2200°F and the solution-treated material was abnormally high, if internal stress control as exemplified by Fig. 10 is considered normal. No fundamental explanation of this phenomenon appears possible at the present time. However, from a technological standpoint the finding is important since the conclusion is that rolling of solution-treated N-155 at temperatures in the vicinity of 2200°F resulted in material which had better creep resistance than other "hot" worked materials.

Key to Symbols Used in Fig. 10

Reduction (percent)	Temperature of Reduction (°F)	Temperature of Annealing (°F)	Symbol
0	-	-	○
5	80	-	◢
5	80	1600	■
5	80	1800	■
13	80	-	◢
13	80	1600	●
13	80	1800	●
50	80	-	◢
50	80	1600	▲
50	80	1800	▲
15	1600	-	◢
15	1600	1600	▼
15	1600	1800	▼
15	1400	-	✕
15	1800	-	●
15	2000	-	■

Conclusions

1—Cold working improves the creep resistance of low carbon N-155 and probably other alloys of the same general type through the presence of elastic stresses left in the lattice after the working operation.

2—For any given reduction, the optimum improvement in creep resistance can be had with any temperature of reduction below that which will allow relaxation of the internal stresses to a marked degree during the working operation itself. For reductions of 15 pct on low carbon N-155 alloy, this useful working temperature range is from 80° to 1500°F.

3—Conversely, increasing amounts of cold working give increasing creep resistance only up to the point where the internal stresses are so high as to permit relaxation to occur in significant amount at the particular service temperature being considered. It further appears that the critical amount of cold reduction decreases as the service temperature is raised. With low carbon N-155 for service or test at 1200°F, the critical cold reduction is approximately 25 pct.

4—A correlation of the logarithm of creep rate against internal stress as measured by diffraction line width existed for solution-treated and cold-rolled low carbon N-155 either with or without subsequent anneals. The full quantitative theoretical significance of this correlation must await more exact interpretation of broadened diffraction lines, although qualitatively it agrees with predictions from the Eyring reaction rate theory for creep.

Acknowledgment

The authors gratefully acknowledge financial support for this investigation from the National Advisory Committee for Aeronautics. The Committee has sponsored this research as part of a continuing program on the fundamentals of high temperature metallurgy at the Engineering Research Institute of the University of Michigan.

References

[1] R. W. James: *X-ray Optics.* (1949) Methuen and Co.
[2] B. E. Warren: *Journal* Amer. Ceramic Soc. (1938) **21**, p. 49.
[3] N. F. Mott and F. R. N. Nabarro: Conference on Strength of Solids. The Physical Soc. (1948).
[4] H. R. Zschokke and K. H. Niehus: *Journal* Iron and Steel Inst. (1947) **156**, p. 271.
[5] L. G. Schultz: *Journal of Applied Physics* (1949) **20**, p. 1030.

Thermal Variation of Young's Modulus in Some Fe-Ni-Mo Alloys

by M. E. Fine and W. C. Ellis

WHEN certain binary Fe-Ni alloys are worked cold and then stabilized by a stress-relief anneal, their Young's moduli are nearly invariant over a substantial temperature range determined by composition and work-anneal history.[1] In the present investigation addition of molybdenum to such alloys (besides increasing the yield strength) was found to diminish the sensitivity of the thermal coefficient of Young's modulus to composition changes. Such alloys are of interest for applications requiring a metal with controlled, low temperature coefficient of Young's modulus and substantial magnetic permeability.[2]

Young's modulus ordinarily decreases with rising temperature. In ferromagnetic alloys a change in modulus on heating due to loss of ferromagnetism modifies the temperature dependence. Far below the Curie temperature ferromagnetism alters the modulus in two ways: a—Addition of the energy of magnetization, a function of interatomic distance, changes the relation between interatomic energy and distance.[3] This lowers the modulus in the Fe-Ni and Fe-Ni-Mo alloys of this investigation. b—An applied stress changes the ferromagnetic domain arrangement so that linear magnetostriction contributes to the strain and further lowers the modulus.[2] Since in the alloys of this investigation both effects lower the modulus, loss of ferromagnetism on heating changes the slope of the modulus-temperature curve in a positive direction. With increasing temperature the slope of the modulus-temperature curve, due to progressive loss of ferromagnetism, becomes less negative, goes through zero (the modulus is minimum), becomes positive, and resumes its normal negative value above the Curie temperature.[3] The increase in modulus and decrease in curvature in the modulus-temperature curve occurring on work hardening have been attributed to a reduction in effect (b).[1, 2] In the absence of ferromagnetism work hardening through introduction of residual strains would be expected to decrease the modulus.[4]

Alloy Preparation—Test Methods

Four series of alloys having nominal molybdenum contents of 5, 7, 9, and 10 pct and containing 47 to 58 pct Fe (the analyzed compositions are given in Table I) were melted in air and cast as bars weighing from 2 to 6 lb. The charge consisted of electrolytic nickel, Armco iron, molybdenum (99+ pct) or ferromolybdenum (62 pct Mo), manganese, and aluminum as a deoxidizer. The bars were swaged cold to the desired diameters with intermediate anneals. Alloys in this composition range are reported[5] to be face-centered cubic and ferromagnetic at room temperature. The Curie temperatures[5] decrease with molybdenum. For example, keeping the Ni/Fe ratio at unity and increasing the molybdenum from 0 to 17 pct decreases the Curie temperature from approximately 500°C to room temperature. (The 17 pct Mo alloy requires quenching to retain a single phase.[5])

Young's modulus at a series of temperatures from −50° to 100°C was determined by a dynamic method previously described.[1, 6] In this method Young's modulus is calculated from the resonant frequency (in this case approximately 50,000 cycles per second) of a rod sample (approximately 2 in. long) vibrating longitudinally in the first mode. The densities of the samples at room temperature, Table I, were determined by the standard method of weighing in air and reweighing in redistilled bromobenzene. The linear coefficients of expansion, Table I, needed to calculate the sample length and density at the temperature of measurement, were obtained by observing the change in length (22° to 100°C) of an 8 in. gage distance with a two microscope cathetometer. The values of density and coefficient of expansion in the few samples checked are independent of treatment to the accuracy reported. This was assumed to be general for all the samples. The modulus values are accurate to $\pm 0.05 \times 10^{11}$ dynes per sq cm. However, values of thermal change in modulus are accurate to $\pm 0.005 \times 10^{11}$ dynes per sq cm.

Young's Modulus

Values at 25°C: The modulus values of 0, 5, and 10 pct Mo alloys at 25°C are plotted in Fig. 1 as functions of nickel. After working cold, the samples were either recrystallized at 950° to 1000°C or given a low temperature stabilizing anneal at 400°C. The 400°C anneal does not reduce the hardness nor cause recrystallization. Annealing at 400°C does

Table I. Compositions, Densities, and Coefficients of Expansion of Fe-Ni-Mo Alloys

Sample Desig.	Chemical Composition, Weight Pct							Density, G per cc	Mean Linear Coefficient of Expansion $\frac{1}{l}\frac{\Delta l}{\Delta T}$ x10⁶
	Mo	Ni	Fe	Mn	Co	Al	C		
6799	5.2	38.4	56.1	0.18				8.27	4.5
6800	5.3	40.2	53.9	0.27	0.35	0.01		8.28	4.4
6801	5.3	41.7	52.6	0.34				8.29	6.0
6837	5.2	43.5	50.6	0.42				(8.30)	(8)
6838	5.2	43.4	50.6	0.48	0.47	0.08		(8.30)	(8)
6882†	7.1	39.4	52.5	0.55				(8.33)	(7)
6883†	7.0	40.4	51.5	0.58				8.33	(7)
6884†	7.2	41.5	50.3	0.61				(8.32)	(7)
6892*	8.8	40.6	49.4	0.64			0.02	8.37	(8)
6902*	9.2	38.6	51.2	0.49				8.36	(8)
6903*	9.1	39.7	50.1	0.61				(8.36)	(8)
6904*	8.9	41.6	48.4	0.62				8.37	(8)
6906*	9.2	41.7	47.9	0.45				(8.37)	(8)
6907*	9.0	40.6	49.2	0.55				(8.37)	(8)
6908*	9.1	41.3	48.5	0.46				(8.37)	(8)
6909*	9.5	42.7	46.6	0.57				8.40	(8)
6802	10.2	36.1	53.4	0.11				(8.40)	8.5
6803	10.7	38.4	50.5	0.13	0.37	0.01		8.42	8.5
6804	10.8	40.1	48.7	0.17				8.43	(8)
6805	9.8	42.8	47.1	0.20				8.43	8.0

* 7 lb melts using ferromolybdenum.
† 7 lb melts using 99+ Mo.
Balance are 2 lb melts using 99+ Mo.
Values in parentheses were interpolated from the measured values.

M. E. FINE and W. C. ELLIS, Members AIME, are Physical Metallurgists, Members of Technical Staff, Bell Telephone Laboratories, Inc., Murray Hill, N. J.

Discussion on this paper, TP 3131E, may be sent, 2 copies, to AIME by Dec. 1, 1951. Manuscript, April 18, 1951. Detroit Meeting, October 1951.

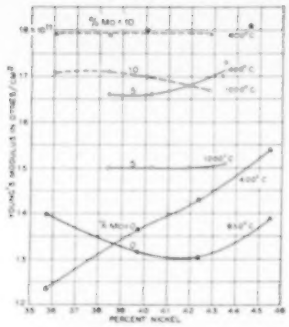

Fig. 1—Young's modulus in Fe-Ni-Mo alloys at 25°C.

Previous to annealing, the binary alloys were swaged cold 74 pct from an initial diameter of 0.390 in.; the ternary alloys, 41 pct from 0.260 in. In the 5 pct Mo series, the molybdenum contents varied from 5.2 to 5.3 pct; in the 10 pct series, from 9.8 to 10.8 pct.
*Annealing temperature. All annealing times were 1 hr.

$$1 \frac{\text{dyne}}{\text{cm}^2} = 1.4504 \times 10^{-5} \text{ psi.}$$

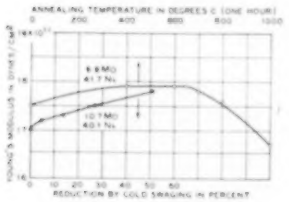

Fig. 2—Effect of annealing temperature and cold reduction on Young's modulus of two 10 pct Mo alloys.

Upper curve—alloy was initially cold reduced 41 pct from 0.260 in. diam.
Lower curve—alloy was cold reduced indicated percentage from 0.210 and annealed at 400°C for 1 hr before testing.
Temperature of test, 25°C.

Fig. 4 (right)—Percentage thermal variation of Young's modulus in cold-worked and stress-relieved 7 and 9 pct Fe-Ni-Mo alloys.

Cold swaged from 0.300 to 0.200 in. diam. (56 pct). Annealed 1 hr at 500°C. An annealing temperature of 500°C was chosen instead of 400°C (Fig. 3b) because in the Fe-Ni-Mo alloys annealed 1 hr at 400°C the modulus increased slightly during a two week treatment at 150°C.

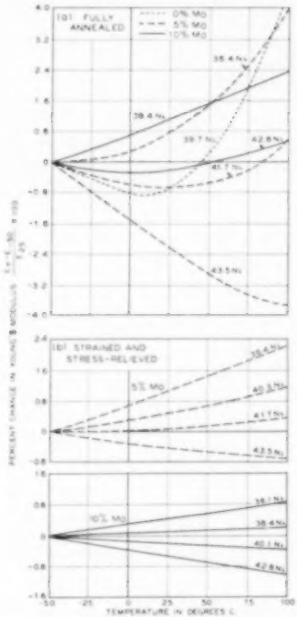

Fig. 3—Percentage thermal variation of Young's modulus in 5 and 10 pct Fe-Ni-Mo alloys.

Cold swaged from 0.260 to 0.200 in. diam. (41 pct).
a—Annealed 1 hr at 1000°C in H_2 and slowly cooled.
b—Annealed 1 hr at 400°C.

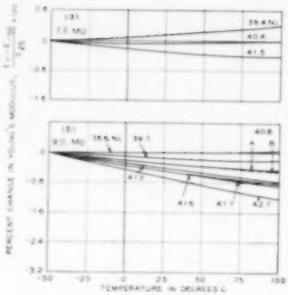

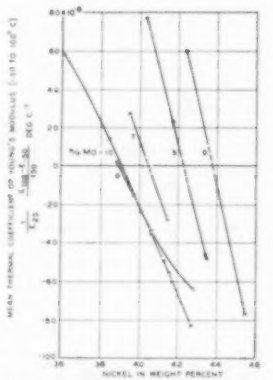

Fig. 5—Mean thermal coefficients of Young's modulus in work-hardened Fe-Ni-Mo alloys between −50° and 100°C.

Δ — Cold reduced 74 pct from 0.390 in. diam. Annealed 1 hr at 400°C.
X — Cold reduced 56 pct from 0.300 in. diam. Annealed 1 hr at 500°C.
○,● — Cold reduced 41 pct from 0.260 in. diam. Annealed 1 hr at 400°C.
The curves for 0, 5, and 7 pct Mo are shown dotted near zero mean coefficient because the slopes of the modulus change-temperature curves reverse and a mean coefficient cannot be simply defined.

relieve residual strains to the extent that subsequent heating to 100°C provides insufficient thermal energy to promote further relaxation.

Young's modulus depends on both composition and the state of strain in the alloy. The addition of molybdenum progressively raises the modulus of alloys in corresponding states of strain. Molybdenum additions, furthermore, render the modulus less sensitive to change in nickel content. The theory of the effect of molybdenum on the modulus is discussed in a later section.

In all the alloys of Fig. 1, except 35.7 pct Ni-Fe,[1] the presence of work hardening increases Young's modulus as shown by comparison of the curves for the 400° and 1000°C anneals (due to a decrease in the stress-produced linear magnetostriction). The effect of cold reduction was studied in more detail in a 10.7 pct Mo, 40.1 pct Ni alloy, lower curve, Fig. 2. The modulus in this alloy increases almost uniformly with the amount of cold reduction. In the upper curve of Fig. 2 annealing temperature (9.9 pct Mo, 41.7 pct Ni alloy) is the variable; the initial cold reduction is kept constant. As the annealing temperature is increased the modulus at first increases, due to stress relief, and then decreases with recrystallization and grain growth.

Temperature Dependence: The change in Young's modulus with temperature in these alloys depends upon a number of factors. Among these are composition, the amount of work hardening, and the degree of recovery* through annealing. Both the temperature of the minimum modulus and the degree of curvature of the modulus-temperature curve about the minimum are affected. The former establishes broadly the thermal region of nearly constant modulus, the latter the degree of constancy. The factors—composition, work hardening, and recovery—do not act independently in their effects, but are interrelated, as will be shown in the following discussion.

The previously mentioned negative, zero, and positive slopes of the modulus-temperature curve, are illustrated in the curves of percentage thermal change in modulus for fully annealed alloys containing 0, 5, and 10 pct Mo, Fig. 3a. In a given alloy the particular slopes observed in the −50° to 100°C temperature range depend upon the location

* Recovery is being used in the sense of including not only reduction of residual strains below the recrystallization temperature but also recrystallization and grain growth.

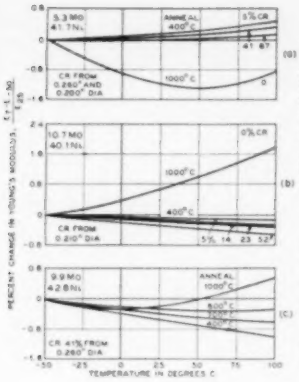

Fig. 6 (left)—Percentage thermal change in Young's modulus as affected by variation in degree of cold work and annealing temperature.

CR (cold reduced) refers to reduction in cross-sectional area.

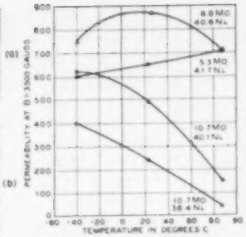

Fig. 7 (left)—Permeabilities of some Fe-Ni-Mo alloys.

● — Cold reduced 41 pct from 0.260 in. diam and annealed 1 hr at 400°C.
△ — Cold reduced 36 pct from 0.300 in. diam and annealed 1 hr at 500°C.
The permeabilities of the 8.8 pct Mo alloy are higher than the 5.3 and 10.7 pct Mo alloys because the former was annealed at a higher temperature.

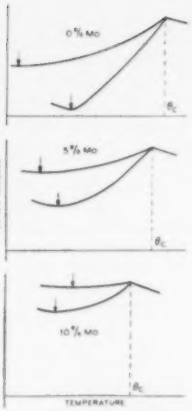

Fig. 8 (right)—Effect of increasing molybdenum on the modulus-temperature curve.

Upper curves—work hardened condition. Lower curves—fully annealed condition. Arrows indicate minima in modulus-temperature curves.

of the Curie temperature, a function of composition. Consistent with the dependence of the Curie temperature on nickel and molybdenum, the temperature of minimum modulus (predicted from the observed slopes in the −50° to 100°C range) increases with nickel content and decreases with molybdenum content. The effects of molybdenum and nickel are interrelated; for a minimum modulus at room temperature the ratio of nickel to iron increases from 0.7 to 0.9 as the molybdenum is increased from 0 to 10 pct.

The curvature in the modulus change-temperature curves (Fig. 3a) about the temperature of minimum modulus decreases on adding molybdenum. (Compare the data for the 0, 5, and 10 pct Mo alloys whose minima are in the temperature range of test). Furthermore, the slopes at temperatures considerably removed from the minimum modulus become numerically less as molybdenum is added.

Cold working of binary Fe-Ni alloys causes the modulus change-temperature curves to be shallower at their minima.[1] Moreover, the slope changes much more gradually at temperatures considerably removed from the minimum. In cold-worked alloys, the presence of the molybdenum to some extent further reduces the curvature in the region of the minimum, but its principal effect is to decrease the sensitivity of the temperature coefficient of modulus to change in nickel content. The evidence for this is in the modulus change-temperature curves for the cold-worked condition (stabilized by a stress-relief anneal at 400° or 500°C) shown in Figs. 3b and 4; the curves fan out less from varying nickel as the molybdenum content is increased. The same effect is illustrated more directly in Fig. 5, showing the mean thermal coefficient of modulus in 0, 5, 7, 9, and 10 pct Mo alloys between −50° and 100°C (slopes of the curves in Fig. 3b and 4). The major effect is for molybdenum contents of more than 5 pct. Adding 9 or 10 pct Mo diminishes the sensitivity of the coefficient to variations in Fe-Ni ratio by a factor of two.

Adding nickel increases the temperature of minimum modulus in both cold-worked and fully annealed alloys. The effect of molybdenum is not so simple. Adding molybdenum to fully annealed alloys decreases the temperature of minimum, but in cold-worked alloys adding molybdenum increases the temperature of minimum modulus. The temperature of minimum in cold-worked binary Fe-Ni alloys is less than in fully annealed alloys. As molybdenum is added the temperatures of minimum for the two conditions approach each other, are equal at approximately 7 pct Mo, and in 10 pct Mo alloys the temperature of minimum is higher for the cold-worked condition (compare Fig. 3a and 3b). This observation has theoretical significance and will be discussed later in the paper.

The effects of cold working were investigated in more detail in two alloys. The results are shown in Fig. 6a and 6b. The samples were first fully annealed at 1000°C and then cold worked the percentages shown in the figure (followed by a stabilizing anneal at 400°C). The initial amounts of cold work produce the greatest effect in flattening and shifting the minimum. This suggests that the principal changes effected by cold work are not due to texture development, since such small amounts of cold work would hardly be expected to develop preferred orientations. These figures again show the opposite effect of the presence of cold work in shifting the minimum in the 5 and 10 pct Mo alloys. The initial cold reduction decreases the temperature of minimum in the former, Fig. 6a, but increases the temperature of minimum in the latter, Fig. 6b. Subsequent cold reduction in both cases decreases the thermal coefficient of modulus.

The effect of change in annealing temperature on the modulus-temperature relation in a 10 pct Mo alloy was studied in detail, Fig. 6c. Increasing the annealing temperature from 400° to 1000°C decreases the temperature of minimum from well above 100°C to approximately 0°C; the slope becomes more positive. Comparing the curves for the 800° and 1000°C anneals at their minima, the latter has more curvature.

The effects of cold work and annealing temperature on the temperature of minimum modulus (Fig. 6b and 6c) are mutually consistent. The largest effect of cold work occurs for small cold reductions; the largest effect of annealing is for removal of the last residual strains introduced by the working (800° to 1000°C). Decrease in temperature of anneal (less removal of strain) has the same effect as increase in strain by cold work.

When the final annealing temperature is constant, the modulus and the thermal variation in modulus depend principally upon the amount of cold reduction after the last full anneal; however, the modulus and thermal variation in modulus depend to some

extent on the working and annealing procedure before the last full anneal. This is not unusual for a property depending upon the state of internal strain.

Magnetic Permeability and Mechanical Strength

Properties of associated importance with the modulus characteristics are the magnetic permeability and the strength. Permeabilities for some alloys are shown in Fig. 7. The thermal permeability variation (at 3500 gauss) is principally due to the decrease in Curie temperature as molybdenum is added. In a 10.7 pct Mo, 38.4 pct Ni alloy cold worked and stress relieved at 400°C, the permeability falls to a low value at 85°C indicating the Curie temperature is not much higher. The permeability of an 8.8 pct Mo, 40.6 pct Ni alloy stress relieved at 500°C remains between 700 and 900 for the temperature variation, −40° to +85°C. The permeabilities are higher in this latter alloy because the annealing temperature is higher.

The strengths of Fe-Ni alloys are substantially increased by addition of molybdenum. For example, an alloy containing 8.9 pct Mo and 41.6 pct Ni, cold worked 56 pct and stress-relief annealed at 500°C has a proportional limit of 115,000 psi. An Fe-Ni alloy containing 45 pct Ni after similar treatment has a proportional limit of 50,000 psi. The ultimate tensile strength of the molybdenum containing alloy is 148,000 psi and the elongation in 2 in. is 2 pct.

Theory of Effect of Mo on the Modulus

Addition of molybdenum to Fe-Ni alloys modifies the modulus through its effects on ferromagnetism and interatomic binding energy. Ferromagnetism, responsible for the observed unusual temperature variation of modulus in Fe-Ni and Fe-Ni-Mo alloys, as previously stated, changes the modulus directly through addition of the energy of magnetization term to the interatomic binding energy. Furthermore, the stress-produced linear magnetostriction increases the strain and lowers the modulus. In the following discussion the former will be referred to as effect (a) and the latter effect (b).

The modulus as it varies with temperature in a 0, 5, and 10 pct Mo alloy (approximately 42 pct Ni) is shown schematically in Fig. 8. The upper curve of each set is for work-hardened alloys, the lower for well-annealed alloys. In the temperature range −50° to 100°C these curves were constructed from actual data. The approximate behavior over a considerably wider temperature range can be deduced from room temperature measurements, since reducing the nickel lowers the Curie temperature and is approximately equivalent to lowering the temperature of test. The curves for the two alloy conditions are shown coming together at the Curie temperature. Actually this may not happen due to the effects of internal strain and crystal orientation on the modulus. To a first approximation the lowering of the upper curve from a straight line extrapolated from above the Curie temperature is due to effect (a); the difference between upper and lower curves is due to effect (b).

Addition of molybdenum, which increases the mechanical strength, by obstructing domain movement reduces the stress-produced linear magnetostriction (b). This partially causes the increase in modulus and decrease in curvature in the modulus-temperature curve on adding molybdenum to well-annealed alloys (Figs. 1 to 3 and 8). Effect (b) increases in magnitude, Fig. 8, over a limited temperature range on heating as in nickel[7] probably because domain movement becomes easier as the temperature is raised.

Effect (a), as molybdenum is increased, diminishes in magnitude and the minimum due to it nears the Curie temperature. Hence, in 0 and 5 pct Mo alloys work hardening, that is, reducing effect (b), decreases the temperature of minimum in the modulus-temperature curve, but in 10 pct Mo alloys work hardening increases the temperature of minimum as shown by the arrows in Fig. 8. Confirming experimental evidence for a diminishing of effect (a) on adding molybdenum comes from expansion data: The coefficient of expansion increases on adding molybdenum, Table I, showing a decrease in the volume effect from loss of ferromagnetism. The decrease in volume effect implies that as molybdenum is added the interatomic distance corresponding to maximum energy of magnetization nears the nonferromagnetic interatomic distance.

Summary

Young's modulus and its temperature coefficient were investigated in low coefficient Fe-Ni-Mo alloys under varying conditions of working and annealing. In the ternary as well as the binary Fe-Ni alloys, the temperature interval of nearly constant Young's modulus is greatly extended by work hardening. A stress-relief anneal is necessary to stabilize the alloys. Addition of 9 or 10 pct Mo decreases the sensitivity of the thermal coefficient to variations in nickel by approximately a factor of two. In these alloys the mean thermal coefficient of modulus for the temperature range −50° to 100°C varies from +50 to -50×10^{-6} degree C^{-1} as the nickel varies from 36.5 to 41.5 pct.

An alloy containing 9 pct Mo, 38 to 41.5 pct Ni, and balance Fe in the cold-worked condition has a low temperature coefficient of Young's modulus, substantial magnetic permeability reasonably constant over a limited temperature range, and high strength. The coefficient of modulus can be controlled by controlling the Fe-Ni ratio. A further measure of control can be exercised by varying the straining-annealing procedure.

The principal effects of molybdenum on the temperature dependence of modulus are explained by assuming that molybdenum decreases the modification in the interatomic energy-interatomic distance relation from the energy of magnetization.

Acknowledgments

The authors are pleased to express appreciation for the valuable assistance of members of the Bell Telephone Laboratories. The alloys were prepared under the direction of D. H. Wenny; the analyses and densities were supplied by H. E. Johnson; C. W. Spencer obtained the expansion data; the magnetic measurements were furnished by V. E. Legg and the mechanical properties by I. V. Williams. E. E. Schumacher assisted greatly through his interest, encouragement, and counsel.

References

[1] M. E. Fine and W. C. Ellis: *Trans.* AIME (1950) **188**, p. 1120. JOURNAL OF METALS (September 1950).
[2] A. C. Keller and L. G. Bostwick: *Trans.* AIEE (1949) **68**, p. 383.
[3] M. Kersten: *Ztsch. Physik* (1933) **85**, p. 708.
[4] C. Zener: *Acta Crystallographica* (1949) **2**, p. 163.
[5] W. Köster: *Arch. f.d. Eisenhüttenwesen* (1934) **8**, p. 170.
[6] R. Wegel and H. Walther: *Physics* (1935) **6**, p. 141.
[7] S. Siegal and S. L. Quimby: *Physical Review* (1936) **49**, p. 663.

Effect of Rate of Cooling on the Alpha-Beta Transformation in Titanium and Titanium-Molybdenum Alloys

by Pol Duwez

The effect of the rate of cooling on titanium, zirconium, and thallium has been measured. For titanium-molybdenum alloys, it has been shown that for molybdenum concentration up to 8 pct the rate of cooling has no effect on the transformation temperature, but this temperature decreases progressively with increasing molybdenum content.

HIGH strength to weight ratio and remarkable corrosion resistance have often been advanced as the main reasons for the present widespread interest in titanium. For the physical metallurgist, the existence of an allotropic transformation in titanium is another important factor. As in the case of iron, an allotropic transformation may be the fundamental property upon which the response of Ti-base alloys to heat treatment will depend. It is therefore important to study the mechanism of the allotropic transformation in pure titanium and the effect of alloying elements on this transformation.

The existence of an allotropic transformation in titanium was reported in 1931 by Schulze.[1] Later, De Boer et al.[2] determined the transformation temperature from a discontinuity in the electrical resistivity at 882°±20°C. According to recent work,[3] the transformation temperature is 882.5°±1°C. The crystal structure of the room temperature α phase is hexagonal close-packed and the high temperature β phase is body-centered cubic.[4]

It is well known that the high temperature β phase of pure titanium cannot be retained by quenching to room temperature. Several investigators[5-7] have shown that in alloys of titanium with metals which are soluble in the β phase (for example, nickel, molybdenum, chromium, or manganese), the β structure can be retained, providing the concentration of the alloying element is greater than a certain critical value. Below this critical value, the alloys transform during quenching, at least partially, into a supersaturated solid solution having the α structure. This behavior is very similar to that found in some iron binary alloys (Fe-Ni and Fe-Mn, for example) and is an indication that the transformation might occur by means of a shear mechanism analogous to that observed in the austenite-martensite reaction.

The present investigation is mostly concerned with the effect of the rate of cooling on the β to α transformation. In the first portion of this paper, the results obtained on pure titanium are described. Two other pure metals, zirconium and thallium, were also investigated, because they both have an allotropic transformation like titanium, from an hexagonal close-packed to a body-centered cubic structure. For purposes of comparison, the effect of rate of cooling of the γ to α transformation of iron was included in the experimental program. The second part of this paper deals with Ti-Mo alloys. The equilibrium phase boundaries involving the solid state reactions on the Ti-rich side of the system were determined and a study was made of the effect of the rate of cooling on the transformation of the high temperature β solid solution.

Experimental Procedure

Since the main object of the present investigation was the determination of the effect of the rate of cooling on a transformation temperature, the best technique available was that used by Greninger[8] in his study of the martensite arrest in carbon steels. This method consists of heating a very small sample of metal to which fine thermocouple wires are attached, cooling the sample rapidly by means of a blast of helium, and recording the temperature vs. time curve on an oscillograph. The apparatus used in the present experiments was very similar to that described by Greninger, except that the heating coil was made of molybdenum wire (0.040 in. in diam) and the assembly was placed in a bell jar under vacuum of 10^{-5} mm Hg or less. The specimen con-

P. DUWEZ, Member AIME, is Associate Professor of Mechanical Engineering, California Institute of Technology, Pasadena, Calif.

Discussion on this paper, TP 3124E, may be sent, 2 copies, to AIME by Dec. 1, 1951. Manuscript, April 12, 1951. Detroit Meeting, October 1951.

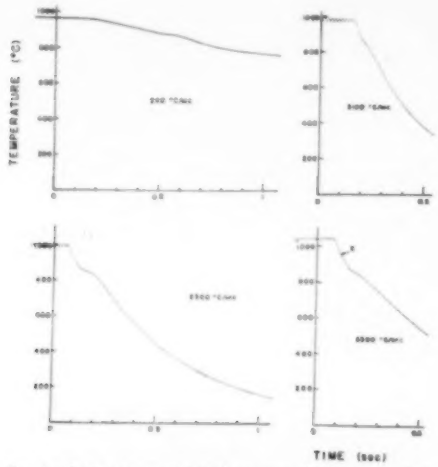

Fig. 1—Cooling curves obtained on pure titanium at various rates of cooling.

sisted of two pieces of metal about 0.020 in. thick and less than 1/16 in. square. The 0.005 in. chromel-alumel thermocouple wires were placed between the two pieces of metal and the assembly spot welded. In an effort to reduce contamination of titanium by any residual oxygen and nitrogen, the specimen was heated as fast as possible (between 5 and 10 sec) above the transformation temperature and immediately quenched. The temperature was recorded on a rotating drum type oscillograph (made by the William Miller Corp., Pasadena, Calif.). The galvanometer was a 65 cycle element, having a resistance of 45 ohms and a sensitivity of 1 in. deflection per 25 microamperes. The instrument was calibrated by means of a Leeds and Northrup portable precision potentiometer. Records were obtained with paper speeds of about 4½ and 8 in. per sec.

The Ti-Mo alloys were prepared by melting in a helium arc furnace. The furnace was very similar to that described in ref. 9, except that the top electrode, made of molybdenum, was water cooled. This electrode was designed so that the cooling water was brought to the tip of the electrode, leaving only 3/16 in. of molybdenum between the arc and the cooling water. The operation of the furnace was frequently checked by melting a specimen of pure titanium and measuring the Vickers hardness before and after melting. It was assumed that no contamination was introduced by melting when the average Vickers hardness number did not increase by more than 5 points.

The melting procedure consisted of loading the desired amount of molybdenum powder into a cavity drilled in a piece of titanium and covering the cavity with a titanium cap. The total weight of a specimen was between 5 and 15 g. Each specimen was melted several times in order to obtain an homogeneous alloy. The alloys were not chemically analyzed after melting. Several specimens, however, were weighed before and after melting and, since the change in weight was found to be less than 0.2 pct, it was assumed that the change in composition, if any, was negligible. After melting, the alloys that were sufficiently ductile (up to about 10 pct Mo) were cold rolled with various reductions in cross-section. All the specimens, whether rolled or not, were sealed in evacuated fused silica tubes (vacuum of 10^{-4} mm Hg or less) and homogenized for 24 hr at 982°C (1800°F). The specimens were then quenched in water from that temperature. All subsequent heat treatments were also carried on in evacuated fused silica capsules. All these heat treatments were made at constant temperature and followed by quenching.

For microscopic observation, the specimens were polished by conventional methods, finishing with 0 to 2 microns diamond powder and etching with a solution of one part 48 pct hydrofluoric acid, one part concentrated nitric acid, and two parts glycerine. A magnification of 250 times was used.

Results of Measurements on Pure Metals

Titanium: Pure titanium obtained by the iodide process was received from the Foote Mineral Co. and from the New Jersey Zinc Co. A small piece of iodide titanium was also obtained from the Naval Research Laboratory through the courtesy of Dr. Chapin. The Vickers hardness (10 kg load) of any of these three specimens varied from about 55 to 75, this variation within a given sample being due probably to crystal orientation. Measurements of Vickers hardness therefore was not suitable for detecting possible differences in the degree of purity of the three samples.

A total of approximately 170 cooling curves was obtained with various rates of cooling ranging from 4° to about 15,000°C per sec. Typical cooling curves obtained with various rates of cooling are shown in Fig. 1. With the exception of a few tests, the break in the cooling curve at the transformation point was quite easy to locate and the accuracy of measurement of the transformation temperature was approximately ±4°C.

The results of measurements on the three samples of iodide titanium are summarized in the graphs of Fig. 2. The scatter between transformation temperatures measured on several samples around a given rate of cooling seems to exceed ±4°C, which is the estimated accuracy of measurement. It is probable that part of the scatter is due to the statistical nature of the nucleation process. In any case, all the measurements seem to be included in a band which has a width of about 10°C at low rates of cooling and of about 20°C at high rates. By taking the center line of such a band as an average curve, it may be concluded that the β to α transformation of titanium decreases slightly with increasing rates of cooling and varies from 882°C at relatively low rates to about 850°C at cooling rates of the order of 10,000°C per sec.

In about half of the 170 cooling curves obtained for the pure titanium specimens, a more or less pronounced heat effect was observed at a temperature higher than that at which the main thermal arrest took place. In many cases a definite change in the slope of the cooling curve was noticeable, as shown at point X on one of the graphs reproduced in Fig. 1. The temperature at which this anomaly was observed varied from specimen to specimen, covering a range from 905° to about 960°C. The variation in the temperature at which the extra thermal arrest was observed excluded the possibility of a second allotropic transformation, although such a transformation has been suggested by McQuillan.[10]

In a more detailed investigation recently published,[3] this same author seems to refute his previous

conclusions and demonstrates that the anomalies observed in the behavior of titanium around the α-β transformation are due to contamination of the specimens by oxygen. In measuring the equilibrium pressure of hydrogen in contact with a titanium specimen as a function of temperature, McQuillan found that, on heating, the discontinuity in pressure is very sharp at the α-β transformation temperature (882.5°C). As the temperature is increased, however, the specimen seems to continue transforming up to (in one case) about 930°C and from there on the pressure-temperature relationship becomes normal (linear relation between log p and 1/T). The explanation for the progressive transformation is that even in a vacuum as low as 10^{-4} mm Hg, there is enough residual oxygen to contaminate the outside layer of the titanium specimen. It is therefore logical to expect that the uncontaminated part of the specimens (the inside core) will transform at 882.5°C with a sharp discontinuity in the pressure. The outside layer, which contains all concentrations of oxygen from zero to a maximum at the surface, will transform gradually over a range of temperatures corresponding to the range of oxygen concentration present. Upon cooling, the reverse mechanism takes place, and the same relationship is observed between the pressure and temperature. By introducing a very small amount of oxygen into the vacuum chamber in order to purposely contaminate the specimen, McQuillan observed that the range of temperature over which the transformation proceeds was increased, and in one case extended from 882.5° to about 960°C.

The conclusions reached by McQuillan concerning the effect of surface contamination on the transformation temperature of titanium clearly explain the anomalies found in the cooling curves discussed in the present study. The very thin specimen used in the quenching experiments is, of course, subject to some contamination by residual oxygen and nitrogen, even if, as stated above, the time necessary for heating the specimen is of the order of seconds only. The oxygen contaminated case around the specimen undergoes the β to α transformation at temperatures above the normal transformation temperature and a decrease in the slope of the cooling curve is observed as shown at point X of Fig. 1. When the transformation temperature of pure titanium is reached, the uncontaminated core of the specimen transforms and the main thermal arrest appears on the cooling curve. Since the degree of contamination is not exactly the same from test to test, the first break in the cooling curve is sometimes more or less pronounced and sometimes absent. When the extra thermal arrest is actually observed, it is not always at the same temperature, but always within a range which is very nearly the same as that found by McQuillan (905° to 960°C).

Table I. Effect of Rate of Cooling on Transformation Temperature of Thallium

Rate of Cooling, °C per Sec	Transformation Temperature, °C
105	231
650	228
950	233
1120	229
1560	231
2150	229
3000	232
8100	230
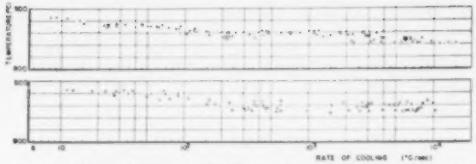
Fig. 2—Effect of rate of cooling on the allotropic transformation temperature of titanium (iodide process).
Upper graph: Foote Mineral Co. titanium. Lower graph: ○—New Jersey Zinc Co. titanium. ●Naval Research Laboratory titanium.

Zirconium: Because zirconium and titanium have very similar physical properties, it was anticipated that the effect of the rate of cooling on the β to α transformation of zirconium would be the same as that found for titanium. About 85 cooling curves were recorded on zirconium specimens cut from a bar of pure zirconium made by the iodide process by the Foote Mineral Co. The results, shown in Fig. 3, indicate that the transformation temperature of zirconium decreases from 865° to about 850°C with increasing rates of cooling. The effect of rate of cooling is therefore smaller for zirconium (about 15°C) than for titanium (about 35°C).

It is interesting to mention that for zirconium no additional thermal arrest of the type found for titanium was observed on any of the cooling curves. Since the experimental conditions were the same for the two metals, it seems that either the rate of absorption of oxygen and nitrogen is smaller in zirconium than in titanium, or that the transformation temperature of zirconium is not greatly affected by oxygen and nitrogen. Since zirconium is generally considered as a better "getter" than titanium, the second hypothesis is probably the more likely one.

Thallium: Besides titanium and zirconium, thallium is the only other element having an allotropic transformation from a high temperature, body-centered cubic form to a low temperature, hexagonal close-packed form.[11]* A few measurements were performed on 99.9 pct pure thallium obtained from Belmont Smelting & Refining Works, Brooklyn. The thermal arrest was not as pronounced as in the case of titanium and zirconium, due to the fact that the latent heat of transformation for thallium is only 0.074 kcal per mol compared with 0.71 for zirconium.[12] However, the arrest could be located easily and the accuracy in the temperature measurement was about ±4°C. The results summarized in Table I indicate that up to a rate of cooling of about 8000°C per sec, the transformation temperature remains within the limits of accuracy of ±4°C. It may be concluded therefore that if rates of cooling up to 8000°C per sec have any effect on the transformation temperature of thallium, this effect is less than about ±4°C.

Iron: Although many studies have been published on the effect of the rate of cooling on the transformation in Fe-base binary alloys, the early results of Esser et al.[13] seem to be the only ones obtained on relatively pure iron and with high rates of cooling. According to these investigators, the α to γ transformation can be depressed from 905°C to as low as about 500°C at cooling rates of the order of 10,000°C per sec. The only information on the carbon content of the material used by Esser is that it was less than 0.017 pct and no definite statement is made concern-

* Since this work was completed, a body-centered cubic to hexagonal close-packed allotropic transformation has been found in hafnium; it will be described in a forthcoming paper.

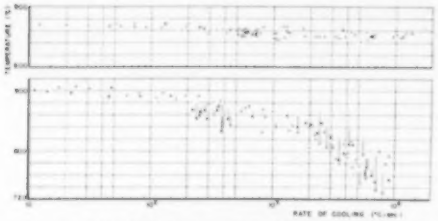

—Bureau of Standards iron. ●—National Research Corp. iron.
Fig. 3—Effect of rate of cooling on the allotropic transformation temperature of zirconium (upper) and iron (lower).

ing other possible impurities. Since Esser's experiments were performed in an atmosphere of hydrogen, there might also be some question about the effect of hydrogen absorption on the allotropic transformation.

Since iron may be obtained at present with a higher degree of purity than at the time the work of Esser was reported, 1933, the effect of rate of cooling on the γ to α transformation temperature was reinvestigated on two different iron samples. The first sample was a small bar of spectroscopically pure iron from the Bureau of Standards. The purity of this particular sample (ingot No. 8) has been described in ref. 14; the carbon content is less than 0.001 pct. The second kind of iron was a 10 lb vacuum-cast ingot purchased from National Research Corp., Boston, Mass. A typical analysis of this type of metal is less than 0.005 pct C, less than 0.02 pct O, less than 0.001 pct N and H, and traces of various metallic impurities (each less than 0.001 pct).

The effect of the rate of cooling on the γ to α transformation is shown in Fig. 3 for the two types of iron tested. In approximately half of the cooling curves, a more or less pronounced recalescence took place at the transformation temperature. This behavior is indicated on the diagram of Fig. 3 by means of a vertical line connecting the minimum temperature corresponding to the beginning of transformation to the maximum temperature reached after recalescence. In spite of the relatively large scatter in experimental results, Fig. 3 indicates clearly that

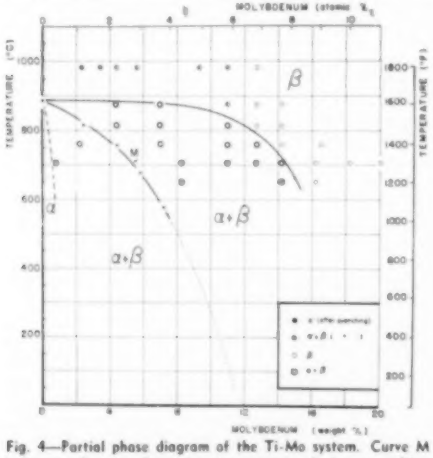

Fig. 4—Partial phase diagram of the Ti-Mo system. Curve M indicates the transformation temperature during quenching from the beta field.

by increasing the rate of cooling it is possible to decrease the allotropic transformation temperature of iron from 905°C to approximately 750°C at a cooling rate of about 10,000°C per sec. This decrease of the γ-α transformation temperature is much smaller than that reported previously by Esser et al.[12] The most probable reasons for the lack of agreement between the two investigations are, first, the difference in the purity of the iron samples, and second, the effect of hydrogen used as an atmosphere in Esser's experiments.

In any case, the rate of cooling has a greater influence on the γ to α transformation temperature of iron than on the β to α transformation temperature of titanium, zirconium, and thallium. In addition, recalescence was frequently observed in iron, but never occurred in any of the measurements made on the other three metals.

Results of thermal analysis measurements are difficult to interpret on a quantitative basis and therefore it is not possible to determine exactly the

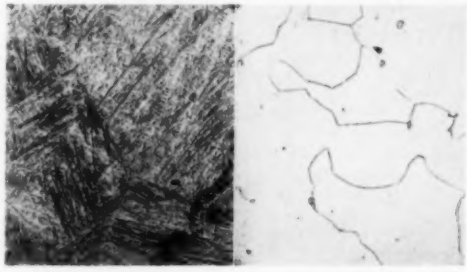

10.85 pct Mo (α'). 12.7 pct Mo (β).
Fig. 5—Structure of Ti-Mo alloys quenched from 980°C.

factors responsible for the differences between the behavior of titanium and that of iron. The change in crystal structure is of course a factor to consider. From this point of view, the results indicate that the rate of cooling has less effect on a body-centered cubic to hexagonal close-packed transformation than on a face-centered cubic to body-centered cubic transformation. This observation, however, does not lead to the conclusion that the atomic processes involved in titanium and in iron are necessarily different. In fact, both transformations are probably of the nucleation and shear type, and apparent lack of similarity in the behaviors of the two metals during fast cooling may simply be the result of differences in the numerical values of the basic factors controlling the rate of nucleation and the energy involved in the shearing process. Further work in the field of phase transformation in pure metals is obviously necessary to answer these questions.

Titanium-Molybdenum System

On the basis of the Hume-Rothery rules governing the formation of solid solutions, titanium and molybdenum should be completely soluble in each other at high temperature. Previous work on this system[6] and additional unpublished results obtained in this laboratory have confirmed this prediction. At temperatures below the α-β transformation of titanium, the solubility of molybdenum in α titanium is apparently very small and the preliminary results[6] indicate that the Ti-Mo phase diagram below 882°C may be similar to the Fe-Ni diagram.

The results of the present study will be described in two parts, the equilibrium phase boundaries be-

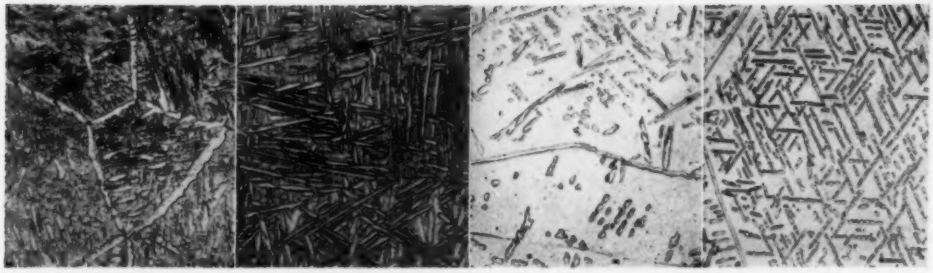

7.1 pct Mo quenched from 871°C ($\alpha+\alpha'$). 4.35 pct Mo quenched from 816°C ($\alpha+\beta$). 10.85 pct Mo quenched from 816°C ($\alpha+\beta$).

Fig. 6—Structure of Ti-Mo alloys quenched from 871° and 816°C.

tween 650° and 882°C and the effect of rate of cooling on the β to α transformation in alloys containing less than 12 pct Mo.

Equilibrium Boundaries Between 650° and 882°C: A series of Ti-Mo alloys containing up to about 20 pct Mo were prepared by the arc-melting method described above. All the alloys were first heated to 980°C for 24 hr and quenched in water. Subsequently they were held at constant temperature for 5 days at 871°C and at 816°C, 10 days at 760°C, 20 days at 700°C, and 30 days at 650°C. The alloy compositions and the structures observed after heat treatment are shown by symbols on Fig. 4.

After quenching from 980°C, the alloys containing 2.3, 3.2, 4.35, 5.6, and 10.85 pct Mo had the typical Widmanstätten microstructure (cf. Fig. 5) found in titanium alloys in which the high temperature β solid solution is transformed, at least partially, into the supersaturated α solid solution. For simplicity, this supersaturated solid solution will be called α', following the nomenclature used by Troiano and McGuire[15] in their study of the Fe-Mn system. The alloy containing 12.7 pct Mo, after quenching, had the β-retained structure (cf. Fig. 5). Hence, the minimum amount of molybdenum necessary to retain the β structure after quenching is around 12 pct Mo.

X-ray diffraction patterns were also taken of the alloys quenched from 980°C. In order to obtain the sharpest possible patterns, the powder was first filed from the quenched specimens, sealed in evacuated quartz tubes, reheated rapidly to 980°C for 5 min, and then quenched in liquid argon.† In spite of these precautions, the patterns were not sharp enough to show resolved doublets in the back-reflection range. This lack of resolution is probably due to the strain introduced by the alloying element in a supersaturated α titanium lattice.

In spite of their lack of sharpness, the X-ray diffraction patterns indicated quite clearly that, in addition to the α' phase, the β phase was also present in alloys containing 4.35, 5.6, 9.35, and 10.85 pct Mo. Judging from the relative intensity of the α' and the β patterns, it was also clear that the amount of the β phase was increasing with molybdenum content. This behavior is very similar to the well-known phenomenon of retained austenite in steels. A quantitative study of the relative amount of α' and retained β could probably be made by using the special X-ray diffraction methods successfully applied by Averbach and Cohen[17] for determining the amount of retained austenite.

The structure of the alloys was investigated by microscopy after attaining equilibrium at 871°C and below. After the 871°C treatment, alloys with 4.35 and 7.1 pct Mo contained α in a matrix of α', the latter formed by the transformation of β during cooling, as shown in Fig. 6. The alloy containing 10.85 pct Mo was α' and the alloys containing 12.7 and 14.3 pct Mo had the β-retained structure. These results, shown by symbols on the diagram of Fig. 4, indicate that at 871°C the phase boundary between the $\alpha+\beta$ and the β fields must cross the 871°C line between 7.1 and 10.87 pct Mo. This location of the phase boundary is compatible with the fact that in the alloys containing 4.35 and 7.1 pct Mo the β phase was not retained after quenching. In these alloys the β phase contains less than the critical value of 12 pct Mo and consequently transforms into α' dur-

† As is explained in ref. 16, titanium powder reacts with water during quenching and a change in lattice parameter of α titanium, probably due to absorption of oxygen, has been observed.

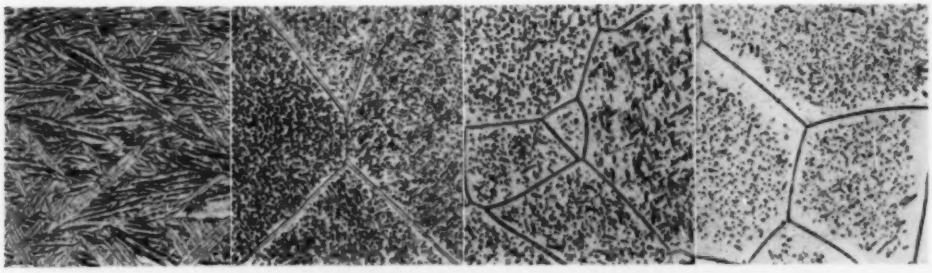

1.8 pct Mo ($\alpha+\beta$). 10.85 pct Mo ($\alpha+\beta$). 12.7 pct Mo ($\alpha+\beta$). 14.3 pct Mo ($\alpha+\beta$).

Fig. 7—Structure of Ti-Mo alloys quenched from 760°C.

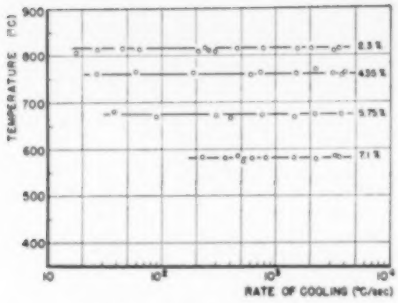

Fig. 8—Effect of the rate of cooling on the transformation temperature of Ti-Mo beta solid solution for various molybdenum concentrations.

ing quenching. The α' structure in the alloy containing 10.85 pct Mo after the 871°C treatment is also logical, since this alloy was in the β field at temperature, but does not contain enough molybdenum to retain the β structure.

After the heat treatments at 816°, 760°, 700°, and 650°C, all the alloys contained either the two phases, α and β, or the β phase only. These results are shown by appropriate symbols in the phase diagram of Fig. 4. Typical microstructures of some of the alloys are shown in Figs. 6 and 7. From these results, the phase boundary between the $\alpha+\beta$ and the β fields may be traced as indicated in Fig. 4. It is, of course, impossible to describe the accuracy in the location of this phase boundary by means of numbers referring to either temperature or concentration. A good estimate of the accuracy can be gained by drawing the boundaries that would be shifted most towards low and high concentration and would still separate the two phase from the one phase alloy. It is believed that these two curves would not be further apart than 1 pct Mo, at the most.

No attempt was made to determine the boundary between the α and the $\alpha+\beta$ phases. The solubility of molybdenum in α titanium, however, is probably very small. The alloy containing 0.8 pct Mo was found to be in a two-phase region at 700°C. A few X-ray diffraction patterns were made from other alloys containing less than 1 pct Mo and no appreciable shift in the powder pattern could be detected. It seems therefore that the solubility of molybdenum in α titanium is less than 1 pct and high accuracy X-ray diffraction measurements will be necessary to establish the solubility limits.

The study of the phase diagram was not pursued at temperatures below 650°C because of the sluggishness of the reactions. It was found, for example, that at 625°C equilibrium structures were not obtained after six weeks at temperature. The knowledge of the phase boundaries below 650°C, however, is not necessary for interpreting the results of the experiments made with high rates of cooling.

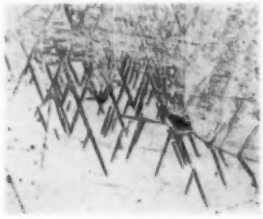

Fig. 9—Typical martensite-like structure in a Ti-Mo alloy (5 pct Mo) quenched from 980°C.

Phase Transformation at High Rates of Cooling: Since the alloys containing less than about 12 pct Mo transform from β to α' during quenching, it was anticipated that the temperature at which this transformation takes place could be detected by thermal analysis. Alloys containing 2.3, 4.35, 5.75, 7.1, 8.15, 9.35, and 12.7 pct Mo were tested and temperature vs. time curves were recorded at various rates of cooling. For the alloys containing 2.3, 4.35, 5.75, and 7.1 pct Mo, a clearly defined thermal arrest was observed. Within the limits of experimental errors, the rate of cooling had no effect on the temperature at which the thermal arrest occurred (cf. Fig. 8). It is therefore established that Ti-Mo alloys containing 0 to 7.1 pct Mo transform from a β solid solution to a supersaturated α solid solution at a temperature which is independent of the rate of cooling. This temperature decreases with increasing molybdenum content following a smooth curve, as shown in Fig. 4 (curve *M*).

The thermal analysis experiments made on the alloys containing 8.15, 9.35, and 12.7 pct Mo failed to reveal a thermal arrest. This is not surprising for the alloy containing 12.7 pct Mo, since in this alloy the β structure is retained after quenching. In the alloys containing 8.15 and 9.35 pct Mo, the results of microscopy and X-ray diffraction described in a previous section indicated that at least some of the high temperature β phase was transformed into supersaturated α during quenching. For these alloys, the failure in measuring a heat effect by thermal analysis may be due to the fact that only a relatively small portion of β is undergoing the transformation and the method of measurement is not sufficiently sensitive to record a heat effect. In any case, it seems logical to assume that the partial transformation from β to α' in the range of concentration from about 8 to about 11 pct Mo takes place at temperatures below 500°C and the transformation temperature vs. concentration curve in this range is probably an extension of the curve measured for lower concentrations. It is interesting to point out that by extrapolating the solid curve M of Fig. 4 to higher concentrations (as shown by the dotted portion of the curve), it appears that the transformation temperature would be below room temperature when the molybdenum concentration is about 12 pct. This is the approximate concentration above which the β phase is actually retained after quenching from high temperature.

Allotropic Transformation in Titanium Alloys

The striking analogy between the Ti-Mo alloys and some of the Fe-base binary alloys, like those with nickel or manganese, strongly suggests that the atomic mechanisms by which the transformation takes place in the two classes of alloys are very similar, and the Ti-Mo transformation would be of the martensitic type. Obviously, the results of the present investigation do not demonstrate that all the characteristic features of a martensite reaction exist in the Ti-Mo system. However, since the reaction takes place, at least partially, at rates of cooling of the order of 10,000°C per sec, it is difficult to refute the conclusion that the reaction is diffusionless. In addition, it was shown that the temperature at

which the reaction takes place is independent of the rate of cooling. Therefore, two important characteristics of the martensite reaction have been found in Ti-Mo alloys.

It may be of interest also to point out that in some cases micrographs showing the typical structure of martensite needles have been obtained. Fig. 9 shows a Ti-Mo alloy containing 9.5 pct Mo prepared with titanium powder obtained from the Bureau of Mines and quenched from the β field.‡ The rather large α' needles in a β matrix are very similar to martensite in austenite. The occurrence of well-defined isolated needles, as shown in Fig. 9, was rather rare in the specimens studied in the present investigation, probably because too large a portion of the β phase was transformed. There is probably a critical and narrow range of molybdenum concentration for which only a small fraction of the β phase would be transformed by quenching to room temperature, and in this range more typical martensitic needles could likely be obtained.

The thermal analysis method used in this investigation is not suitable for a complete study of the finer details involved in a martensite reaction. It is probable that there is a temperature interval between the beginning and the end of the reaction. By thermal analysis, it is possible to detect only the temperature at which the bulk of the heat is released. This temperature probably corresponds to that which is sometimes referred to as the burst temperature for the martensite reaction.

Finally, the atomic mechanism of the transformation in titanium alloys of the Ti-Mo type remains unknown. The only clue to a possible mechanism is the work of Burgers on the crystallographic relationships in the transformation of pure zirconium.[18]

Conclusions

1—The temperature at which titanium transforms from the β form (body-centered cubic) to the room temperature α form (hexagonal close-packed) decreases progressively from 882°C to about 850°C with increasing rate of cooling from 4° to 10,000°C per sec. A similar effect has been found for zirconium, for which the drop in temperature is from 865° to 850°C. The transformation temperature of thallium (also from body-centered cubic to hexagonal close-packed) is not affected by rates of cooling up to 8000°C per sec. The body-centered cubic to hexagonal close-packed transformation in these three metals is therefore a diffusionless transformation and is probably the result of a combination of shear and homogeneous change in volume.

2—The solid state phase boundaries in the Ti-Mo system have been established above 650°C. Alloys quenched from the β field transformed into an α supersaturated solid solution (called α') for molybdenum concentration up to about 12 pct. The transformation is only partial from about 4 to 12 pct Mo. Above 12 pct Mo, the β structure is retained.

3—From 0 to 8 pct Mo, the temperature at which β transforms entirely or partially to α' was measured by thermal analysis. This temperature is not affected by the rate of cooling. For molybdenum concentration between 8 and 12 pct, no heat effect was detected during cooling although it was found by both X-ray diffraction and microscopy that α' was present after quenching. The heat released in the case of partial transformation was probably too small to be detected by thermal analysis.

4—The analogy between the Ti-Mo alloys and some binary Fe-base alloys (such as iron with nickel or manganese) suggests that the transformation in the Ti-Mo system is of the martensite type. The same type of transformation has been found in the Ti-Cr system and probably exists in other binary alloys for which there is an extensive solid solubility in β titanium.

‡ Such specimens prepared by powder metallurgical methods were not as pure as those used for the phase diagram study and the presence of impurities might have had an effect on the microstructure.

Acknowledgment

This work was sponsored by the Office of Naval Research, U. S. Navy, under contract number N6ONR-24430. The author wishes to express his appreciation to I. R. Kramer, Head, Materials Branch, Office of Naval Research, who pointed out the importance of the kinetics of the phase transformation in titanium alloys. Thanks are also due to D. S. Clark for his valuable cooperation and to J. O. McCaldin, J. M. Denney, and W. V. Wright, Jr., who carried out most of the experiments.

References

[1] A. Schulze: Transformation in Metals. *Ztsch. für Metallkunde* (1931) **23**, p. 261.

[2] J. H. De Boer, W. G. Burgers, and J. D. Fast: The Transition of Hexagonal Alpha Titanium into Cubic Beta Titanium at High Temperature. *Proc.* Acad. Sci. Amsterdam (1936) **39**, p. 515.

[3] A. D. McQuillan: Some Observations on the Alpha-Beta Transformation in Titanium. *Journal* Inst. of Metals (1950) **18**, p. 249.

[4] W. G. Burgers and F. M. Jacobs: Crystal Structure of Beta Titanium. *Ztsch. für Krist.* (1936) **94**, p. 299.

[5] J. R. Long, E. T. Hayes, D. C. Root, and C. E. Armantrout: A Tentative Titanium-Nickel Diagram. U. S. Bur. of Mines, *R. I.* No. 4463 (February 1949).

[6] C. M. Craighead, O. W. Simmons, and L. W. Eastwood: Titanium Binary Alloys. *Trans.* AIME (1950) **188**, p. 485; JOURNAL OF METALS (March 1950).

[7] W. Finlay, J. Resketo, and M. Vordahl: *Industrial and Engineering Chemistry* (1950) **42**, pp. 218-222.

[8] A. B. Greninger: The Martensite Thermal Arrest in Iron-Carbon Alloys and Plain Carbon Steels. *Trans.* ASM (1942) **30**, p. 1.

[9] C. H. Schramm, P. Gordon, and A. R. Kaufmann: The Alloy Systems Uranium-Tungsten, Uranium-Tantalum, and Tungsten-Tantalum. *Trans.* AIME (1950) **188**, p. 195; JOURNAL OF METALS (January 1950).

[10] A. D. McQuillan: Allotropic Transformation in Titanium. *Nature* (1949) **164**, p. 24.

[11] H. Lipson and A. R. Stokes: The Structure of Thallium. *Nature* (1941) **148**, p. 437.

[12] C. J. Smithells: *Metals Reference Book*. p. 419. (1949) New York. Interscience Publishers, Inc.

[13] H. Esser, W. Elender, and E. Spenle: The Hardening of Iron-Carbon Alloys. *Archiv für der Eisenhüttenwesen* (1933) **6**, p. 389.

[14] H. E. Cleaves and J. M. Hiegel: Physical Properties of Pure Iron. U. S. Bur. of Standards *Journal of Research* (1942) **28**, p. 643.

[15] A. R. Troiano and F. T. McGuire: A Study of the Iron Rich Iron-Manganese Alloys. *Trans.* ASM (1943) **31**, p. 340.

[16] P. Duwez and J. L. Taylor: A Partial Titanium-Chromium Phase Diagram and the Crystal Structure of $TiCr_2$. To be published.

[17] B. L. Averbach and M. Cohen: X-Ray Determination of Retained Austenite by Integrated Intensities. *Trans.* AIME (1948) **176**, p. 401; METALS TECHNOLOGY (September 1947).

[18] W. G. Burgers: On the Process of Transition of the Cubic Body-Centered Modification into the Hexagonal Close-Packed Modification of Zirconium. *Physica* (1934) **1**, p. 561.

Crystal Structure of Ti_5Si_3, Ti_5Ge_3, and Ti_5Sn_3

by Paul Pietrokowsky and Pol Duwez

The crystal structure of the compound Ti_5Ge_3 has been determined from X-ray powder diffraction data. Related silicon and tin compounds have been found to be isomorphous. Unit cell dimensions, axial ratios, and parameters for equivalent atomic positions are given.

THERE is, at present, only meager information pertaining to the solid state reactions of titanium with the elements in group 4B of the periodic table (silicon, germanium, tin, and lead). The only two compounds whose crystal structure has been established are $TiSi_2$ and $TiGe_2$ (references 1 and 2 respectively). These two compounds are isomorphous and have an orthorhombic symmetry D^{24}_{2h} — *Fddd*. The titanium-rich regions of the constitution diagrams of titanium-silicon,[3] titanium-tin, and titanium-lead have been investigated by Craighead et al.[3] While valuable information concerning the alpha solid solubility of these three elements in titanium was obtained, no light was shed on the existence or nature of the titanium-rich compound in these systems. The present study is concerned with the crystal structure of the intermediate phases Ti_5Si_3, Ti_5Ge_3, and Ti_5Sn_3, which were found to be isostructural.

The alloys were prepared by mixing the pure metal powders in the desired proportions, pressing the mixture into pellets, and melting them in an electric arc furnace in the presence of a helium atmosphere.[4] After melting, the specimens, weighing approximately 5 g, were sealed in evacuated quartz vials, homogenized at 1038°C for three days, and quenched from that temperature. Powder diffraction patterns were made with a 143.2 mm diam Debye-Scherrer X-ray camera in which the Ievins and Straumanis film arrangement was utilized. Filtered copper radiation was used throughout the entire investigation.

A study of the powder patterns of a series of alloys of various compositions indicated the presence of a compound around a composition corresponding approximately to a ratio of 3 titanium to 2 silicon, germanium, or tin. From a visual examination of the diffraction patterns, it was evident that the silicon and germanium alloys were isomorphous. For small angle reflections, the powder pattern of the tin compound was analogous to that of the silicon and germanium compounds, but after the first ten reflections, the similarity was no longer clear. The powder pattern of the germanium compound was selected for indexing, since it exhibited a weak small angle reflection and clearly resolved doublets in the back-reflection range. Good agreement between observed and calculated values of $(1/d)^2$ was found by indexing the pattern on the basis of hexagonal symmetry. For the hexagonal system:

Table I. Debye-Scherrer Powder Diffraction Data for Ti_5Ge_3. Filtered Copper Radiation.

hkl	d Obs. (A)	$(1/d)^2$ Obs. (A^{-2})	$(1/d)^2$ Calc. (A^{-2})	Intensity, Obs.	Relative Intensity, Calc.
10.0	6.5	0.0236	0.0235	w	A*
10.1	—	—	—	—	0
11.0	3.79	0.0697	0.0705	w	29
20.0	—	—	—	—	13
11.1	3.07	0.1064	0.1072	m	175
20.1	—	—	—	—	0
00.2	2.61	0.1473	0.1465	ms	270
21.0	2.47	0.1632	0.1645	ms	250
10.2	2.42	0.1700	0.1703	wm	201
21.1	2.22	0.2022	0.2012	vs	1000
30.0	2.17	0.2115	0.2115	ms	302
11.2	2.14	0.2175	0.2173	s	546
20.2	2.03	0.2417	0.2408	m	125
22.0	—	—	—	—	3
31.0	1.81	0.3041	0.3055	w	78
21.2	—	—	—	—	8
22.1	1.77	0.3179	0.3187	m	118
00.3	—	—	—	—	0
31.1	1.71	0.3406	0.3422	s	321
10.3	—	—	—	—	0
30.2	1.67	0.3572	0.3583	w	13
40.0	—	—	—	—	3
11.3	1.58	0.3990	0.4006	w	21
20.3	—	—	—	—	0
22.2	1.53	0.4311	0.4288	m	85
32.0	—	—	—	—	5
31.2	—	—	—	—	3
32.1	1.441	0.4817	0.4823	w	6
41.0	1.422	0.4946	0.4935	s	42
21.3	1.422	0.4946	0.4948	s	209
40.2	1.383	0.5229	0.5228	m	39
50.0	1.366	0.5867	0.5875	—	198
00.4	1.306	0.5867	0.5872	s_s**	66
32.2	1.301	0.5911	0.5933	m	66
22.3	1.278	0.6126	0.6133	wm	42
***					

* Calculated intensity not significant because of absorption.
** A broad strong reflection due to overlapping.
*** Thirty-five additional reflections with spacing smaller than 1.27 A were observed.
vs = very strong, s = strong, ms = medium strong, m = medium, wm = weak medium, w = weak.

P. PIETROKOWSKY, Junior Member AIME, is Research Engineer and POL DUWEZ, Member AIME, is Associate Professor of Mechanical Engineering and Chief of the Materials Section, Jet Propulsion Laboratory, California Institute of Technology, Pasadena, Calif.

Discussion on this paper, TP 3121E, may be sent, 2 copies, to AIME by Dec. 1, 1951. Manuscript, April 10, 1951. Detroit Meeting, October 1951.

$$(1/d)^2 = A\,(h^2 + hk + k^2) + B\,(1)^2 \qquad [1]$$

$$A = \frac{4}{3\,a^2}, \quad B = \frac{1}{c^2}$$

The results of these computations are shown in Table I.

A similar method of indexing was applied to the titanium-silicon and titanium-tin compounds, and in all cases, good agreement was obtained between calculated and observed interplanar spacings. The values of the constants A and B in the quadratic eq 1 and the lattice parameters of the three compounds are given in Table II. The parameters were obtained by applying the least squares method to the large angle reflections.

Table II. Unit Cell Parameters for Ti_5Si_3, Ti_5Ge_3, and Ti_5Sn_3. Parameters are expressed in A.

Compound	A	B	a_0	c_0	c_0/a_0
Ti_5Si_3	0.0239	0.0375	7.465±0.002	5.162±0.002	0.692
Ti_5Ge_3	0.0235	0.0367	7.537±0.002	5.223±0.002	0.693
Ti_5Sn_3	0.0258	0.0336	8.049±0.002	5.454±0.002	0.678

An attempt to elucidate the structure of the titanium-germanium compound was made on the basis of the powder pattern. The only systematic extinctions in the Debye-Scherrer patterns are those of the $(h0l)$ reflections for $l \pm 2n$. This indicates the presence of a mirror glide plane with a displacement $c/2$ parallel to the c axis. Since no other systematic extinctions were observed, five space groups are possible, namely D^1_{4d}, C^6_{2v}, D^3_{4h}, C^6_{4v}, and D^5_{2h}. Since a further reduction in the number of likely space groups is not possible from the powder data, it was decided to initiate a survey of the literature prior to finding the Laue symmetry. This survey failed to uncover any similitude with a compound of the A_5B_3 type, but an analogy was found with Mn_5Si_3. The structure of Mn_5Si_3 determined by Åmark, Borén, and Westgren,[5] is hexagonal and belongs to the space group $D^3_{6h} - C\ 6/mcm$ (type $D8_8$). The unit cell contains 16 atoms in the following positions: *

4 Mn I in (d): 1/3 2/3 0; 2/3 1/3 0; 1/3 2/3 ½; 2/3 1/3 ½.

6 Mn II in (g): $x0\frac{1}{4}$; $0x\frac{1}{4}$; $\bar{x}\bar{x}\frac{1}{4}$; $\bar{x}0\frac{3}{4}$; $0\bar{x}\frac{3}{4}$; $xx\frac{3}{4}$. $x = 0.23$.

6 Si in (g): $x = 0.60$.

A perspective drawing of the structure is shown in Fig. 1.

Assuming this structure to be the correct one for the titanium-germanium compound, intensity computations were made using the well-known formula:

$$I = \text{constant}\ [F\,(hkl)]^2\ p\ \frac{1 + \cos^2 2\theta}{\sin^2\theta \cos\theta}$$

In view of the large number of reflections present (57 for Ti_5Ge_3), no correction for absorption was included in the calculated intensities. Only the first reflection (100) suffers greatly from this oversight. With the exception of the (100) reflection, the agreement between calculated and observed intensities (Table II) is quite satisfactory. Similar computations were made for Ti_5Si_3 and Ti_5Sn_3, and in all cases, the observed intensities were in good agreement with the calculated values.

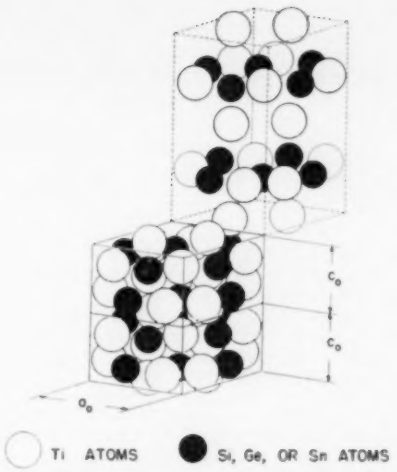

Fig. 1—Perspective drawing of two cells of Ti_5 (Si, Ge, Sn)$_3$ (lower left) and of one cell expanded in the c axis direction (upper right).

From the point of view of a systemization of the structure of intermetallic compounds between the transition elements of the first series and the elements of the 4B group of the periodic table, it is interesting to note that the only other intermetallic compound reported so far as being isomorphous with Mn_5Si_3 is the η phase (Fe_5Si_3) in the iron-silicon system.[7, 8] It is probable that other compounds of the Mn_5Si_3 type exist between the transition elements and silicon, germanium, and tin.

Acknowledgments

This work was done at the Jet Propulsion Laboratory, California Institute of Technology, under contract number W-04-200-ORD-455 with the Army Ordnance Department, Washington, D. C. The authors wish to thank this agency for the permission to publish the results of this investigation.

References

[1] F. Laves and H. J. Wallbaum: The Crystal Structure of Ni_2Ti and Si_2Ti. *Ztsch. für Kristallographie* (1939) **101**, pp. 78-93.

[2] C. J. Smithells: *Metals Reference Book*, p. 218 (1949) New York. Interscience Publishers, Inc.

[3] C. M. Craighead, O. W. Simmons, and L. W. Eastwood: Titanium Binary Alloys. *Trans.* AIME (1950) **188**, pp. 485-513; JOURNAL OF METALS (March 1950).

[4] C. H. Schramm, P. Gordon, and A. K. Kaufman: The Alloy Systems Uranium-Tungsten, Uranium-Tantalum, and Tungsten-Tantalum. *Trans.* AIME (1950) **188**, pp. 195-204; JOURNAL OF METALS (January 1950).

[5] K. Åmark, B. Borén, and A. Westgren: X-Ray Analysis of Manganese-Rich Manganese-Silicon System. *Metallwirtschaft* (1936) **15**, pp. 835-836.

[6] *Strukturbericht*, Ed. by C. Gottfried. Akademische Verlagsgesellshaft M. B. H. Leipzig. (1936) **4**, pp. 24-25.

[7] A. R. Weill: Structure of the Eta Phase of the Iron-Silicon System. *Nature* (1943) **152**, p. 413.

[8] H. Lipson and A. R. Weill: The Mechanism of Phase Change on Some Iron-Silicon Alloys. *Trans.* Faraday Soc. (1943) **39**, pp. 13-18.

* An error in the tabulation of nearest neighbors to the silicon atom in the position $\bar{x}\bar{x}\frac{1}{4}$, $x = 0.60$, should be corrected in ref. 6. The atom designated f' and the two atoms marked f'' are Mn II atoms and not Si atoms; the number of nearest neighbors to the silicon atoms having the structural symmetry $C\ 2v - mm$ are 4 Mn I atoms, 3 Mn II atoms, and 6 Si atoms.

Role of Gases in the Production of High Density Powder Compacts

by Donald Warren and J. F. Libsch

THIS investigation originated as a result of a previous experimental study[1] of the magnetic properties of Fe-Co alloys fabricated by the powder metallurgy technique. Densities of powder compacts prepared for the magnetics investigation varied from 7.45 to 7.70 g per cu cm or from 93 to 95 pct of the experimental value of 8.08 g per cu cm for a fused alloy of the same composition.[2] While this range of density is considered sufficiently high for most applications, the highest possible density is to be desired for maximum magnetic properties.

By applying a technique similar to the one described above to a pure electrolytic iron powder, Rostoker[3] was able to achieve a density of 7.895 g per cu cm, which is the highest density ever reported for sintered iron. While Rostoker's work involved the sintering of an elemental powder rather than a mixture, it was believed that higher densities should also have been obtained for alloys using the above technique because of the recoining operation and the high sintering temperature. Consequently, it was decided to investigate the various factors affecting the density of this alloy with the idea that such a study might lead to higher densities and, as a result, powder alloys having magnetic properties identical with those of the fused alloys.

It was believed that the principal reason that near-theoretical densities for the powdered alloy were not obtained was the interference of gases with the normal sintering mechanism. When present during the sintering operation, gases can exert several harmful effects: they can remain on the particle surface and interfere with surface diffusion and plastic flow; they can be released and, under certain conditions, expand the void spaces through gas pressure; or they can remain trapped in the pores and exert a hydrostatic pressure that retards elimination of the pores.

Jones,[4] Rhines,[5] Goetzel,[6] and others have given the effect of gases in the sintering of powder compacts an extensive treatment. Among the more important sources of gases in the sintering process are dissolved gases, adsorbed gases, air entrapped during pressing, and gaseous products of chemical reactions. During sintering adsorbed gases are partly released at a relatively low temperature, while those gases entrapped during pressing cannot escape until their pressure is increased sufficiently through increasing temperature to expand the interparticle openings. The remaining adsorbed gases, gaseous reduction products, and dissolved gases produce a similar effect at the higher temperatures. If, in the sintering process, gas evolution occurs after the interpore channels have been sealed, an exaggerated expansion of the void spaces results. This is particularly true if the temperature is high enough for extensive plastic flow.

In his fabrication of powder bars from tantalum, Balke[7] had to consider the effect of adsorbed hydrogen and provide for its escape during sintering by limiting the compacting pressure to a maximum of 50 tons per sq in. The effect of gases entrapped during pressing was first noted by Trzebiatowski[8] when he found that gold and silver powders decrease in density with increasing sintering temperature if pressed at 200 tsi, while they exhibit the usual increase when pressed at 40 tsi. Recent investigators[9-11] have also noted that entrapped gases have an effect on the expansion of copper compacts during sintering. Proper provision for the escape of gaseous products of reduction must be made in order to avoid deleterious effects. Myers[12] states that in the sintering of electrolytic tantalum powder, the temperature was gradually raised to 2600°F with a pause at 2000°F to permit reduction of the oxides.

Experimental Details

For the present study, 50 pct Co-50 pct Fe compacts in the form of circular disks 1½ in. in diam and 0.15 in. thick were fabricated by the pressing and sintering of a mixture of the elemental powders. It was decided to follow the sintering process by means of liquid permeability measurements, because it was thought that such measurements might serve as a measure of relative pore sizes, as well as a possible indication of the point at which most of the interpore channels become sealed. However, since the permeability as measured by the flow of a liquid, such as ethylene glycol, does not give an absolute indication of the point where the pores have become isolated, a method for determining the percentage of pores connected to the surface was set up. As an additional cross check on the permeability measurements, metallographic methods were used to study the relative pore size. Finally, the property of ultimate interest, the density, was measured.

Raw Materials: The powders used consisted of an annealed, 99.9 pct pure, −150 mesh grade of electrolytic iron powder, and a 98 pct pure, −200 mesh grade of reduced and comminuted cobalt powder. The cobalt powder was not further processed either by hydrogen reduction or annealing.

The screen analyses for the iron and cobalt powders are given in Table I, while the chemical analyses for each type of powder are listed in Table II. Table III gives the hydrogen loss measurements for the powders according to the M.P.A. Standard Method and for a higher temperature as well.

Preparation of Compacts: Equal amounts of the elemental powders were mixed by rotation for 1 hr and then pressed into compacts approximately 0.15

D. WARREN, Student Associate AIME, and J. F. LIBSCH, Junior Member AIME, are du Pont Fellow in Metallurgical Engineering and Associate Professor, respectively, Department of Metallurgy, Lehigh University, Bethlehem, Pa.

Discussion on this paper, TP 3135E, may be sent, 2 copies, to AIME by Dec. 1, 1951. Manuscript, April 16, 1951; revision, July 12, 1951. Detroit Meeting, October 1951.

Table I. Screen Analyses of Powders

Size Range	Fe Powder, Pct	Co Powder, Pct
+80 mesh	Trace	Trace
−80 +100	Trace	Trace
−100 +150	Trace	Trace
−150 +200	8.75	Trace
−200 +325	22.80	0.96
−325	68.40	99.00

in. thick in a single acting die lubricated with a 3 pct stearic acid solution. The equipment used for pressing and sintering the compacts has been described previously.[8] It should be mentioned that the compacts, except where otherwise stated, were placed in the furnace directly at the sintering temperature and required about 5 to 10 min to reach temperature.

Permeability Measurements: The permeability of the compacts was measured by a method similar to the one devised by Chadwick and Broadfield.[10] The apparatus consisted of a Witt filter flask in which was mounted a filter funnel feeding into a graduated cylinder inside the flask. When the flask was evacuated with a Cenco Hy-Vac pump, the atmospheric pressure caused the compact to seat itself against a thin rubber sleeve placed in the filter funnel and thus provide an air-tight connection. Ethylene glycol was used as the permeating medium because of its low viscosity and vapor pressure and lack of corrosive action. The time required for 5 ml of glycol at a temperature of 30°C to pass through a compact of approximately 0.15 in. thickness under a pressure difference of more than 75 cm of mercury was measured. In some instances where the permeability was very low and the times required were very long, the measurement was limited to only 2 or 3 ml of flow. In all cases, the permeability was reported as ml per in.^{2} min where in.^{2} refers to the surface area of the compact.

Pore Volume and Density Measurements: After a compact had been given its final fabricating treatment, it was cleaned in acetone, oven-dried, and weighed on an analytical balance. The compact was then immersed in xylene, and a vacuum pulled on it to remove the air from the pores and allow the xylene to enter. The weight of the compact in xylene, maintained at a temperature of 30°C ±1°C, was then measured. After being oven-heated to drive off the xylene, the compact was given several applications of Dekadhese to provide a thin coating that was impervious to water. Next, the coating was oven-baked, and finally, the weight of the compact in air and in water was determined. Those compacts which had densities equal to 95 pct or more of the theoretical density were not coated with Dekadhese but were weighed directly in water.

The following is an outline of the method used for calculating pore volume and density from the measurements described above:

$$\text{Bulk volume of the compact} = \frac{W_{CA} - W_{CW}}{D_W} \quad [1]$$

Table II. Chemical Analyses of Powders

	C, Pct	Mn, Pct	Si, Pct	Cu, Pct	Ni, Pct
Fe powder	0.048	0.04			
Co powder	0.069	0.11	0.13	0.075	0.5

where W_{CA} is the weight of compact in air after coating with Dekadhese; W_{CW}, the weight of compact in water after coating with Dekadhese; and D_W, the density of water at temperature of measurement.

$$\text{Subsurface volume of the compact (volume of the metal itself plus isolated pores)} = \frac{W_A - W_X}{D_X} \quad [2]$$

where W_A is the weight of compact in air; W_X, the weight of compact in xylene; and D_X, the density of xylene at temperature of measurement (for these experiments D_X = 0.855 g per cu cm at 30°C).

Table III. Hydrogen Loss Measurements

	Fe Powder, Pct	Co Powder, Pct
1 hr at 1050°C (Standard M.P.A. Method)	0.4	1.3
30 min at 1400°C	0.4	1.4
1 hr at 1400°C	0.4	1.4

$$\text{Volume of surface connected pores} = \frac{W_{CA} - W_{CW}}{D_W} - \frac{W_A - W_X}{D_X} \quad [3]$$

$$\text{Volume of metal alone} = \frac{W_A}{8.08} \quad [4]$$

where 8.08 g per cu cm is the density of the fused 50 pct Fe-50 pct Co alloy.[7]

$$\text{Total volume of the pores} = \frac{W_{CA} - W_{CW}}{D_W} - \frac{W_A}{8.08} \quad [5]$$

$$\text{Density of the compact} = W_A \div \frac{W_{CA} - W_{CW}}{D_W} \quad [6]$$

The densities of those compacts which had to be coated with Dekadhese before weighing in water are accurate only to about 0.01 g per cu cm because of the error introduced by the coating. However, for those compacts having a density equal to or greater than 95 pct of the theoretical density, the density is correct to 0.001 g per cu cm.

In the experimental results the volume of the surface connected pores is expressed as a percentage of the total pore volume. The accuracy of this value depends upon the error introduced by the Dekadhese coating in the bulk volume measurement and as such it varies with the total amount of porosity. Where the total porosity is high, the percentage of surface connected pores is correct to ±1 pct and where the total porosity is low, this value is correct only to ±5 pct.

Metallographic Examination: The samples for metallographic examination were first impregnated with a very thin varnish and oven-baked. After being ground and polished, the compacts were electrolytically etched in a 10 pct nitric acid solution in order to remove the flowed metal covering the pores and then etched for 2 to 3 min by immersion in a 4 pct picral solution to reveal the grain boundaries.

Experimental Observations on Compacting and Sintering Procedures

Effect of Compacting Pressure: The effect of compacting pressure upon the permeability, density, and percentage of pores connected to the surface of green compacts is shown in Fig. 1.

The fact that practically 100 pct of the pores are connected to the surface in specimens compacted at

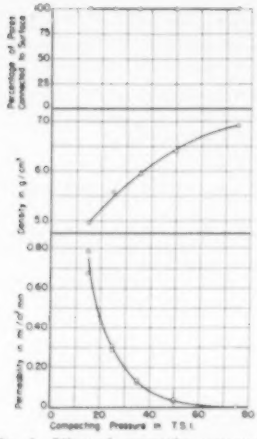

Fig. 1—Effect of compacting pressure.

pressures up to 75 tsi indicates that there is little likelihood of entrapped gases in these compacts. This is in accordance with the views of Kamm, Steinberg, and Wulff,[9] who feel that there is very little possibility of entrapping gases during the pressing of relatively hard powders, such as iron and nickel.

Figs. 2 and 3 are micrographs of compacts pressed at 25 and 75 tsi, respectively. (It was necessary to sinter these compacts at 800°C for metallographic preparation.) The larger particles of iron are most prominent, while the lighter areas consist of the finer particles of iron and cobalt which have already begun to sinter.

Effect of Sintering Time and Temperature upon Compacts Pressed at 25 tsi: The results of these experiments are summarized in Figs. 4 and 5. It is important to stress the fact that none of the increases in permeability would be predicted if the sintering process were being followed by means of density measurements alone, as can be seen from the lower set of curves in Fig. 5. The only irregularity observed in the density vs. sintering time curves is that the entire curve for 1000°C lies below that for 800°C. This apparent anomaly has been noted by other investigators[10, 11] and has been attributed to various factors connected with the α to γ phase transformation.

While a study of the density values gives no

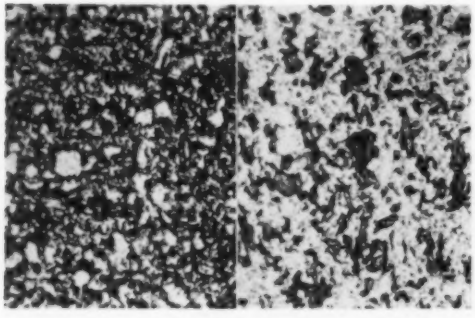

Fig. 2—Pressed at 25 tsi, sintered 15 min at 800°C. X100.

Fig. 3—Pressed at 75 tsi, sintered 15 min at 800°C. X100.

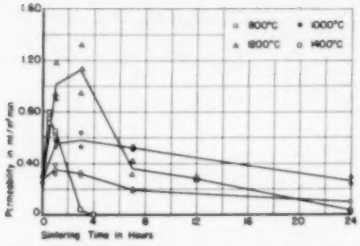

Fig. 4—Effect of sintering time and temperature upon the permeability of compacts pressed at 25 tsi.

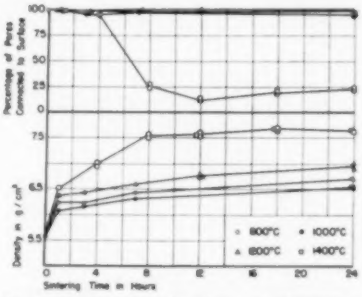

Fig. 5—Effect of sintering time and temperature upon the density and pore volume of compacts pressed at 25 tsi.

reason for the increases observed in the permeability values, metallographic examination does. Figs. 6, 7, 8, and 9 are micrographs of compacts sintered 1 hr at 800°, 1000°, 1200°, and 1400°C, respectively. It can be seen that the individual pores become increasingly well-defined with increasing sintering temperature, and that those pores in the compact sintered at 1400°C have been blown up tremendously. Metallographic examination showed that the microstructure of the compact sintered 3 hr at 1200°C was essentially the same as that of Fig. 8.

Since the individual pores have been expanded to a greater extent after an hour sinter at 1400°C than after a similar sinter at 1200°C, it might be expected that the permeability values for the former will be greater than those for the latter. But such is not the case. In order to resolve the apparent disagreement, it should be remembered that the resistance of a powder compact to liquid flow in a permeability measurement depends not only upon the pore size but also upon the degree to which the pores are interconnected. It is here that a metallographic study fails to tell the complete story. It would be expected that at 1400°C, the interpore channels would be sealed more rapidly than at 1200°C. This is borne out by the following observations: 1—the greater expansion of individual pores at 1400°C, which requires the prior sealing of interpore channels; 2—the absence in Fig. 9 of the network of fine pores present in Fig. 8; and 3—the large decrease in percentage of pores connected to the surface for compacts sintered more than 4 hr at 1400°C, Fig. 5. From the above discussion, it can be seen that the permeability value for a powder compact depends upon the balance between the shrinkage produced by normal sintering and the expansion due to the presence of evolved gases.

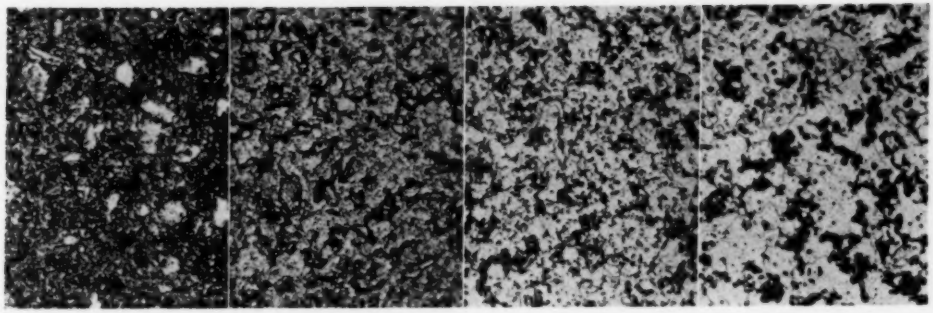

Fig. 6—Pressed at 25 tsi, sintered 1 hr at 800°C. X100.

Fig. 7—Pressed at 25 tsi, sintered 1 hr at 1000°C. X100.

Fig. 8—Pressed at 25 tsi, sintered 1 hr at 1200°C. X100.

Fig. 9—Pressed at 25 tsi, sintered 1 hr at 1400°C. X100.

Of the sources of gases in the sintering process, it is believed that chemisorbed gases and gaseous reduction products are primarily responsible for the pore expansion observed in compacts sintered at 1200° and 1400°C. Some idea of the oxide content of the cobalt and iron powders can be obtained from the hydrogen loss values given in Table III. The existence of such oxides, either as surface films or inclusions in the powder, is detrimental because the reduction of oxides by hydrogen used as a sintering atmosphere or by carbon in the powders themselves (see Table II) will lead to the evolution of gases. The detrimental effect of oxides has been shown by Cordiano,[15] who obtained a decrease in density with increase in hydrogen loss for iron compacts sintered for short times. The reduction of cobalt and iron oxide by hydrogen begins below 500°C and is rapid at 700° to 1100°C. The fact that reduction occurs at these higher temperatures means that oxides probably contribute more to pore expansion than any other source of gases, because their gaseous reduction products must make their escape after considerable sintering (sealing of the interpore channels) has occurred.

There is no data to show the amount of chemisorbed gases present in the powders used for this study. However, Taylor and Burns[16] have studied the adsorption of gases by iron and cobalt powders. Their data indicate that appreciable quantities of CO and CO_2 were adsorbed by cobalt powder, while only small quantities were adsorbed by iron powder. It was also indicated that there was considerably more adsorption by a partially oxidized lot of cobalt powder than by a completely reduced lot of the same powder. Since their adsorption values decrease with increasing temperature, it is reasonable to expect that in the heating of a green compact, the bulk of adsorbed gases would be driven off before appreciable sintering could occur. Whether or not the escape of such gases expands the pores depends upon the degree of powder compaction and the heating rate during sintering. In the case of the present experiments, the compacts were placed in the furnace at the sintering temperature and required only 5 to 10 min to reach that temperature. With such a high heating rate, the presence of adsorbed gases becomes significant.

Effect of Sintering at 1400°C upon Compacts Pressed at 25, 50, and 75 tsi: The results of these experiments are presented in Fig. 10. A study of this figure shows that for the first time, the pore expansion (as indicated by an increase in permeability) could be detected by a decrease in density. However, this was true only of the density curve for a pressure of 75 tsi. It is important to note that the density values after a 24 hr sinter at 1400°C decrease in order of increasing compacting pressure, which is just the opposite of what might be expected.

That the early increases in the permeabilities are caused by expansion of the pores is borne out by Figs. 11 and 12, which present a clear picture of the relative pore sizes in compacts pressed at 25 and 50 tsi, respectively, and then sintered for 30 min at 1400°C. The microstructure of the compact pressed at 75 tsi and sintered 30 min at 1400°C was similar to that of Fig. 12. Because the compacts pressed at 25 tsi were more porous in the green condition than the compacts pressed at 50 and 75 tsi, the individual pores have not been blown up to as great an extent in these as in the denser compacts.

The lesser degree of pore expansion in compacts pressed at 25 tsi is reflected in Fig. 10 by the more rapid decrease in permeability and in the percentage of pores connected to the surface between 1 and 2½ hr at 1400°C for compacts pressed at 25 tsi.

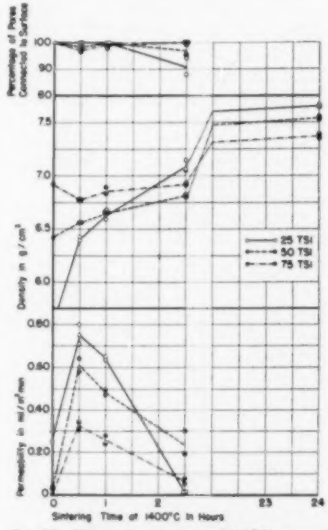

Fig. 10—Effect of sintering at 1400°C on compacts pressed at 25, 50 and 75 tsi.

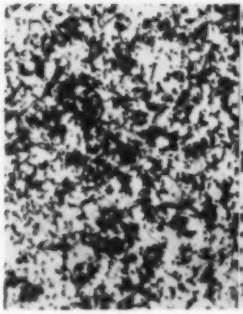

Fig. 11—Pressed at 25 tsi, sintered 30 min at 1400°C. X100.

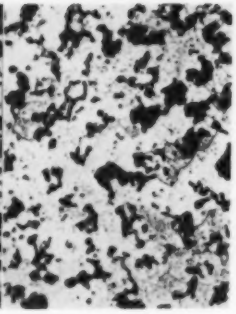

Fig. 12—Pressed at 50 tsi, sintered 30 min at 1400°C. X100.

The lesser expansion of individual pores that occurs with the lower compacting pressures can be attributed to two factors: 1—the hydrogen has greater access to the surfaces of loosely compacted powder particles, and 2—the slower initial rate of sintering provides a greater opportunity for the oxides to be reduced and for the gaseous reduction products to escape. In the highly compressed compacts, sealing of the interpore channels begins earlier and takes place more rapidly. In such a case, the relatively small hydrogen atoms can easily diffuse into the interior of the compact, but the larger molecules of water formed by the reduction cannot diffuse outward through the lattice interstices. Thus, they must remain in the sealed off pores to either produce an actual expansion or to retard sintering.

The decrease in final density that occurs with an increase in compacting pressure for compacts sintered 24 hr at 1400°C is a reflection of the larger degree of pore expansion with the higher compacting pressures, because these larger pores are closed up at a very slow rate. Also, there is a greater possibility with the higher compacting pressures of gases being sealed off in the pores and thus retarding the later phases of sintering. Both Shaler[17] and Mackenzie and Shuttleworth[18] have given the effect of gases trapped within the pores of powder compacts an extensive mathematical treatment.

Study of the Gases Evolved During Sintering

In the second phase of this investigation, an effort was made to relate the effects observed in the original experimental results with the evolution of gases and to determine, if possible, the nature of these gases.

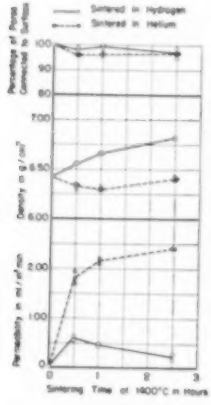

Fig. 13—Effect of sintering at 1400°C in hydrogen and helium on compacts pressed at 50 tsi.

Effect of Sintering at 1400°C in Hydrogen and Helium on Compacts Pressed at 50 tsi: Since it was believed that gases resulting from the reduction of oxides in or on the powder particles by the hydrogen of the sintering atmosphere was primarily responsible for the expansion of the pores, a series of compacts was pressed at 50 tsi and sintered at 1400°C in a helium atmosphere for comparison with the previous series of compacts pressed at 50 tsi and sintered at 1400°C in hydrogen. The results of this experiment are shown in Fig. 13.

The large increase in the permeability, as well as the significant decrease in the density, of a compact sintered at 1400°C in helium suggests the occurrence of a severe expansion of the individual pores leading to an overall growth in the size of the compact. That such is actually the case is shown by the microstructure of a compact pressed at 50 tsi and sintered for 30 min at 1400°C in helium, see Fig. 14.

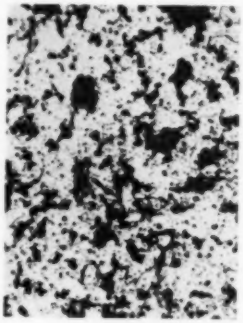

Fig. 14—Pressed at 50 tsi, sintered 30 min at 1400°C in helium. X100.

This experiment tends to relegate the effect of chemisorbed gases to a relatively minor role as far as pore expansion is concerned, because if chemisorbed gases, alone, were responsible for the effects observed, then there seems to be no obvious reason why the properties of compacts sintered in hydrogen and helium would not be fairly similar. The most logical explanation for the results observed for compacts sintered in helium seems to be that the gases were produced either by the reduction of oxide films by carbon in the powders or by thermal decomposition of the oxides.

Reduction of the oxides by carbon would probably be slower than reduction by hydrogen, because the diffusion of carbon is necessary for appreciable reduction to occur, whereas hydrogen can readily permeate the pores of the compact. According to the available data,[19] the only oxide of either cobalt or iron that decomposes at 1400°C or below is cobaltic oxide (Co_2O_3) which decomposes at 895°C. Such a thermal decomposition would therefore occur at a temperature higher than that required for reduction by hydrogen. Thus, either of the two proposed mechanisms would lead to the evolution of gases at a later stage in the sintering process than if the same gases had been liberated by reduction of the oxides by hydrogen. This evolution of gases after appreciable sintering (sealing of interpore channels) had already occurred seems to account for the greater expansion of pores observed for the compacts sintered in helium.

Effect of Sintering at Various Temperatures in

Helium on Compacts Pressed at 50 tsi: In order to determine if gases were actually being evolved by the thermal decomposition of oxides contained in the powders, the oxygen content of compacts pressed at 50 tsi and sintered for 4 hr in helium at 1100°, 1200°, 1300°, and 1400°C was determined by means of vacuum-fusion analyses. A 4 hr time limit was chosen, because it was believed that the largest part of any thermal decomposition would have occurred in that length of time. As a basis for determining the original oxygen content of the compacts, vacuum-fusion analyses for oxygen were made on a compact pressed at 50 tsi and sintered in helium for 15 min at 800°C and also on a green compact of the same powder mixture. In conjunction with the vacuum-fusion analyses, the usual measurements were also made. These data are presented in Fig. 15.

The results of the vacuum-fusion analyses are expressed in terms of the original oxygen content of the green compacts (0.84 pct O) as determined by vacuum fusion. The fact that sintering 4 hr at 1100° and 1400°C in helium has eliminated 53 and 86 pct, respectively, of the original oxygen content of the compacts clearly indicates that gases are evolved during the sintering process.

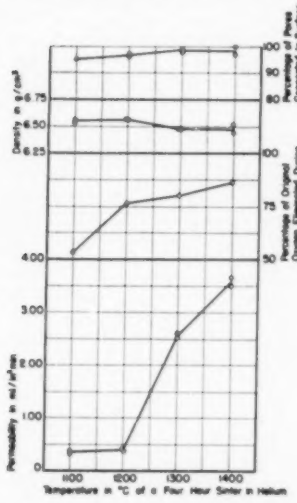

Fig. 15—Effect of sintering at various temperatures in helium on compacts pressed at 50 tsi.

In Fig. 15, the evolution of gases is also reflected by the rapid increase in permeability between 1200° and 1400°C accompanied by a small decrease in density and a small increase in the percentage of pores connected to the surface. The main reason for the difference between the properties of compacts sintered for 4 hr at 1200°C and for 4 hr at 1300° or 1400°C would seem to be due to the greater plasticity of the metal at the higher temperatures, because the difference in the amount of gas liberated at each of these three temperatures is obviously not enough to account for it. The fact that the expansion of individual pores has occurred during the sinter at 1200°C, but to a lesser extent than that at 1400°C, is shown by a comparison of Figs. 16 and 17.

Effect of Heating Cobalt Powder to 1000°C in a Vacuum: Because the cobalt powder had a hydrogen loss three times that for the iron powder (see Table III) and because its oxygen content by vacuum-fusion analysis was 1.04 pct compared to 0.41 pct

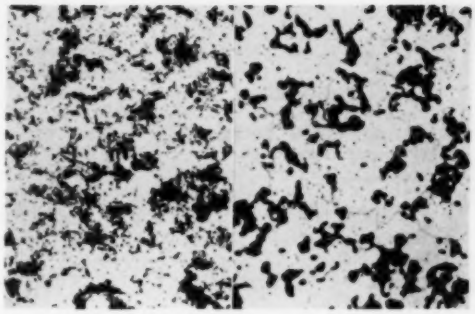

Fig. 16—Pressed at 50 tsi, sintered 4 hr at 1200°C in helium. X100.

Fig. 17—Pressed at 50 tsi, sintered 4 hr at 1400°C in helium. X100.

for the iron powder, a study was made of the evolution of gases upon heating from the cobalt powder alone. This was done by degassing in a vacuum a 4 g sample of cobalt powder for 2 hr at 225°C, sealing off the system at a vacuum of 10^{-5} cm after degassing, and then measuring the pressure of the closed system as the cobalt powder was gradually heated (5°C per min) from 250° to 1000°C (the upper temperature limit of the apparatus). The results of this experiment, which are given in Fig. 18, show that rapid gas evolution occurs between 350° and 450°C and between 800° and 1000°C.

The volume of gas liberated upon heating to 1000°C was calculated to be 1.6 ml per g of cobalt powder. While this is an appreciable quantity of gas, it represents less than one fourth of the total gas available (7.3 ml per g) as calculated on the basis of the vacuum-fusion analysis (1.04 pct O). Vapor pressure and chemical solubility measurements showed that the gas evolved from the cobalt powder was largely carbon dioxide.

This carbon dioxide could be formed by the reaction between the carbon and oxides of the powders or by the release of chemisorbed gases. In their study of gas evolution on rise of temperature for carbonyl iron powder, Duftschmid, Schlecht, and Schubardt[20] found that the reaction between the carbon and iron oxide of the powders produced a major gas evolution at 450°C with the bulk of the gas being carbon dioxide with some carbon monoxide also present.

If all the carbon (0.069 pct) present in the cobalt powder were oxidized to carbon dioxide during the heating to 1000°C, then 1.3 ml of carbon dioxide per gram of powder would be produced. This leaves 0.3

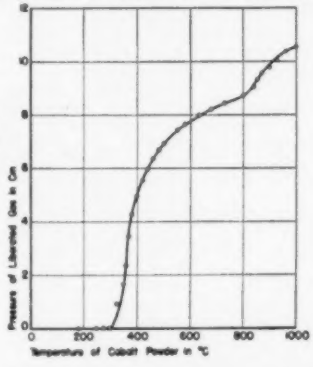

Fig. 18—Pressure of liberated gas vs. temperature for cobalt powder heated in a vacuum.

ml to be supplied by some other source, such as chemisorbed carbon dioxide.

The above discussion leads to the belief that the evolution of gas from the cobalt powder occurring at 400°C is largely due to the reduction of oxides by carbon in the powder and that the second evolution occurring at 800° to 1000°C is probably the result of the thermal decomposition of cobaltic oxide (decomposes at 895°C).

Minimizing the Influence of Gases on Sintering Process

The final part of this investigation consisted of experiments that were designed to minimize or even eliminate, if possible, the influence of gases upon the sintering process.

Effect of Reduction of Powder upon Influence of Gases during Sintering: The most obvious method of minimizing the influence of gases upon the sintering process is to eliminate the source of these gases. An attempt was made to accomplish this purpose, first by reduction of the cobalt powder alone (because of its higher oxygen content) and then by reduction of both the iron and the cobalt powder just prior to compacting and sintering.

A series of compacts were prepared from cobalt powder, annealed in pure dry hydrogen for 1 hr at 600°C, and unannealed iron powder by pressing at 50 tsi and sintering for 30 min and for 24 hr at 1400°C. The properties of these compacts along with the properties of compacts fabricated in a similar manner from both unannealed cobalt and iron powder are listed in Table IV for comparison. The fact that the prior reduction of cobalt powder resulted in a lower permeability and a higher density for the compacts sintered 30 min at 1400°C would certainly seem to indicate that less pore expansion had occurred, and that, as a result, a higher density might be obtained for similar compacts sintered 24 hr at 1400°C. But as can be seen, this is not the case.

A glance at the microstructure of a compact prepared using the annealed cobalt powder and sintered for 30 min at 1400°C helps to resolve this difficulty, see Fig. 19. It should be noted that even though the hydrogen loss for the powders used in making the compact was reduced to one third of its original value by the prior reduction, the pores have still been enlarged sufficiently to interfere with the achievement of a high final density (24 hr at 1400°C).

In order that the maximum amount of gases might be eliminated prior to sintering, both the iron and the cobalt powder were annealed for 1 hr at 600°C in pure dry hydrogen, and a series of compacts were pressed at 25 tsi and sintered 24 hr at 1400°C. As shown in Table IV, even this reduction treatment did not result in a higher final density.

Effect of Variations in Sintering Cycle to Allow for Removal of Gases from Compacts: Because the minimization of the deleterious effects of gases by variation in the sintering cycle had been successfully carried out by other investigators,[11] it was decided to use two such methods in order to eliminate the gases from the compacts before the interpore channels could become sealed. The first method was to place the compacts in the furnace at 800°C and heat slowly (2.5° to 3° per min) from 800° to 1400°C in order to allow the oxides to be gradually reduced with the gaseous reduction products making their escape while the interpore channels are still open. The second method was to place the compacts in the furnace at 800°C and hold at that temperature for 4 hr in order to provide for the maximum reduction of oxides before the sintering temperature was increased to 1400°C. At 800°C the gaseous reduction products can make their escape without disrupting the compact because the sintering action is relatively slow.

The results of these two experiments which are given in Table V show that both of the treatments described above have had a very beneficial effect in increasing the density. While the second method of varying the sintering cycle decreased the sintering time at 1400°C to 19 hr, it still resulted in higher final densities, even in the case of those compacts pressed at 25 tsi and having a low green density.

Fig. 20 shows the microstructure of a compact pressed at 25 tsi and placed in the furnace at 1400°C and sintered for 24 hr at that temperature, while Fig. 21 shows the microstructure of a compact pressed at 25 tsi and placed in the furnace at 800°C and given a slow heating rate from 800° to 1400°C before the final sinter at that temperature. A comparison of the two figures shows clearly that the use of a slow heating rate preceeding the high temperature sinter results in both fewer and smaller pores. This in turn, is reflected in a higher density for this type of treatment.

Summary

1—Data are presented to show the influence of various pressing and sintering conditions upon the

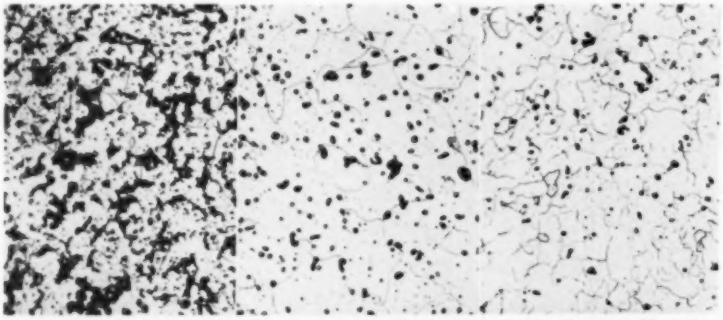

Fig. 19—Pressed at 50 tsi from annealed cobalt powder and unannealed iron powder. Sintered 30 min at 1400°C. X100.

Fig. 20—Pressed at 25 tsi, sintered 24 hr at 1400°C. X100.

Fig. 21—Pressed at 25 tsi. Slow heating rate from 800° to 1400°C preceding sinter at 1400°C. Total sintering time was 24 hr. X100.

Table IV. Comparison of Properties of Compacts Fabricated from Annealed and Unannealed Powders

Powder Treatment		Compacting Pressure	Sintering Treatment	Permeability (Millidarcys per In.^{2} Min)	Density (G per Cm^3)
Annealed Co Powder Unannealed Fe Powder	Total H_2 loss for both was 0.3 pct	50 tsi	30 min at 1400°C	0.18 0.25	6.75 6.75 6.76
Unannealed Co Powder Unannealed Fe Powder	Total H_2 loss for both was 0.9 pct	50 tsi	30 min at 1400°C	0.63 0.57	6.56 6.56
Annealed Co Powder Unannealed Fe Powder	Total H_2 loss for both was 0.3 pct	50 tsi	24 hr at 1400°C		7.570
Unannealed Co Powder Unannealed Fe Powder	Total H_2 loss for both was 0.9 pct	50 tsi	24 hr at 1400°C		7.571 7.537
Annealed Co Powder Annealed Fe Powder		25 tsi	24 hr at 1400°C		7.665 7.665 7.645
Unannealed Co Powder Unannealed Fe Powder		25 tsi	24 hr at 1400°C		7.661 7.654

permeability, density, and percentage of pores connected to the surface of Fe-Co powder compacts. This data has led to a study of the effect of evolved gases on the sintering process and to a successful minimization of the influence of such gases.

2—It has been shown that a density study does not always afford a reliable means of following the sintering process in powder compacts. On the other hand, liquid permeability measurements have indicated changes occurring in the sintering process not revealed by density measurements. Permeability has been shown to be a fairly good measure of the relative pore sizes of powder compacts, as well as the degree to which these pores are interconnected. While a metallographic study offers a reliable check on the relative pore sizes, it is lacking in that it does not show the degree of interconnection of the pores. The pore volume measurements introduced here offer a new method of determining the percentage of the total pores in a compact that are actually connected to the surface.

3—The experiments performed indicate that the role of gases during the initial stages of the sintering process have an important influence upon the final density of compacts sintered to achieve theoretical density. In this connection, high compacting pressures, rapid heating rates, and high sintering temperatures exaggerate the effect of evolved gases and promote the formation of large initial pores which are eliminated during continued sintering only with difficulty.

4—A density close to that for the fused alloy (97.5 pct) has been obtained for 50 pct Fe-50 pct Co powder compacts by providing for the escape of liberated gases before appreciable sintering has occurred.

5—The results of this investigation should prove of interest to powder metallurgists concerned with the production of very high density materials or with the production of parts having a controlled porosity, such as bearings and filters.

Table V. Effect of Variations in Sintering Cycle upon Final Density of Compacts Pressed at 25, 50, and 75 tsi

Compacting Pressure (Tsi)	Sintered 24 Hr at 1400°C	Slow Heating Rate (2.5°-3° Per Min) from 800° to 1400°C. Held at 1400°C Until Total Sintering Time Was 24 Hr	Held at 800°C for 4 Hr. Rapid Heating Rate (10°C Per Min) from 800° to 1400°C. Held at 1400°C Until Total Sintering Time Was 24 Hr
25	7.661	7.863	7.771
	7.654	7.859	7.773
		7.857	7.766
50	7.525	7.843	7.886
	7.553	7.845	7.879
		7.848	7.881
75	7.362	7.785	7.836
	7.391	7.783	7.816
		7.757	7.825

Acknowledgments

The authors wish to express their appreciation to the U. S. Signal Corps for the supply of materials and equipment used in this investigation. For the vacuum fusion and other chemical analyses, the authors are grateful to the Allegheny Ludlum Steel Corp. The authors are especially indebted to W. C. Walker, of the Department of Chemistry, Lehigh University, for outlining the method for making the pore volume measurements. Finally, gratitude is expressed to the E. I. du Pont de Nemours and Co., who made this investigation possible by their grant of a fellowship in metallurgical engineering.

References

[1] J. F. Libsch, E. Both, et al.: *Trans.* AIME (1950) **188**, p. 287: JOURNAL OF METALS (February 1950).
[2] A. Kussman, B. Sharnow, and A. Schultz: *Ztsch. Techn. Physik* (1932) **13** (10), p. 449.
[3] W. Rostoker: *Trans.* AIME (1949) **180**, p. 684; METALS TECHNOLOGY (October 1948).
[4] W. D. Jones: *Principles of Powder Metallurgy*, pp. 37-54, (1937) London. Edward Arnold and Co.
[5] F. N. Rhines: *Trans.* AIME (1946) **166**, pp. 474-491; METALS TECHNOLOGY (August 1946).
[6] C. G. Goetzel: *Treatise on Powder Metallurgy I.* pp. 120-125, 518-524. (1949) New York. Interscience Publishers, Inc.
[7] C. W. Balke: *Symposium on Powder Metallurgy* ASTM (March 1943) p. 12.
[8] W. Trzebiatowski: *Ztsch. f. Phys. Chem.* (1934) **B-24**, pp. 75-97.
[9] R. Kamm, M. A. Steinberg, and J. Wulff: *Trans.* AIME (1949) **180**, pp. 705, 703; METALS TECHNOLOGY (December 1948).
[10] A. J. Shaler and J. Wulff: *Industrial and Engineering Chemistry* (May 1948) **40**, p. 838.
[11] P. Duwez and H. Martens: *Trans.* AIME (1949) **185**, pp. 573-574: JOURNAL OF METALS (September 1949).
[12] R. H. Myers: *Metallurgia* (1948) **38**, pp. 307-310.
[13] R. Chadwick and E. R. Broadfield: Symposium on Powder Metallurgy, *Special Report N38*, Iron and Steel Inst. (1947) p. 126.
[14] J. Libsch, R. Volterra, and J. Wulff: *Powder Metallurgy.* (1942) p. 387. ASM. Cleveland, Ohio.
[15] J. J. Cordiano: *Proc.* Fifth Annual Meeting, M. P. A. (April 1949) p. 26.
[16] H. S. Taylor and R. M. Burns: *Journal* Amer. Chem. Soc. (1921) **43**, pp. 1273-1287.
[17] A. J. Shaler: *Trans.* AIME (1949) **185**, p. 803; JOURNAL OF METALS (November 1949).
[18] J. K. Mackenzie and R. Shuttleworth: *Proc.* Phys. Soc. London (1949) **62B**, pp. 848-851.
[19] *Handbook of Chemistry and Physics.* Cleveland. Chemical Rubber Publishing Co.
[20] F. Duftschmid, L. Schlecht, and W. Schubardt: *Stahl u Eisen* (1932) **52** (2), pp. 845-849.

Constitution and Precipitation-Hardening Properties of Copper-Rich Copper-Tin-Beryllium Alloys

by R. A. Cresswell and J. W. Cuthbertson

THE constitution of Cu-rich alloys with 1.5 to 13.5 pct Sn and 0.25 to 3.0 pct Be and the precipitation-hardening characteristics of alloys with 1.5 to 13.5 pct Sn and 0.25 to 1.0 pct Be have been examined.

The hardness and tensile strength of the alloys examined increase markedly after solution treatment at 700°C followed by heat treatment at temperatures between 200° and 450°C. By a combination of cold work and heat treatment, hardness values similar to those exhibited by commercial Be-Cu alloys containing 2.25 pct Be can be obtained with ternary alloys containing 9 pct Sn and 0.75 pct Be and containing 10 pct Sn and 0.5 pct Be. Marked hardening effects occur with alloys containing even less beryllium. By heat treatment alone, a hardness value of 310 diamond pyramid hardness can be obtained from an alloy containing 10 pct Sn and 0.75 pct Be. Preliminary tensile tests have shown that an ultimate tensile strength of 110,000 psi with an elongation of 23 pct is obtainable by precipitation hardening an alloy with 8 pct Sn and 0.75 pct Be.

The precipitation-hardening process has been followed microscopically for certain alloys and the inference is that, while the initial hardening effect is probably explained by the precipitation of the β' phase of the Cu-Be system, further hardening, proceeding at a much slower rate, also occurs, apparently as a result of precipitation of phases of the Cu-Sn system, particularly precipitation of the ϵ phase at temperatures below 350°. The presence of the ϵ phase of the Cu-Sn system in certain alloys at temperatures below 350°C has been confirmed.

Tin-bronzes are widely used in engineering applications where a combination of high strength and good resistance to corrosion is wanted. The maximum strength is induced in these alloys by cold working, and it would be an advantage for many purposes if high strength could be achieved alternatively by an age-hardening process. While Cu-Sn alloys have a good fatigue resistance they can be surpassed in this respect by Cu-Be, but the use of the latter alloy is limited by its high cost. If, by adding beryllium to tin-bronze, the properties of the respective binary alloys could to some extent be combined, a most attractive alloy should result.

As pointed out by Raynor,[1] beryllium is on the borderline of the zone of favorable size factors for copper, and the solid solubility of beryllium in copper is consequently much more restricted than if the size factor were strongly favorable. The size factor is sufficiently favorable, however, to permit an increase in solid solubility with rise in temperature, and there is thus a composition range in which Cu-Be alloys are susceptible to hardening by precipitation heat treatment. Although the α phase of the Cu-Sn system is similarly susceptible to precipitation treatment, the time necessary to establish equilibrium in commercial alloys of this type is usually so great that age hardening becomes impracticable.

The addition of beryllium to Cu-Sn alloys would appear to offer a means of conferring on the latter useful age-hardening properties. Masing and Dahl[2] and others have, in fact, shown that the addition of beryllium to Cu-Sn α solid solutions renders these alloys susceptible to precipitation hardening and after such hardening confers on them an encouraging improvement in physical properties. If this improvement could be achieved by the addition of substantially smaller amounts of beryllium than are customarily found in binary Cu-Be alloys, the ternary alloys should possess economic advantages which might make them more attractive than the binary alloy for some applications.

Binary Systems

Copper-Tin: The constitution of these alloys is now reasonably well known and is summarized in the equilibrium diagram published by Raynor.[3]

The following observations, due to Raynor,[1] on the structure of those phases of the Cu-Sn system that are likely to be found in the ternary alloy system will facilitate the subsequent discussion on the examination of that system. The β phase is an electron compound at the electron-atom ratio 3:2 and has a body-centered cubic crystal structure. This phase is stable only down to 586°C, at which temperature it decomposes eutectoidally into the α and γ phases. The γ phase has a structure that is also based on the cubic system. This phase is stable down to 520°C, at which temperature it decomposes eutectoidally into the α and δ phases. The δ phase is an electron compound ($Cu_{31}Sn_8$) which has a crystal structure analogous to that of γ brass. This phase is stable from 590° to 350°C; on prolonged annealing at the latter temperature it breaks down into a mixture of the α and ϵ phases. The ϵ phase is an electron compound (Cu_3Sn) having the electron-atom ratio 7:4. Its structure may be regarded as a superlattice based on the close-packed hexagonal system. This phase is stable from 676°C to room temperature.

The primary solid solubility of tin in copper increases to a maximum of 15.8 pct as the temperature falls from that of the peritectic reaction to 586°C. The solid solubility remains constant from 586° to 520°C. At lower temperatures the solubility decreases progressively. Below 350°C the fall in solubility is pronounced and is associated with the precipitation of the ϵ phase. This precipitation is very sluggish and does not normally occur under service conditions.

Copper-Beryllium: The Cu-Be system has been investigated by Borchers[4] and others. Raynor[5] summarized the present state of information on it.

R. A. CRESSWELL is Research Metallurgist and J. W. CUTHBERTSON is Assistant Director of Research, Tin Research Institute, Perivale, Greenford, Middlesex, England.

Discussion on this paper, TP 3134E, may be sent, 2 copies, to AIME by Dec. 1, 1951. Manuscript, April 10, 1951. Detroit Meeting, October 1951.

The solid solubility of beryllium in copper does not exceed 2.1 pct. Beyond the α range increase in beryllium content up to about 12 pct leads to the appearance of first the β phase and subsequently the β' phase (the latter phase is designated γ by Borchers). The β and β' phases both have body-centered cubic structures, the former being disordered and the latter ordered. Hume-Rothery, Reynolds, and Raynor[6] consider that both of these phases are probably derived from the same 3:2 electron compound. The β phase decomposes eutectoidally at 575°C giving the α and β' phases.

Tin-Beryllium: So far as could be traced no information has been published on the Sn-Be system. Raynor considers that the size factor relationships in this case are unfavorable.

Ternary System

The first work carried out on the Cu-Sn-Be system was done by Masing and Dahl in 1929.[7] They determined the limits of the α phase at 750°C and examined the possibilities of precipitation hardening in these alloys. Rowland and Upthegrove[1] have pointed out, however, that owing to insufficient annealing the specimens on which Masing and Dahl based their conclusions were not in equilibrium and the results of the latters' findings in regard to the constitution diagram are thus open to criticism. Rowland and Upthegrove have examined the structure of Cu-Sn-Be alloys containing up to 1 pct Be. They have not, however, studied the age-hardening properties of these alloys in detail, and since in their investigation they used the older type of Cu-Sn constitution diagram based on the work of Heycock and Neville, they appear to have overlooked the transformation of the δ phase of that system at approximately 350°C. In the light of later work on the Cu-Sn system it would seem the β', $\beta + \gamma$, and γ fields reported by Rowland and Upthegrove can almost certainly be identified with one continuous γ field.

Scope of Present Investigation

In planning this investigation the general form of Rowland and Upthegrove's diagram and the results of their thermal analyses were accepted, and it was decided only to consider those sections of the system which, in view of the information that has become available since these investigators published their results, might justify re-examination. In view of these uncertainties it was deemed advisable to redetermine certain parts of the ternary diagram in order to settle what phases are most likely to be precipitated on heat treatment of alloys near the α phase boundary, i.e., alloys in which the maximum degree of precipitation hardening is to be expected.

The boundaries of selected isothermal sections of the ternary model were determined by microscopical examination of annealed and quenched specimens. The effects of heat treatment on selected alloys were examined and a limited study was made of the mechanical properties of these alloys.

Experimental Procedure

In all, 68 different alloys were prepared. Of these 58 were made from electrolytic copper, Chempur tin, and a Cu-Be master alloy containing 4 pct Be. The remaining 10 alloys, which were used to settle any doubtful questions in the constitution work, were made from raw materials that were spectrographically standardized and of very high purity.

The analyses of the copper, tin, and master alloy are given in Table I, and the tin and beryllium contents of the prepared alloys are reported in Table II. All samples were analyzed for tin content by precipitation with tannin and for beryllium content by precipitation with 8-hydroxy quinoline and ignition to oxide, traces of iron and aluminium being removed first. The impurity content of selected alloys was determined and the total amount of impurity found did not exceed 0.1 pct. The average silicon content was 0.03 to 0.05 pct and traces of iron and aluminium were detected.

Table I. Analyses of Raw Materials

Material	Impurity Content			
Copper	Fe 0.005 pct	As 0.001 pct	Cd 0.001 pct	
	CuO 0.04 pct approx.			
Tin	Typical analysis for Chempur tin:		Fe 0.0013 pct	
	Pb 0.0027 pct	Sb 0.003 pct	Bi 0.0006 pct	
	Cu 0.0005 pct	As nil.		
Cu-Be Master Alloy	0.3 pct total impurity, mainly Fe, Al and Si in approximately equal amounts.			

In preparing the majority of the alloys for the constitution work, the metals were melted in a salamander crucible heated in an electric furnace of the silicon-carbide resistor type. During melting, a stream of oxygen-free nitrogen was passed through the furnace and melting was carried out as quickly as possible. The usual procedure in making up alloys of low beryllium content was first to melt the copper and bring its temperature rapidly to about 1300°C and then to add the tin and master alloy which were first preheated. The normal casting temperature was 1150°C. Before casting, the melts were stirred with a carbon rod and casting was effected through a preheated tundish into a chill mold $\frac{3}{4}$ in. in diam preheated to 200°C. In the case of the alloys of higher beryllium content, the total charge was placed in the crucible at the outset and melting and casting were carried out as before. The usual weight of the melts prepared in the electric furnace was 250 g. Experience indicated that provided the melting was done quickly there was no significant increase in the silicon content of alloys prepared in this way. With prolonged heating the silicon in the alloy may increase as a result of reduction of the silica in the crucible by the beryllium in the melt.

Larger melts were required for studying precipitation hardening and the mechanical properties of the alloys, and these were prepared as follows. Melting was done in a gas-fired injector furnace. The

Table II. Analyses of Alloys

Alloy No.	Sn, Pct	Be, Pct	Alloy No.	Sn, Pct	Be, Pct	Alloy No.	Sn, Pct	Be, Pct
1	1.5	0.93	24	3.85	1.88	47†	8.45	2.80
2	1.5	1.45	25	4.25	2.40	48†	9.1	0.21
3	1.5	1.85	26	5.2	0.24	49*	10.15	0.48
4	1.9	0.18	27	4.65	0.50	50*	8.8	0.75
5	2.1	0.47	28	4.7	0.87	51	8.95	1.52
6*	1.9	0.70	29	5.3	1.10	52†	9.3	1.80
7	2.05	1.50	30	4.9	2.29	53†	9.39	0.26
8*	2.5	0.48	31	5.9	0.15	54†	9.54	0.21
9*	2.6	0.95	32	6.15	0.55	55*	9.8	0.17
10†	2.4	1.30	33	5.75	0.79	56*	10.0	0.47
11	2.65	1.65	34	6.2	2.77	57*	9.88	0.73
12	2.45	1.90	35†	6.35	2.85	58	10.25	0.87
13	2.9	0.20	36	7.25	1.0	59	9.95	2.06
14†	3.10	0.31	37	7.05	1.60	60	11.05	0.13
15	3.1	2.05	38	7.25	1.95	61*	11.15	0.47
16*	3.5	0.52	39	7.1	2.75	62*	10.75	0.77
17†	3.6	1.15	40	7.65	1.10	63*	11.4	0.73
18	3.5	1.90	41*	7.75	0.67	64*	12.2	0.31
19	3.85	0.005	42	8.45	0.96	65*	12.25	0.47
20	4.1	0.53	43	7.75	2.45	66*	13.35	0.47
21*	3.9	0.97	44	8.15	2.88	67*	12.75	0.73
22†	3.7	0.80	45†	8.64	0.27	68*	13.55	0.24
23	4.0	1.73	46	8.55	1.05	69	14.55	

* Alloys melted in the gas-fired injector furnace.
† Alloys made up from spectrographically standardized materials.

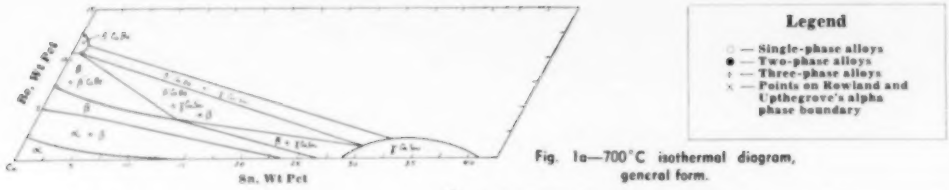
Legend
○ — Single-phase alloys
● — Two-phase alloys
† — Three-phase alloys
× — Points on Rowland and Upthegrove's alpha phase boundary
Be, Wt Pct
Sn, Wt Pct

Fig. 1a—700°C isothermal diagram, general form.

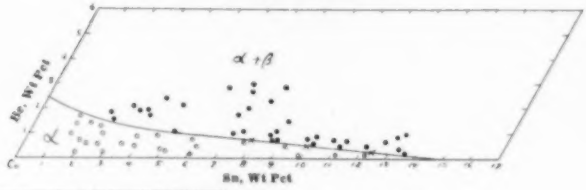

Fig. 1b—700°C isothermal diagram, alpha phase boundary.

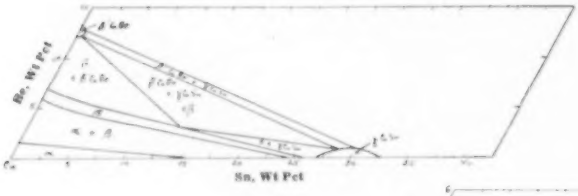

Fig. 2a—600°C isothermal diagram, general form.

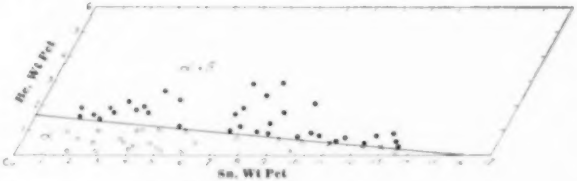

Fig. 2b—600°C isothermal diagram, alpha phase boundary.

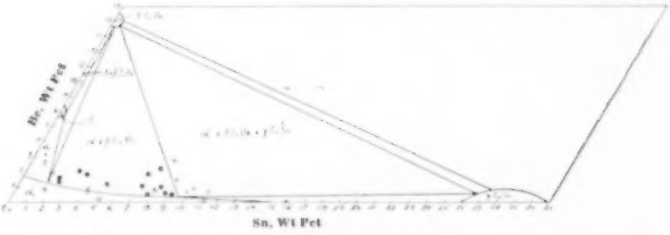

Fig. 3—580°C isothermal diagram.

copper was melted under an oxidizing flux consisting of equal parts of cupric oxide, borax, and sand, and was raised to a temperature of 1250° to 1300°C. The flux was thickened with sand and removed. The copper was deoxidized with 15 pct phosphor-copper and the Sn and Cu-Be alloy were added in that order. The melts were poured at 1150°C into a cast iron mold measuring 10x2x½ in. preheated at 150°C. Slow pouring was insured by the use of a tundish having an outlet orifice ⅛ in. in diam. The weight of the castings made in this way was approximately 1200 g. Before use, these castings were annealed at 700°C for 15 hr. While these samples were prepared primarily for the purposes mentioned above, melts thus made that on analysis were found to be substantially free from phosphorus were also used to provide additional data on alloy constitution, particularly in the higher tin regions.

Preparation of Microspecimens

The cast alloys were annealed for 2 hr at 700°C, hammered while hot, reannealed at 700°C for 16 hr, and water quenched. Drillings for chemical analysis were taken from the bottom of each ingot and the specimens for microscopic examination were cut from the portion just above. No variation in composition along the lengths of the castings was detectable, and it is considered that the chemical analyses correspond very closely with that of the microspecimens taken from adjacent parts of the castings. Six batches of microspecimens were cut from castings of the desired compositions, and all of the specimens were annealed at 700°C for 96 hr. At the end of this time the first batch of specimens was withdrawn and water quenched. The temperature of the annealing furnace was then slowly lowered to 600°C and maintained at this temperature for a further 96 hr, following which the second batch of specimens was water quenched. This procedure was repeated, with progressive decrease in the intermediate cooling rate, at 580°, 500°, and 400°C. The final batch of specimens was held at 300°C for 168 hr before quenching. On examination of the samples in this batch it was found that soaking for 168 hr was not

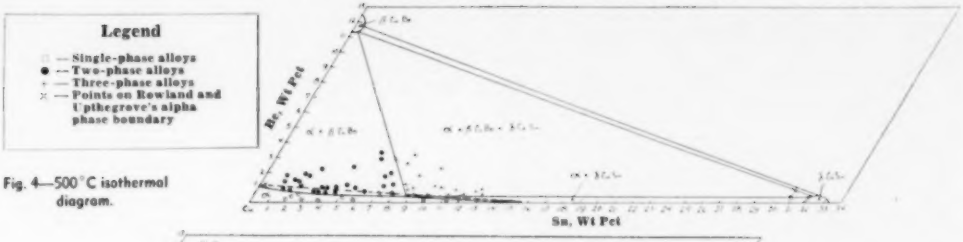
Legend
□ — Single-phase alloys
● — Two-phase alloys
+ — Three-phase alloys
× — Points on Rowland and Upthegrove's alpha phase boundary
Be, Wt Pct
Sn, Wt Pct

Fig. 4—500°C isothermal diagram.

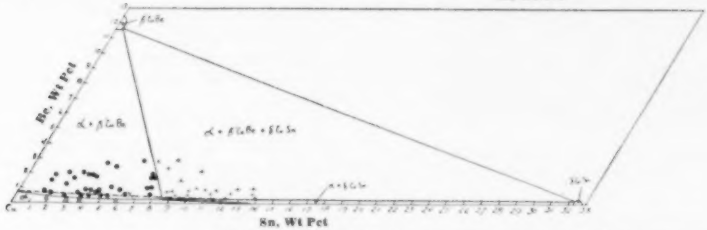

Fig. 5—400°C isothermal diagram.

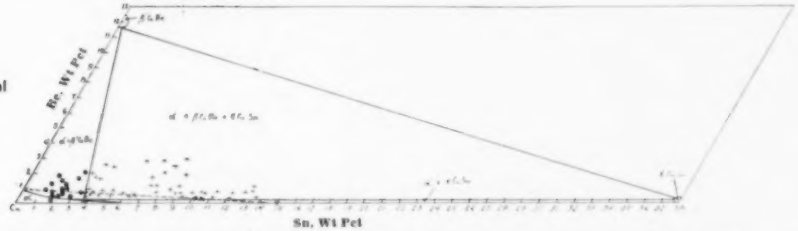

Fig. 6—300°C isothermal diagram.

sufficient to establish equilibrium in all of the alloys, and selected alloys near phase boundaries were therefore reannealed for a further 60 days to insure that equilibrium was established.

The microsections were prepared by hand polishing on Selvyt cloth moistened with Silvo metal polish and soap, and were etched in alcoholic ferric chloride or preferably in alkaline cuprammonium chloride: The latter etchant was found to give excellent phase differentiation in the majority of the three-phase alloys.

Results of the Constitution Investigation

The ternary isothermals at 700°, 600°, 580°, 500°, 400°, and 300°C are shown in Figs. 1 to 6.* For purposes of comparison some of the points on the phase boundaries of Rowland and Upthegrove's diagram have been included.

Sections at 700° and 600°C: It is confirmed, Figs. 1 and 2, that the β phases of the Cu-Sn and Cu-Be systems form a continuous series of solid solutions and that at these temperatures alloys in the copper corner of the diagram consist of α, or $\alpha + \beta$. The β phase is retained by quenching and is easily recognizable as white island in the darker α matrix. The phase boundaries at these temperatures are in close agreement with those of Rowland and Upthegrove.

* In Figs. 1 to 6 the abbreviation CuSn, etc., merely indicates the constituent metals and not the compositions of the respective phases.

Fig. 7—Equilibrium structure at 580°C of alloy No. 12, 2.5 pct Sn-2 pct Be. X750.

Fig. 8—Equilibrium structure at 500°C of alloy No. 61, 11 pct Sn-0.5 pct Be. X500.

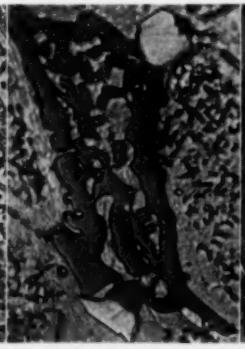

Fig. 9—Equilibrium structure at 500°C of alloy No. 57, 10 pct Sn-0.75 pct Be. X2000.

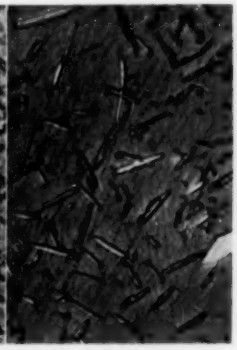

Fig. 10—Equilibrium structure at 500°C of alloy No. 41, 8 pct Sn-0.75 pct Be. X500.

Nominal compositions are given for these and all other micrographs.

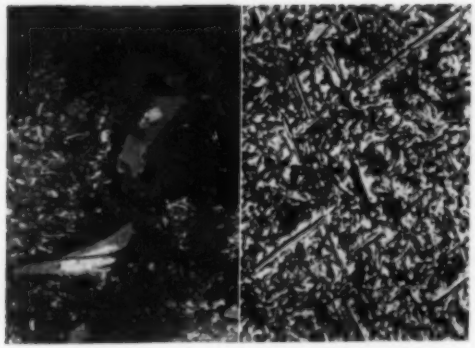

Fig. 11—Equilibrium structure at 300°C of alloy No. 68, 13.5 pct Sn-0.25 pct Be. X1750.

Fig. 12—Equilibrium structure at 300°C of alloy No. 22, 4 pct Sn-1 pct Be. X2000.

Section at 580°C: Owing to the transformation at 586°C of the β phase of the Cu-Sn system into $\alpha + \gamma$, this section, Fig. 3, shows a marked change from the one at 600°C. Pseudobinary systems are formed between the α and the β' phases of the Cu-Be system and between the γ phase of the Cu-Sn system and the β' phase of the Cu-Be system. One three-phase field appears between the α, β, and β' phases of the Cu-Be system and another between the α, β' CuBe, and γ phase of the Cu-Sn system. In the $\alpha + \beta'$ CuBe + γ Cu-Sn field, the islands that were originally β now consist of γ Cu-Sn and/or β' CuBe and α, and have become coarse in structure. The γ Cu-Sn phase is light gray in color and similar in form to the β phase of the Cu-Sn system. The β' CuBe phase, designated θ by Rowland and Upthegrove, is readily recognized by its white color and acicular form. Fig. 7 shows the equilibrium structure of an alloy containing approximately 2.5 pct Sn and 2 pct Be and reveals needles of CuBe and islands of Cu-Sn in a matrix of α.

Sections at 500° and 400°C: In these sections, Figs. 4 and 5, the γ phase of the Cu-Sn system is no longer present having undergone a eutectoid inversion into $\alpha + \delta$. At these lower temperatures the α solid solubility is reduced and β' CuBe or δ Cu-Sn (or both) phases precipitate from the α. The δ phase of the Cu-Sn system is precipitated from the α at the grain boundaries and within the grains themselves and is readily distinguished by its bluish-gray color. The β phase no longer exists and is replaced by a more complex structure consisting of α and either β' CuBe or δ Cu-Sn, or both, depending on the composition (see Figs. 8 to 10).

The range of α solid solubility at 500°C was found to be more restricted than is indicated in Rowland and Upthegrove.

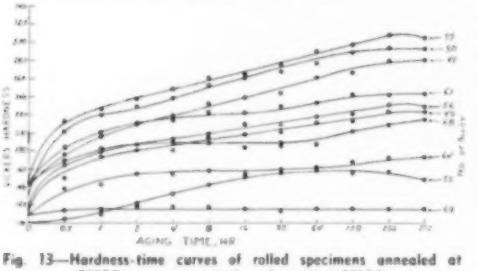

Fig. 13—Hardness-time curves of rolled specimens annealed at 700°C, water quenched, and aged at 250°C.

Section at 300°C: Only a trace of the δ phase was observed in specimens annealed at 300°C for 8 weeks, Fig. 6: the δ phase had practically all decomposed to give α and ϵ, Figs. 11 and 12. Some ϵ is also precipitated from the α in form of very small gray particles, some of which are barely resolved at a magnification of 2000. X-ray examination confirmed the existence of this phase in alloys in equilibrium but failed to detect its presence in alloys annealed for only two weeks.

The restriction in α solid solubility at this temperature was found to be very marked, and diverged considerably from that observed by Rowland and Upthegrove.

General Discussion

All phase boundaries were found to shift toward lower tin contents with increase in beryllium content. Also, the α field of the ternary system was found to decrease in area with decrease in temperature below 600°C. This decrease becomes marked at temperatures below the $\gamma \rightarrow \alpha + \delta$ transformation of the Cu-Sn system and is still more marked below the temperature of the $\delta \rightarrow \alpha + \epsilon$ transformation of the Cu-Sn system. This decrease in solubility accounts for the susceptibility to precipitation hardening in certain alloys of the ternary system noted by Masing and Dahl. The effect of composition and temperature on the limits of α solid solubility can be appreciated from the figures given in Table III.

Precipitation Hardening of Cu-Sn-Be Alloys

Masing and Dahl showed that Cu-Sn-Be alloys of suitable composition could be heat treated in the same way as binary Cu-Be alloys and demonstrated that the hardness of ternary alloys could be very considerably increased by aging after solution treatment. Further, aging was shown to be possible at temperatures below the recrystallization temperature, and the effect of cold working and precipitation hardening could therefore be superimposed.

The majority of Masing and Dahl's alloys contained 1.25 pct Be, or more. As such alloys would offer little economic advantage over the standard binary alloy containing around 2 pct Be, it was decided to investigate alloys of lower beryllium content. The alloys investigated had nominal contents of 2.0 to 13.5 pct Sn and 0.25 to 1.0 pct Be.

Rolled specimens were mainly used for the study of precipitation hardening. The melting procedure adopted in making ingots for this part of the work has already been described. After annealing the ingots at 700°C for 15 hr attempts were then made to hot roll them, but serious cracking occurred with all compositions. Cold rolling was therefore substituted and a number of ingots were successfully cold rolled down to a thickness of 0.1 in. Some ingots cracked badly in the early stages of rolling, especially those of alloys containing a large amount of a second phase. By adopting certain expedients the

Table III. Limiting Tin Content of α Solid Solutions

Temperature, °C	Tin, Pct		
	At 0.25 Pct Be	At 0.5 Pct Be	At 1 Pct Be
700	12.7	9.6	5.4
600	13.0	9.3	4.7
500	9.3	2.5	
400	4.4	1.0	
300	1.6	0.4	

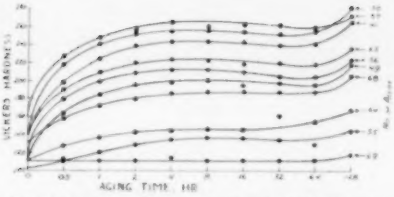

Fig. 14—Hardness-time curves of rolled specimens annealed at 700°C, water quenched, and aged at 300°C.

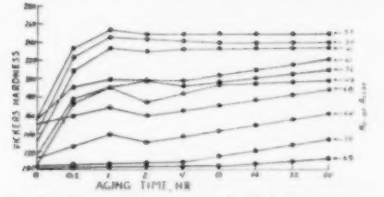

Fig. 15—Hardness-time curves of rolled specimens annealed at 700°C, water quenched, and aged at 350°C.

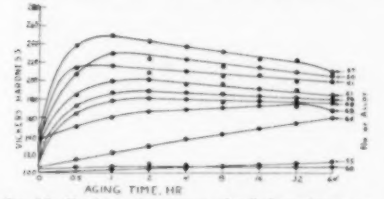

Fig. 16—Hardness-time curves of rolled specimens annealed at 700°C, water quenched, and aged at 400°C.

tendency to cracking was reduced and in many cases cracking was completely eliminated.

The procedure finally adopted was as follows: The annealed ingots were cold rolled to a reduction of 30 to 40 pct in several passes; they were then annealed for 15 min and again cold rolled as before. The whole procedure was repeated until a thickness of 0.1 in. was attained. In this way alloys Nos. 6, 8, 9, 16, 20, 21, 41, 49 50, 55, 56, 57, 61, 64, and 68 selected from the list given in Table II were successfully worked. For comparison, a binary tin-bronze containing 14.55 pct Sn was also prepared, and no trouble was experienced in working this alloy. The remaining alloys selected, namely, Nos. 62, 63, 65, 66, and 67, contained a large amount of a second phase in addition to the α constituent, and these alloys cracked severely on cold working.

All specimens were subjected to a solution heat treatment at 700°C before aging. This temperature is below the solidus for all of the alloys examined. Equilibrium was established in worked alloys after annealing at this temperature for 16 hr. Aging after solution treatment was carried out at 250°, 300°, 350°, 400°, and 450°C, the times of treatment being 0.5, 1, 2, 4, 8, 16, 32, and 64 hr: In addition, at 250°C the effect of prolonged aging for 128 and 256 hr was studied. Some alloys containing low amounts of tin and beryllium were also examined after aging at only 200°C.

Effect of Aging on Hardness: Hardness tests were made with a Vickers machine using a load of 50 kg and a time of application of 15 sec. At least three impressions were made for each test. The results obtained on rolled material were consistent, but there was some scatter in the hardness readings for as-cast samples.

The relationship between hardness and time of aging is shown in Figs. 13 to 16. For all ternary alloys aging at 250°C causes a rapid increase in hardness during the first hour, after which the hardness increases at a steady rate that is almost directly proportional to the logarithm of the time. The latter increase continues up to 256 hr. After 256 hr alloy No. 57 had a hardness of 310, which is the maximum figure recorded for any preannealed alloy. On aging at 300°C, the increase in hardening during the first hour is greater than at 250°C: On further aging at 300°C, the hardness remains fairly constant except in the case of alloys low in tin and beryllium for which the hardness increases progressively.

On aging at 350°C, the hardness of alloys containing 0.75 pct Be reaches a maximum after about 1 hr and thereafter remains substantially constant. Alloys of lower beryllium content continue to increase in hardness after 1 hr, but less markedly than when aged at 250° and at 350°C. On aging at 400°C and at 450°C, the hardness after the first hour of alloys with 0.5 to 0.75 pct Be diminishes with time; alloys with 0.25 pct Be show a progressive increase in hardness, as in the lower temperature treatments.

The extent to which hardness increases on aging appears to be determined almost entirely by the beryllium content of the alloys. Increase in the tin content of the alloys raises the general level of the hardness-aging time curves but does not significantly affect age hardening. Except in the case of alloys high in tin and beryllium, where the maximum hardness is reached after aging at 400° to 450°C, the remaining alloys attain their greatest hardness after aging at 250°C for 256 hr.

It was observed that many of the alloys examined could be cold worked in the solution-treated condition and the effect of age hardening superimposed on work hardening was next investigated. Figs. 17

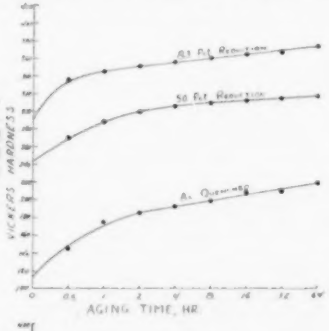

Fig. 17—Hardness-time curves for alloy No. 56 quenched from 700°C, cold rolled, and aged at 250°C.

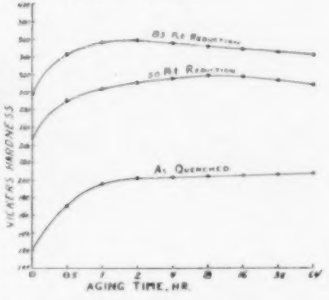

Fig. 18—Hardness-time curves for alloy No. 56 quenched from 700°C, cold rolled, and aged at 300°C.

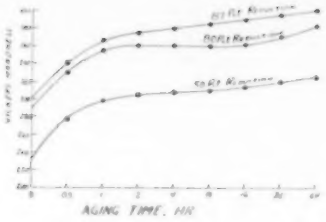

Fig. 19 (left) — Hardness - time curves for alloy No. 50 quenched from 700°C, cold rolled, and aged at 250°C.

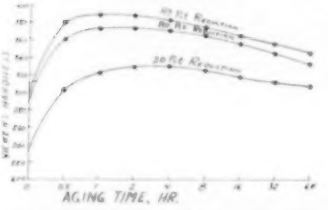

Fig. 20 (lower left) — Hardness-time curves for alloy No. 50 quenched from 700°C, cold rolled, and aged at 300°C.

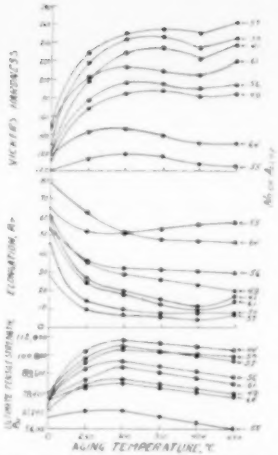

Fig. 21 (right) — Effect of aging temperature on the hardness, tensile strength, and elongation of rolled alloys.

to 20 show the hardness-time curves for two selected alloys solution treated and subjected to varying degrees of cold working followed by aging at 250° or 300°C. These alloys showed an increase in hardness of about 170 as a result of heavy cold working and on aging at 250°C showed a further rapid increase in hardness during the first hour followed by a slower progressive hardening which continued up to 64 hr without any sign of diminishing.

Table IV compares the maximum hardness values obtained for Cu-Sn-Be alloys with the hardness of commercial Cu-Be alloy containing 2.25 pct Be. It is apparent that although the hardness of the ternary alloys when aged from the solution-treated condition does not approach that of the binary Cu-Be alloy, the hardness of the ternary alloys can, if their beryllium content approaches 0.75 pct, be made equal to that of the binary alloy by a combination of cold work and precipitation heat treatment.

Where composition permits a direct comparison to be made, it is noteworthy that the initial and final hardness figures obtained in this work are considerably higher than the corresponding figures reported by Masing and Dahl.

The effects of heat treatment on a few as-cast alloys were examined and were found to be much the same as in the case of the rolled alloys, but the cast alloys gave somewhat lower initial and final hardness figures. The maximum hardness developed at a given temperature was reached in about the same time for both cast and rolled materials. Those alloys which failed to roll satisfactorily, owing to the high proportion of second phase present therein, all reached high hardness values on heat treatment in the as-cast condition.

Table IV. Comparative Hardness Values for Cu-Sn-Be and Cu-Be Alloys

Alloy	Vickers Hardness Number			
	Annealed	Cold Rolled	Heat Treated	Heat Treated after Cold Rolling
Commercial Cu-Be (2.5% Be)*	80-100	215-240	375	390
9% Sn, 0.75% Be, Bal. Cu	130	290-300	260	402
10% Sn, 0.5% Be, Bal. Cu	120	280	210	375
13.5% Sn, 0.25% Be, Bal. Cu	135	280	190	346
10% Sn, 0.2% Be, Bal. Cu	100	260	160	298

Effect of Aging on Tensile Strength and Elongation: Tensile tests were carried out on flat specimens 0.1 in. thick having a gage length of 2 in. Specimens were tested after solution treatment at 700°C followed by aging for 1 hr at 250°, 300°, 350°, 400°, and 450°C, respectively. The results obtained are shown in Fig. 21, which also includes comparison curves showing the effect of aging temperature on hardness. For single-phase alloys there is a reasonable correspondence between the effects of aging on hardness and on tensile properties. Perhaps the only significant divergence between the two properties is the lack of any marked increase in ductility in those cases where an increase in aging temperature has led to a fall in hardness. The best tensile properties were revealed by alloy No. 41 (8 pct Sn, 0.75 pct Be, nominal) which, after aging at 300°C, gave a tensile strength of 110,000 psi and an elongation of 23 pct. A similar tensile strength can be induced in high tin-binary bronze by cold working, but the accompanying elongation is much lower than that for the ternary alloy.

Effect of Aging on Electrical Resistivity: Resistivity-aging time curves are given in Figs. 22 to 25. There is little correlation between the effect of heat treatment on electrical resistivity and its effect on hardness. On aging at 250° and at 300°C the electrical resistivity of all of the alloys rises slightly at first and then falls continuously. On aging at higher temperatures there is a continuous fall in resistivity. An increase in electrical resistivity frequently occurs during the early stages of precipitation hardening, and the maxima in the hardness and electrical resistivity curves do not necessarily coincide. The maximum resistivity was developed in these alloys before precipitation could be detected under the microscope; this is usual in precipitation hardening.

Effect of Aging on Microstructure: After annealing and quenching, alloys outside the α phase boundary at 700°C were duplex in structure, the second phase being retained β; the presence of beryllium aids the retention of β.

The metallographic changes during aging were closely followed for alloys containing 10 pct Sn and 0.75 pct Be and those containing 11 pct Sn and 0.5 pct Be (nominal compositions). At all aging tem-

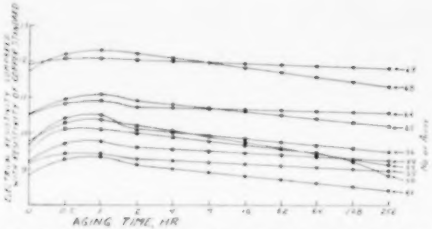

Fig. 22—Electrical resistivity-time curves for rolled specimens annealed at 700°C, water quenched, and aged at 250°C.

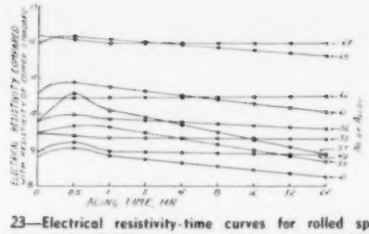

Fig. 23—Electrical resistivity-time curves for rolled specimens annealed at 700°C, water quenched, and aged at 300°C.

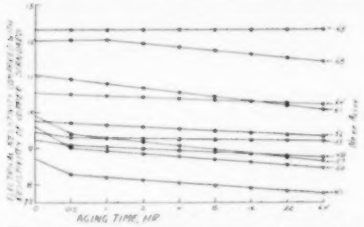

Fig. 24—Electrical resistivity-time curves for rolled specimens annealed at 700°C, water quenched, and aged at 350°C.

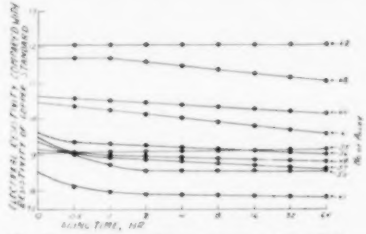

Fig. 25—Electrical resistivity-time curves for rolled specimens annealed at 700°C, water quenched, and aged at 400°C.

peratures the β phase commences to decompose in the first 30 min. According to the equilibrium diagram, the β phase should be converted to $\alpha + \delta$ above 350°C and to $\alpha + \epsilon$ below 350°C; generally speaking, it is impossible to resolve the precipitated individual phases under the microscope. Precipitation occurs in the α phase of all of the alloys examined and takes place in three stages. In the first stage there is a thickening of the grain boundaries leading to a definite precipitate on further aging. In the next stage martensitic markings develop within the α grains and increase in intensity as aging proceeds. The third stage, which at 400°C is reached after aging for 4 to 8 hr, corresponds to the disappearance of the martensitic markings and the appearance of precipitated particles within the α grains, Fig. 26.

Grain boundary precipitation is most marked in alloys that are originally duplex in structure. Precipitation commences from the β areas and the precipitated phase ultimately forms a continuous network surrounding the α grains, Fig. 27. The presence of this intergranular network is thought to account for the lower tensile strength of high tin as compared with that of lower tin alloys containing a high percentage of beryllium, see Fig. 21. At higher aging temperatures there is a tendency for the grain-boundary precipitate to ball up and form a discontinuous chain of particles, Fig. 28.

In alloys that are three phase after aging it is impossible to distinguish the two separate phases precipitating in the α as the structures are so complex, Fig. 29. In these alloys the structure probably consists of an intimate mixture of fine particles of β' CuBe and δ or ϵ embedded in a matrix of α. It is only possible in two-phase alloys to obtain structures that can be correlated with the equilibrium diagram by aging the alloys at high temperatures for a long time. Typical structures obtained in this way are shown in Figs. 30 and 31.

The course of precipitation in the low tin, low beryllium alloys is marked at the outset by a thickening of the α grain boundaries and the appearance of lines of precipitation along lattice planes within the α crystals, Fig. 32. On further aging, the lines

Fig. 26—Structure of alloy No. 57, 10 pct Sn-0.75 pct Be, after aging at 400°C for 8 hr. X500.

Fig. 27—Structure of alloy No. 68, 13.5 pct Sn-0.25 pct Be, after aging at 350°C for 32 hr. X1000.

Fig. 28—Structure of alloy No. 61, 11 pct Sn-0.5 pct Be, after aging at 400°C for 1 hr. X1000.

Fig. 29—Structure of alloy No. 57, 10 pct Sn-0.75 pct Be, after aging at 450°C for 128 hr. X500.

Fig. 30—Structure of alloy No. 68, 13.5 pct Sn-0.25 pct Be, after aging at 400°C for 64 hr. X500.

Fig. 31—Structure of alloy No. 41, 8 pct Sn-0.75 pct Be, after aging at 450°C for 256 hr. X2000.

Fig. 32—Structure of alloy No. 27, 5 pct Sn-0.5 pct Be, after aging at 300°C for 4 hr. X2000.

Fig. 33—Structure of alloy No. 5, 2 pct Sn-0.5 pct Be, after aging at 300°C for 8 hr. X500.

of precipitation along the planes within the α grains become more numerous and it is easy to follow this change of direction at the α grain boundaries and at twin discontinuities, Fig. 33. On still further prolonging the time of aging, the grain boundaries and lines within the grains become thicker and ultimately it is possible to resolve the latter as particles of the precipitated second phase, Fig. 34.

Effect of Aging

The fall in resistivity which occurs on aging Cu-Sn-Be alloys precedes slightly the onset of grain-boundary precipitation. This is in accordance with the hypothesis that maximum lattice strain is reached before visible precipitation occurs. It is somewhat surprising that the appearance of resolvable particles in the α is not accompanied by a fall in hardness, except for aging at 400° and at 450°C, as in age-hardening systems the hardness generally reaches a maximum before visible precipitation occurs. It is possible that there is some undetected heterogeneity in the α phase of these ternary alloys and that the softening in certain areas, which theoretically should occur when visible particles form, is offset by hardening in other areas in which precipitation is less advanced. Such heterogeneity might arise through differential stress resulting from non-uniform rolling. However, it is tentatively suggested that in the case of three-phase alloys, which have been annealed at temperatures not exceeding 350°C, the initial hardening and the first visible precipitation is attributable to precipitation of the β' phase of the Cu-Be system and that subsequent softening is overshadowed by slow, progressive hardening resulting from the sluggish precipitation of the ϵ phase.

Fig. 34—Structure of alloy No. 27, 5 pct Sn-0.5 pct Be, after aging at 250°C for 32 hr. X2000.

Summary and Conclusions

Isothermal sections of the ternary Cu-Sn-Be system have been determined by microscopic methods for alloys in equilibrium at 700°, 600°, 580°, 500°, 400°, and 300°C and for the composition range 0.25 to 3.0 pct Be and 1.5 to 13.5 pct Sn. The decrease in the limit of α solid solubility with fall in temperature is found to be more marked than is indicated by the work of previous investigators, particularly at temperatures below 350°C, where the field is restricted by the eutectoid transformation of the Cu-Sn system. The presence of the ϵ phase of the Cu-Sn system in specimens that had been annealed at 300°C for 8 weeks was confirmed by X-ray examination.

Alloys containing 0.25 to 0.75 pct Be and 2.0 to 13.5 pct Sn have been shown to possess age-hardening properties. The extent of precipitation hardening obtainable depends primarily on the beryllium content of the alloy. After appropriate aging of rolled and solution-treated material, the maximum hardness is obtained with a nominal composition of 10 pct Sn, 0.75 pct Be. For the same pretreatment, the maximum tensile strength is obtained with a nominal composition of 8 pct Sn, 0.75 pct Be; this alloy can show an ultimate tensile strength of 110,000 psi with an elongation of 23 pct on 2 in. The hardness of the ternary alloys, aged from the solution-treated condition, does not reach that of heat-treated binary Be-Cu alloys with around 2 pct Be, but by cold working solution-treated alloys prior to aging, hardness figures comparable with those exhibited by commercial Cu-Be alloys can be obtained from ternary alloys of suitable composition.

Annealed alloys containing a large amount of second phase tend to crack on cold rolling. These alloys can be heat treated, however, to give high hardness values, a hardness of 260 being attainable for alloys of high tin and high beryllium content.

The constitution changes taking place during precipitation heat treatment have been examined. It is suggested that, on aging three-phase alloys below 350°C, the observed initial hardening is attributable

to precipitation of the β' phase of the Cu-Be system and that the subsequent hardening is explained by slow precipitation of the ϵ phase of the Cu-Sn system.

In view of the high cost of beryllium, the fact that approximately the same properties can be obtained in a ternary alloy containing 0.75 pct Be as in a binary alloy containing 2.0 pct Be is noteworthy, and there seems no reason to believe that the cheaper alloy might not function satisfactorily in some of the applications where the binary alloy is now used.

Acknowledgments

This research was carried out in the laboratories of the Tin Research Institute. The authors are indebted to the International Tin Research and Development Council for permission to publish this paper. Grateful acknowledgment is made for guidance given throughout the course of the work by D. Hanson and G. V. Raynor, of the Department of Metallurgy, University of Birmingham, England, the former to whom thanks are also due for carrying out the X-ray examination mentioned in the paper, and the latter for helpful advice and criticism.

References

[1] G. V. Raynor: Private communication.

[2] G. Masing and O. Dahl: *Wiss. Veröff. Siemens-Konzern* (1929) **8**, p. 202.

[3] G. V. Raynor: Annotated Equilibrium Diagrams, Inst. of Metals (1944) No. 2.

[4] H. Borchers: *Metallwirts.* (1932) **11**, pp. 317, 329; cf. *Metallurgist* (1932) **8**, p. 152; H. Borchers and H. J. Otto, *Metallwirts.* (1942) **21**, p. 215.

[5] G. V. Raynor: Annotated Equilibrium Diagrams. Inst. of Metals (1949) No. 7.

[6] W. Hume-Rothery, P. W. Reynolds, and G. V. Raynor: *Journal* Inst. of Metals (1940) **66**, p. 191.

[7] E. S. Rowland and C. Upthegrove: *Trans.* AIME (1935) **117**, p. 190.

[8] D. W. Crossley and E. M. Foster: *Journal of Scientific Instruments* (1943) **20**, p. 7.

Technical Note

Lattice Parameter of InSb

by T. S. Liu and E. A. Peretti

A LITERATURE survey of the In-Sb system, which was made before a study of the binary diagram was undertaken, revealed that the intermediate phase InSb existed and that its crystal structure is face-centered cubic of the zinc blend type. In 1929 Goldschmidt[1] determined the lattice constant for InSb and obtained a value of 6.452A. A more recent value, 6.461A was reported by Iandelli[2] in 1941. The purity of the indium used was not very high, however. The indium used by Iandelli contained 2 pct Ge. In view of this fact it was decided to remeasure the lattice parameter using high-purity indium (99.97+ pct In) and spectrographically standardized antimony of the highest purity available (99.91 pct Sb).

Specimens corresponding to the InSb composition were made by carefully weighing the ingredients on an analytical balance and heating them in vacuo in a quartz tube at 700°C. As melting losses were negligible, the alloys were not analyzed chemically, but the intended analysis was taken as being accurate. Powder samples were prepared by either filing or crushing of the brittle alloy, followed by screening at 325 mesh. The powders were then annealed at 400°C in evacuated capsules for about an hour.

X-ray photograms were taken with a Debye and a back-reflection focusing camera, using characteristic cobalt K_α radiation. Lattice parameters were calculated by Cohen's[3] method. The results of a Debye pattern and of a back-reflection pattern at 25°C are given in Tables I and II.

The lattice parameter at 25°C is 6.4760A.

Table I. Debye Pattern of InSb*

θ	$\sin\theta$	d	Observed Intensity	hkl	λ
81.18	0.9881	0.9054	m	711 551	α_2
80.50	0.9863	0.9050	vs	711 551	α_1
73.55	0.9590	0.9328	w	444	α_2
73.23	0.9574	0.9324	w	444	α_1
69.43	0.9362	0.8638	w	642	β
65.33	0.9086	0.9846	vw	533	α_2
65.10	0.9070	0.9842	m	533	α_1
61.23	0.8765	1.021	vw	620	α_2
61.05	0.8750	1.020	m	620	α_1
55.08	0.8200	1.089	s	531	α
51.68	0.7846	1.136	vw	440	α
48.13	0.7446	1.086	w	531	β
46.23	0.7231	1.236	m	333 511	α
42.90	0.6807	1.311	s	422	α
37.38	0.6070	1.471	m	331	α
33.93	0.5581	1.599	w	400	α
27.63	0.4637	1.925	s	311	α
25.08	0.4238	1.918	vw	311	β
23.40	0.3971	2.248	vs	220	α
21.18	0.3612	2.239	vw	220	β
14.28	0.2464	3.623	vw	111	α

* Cobalt radiation with iron filter.
s, strong; m, medium; w, weak; vw, very weak.

Table II. Lattice Constant Calculation for Focusing Back-Reflection Pattern Taken at 25°C

Plane		$\sin^2\phi$	$h^2+k^2+l^2$	δ^*
711 551	α_2	0.976348	51	5.3
711 551	α_1	0.972111	51	6.4
444	α_2	0.922410	48	17.4
444	α_1	0.917841	48	18.4
731 553	β	0.913711	89	19.2
642	β	0.874521	56	27.5
533	α_2	0.820171	43	38.6
533	α_1	0.816538	43	39.3

Normal Equations

$184596K\dagger + 2571.3D = 1097.96^2$
$25171.3K + 4868.44D = 149.578^2$
$K = 0.00596105 \quad D = -0.00009037 \quad a_o = 6.4760$

* $\delta = 2\phi \sin^2\phi$, where $\phi = 90° - \theta$.
† $K = \frac{1}{4}a^2\lambda^2$, λ is incorporated into the equations.
Values of λ are based on those adopted at the conference of the X-ray Analysis Group of the Institute of Physics, London (1946).[4]

References

[1] V. M. Goldschmidt: Crystal Structure and Chemical Constitution. *Trans.* Faraday Soc. (1929) **25**, p. 253.

[2] Aldo Iandelli: Sulla Struttura Dei Composti InP, InAS e InSb. *Gazzetta Chimica Italiana* (1941) **71**, No. 1, p. 58.

[3] M. U. Cohen: Precision Lattice Constants from X-ray Powder Photographs. *Review of Scientific Instruments* (March 1935) **6**, p. 68.

[4] *Journal of Scientific Instruments* (1947) **24**, p. 27.

T. S. LIU, Student Associate AIME, is Teaching Fellow and E. A. PERETTI, Member AIME, is Professor of Metallurgy, University of Notre Dame, Notre Dame, Ind.

TN 87E. Manuscript, May 18, 1951.

Creep Behavior of Zinc Modified by Copper in the Surface Layer

by Milton R. Pickus and Earl R. Parker

THE modern theories of creep[1-4] in general have been based upon the concept of generation and migration of dislocations, with the generation process normally assumed to be rate controlling. The theories are generally deficient in that they fail to take into account many factors that are known to influence creep. The influence of the state of the surface of the test specimen has been almost completely overlooked; yet the present report shows that the nature of the surface may, in certain cases, govern the creep characteristics of a specimen.

In the period since Taylor[5] applied the concept of dislocations to a study of metals, a school of thought has developed that closely relates the plastic deformation of metals to the generation and migration of dislocations through the crystal lattice. It might be expected that the thermal energy required for the generation of a dislocation would be different from that for migration of the dislocation through the lattice. Furthermore, the activation energy for generation would be expected to vary for different parts of the solid metal. It has been predicted that dislocations would be generated most easily at external surfaces, but could also be activated at certain internal surfaces such as grain or phase boundaries. Within the body of the metal a range of values for the activation energy might be expected because of different degrees of disorder at such regions as grain boundaries, impurities, and second-phase particles. The particular value of the activation energy that was rate determining could then depend on the specific conditions of a test. If, for example, the surface atoms were by some means constrained, the generation of dislocations in the body of the metal might become the important factor. On the other hand, other conditions may favor generation at the surface. It is possible then that the creep behavior may not be completely determined by the inherent properties of the metal. Even the environment in which a test is carried out could have a significant effect. In fact it is conceivable that in order to obtain the maximum creep resistance from a given alloy, the surface atoms must be so constrained that the activation energy for generating dislocations on the surface is at least equal to that required for generation in the body of the metal. On the basis of such considerations, and in view of the limited number of publications discussing this subject, it seemed that an investigation of the influence of the state of the surface on creep might yield information of both theoretical and engineering interest.

Experiments on single crystals, demonstrating a variation in the mechanical properties due to alterations in the surface layer, have been reported by several investigators.[6-10] The results of these experiments have been briefly summarized;[11] consequently, the earlier work will not be reviewed here. As an example of these findings the observations of Cottrell and Gibbons may be cited. They reported the critical shear stress of a lightly oxidized cadmium single crystal is greater by a factor of 2½ than a specimen with a clean surface.

M. R. PICKUS and E. R. PARKER, Members AIME, are Research Metallurgist and Professor of Physical Metallurgy, respectively, University of California, Berkeley, Calif.

Discussion on this paper, TP 3122E, may be sent, 2 copies, to AIME by Dec. 1, 1951. Manuscript, April 10, 1951. Detroit Meeting, October 1951.

This paper represents part of the work done on a research program under the sponsorship of the Office of Naval Research.

Materials and Methods

Single crystals ½ in. in diam and 8 in. long were prepared from Horse Head Special zinc, melted under an atmosphere of helium in a large pyrex test tube, and drawn up into a long ½ in. diam pyrex tube by means of a vacuum pump. The cast zinc rods thus produced were cut into convenient lengths and sealed in evacuated pyrex tubes. Single crystals were grown by gradual solidification of the remelted rods. Cleaving the ends of the single crystal specimens chilled by liquid nitrogen proved a simple method for determining orientations from the exposed basal plane from the markings left on the cleaved surface that gave the slip directions with sufficient accuracy for the experimental work. The specimens chosen for the experiments were those having the angle between the basal plane and the specimen axis within the range of 15° to 65°.

Since zinc single crystals are quite delicate, it was necessary to devise an appropriate method of gripping the specimens in order to suspend them in the furnace and apply the load. Stainless steel collars were prepared having an inside taper, the smaller end of the taper being of such a size that the specimen could just pass through freely. The tapered hole did not extend the full length of the collar; a sufficient thickness of metal remained so that a hook could be attached to provide a means of applying the load and suspending the specimen. One of the collars was slipped over the upper end of a specimen which was supported vertically in a steel jig. The collar was then heated electrically until the end of the crystal melted and filled the collar with molten zinc. At this point the application of heat was discontinued, whereupon the molten zinc quickly solidified, due to the chilling effect of the jig. The specimen was then inverted and the second collar applied in a similar manner. The jig served several purposes: limiting the length of specimen that was melted, providing excellent alignment of the collars with respect to the specimen axis, and protecting the specimen from mechanical damage.

Once the specimen was suspended in the furnace and loaded, it was desired to accomplish the surface treatment with a minimum of disturbance of the specimen. Around the specimen was a long pyrex tube, the upper portion of which was approximately 1 in. in diam, and in it was a copper coil of such a diameter to fit snugly against the tube. A specimen, approximately ½ in. in diam and 4 in. long, was suspended by means of a stainless steel rod so that it hung within the copper coil. The lower portion of the glass tube was approximately ¼ in. in diam, and passing through it was a 5/32 in. diam stainless steel rod which hung from the lower specimen collar. This portion of the glass tube and the stainless steel rod extended through the bottom of the furnace. A T-connector, with suitable packing, was attached to the lower end of the stainless rod to provide a water-

tight seal. A yoke, attached to this rod by a gimbal joint, was used to activate a dial gage and from which the load was suspended by a coil spring. Fig. 1 shows the main features of the assembly.

The furnace consisted of an insulated rectangular box with two nichrome heating elements and a small fan so disposed that a uniform temperature over the gage length of the specimen was obtained. Three thermocouples mounted on a dummy specimen, one at each end, and one at the center of the gage length, showed less than 1°C difference in temperature. Three specimens could be tested simultaneously. A pyrex panel mounted in one of the sides made it possible to observe the specimens.

The gage length consisted of the 4 in. length of crystal between the gripping collars. Overall extension was measured by means of a dial gage graduated in divisions corresponding to a plunger travel of 0.0001 in. The range of the gage was 0.4 in.

The method of achieving reproducible surface changes decided upon consisted in applying electrolytically a thin layer of copper. With respect to zinc, copper may be considered a thermally inactive metal in the sense that at 200°C, for example, the kinetic energy of the copper atoms is still far below that required to overcome the bonding energy that holds the copper atoms in their lattice positions, whereas zinc atoms, in view of the relatively low melting point of 419°C, have kinetic energies more nearly commensurate with the magnitude of the energy holding the zinc atoms together. From these considerations, it was supposed that under the influence of stress and temperature, dislocations could be generated much more easily in a surface layer consisting of zinc atoms than in one containing copper atoms, or for the case where dislocations were generated internally, their escape to the surface would be hampered by the layer of copper.

In order to accomplish the desired changes in the surface layer, procedures were required for cleaning the zinc surface prior to the electrodeposition of copper, and for removing the electrodeposited copper while the specimen was in the assembled apparatus. Fortunately it was found that both of these requirements were met by an anodic treatment of the specimen in an electrolyte consisting of a 10 pct aqueous solution of sodium cyanide, the copper coil (Fig. 1) serving as a cathode. During the development of the anodic treatment, an interesting relationship was observed between the applied voltage and current. Several discontinuities were found, the best cleaning being obtained just after the first. The current was not a single valued function of the voltage; the same current could be obtained at several different voltages, depending on which of the discontinuous curves was applicable. Although the values of the current and voltage at the discontinuities depended on the size of the specimen and the temperature, the cleaning procedure proved to be quite simple, since it was necessary only to apply approximately 4 v and watch the ammeter needle. With the cell filled with electrolyte and the electrical connections made, the current slowly rose to a maximum and then dropped sharply. After 10 or 15 sec at the lower current the specimen was found to be cleaned effectively.

If the specimen was to be copper plated, the sodium cyanide solution was drained off, the polarity of the electrodes reversed, and the cell filled with a copper-plating solution. The zinc specimen was plated at a current density of 0.10 amperes per sq

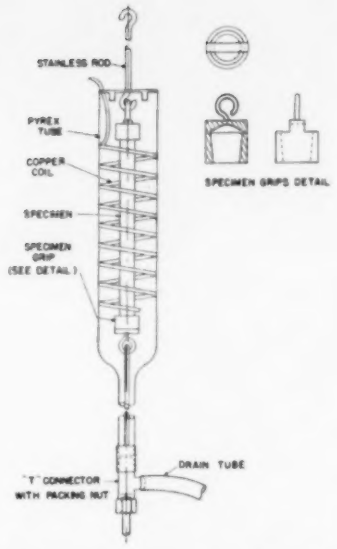

Fig. 1—Specimen assembly.

in. for 90 sec. Both the specimen and electrolyte were at room temperature during the plating. The composition of the plating bath was as follows: Copper cyanide, 22.5 g per liter; sodium cyanide, 33.8; sodium carbonate, 15. The average thickness of the copper layer deposited under these conditions is 10^{-4} in. After plating, or cleaning if that was to be the final step, the cell was rinsed first with water and then with alcohol. Finally the specimen and cell were dried by the passage of a stream of air.

In order to determine the effects of the copper deposit, it was found necessary to employ a single specimen for a complete test involving alternate changes in the surface layer. This procedure had the advantage of reducing the number of variables, although it did require an interruption in the test. Earlier experiments had shown that despite the care employed in the preparation of the single crystals, they nevertheless differed from one another in that the same creep rates for different orientations could not be obtained by adjusting the load to provide the same shear stress in the direction of slip. For one thing the extension was by no means uniform over the 4 in. gage length. In this respect there was a variation from one specimen to another. In an extreme case the entire deformation was localized in a small portion of the specimen, which had the appearance of two substantially undeformed portions markedly offset from each other over the width of a narrow slip band. This of course means that measuring the overall extension of the 4 in. specimen can give only a fictitious strain rate, since the true gage length is indeterminate. However, the measurement of the overall extension served as a convenient means of observing changes in a particular specimen. A few of the specimens subjected to elevated temperature creep tests are shown in Fig. 2. It should also be mentioned in this connection that the loading of the specimens to obtain the desired creep rate proved to be quite a problem. In many cases only a small increment of load beyond that producing a very slow rate of secondary creep resulted in the sudden onset of the third stage, with

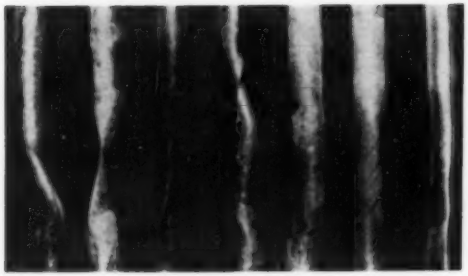

Fig. 2—Examples of unplated zinc single crystals tested in creep at elevated temperatures.

large extensions occurring in a relatively short time. In some instances this increment of load was supported by the specimen for several hours, the creep progressing at a slow steady rate; then the creep rate would rise sharply, producing such excessive extension the particular test had to be abandoned.

After the specimen assemblies were suspended in the furnace, the specimens were cleaned anodically in the sodium cyanide solution and then rinsed and dried. The furnace then was heated to a higher temperature than was to be used for the tests, and a period allowed for temperature stabilization with the object of minimizing any changes in the state of the specimens due to heating at the test temperature. The furnace was cooled and brought to equilibrium at the test temperature before the load was applied. After the secondary creep rate was determined, the furnace was cooled to room temperature, with the specimens still under load. They were again cleaned anodically in the sodium cyanide solution, after which they were copper plated in the manner already described. The furnace was reheated to the test temperature and the secondary creep rate for the copper-plated condition determined. As already mentioned, the copper layer was effectively removed by the anodic cleaning procedure. Thus several cycles of creep for each condition of the specimen surface could be observed.

This procedure was adopted after several unsuccessful modifications. It was thought that for tests at temperatures near 100°C hot solutions could be employed, thus eliminating the necessity for interrupting the test by cooling down the furnace. However, the anodic treatment in sodium cyanide solution was not controllable in hot solutions.

On the other hand, if the furnace was maintained at the test temperature, and the specimens momentarily chilled by filling the cells with cool liquid, an effect of the cooling on the creep rate was invariably observed. This effect was analogous to that obtained by adding an increment to the load. The creep rate increased rather sharply and the effect persisted for several hours.

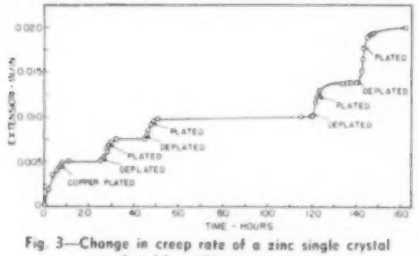

Fig. 3—Change in creep rate of a zinc single crystal produced by a thin copper plate.
Test temperature, 100°C. Resolved shear stress, 31.5 psi.

Several tests were performed wherein during a period of steady creep no change was made other than to cool the furnace to room temperature, and then reheat it to the test temperature. In all cases the creep rate was unchanged by the slow cooling and heating cycle. It appeared, therefore, that in order for there to be an effect on the creep rate due to cooling the specimen, a temperature differential must be set up between the surface and interior of the specimen. The fact that no noticeable effect was introduced by gradual cooling was regarded as justification for the test procedure that was adopted.

In this manner the effect of copper in the surface layer on the secondary creep rate was studied at constant temperature and constant load. This was done for polycrystalline zinc and for single crystals. The temperature dependence at constant load of the secondary creep rate was also determined for both forms of zinc with and without the presence of an electrolytically deposited layer of copper.

The polycrystalline specimens were in the form of cast rods of chemically pure zinc. While the grain size of these specimens was somewhat coarse, a cross-section contained many grains so that a comparison between single crystal and polycrystalline zinc could be obtained. The polycrystalline specimens were 5½ in. long and ¼ in. in diam, with a 2 in. reduced section of 0.187 in. diam which served as the gage length.

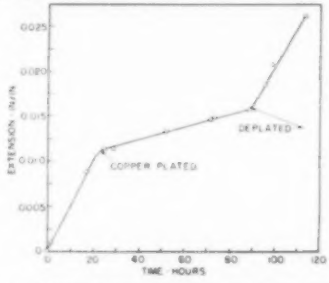

Fig. 4—Change in creep rate of a zinc single crystal produced by a thin copper plate.
Test temperature, 200°C. Resolved shear stress, 26.5 psi.

Experimental Results

In the course of the experimental work a large number of single crystals in a considerable range of orientations were tested. The results in all cases followed the same general pattern. The creep rate was sharply decreased by the presence of the thin copper layer. When the copper was removed, the creep rate increased to the value obtained for the unplated specimen. The effect of the copper was large, amounting in some cases to essentially a complete cessation of flow. In an extreme case when a test was carried to a point where the cross-sectional area was noticeably diminishing, the application of the copper deposit arrested the acceleration of creep rate.

The results of typical tests are shown graphically in Figs. 3 and 4. In Fig. 3 is recorded a test at 100°C showing the effect of a series of plating and deplating cycles. Even though necking had begun in the latter stages of the test, the effect of the copper was still definite. Fig. 4 shows the results of a similar test at 200°C.

Numerous tests on the polycrystalline specimens

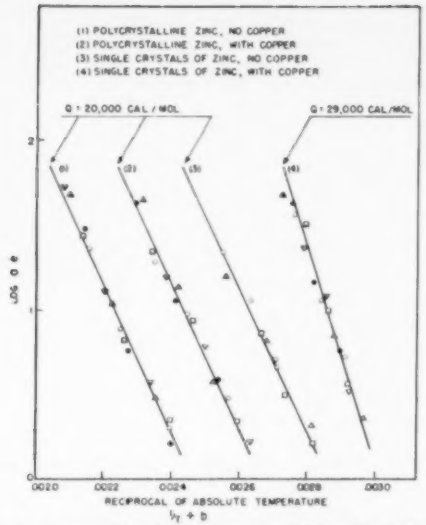
(1) POLYCRYSTALLINE ZINC, NO COPPER
(2) POLYCRYSTALLINE ZINC, WITH COPPER
(3) SINGLE CRYSTALS OF ZINC, NO COPPER
(4) SINGLE CRYSTALS OF ZINC, WITH COPPER
Q = 20,000 CAL / MOL
Q = 29,000 CAL/MOL
LOG ė
RECIPROCAL OF ABSOLUTE TEMPERATURE
1/T + b

Fig. 5—Composite plot of data from 18 tests designed to establish the temperature dependence of creep for polycrystalline and single crystal zinc both with and without copper on the surface.

Creep rate designated as ė. The constants a and b were selected to shift the curves parallel to their original positions for ease of comparison. All the experiments were in the temperature range of 200° to 325°C.

show conclusively that the presence of a thin layer of copper has no effect on the creep behavior of polycrystalline zinc. While particular experiments might indicate an effect of small magnitude, the effect is so small as to be within the scatter of results obtained over many experiments.

The secondary creep rates for zinc in four different conditions were determined in the temperature range 200° to 375°C. The four conditions comprised single crystal and polycrystalline zinc, both with and without the presence of copper in the surface layer. The test procedure consisted of determining for each specimen the creep rates at three different temperatures. After the creep rates were determined for each of the three temperatures, the test at the first temperature was repeated as a check that no appreciable change in the state of the specimen had occurred. The data were plotted with the logarithm of the creep rate as ordinate and the reciprocal of the absolute temperature as abscissa. It is characteristic of the second stage of creep that the creep rate changes very little for relatively large strains. The approximately steady secondary creep rate is known to vary with temperature in close accord with the expression:

$$\text{Creep rate} = A\, e^{-Q/RT}$$

where A is a constant; e, the natural logarithm base; Q, a quantity known as the activation energy; R, the gas constant; and T, the absolute temperature.

The results of these tests have been summarized in the composite plot shown in Fig. 5. In this series of experiments, the objective was to determine the effect of the copper plate on the temperature dependence of creep. Both single and polycrystalline specimens were tested. The lines drawn through the points represent a graphical averaging of the data obtained from numerous tests. The lines have been separated for clarity by shifting the ordinates to a different position on the graph for each type of specimen. However, the range of temperatures and creep rates were approximately the same for all tests (see Figs. 3 and 4 for typical creep rates), so that a direct comparison of temperature dependence could be made. Individual tests are distinguished by the use of different symbols. The values of Q were determined from the slopes of these four lines. It will be noted that the same value of Q was obtained for single crystals without copper, and for polycrystalline zinc with and without copper in the surface layer. Of the four conditions studied only the copper-plated single crystals showed an appreciably different temperature dependence.

An observation was made in regard to the copper-plated single crystals that is of considerable interest. It was found that if, after the creep rate had been determined at three successively higher temperatures, the temperature was lowered for a period of 15 hr, or so, to a point where creep progressed very slowly, reheating the specimen to the original three test temperatures gave appreciably lower creep rates. The log (creep-rate) vs. $1/T$ plot was a straight line parallel to the line obtained originally, but displaced in the direction of lower creep rates. This effect was observed consistently and is illustrated for a particular test in Fig. 6. The magnitude of the effect may be appreciated by comparing points (1) and (4) which show corresponding creep rates obtained at 275°C before and after the low temperature treatment. This strengthening effect may be due to the clustering of solute atoms around dislocations which reduces their mobility.

Discussion of Results

Since a relatively thin deposit of copper had such a pronounced effect on the creep behavior of zinc single crystals, it becomes important to consider in what manner the copper exerts its influence. Before discussing the various mechanisms that might account for these results, it is necessary to take into account an additional experimental observation. In all the tests that were performed, diffusion between zinc and copper occurred. The diffusion was quite

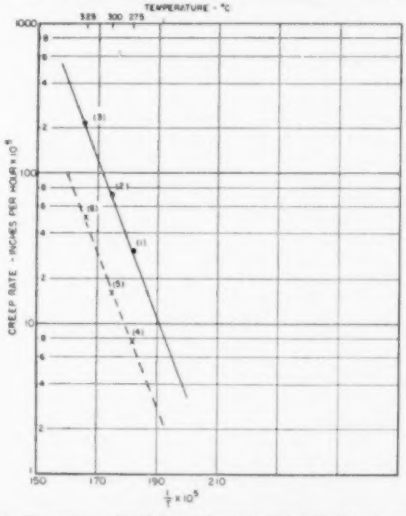

Fig. 6—Temperature dependence of copper-plated zinc single crystal showing effect of a period of very slow creep.

After determining points 1, 2, and 3, specimen was cooled under load to 250°C and held at this temperature for 15 hr. Then points 4, 5, and 6 were determined.

rapid; before the specimens attained the test temperature, little visible evidence of the copper deposit remained. However, that the copper remained in the extreme surface layer of the specimen was indicated by the fact that the slight amount of material removed by the anodic treatment in sodium cyanide solution caused the creep rate to increase to the value obtained before plating with copper. It has already been mentioned that during the anodic treatment of the zinc specimens a discontinuous relationship was observed between the applied voltage and the current. When copper was present these discontinuities did not occur. As soon as a surface of essentially pure zinc was exposed, the discontinuities reappeared. This served as a convenient control of the cleaning procedure. Any attempt, therefore, to rationalize the results must take into account the fact that the surface layer consists of a Cu-Zn alloy.

The question arises as to whether the effect of the copper on the creep of zinc single crystals is simply a mechanical one; that is to say, the Cu-Zn surface layer produces a strengthening effect analogous to increasing the specimen diameter by an equivalent thickness of zinc. Stress analyses indicate that this is unlikely and furthermore, if this were the case, no difference in the temperature dependence would be expected between the plated and unplated crystals. The fact that a difference was found suggests that there is a fundamental difference in the creep process for the two surface conditions.

The possibility of developing stresses in the surface layer as a consequence of the application of the copper must also be considered. Such stresses could arise from at least two sources. The existence of stresses in electrodeposited metal is common knowledge. Such stresses may be either tensile or compressive in nature, depending on the metal being deposited and the conditions of electrodeposition. Another source of surface stress lies in the fact that diffusion occurs between the copper and zinc. This causes a change in the lattice parameter at the surface and thus produces a potential localized stress field. While such stresses might conceivably affect the creep rate at a given temperature, it is difficult to see how they could account for a change in the temperature dependence, particularly since the temperature coefficient for unplated zinc was found to be rather insensitive to changes in the stress level. Moreover, the fact that the tests were conducted at elevated temperatures would tend to limit the magnitude of the localized stresses.

Another pertinent question is why the copper deposit had no effect on the creep behavior of polycrystalline zinc. If it is assumed that the generation of dislocations, rather than their migration through the lattice, is rate determining, a possible explanation for this difference in behavior can be offered. It is a reasonable assumption that dislocations can be more easily generated at a surface than in a volume of perfect crystal. In a single crystal the only surface is the external one (neglecting domain boundaries); whereas in a polycrystalline specimen there is a network of internal surfaces as well. Since, in the latter case the external surface is only a small percentage of the total available surface area, a polycrystalline specimen would not be expected to be sensitive to alterations in the external surface. However, evidence has been obtained that indicates such a conclusion may be incorrect. Some tests were performed on polycrystalline "A" nickel, the results of which have been published.[16] A comparison was made of the creep behavior of "A" nickel in different environments and surface conditions. It was found that resistance to high temperature creep was much greater in air than in either purified hydrogen or nitrogen. The experiments with "A" nickel were therefore interesting with respect to the strengthening effects that have been reported for single crystals due to an oxide film. Similar results recently have been obtained for copper. It now appears that oxide films are also significant for polycrystalline metals.

In the case of the zinc single crystals the possibility of a volume, rather than a surface effect, would appear to be ruled out by the observation that the removal of a small amount of surface material from a copper-plated specimen caused the creep rate to increase to the value obtained for unplated specimens.

The results presented herein do not constitute a proof that dislocations originate at the surface of single metal crystals during a creep test. It may well be that dislocations are generated internally as postulated by Frank and Reed[15] and that their egress is blocked by the surface layer. At the present time it is not possible to locate the origin of the dislocations. However, additional experiments are now under way which may prove sufficiently critical to establish whether dislocations are generated within the volume of a crystal or at external or grain surfaces.

References

[1] R. Becker: Über die Plastizität amorpher und kristalliner fester Körper. *Ztsch. Physik* (1925) **26**, p. 919.

[2] E. Orowan: The Creep of Metals. *Journal* West of Scotland Iron and Steel Inst. (February 1947) p. 45.

[3] J. M. Burgers: Some Considerations on the Fields of Stress Connected with Dislocations in a Regular Crystal Lattice. *Proc.* Royal Acad. Sci. Amsterdam (1939) **42**, pp. 293, 378.

[4] N. F. Mott: Theories of the Mechanical Properties of Metals. *Research* (1949) **2**, p. 162.

[5] G. I. Taylor: The Mechanism of Plastic Deformation of Crystals. *Proc.* Royal Soc. (London) (1934) **145A**, p. 362.

[6] R. Roscoe: The Plastic Deformation of Cadmium Single Crystals. *Philosophical Magazine* (1936) **21**, Series 7, p. 399.

[7] P. A. Rehbinder, V. I. Lichtman, and V. M. Maslennikov: Deformation of Single Crystals of Metals as Facilitated by Adsorption of Surface Active Substances. *Akademiia Nauk Comptes Rendus N.S.* (1941) **32**, p. 125.

[8] A. H. Cottrell and D. F. Gibbons: Thermal Hardening of Cadmium Crystals. *Nature* (1948) **162**, p. 488.

[9] S. Harper and A. H. Cottrell: Surface Effects and the Plasticity of Zinc Single Crystals. *Proc.* Physical Soc. (May 1950) **63B**.

[10] E. N. da C. Andrade and R. F. Y. Randall: Surface Effects with Single Crystal Wires of Cadmium. *Nature* (1948) **162**, p. 890.

[11] E. N. da C. Andrade: Effect of Alpha Ray Bombardment on Glide in Metal Single Crystals. *Nature* (1945) **156**, p. 113.

[12] W. Boas: Discussion of a paper by N. F. Mott, Mechanical Properties of Metals. *Physica* (April 1949) p. 131.

[13] E. N. da C. Andrade: Surface Effect and Structure of Single Crystal Wires. *Nature* (September 1949).

[14] Milton R. Pickus and Earl R. Parker: Creep as a Surface Dependent Phenomenon.Symposium on Corrosion and Erosion of Materials at Elevated Temperatures. A.S.T.M. Special Tech. Pub. No. 108, p. 26 (February 1951).

[15] F. C. Frank and W. T. Read, Jr.: Multiplication Processes for Slow Moving Dislocations. *Physical Review* (August 1950) **79**, No. 4, p. 722.

Equilibrium Relations in Magnesium-Aluminum-Manganese Alloys

by Benny J. Nelson

As a part of the fundamental research program of Aluminum Research Laboratories, some data were obtained on the ternary system Mg-Al-Mn. As very little information on the magnesium corner of this diagram has heretofore been published, it seems desirable to make available the values found for the liquidus and solidus surfaces of this system.

Procedure

The settling procedure was used for the determination of the liquidus compositions. Metallographic examination of quenched samples, and stress-rupture upon incipient melting, were used for the solidus determinations.

The settling procedure has been described in a previous paper.[1] Briefly, this method involved saturating the alloy with manganese at a temperature substantially above that at which the solubility was to be determined, then cooling the melt to the latter temperature, and holding it at that temperature for a substantial period of time. Samples for analysis were carefully ladled from the upper portion of the melt at hourly intervals during the holding period. After the ladling of each sample, the melt was stirred to redistribute some of the manganese that had already settled, because it appeared that when the latter particles of manganese again settled, they aided in carrying down more of the manganese and thus hastened the attainment of equilibrium.

The melts were prepared and held in a No. 8 Tercod crucible holding approximately 4 lb of metal. The manganese was added either in the form of a prealloyed ingot (Dow M) containing about 1.5 pct Mn or by the use of a flux (Dow 250) containing manganese chloride. In calculating the flux additions, it was assumed that the manganese introduced would be equal to 22 pct of the total weight of the flux. Temperatures were measured with an iron-constantan thermocouple enclosed in a seamless steel tube, the lower end of which was welded shut. This protection tube also served as a stirring rod. The samples ladled from the upper portions of the melts at the various intervals were analyzed for aluminum, manganese, and iron.

When making the alloys which were to be used for the determination of the solidus, 2½ in. diam tilt mold ingots were cast, scalped to 2.0 in. in diam, and extruded into ⅛ in. diam wire. The principal impurities in the melts for this investigation were iron and silicon; their total not exceeding 0.03 pct.

Portions of the wire, approximately 2 in. in length, were enclosed in stainless steel capsules for protection from the atmosphere. Bundles of these capsules, with a dummy capsule containing an iron-constantan thermocouple, were heated inside a large steel block (acting as a heat reservoir) in a closed circulating-air type electric furnace. At appropriate times, the capsules were removed and quenched in water. The wires were examined metallographically to determine the temperature of initial melting.

Short times at temperature were used at the beginning for wire specimens of all alloys to obtain quickly the approximate temperatures at which melting could be first observed. When approximate solidus temperatures had thus been determined, equilibrium heating was attempted. This equilibrium heating consisted of an 8 or 16 hr period at a temperature, about 50°F below the lowest temperature at which melting occurred when short heating cycles were used, followed by further heating for 1 hr periods at consecutive 10° higher temperatures.

The theory for the method of stress-rupture at incipient melting has been well covered[2] and its limitations are recognized. Thus, if the interfacial tensions are such that the first minute quantity of liquid is "bunched up" at the grain boundary junctions instead of spreading out along the grain boundaries,[3] temperatures higher than the solidus are required before melting will be manifested by rupture of the specimen. This point will be elaborated later.

Specimens of the wires with a reduced section (approximately 1/16 in. diam) were suspended vertically in a tubular furnace. The setup used is shown in Fig. 1. The clamp holding the specimen was made from alumel thermocouple wire and the thermocouple was thus completed across the specimen by attaching a chromel wire to its lower end. Temperatures were read from a Speedomax recorder used in conjunction with a calibrated thermocouple. The small weight attached to the specimen and a vibrator attached to the furnace tube, to aid in distributing the molten constituent along the grain boundaries, were used to bring about rupture at a temperature closely approximating the solidus. The specimens were heated at a rate of about 5°C per min. The rupture of the specimens was indicated both by sound and by the action of the recorder. An argon atmosphere containing a small amount of SO_2 was used for protection of the specimen. The assembly was taken out of the furnace immediately following rupture and the specimen removed. Some of the broken specimens were examined metallographically and will be referred to later.

Results and Discussion

Fig. 2 shows a set of typical time-composition curves for liquid samples of the Mg-Al-Mn alloys used for the settling tests. The data as presented

Table I. Limiting Values for Liquid Solubility of Manganese in Mg-Al-Mn Alloys

Settling Temperature, °F	Nominal 0.8% Al		Nominal 1.6% Al		Nominal 4.3% Al		Nominal 7.5% Al	
	Al Pct	Mn Pct	Al Pct	Mn Pct	Al Pct	Mn Pct	Al Pct	Mn Pct
1500	0.57	2.66	1.63	2.05	4.62	1.70	7.56	1.43
1475	0.65	2.28	1.66	1.95	4.43	1.55	7.45	1.31
1450	0.55	1.94	1.91	1.76	4.31	1.40	7.13	1.10
1400	0.86	1.75	1.53	1.54	4.17	1.18	7.31	0.98
1350	0.52	1.46	1.31	1.31	4.35	0.83	7.06	0.80
1300	0.50	1.30	1.45	1.02	4.27	0.73	6.82	0.63
1250	0.58	0.90	1.55	0.76	4.05	0.56	7.02	0.40
1200			1.58	0.50			6.99	0.32

B. J. NELSON, Junior Member AIME, is Research Metallurgist, Physical Metallurgy Division, Aluminum Research Laboratories, Aluminum Company of America, New Kensington, Pa.

Discussion on this paper, TP 3133E, may be sent, 2 copies, to AIME by Dec. 1, 1951. Manuscript, April 11, 1951. Detroit Meeting, October 1951.

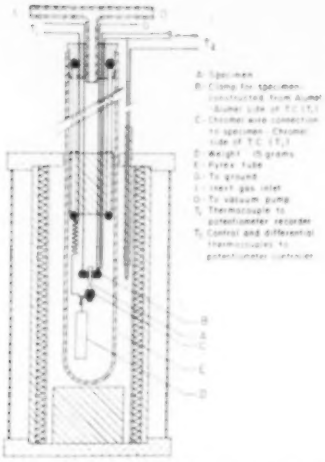

Fig. 1 (left)—Apparatus for determining solidus temperatures in magnesium alloys by the stress-rupture method.

Fig. 2 (right)—Liquid solubility of manganese in Mg-4.5 pct Al alloy as determined by settling tests.

Fig. 3 (lower left)—Liquid solubility of manganese in Mg-Al alloys as determined by limiting values on settling test curves.

Fig. 4 (lower right)—Liquid solubility of manganese in Mg-Al-Mn alloys plotted as the logarithm of atomic percentage of manganese vs. the reciprocal of absolute temperature.

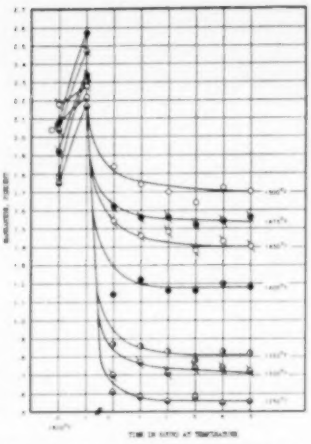

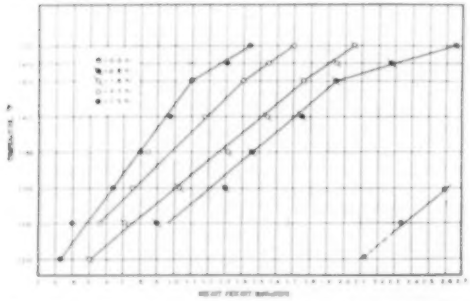

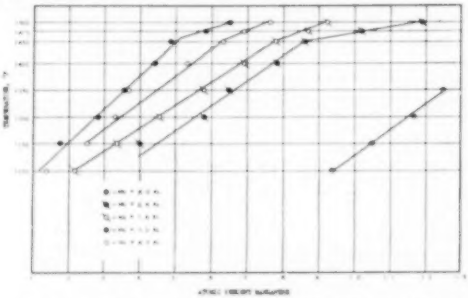

show that, in general, supersaturation is established before the settling period begins. The manganese concentration usually rises during the period in which the melt is held at 1600°F and after the temperature is lowered, falls rather quickly to a limiting value, which is taken as the solubility of manganese in the alloy at the lower temperature. In all cases, solubility curves were determined on the basis of the average manganese contents during the last few hours of settling. It should further be brought out that the aluminum content as given for the curves is the nominal composition; the actual content for each sample varied somewhat from this nominal. Table I gives the "limiting" values at each temperature for both aluminum and manganese for the different nominal aluminum content series.

Fig. 3 shows the liquidus curves in weight percentage of manganese for these alloys vs. degrees F, while Fig. 4 shows the solubility of manganese in atomic percentage vs. the reciprocal of the absolute temperature (corresponding degrees F being indicated). The values for zero pct Al are taken from the results of Tiner.[4] The liquidus curves take a decided change in slope in the neighborhood of 1450°F, possibly indicating a peritectic reaction.

As would be expected, the addition of aluminum to the Mg-Mn alloys lowers the solubility of man-

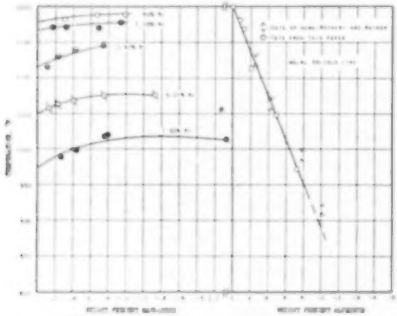

Fig. 5—Solidus temperatures in magnesium base Mg-Al-Mn alloys and the Mg-Al solidus line.

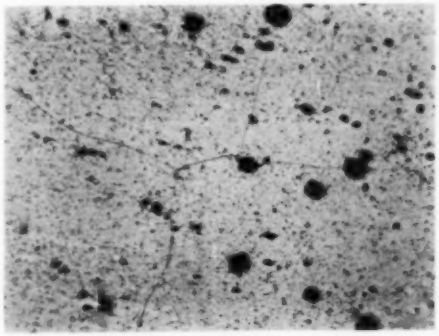

Fig. 6—Microstructure of Mg-7.25 Al-2.11 Mn alloy fractured at 1013°F. Notice narrowness of grain boundaries and the absence of bunching up at the grain junctions. Etched with Keller's etch. X500.

Table II. Solidus Temperatures in Mg-Al-Mn Alloys

S-No.	Al %	Mn %	Fe %	Si %	Temperature Determined by Metallographic Examination of Quenched Wires: Non-Equilibrium	Temperature Determined by Metallographic Examination of Quenched Wires: Equilibrium	Temperature Determined by Stress-Rupture Upon Incipient Melting: No. of Tests	Temperature Determined by Stress-Rupture Upon Incipient Melting: Average Temperature, °F	Temperature Determined by Stress-Rupture Upon Incipient Melting: Standard Deviation, °F
117654	0.81	0.31	0.028	<0.01	*	*	3	1182	1.0
117656	0.81	0.79	0.020	<0.01	—	1180	*	*	*
117657	0.80	0.99	0.018	<0.01	1180	**	3	1188	0
117659	0.79	0.67	0.001	*	—	1180	4	1188	1.8
117648	1.32	0.17	0.027	<0.01	—	1190	3	1171	1.8
117649	1.32	0.32	0.024	<0.01	1180	—	3	1171	4.8
117652	1.30	0.94	0.011	<0.01	—	1180	3	1177	2.9
117658	1.47	0.69	0.001	*	—	1170	3	1170	1.0
94369-1	2.42	0.11	0.021	—	1106	1120	3	1117	1.0
94369-2	2.50	0.24	0.028	—	1120	1130	3	1130	2.5
94369-3	2.53	0.43	0.027	—	1130	1140	3	1139	5.2
94369-4	2.44	0.75	0.009	—	1120	—	3	1146	2.3
94370-1	5.09	0.15	0.029	—	1050	1050	7	1058	5.1
94370-2	5.07	0.23	0.022	—	1060	1070	6	1063	9.1
94370-3	5.07	0.41	0.027	—	1060	1060	7	1067	7.1
94370-4	5.09	1.33	0.025	—	1070	1080	3	1076	2.3
94370-5	4.75	0.75	0.001	—	1070	1080	3	1076	1.4
94371-1	7.85	0.26	0.029	—	980	980	4	988	3.8
94371-2	7.81	0.44	0.020	—	980	990	4	997	3.8
94371-3	7.49	0.66	0.008	—	1000	1000	*	*	*
94371-4	7.25	2.11	0.010	—	1010	1020	11	1013	13.4
94371-5	7.28	0.76	0.001	—	1020	1020	8	1017	11.4
94371-6	7.34	0.80	0.001	—	1020	1030	10	1020	5.0

* Not determined.
** Equilibrium conditions not attained.

ganese in the ternary alloy. The striking influence of small amounts of aluminum in decreasing the liquid solubility of manganese in these alloys is readily apparent.

It should be emphasized that the numerical value of atomic percentage of manganese for each point on all of these curves was calculated separately. This was necessary because in all cases there was some change in the aluminum content as the limiting solubility of manganese was reached; the best average for the limiting values of both aluminum and manganese was used as is shown in Table I.

Solidus Temperatures in Mg-Al-Mn Alloys

As stated earlier, both metallographic examination and the stress-rupture method were used to determine the solidus temperatures of the Mg-Al-Mn alloy wires.

Table II gives the solidus temperatures of the wires as determined by these two methods. Considering the limitations of each method, the agreement between the results is fairly good, particularly for the alloys of low to medium aluminum content.

Fig. 5 shows the effect of manganese on the solidus temperature as determined by the stress-rupture method; the aluminum values listed for the curves are averages. It is seen that the manganese significantly raises the solidus temperature of Mg-Al alloys. This figure also shows the Mg-Al solidus line when these curves are extrapolated to zero pct Mn, together with the Mg-Al solidus data of Hume-Rothery and Raynor.[5] The agreement between the present data and that of ref. 5 for the solidus is fair.

It was mentioned earlier that the distribution of the liquid phase would have an influence upon the temperature of fracture. The microstructure of one of the specimens from the stress-rupture test is shown in Fig. 6. No tendency for the melted constituent to "bunch up" at the grain boundaries is noted; the film of liquid along the grain boundaries is so thin it is difficult to show in the micrograph.

Conclusions

Liquidus and solidus determinations have been made in the ternary system Mg-Al-Mn and these are shown by a series of curves. The following conclusions can be drawn:

1—The solubility of manganese in liquid magnesium is greatly depressed by the addition of a small amount of aluminum, and is further depressed by increasing amounts of aluminum in the alloys.

2—There is a discontinuity in the slope of the liquidus surface in the magnesium corner at about 1450 °F.

3—The solidus temperature of alloys in the magnesium corner decreases markedly with increasing aluminum content for alloys having approximately equal manganese contents.

4—The solidus temperature increases substantially with increasing manganese.

Acknowledgment

The author wishes to express his appreciation of the assistance given by his associates in Aluminum Research Laboratories, and especially to L. A. Willey who designed and built the apparatus for the stress-rupture determinations.

References

[1] Nelson and Sager: *Trans.* AIME (1949) **185**, p. 405.
[2] Pellini and Rhines: *Trans.* AIME (1943) **152**, p. 65.
[3] Smith: *Trans.* AIME (1948), **175**, p. 15. Metals Technology.
[4] Tiner: *Trans.* AIME (1945) **161**, p. 351.
[5] Hume-Rothery and Raynor: *Journal* Inst. of Metals (1938) **63**, p. 201.
[6] Hildebrand: *Solubility.* (1924) **37**, p. 186, New York. The Chemical Catalog Co.
[7] Gann: *Trans.* AIME (1929) **83**, p. 309.
[8] Leemann: *Aluminium-Archiv* (1938) (9).
[9] Imaki: *Suiyokwai-Shi* (1938) **9**, p. 665.
[10] Fahrenhorst and Hofman: *Metallwirtschaft* (1940) **19**, p. 891.
[11] Butcher, Raynor, and Hume-Rothery: *Journal* Inst. of Metals (1943) **69**, p. 216.

Crystal Structure of UAl_4

by Bernard S. Borie, Jr.

THE U-Al binary system has been studied by Kaufmann and Gordon.[1] They have shown that three intermetallic compounds occur in the system: UAl_2, UAl_3, and a third compound tentatively identified as UAl_4. UAl_4 is simple cubic, $a_o = 4.26$A. Its unit cell contains one formula weight, and it is isomorphous with $AuCu_3$. UAl_2 is face-centered cubic, $a_o = 7.72$A, with eight formula weights per unit cell. Rundle and Wilson have shown that it is isomorphous with Cu_2Mg.[2] A Debye-Scherrer pattern of the Al-rich compound indicated a more complex structure than either UAl_4 or UAl_3. The following is a report of an investigation of the crystal structure of this compound and a determination of its stoichiometric formula.

A melt of uranium (99.9 pct pure) and aluminum (99.9 pct pure) was prepared which contained about 25 pct U by weight. It was cooled from 950° to 650°C at a rate of 500° per hr and then taken from the furnace and air cooled. An X-ray diffraction pattern of the ingot showed only lines of aluminum and the Al-rich compound. Filings from the ingot were reacted with a solution of sodium hydroxide, producing a fine black powder, the diffraction pattern of which showed no traces of aluminum. A comparison of the Debye-Scherrer pattern of our sample with the data published by Kaufmann and Gordon[1] showed that it is identical with the Al-rich phase which they reported.

Single crystals were obtained by cooling the melt more slowly (about 50°C per hr). After reaction with sodium hydroxide, the crystals appeared as small black needles attached to the ingot surface.

Cell Size, Space Group, and Uranium Positions

A series of Weissenberg photographs for rotation about two of the crystallographic axes, taken with copper radiation filtered through nickel foil, revealed an orthorhombic cell of dimensions:

$$a = 4.41 \pm 0.02\text{A}$$
$$b = 6.27 \pm 0.02\text{A}$$
$$c = 13.71 \pm 0.03\text{A}$$

Reflections of the type hkl were observed only if:

$$h + k + l = 2n,$$

of the type $hk0$ only if:

$$h = 2n \text{ and } k = 2n,$$

of the type $h0l$ only if:

$$h + l = 2n,$$

and of the type $0kl$ only if:

$$k + l = 2n.$$

Hence, the cell is body-centered with an $00l$ glide plane. The evidence for the existence of the glide plane is the observed extinction of 23 possible reflections of the type $hk0$ with at least one index odd.

B. S. BORIE, JR., is with the Metallurgy Division, Oak Ridge National Laboratory, Oak Ridge, Tenn.

Discussion on this paper, TP 3126E, may be sent, 2 copies, to AIME by Dec. 1, 1951. Manuscript, April 20, 1951. Detroit Meeting, October 1951.

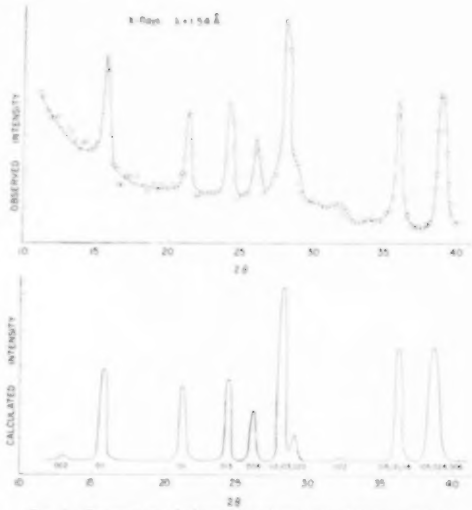

Fig. 1—Comparison of observed and calculated X-ray patterns for UAl_4.

There are only two space groups consistent with these data: $C^{12}_{2v} - I2ma$ and $D^{28}_{2h} - Imma$.[3] The possible sets of atomic positions for these space groups are:

I2ma:

(0 0 0; ½ ½ ½) +

4: (a) $x\ 0\ \frac{1}{2};\ \bar{x}\ \frac{1}{2}\ \frac{1}{2}$

(b) $x\ \frac{1}{4}\ z;\ \bar{x}\ \frac{3}{4}\ \bar{z}$

8: (c) $x\ y\ z;\ \bar{x}\ \bar{y}\ \bar{z};\ x,\ \frac{1}{2} + y,\ \bar{z};\ \bar{x},\ \frac{1}{2} - y,\ z$

Imma:

(0 0 0; ½ ½ ½) +

4: (a) 0 0 0; 0 ½ 0

(b) 0 0 ½; 0 ½ ½

(c) ¼ ¼ ¼; ¾ ¼ ¼

(d) ¼ ¼ ¾; ¾ ¼ ¾

(e) $0\ \frac{1}{4}\ z;\ 0\ \frac{3}{4}\ \bar{z}$

8: (f) $x\ 0\ 0;\ \bar{x}\ 0\ 0;\ x\ \frac{1}{2}\ 0;\ \bar{x}\ \frac{1}{2}\ 0$

(g) $\frac{1}{4}\ y\ \frac{1}{4};\ \frac{3}{4}\ \bar{y}\ \frac{3}{4};\ \frac{3}{4}\ y\ \frac{1}{4};\ \frac{1}{4}\ \bar{y}\ \frac{3}{4}$

(h) $0\ y\ z;\ 0\ \bar{y}\ \bar{z};\ 0,\ \frac{1}{2} + y,\ \bar{z};\ 0,\ \frac{1}{2} - y,\ z$

(i) $x\ \frac{1}{4}\ z;\ \bar{x}\ \frac{3}{4}\ \bar{z};\ \bar{x}\ \frac{1}{4}\ z;\ x\ \frac{3}{4}\ \bar{z}$

16: (j) $x\ y\ z;\ \bar{x}\ \bar{y}\ z;\ x\ \bar{y}\ z;\ \bar{x}\ y\ z;\ x,\ \frac{1}{2} + y,\ \bar{z};$
$\bar{x},\ \frac{1}{2} - y,\ z;\ x,\ \frac{1}{2} - y,\ z;\ \bar{x},\ \frac{1}{2} + y,\ \bar{z}$

Though density measurements on different samples were found to vary somewhat, they were all within the range 5.7 ± 0.3 g per cu cm. If it is assumed that the unit cell contains four formula weights of UAl_4, it is 6.5 g per cu cm. If there were as many as eight uranium atoms per unit cell, the

density would be in excess of 8.5 g per cu cm. Therefore the cell contains four uranium atoms.

If the uranium atoms occupied four-fold positions (a), (b), (c) or (d) of *Imma* or (a) of *I2ma*, for reflections of the type 00*l* the uraniums would all be in phase and the reflections should all be fairly uniformly strong. However, the reflections of this type not suppressed by the space group were observed to vary from very strong to very weak. Hence the uranium atoms must occupy either positions (e) of *Imma* or (b) of *I2ma*. By a proper choice of the origin for positions (b) of *I2ma*, so the uraniums all lie in planes $x/a = 0$ and $x/a = \frac{1}{2}$, these positions may be made equivalent. It was found that a parameter of $z/c = 0.111$ fits the observed intensities quite well.

Determination of the Stoichiometric Formula

Since the space group requires that the number of aluminum atoms per unit cell be a multiple of four, and since there are four uranium atoms per unit cell, the ideal cell must contain four formula weights and the formula must be of the type UAl_x.

Chemical analyses, as did the density measurements, suggest that the structure occurs over a range of composition. Various samples, which by spectrographic methods were found to contain only traces of impurities and the X-ray patterns of which showed no lines other than those of the compound, were found to have uranium compositions ranging from 64.2 to 66.3 pct by weight. This corresponds to a range in the formula of from $UAl_{3.0}$ to $UAl_{3.3}$. Hence these data yield little information other than that the ideal formula must be either UAl_3 or UAl_4.

However, it may be shown, on the basis of the atomic radii of uranium and aluminum and the symmetry of the possible space groups, that the formula must be UAl_4. On the basis of the atomic diameters of the two elements, the U-Al interatomic distance should not be less than 2.73A, and the Al-Al distance should be about 2.7A.

Positions (a), (c), (d), (f), (g), (i), and (j) of space group *Imma* would all require either a U-Al distance or an Al-Al distance to be less than 2.3A. Hence the aluminums must not occupy these positions. It is found, when the remaining three sets of positions are considered, that to satisfy the atomic radii, not more than 16 aluminum atoms may occupy the unit cell; they must be in a set of four in positions (b), a set of four in (e), and a set of eight in (h).

For space group *I2ma*, to satisfy the atomic radii, the 16 aluminums must be in a set of four in (a), a set of four in (b), and a set of eight in general positions (c).

Determination of the Aluminum Positions

Except for the x parameters, positions (b), (e), and (h) of *Imma* are equivalent to (a), (b), and (c) of *I2ma*. It was found that to satisfy the interatomic distances, the aluminum atoms must lie in planes $x/a = 0$ and $x/a = \frac{1}{2}$, as described by *Imma*, or very nearly so. It was assumed that this is the case.

A set of approximate aluminum positions for space group *Imma*, chosen to be consistent with the observed X-ray intensities and the atomic radii, are:

4 Al in (b)
4 Al in (e), $z/c = -0.111$
8 Al in (h), $y/b = -0.033$, $z/c = 0.314$

A comparison of the observed and calculated X-ray patterns for these positions is shown in Fig. 1. The observed pattern was obtained using a North American Phillips spectrometer. The pattern was calculated using the formula:

$$I \propto \frac{(1 + \cos^2 2\theta)\ pF^2}{\sin^2\theta \cos\theta}$$

The line widths were chosen to correspond to those observed. An effort to refine these parameters by a Fourier synthesis of the electron density projected on the xy plane failed. In spite of the fact that the crystal used was quite small, its absorption coefficient was large enough and its shape sufficiently irregular to make accurate determination of the structure factors impossible.

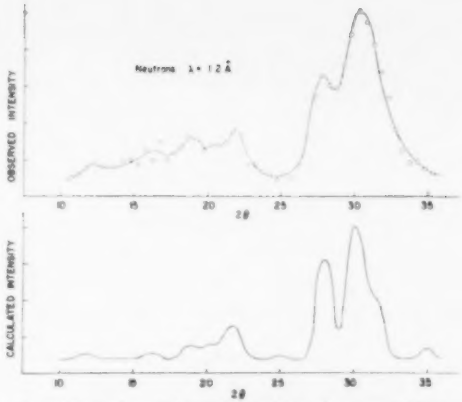

Fig. 2—Comparison of observed and calculated neutron patterns for UAl_4.

Since the scattering factor of uranium is about seven times that of aluminum, the general characteristics of the calculated diffraction pattern are not very sensitive to variations in the aluminum positions. However, for neutrons the scattering factor of uranium is only slightly more than twice that of aluminum. Hence, the neutron diffraction pattern should provide valuable evidence for the light atom positions. A neutron pattern was obtained and is shown in Fig. 2, compared with the calculated pattern for the aluminum positions listed above. The intensity was taken to be proportional to:

$$\frac{1}{\sin\theta \cos\theta}\ pF^2$$

Table I. Interatomic Distances of UAl_4

Atom	No. of Neighbors	Kind of Neighbors	Distance, A
U (4e)	2	Al (4e)	3.14
	4	Al (4b)	3.10
	4	Al (8h)	3.02
	2	Al (8h)	3.30
Al (4e)	2	U (4e)	3.14
	4	Al (4b)	3.10
	4	Al (8h)	2.79
	2	Al (8h)	3.09
Al (4b)	4	U (4e)	3.10
	4	Al (4e)	3.10
	2	Al (4b)	3.14
	2	Al (8h)	2.57
Al (8h)	2	U (4e)	3.02
	1	U (4e)	3.30
	2	Al (4e)	2.79
	1	Al (4e)	3.09
	1	Al (4b)	2.57
	2	Al (8h)	2.81
	1	Al (8h)	3.56
	1	Al (8h)	2.72

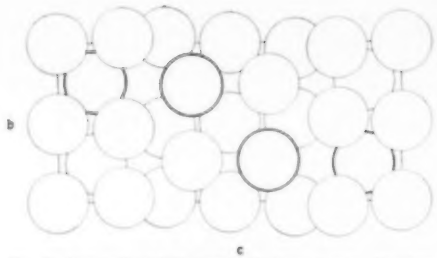

Fig. 3—Unit cell of UAl_4 projected along a axis. Uranium atoms shown in heavy outline.

The line widths were again chosen to correspond to the observed pattern.

Summary and Discussion

The Al-rich, U-Al intermetallic compound has the formula UAl_4. Its unit cell is body-centered orthorhombic, $a = 4.41$A, $b = 6.27$A, and $c = 13.71$A. The cell contains four formula weights and the space group is either *I*2*ma* or *Imma*. The atoms occupy the following positions of *Imma*:

$(0\,0\,0;\ \tfrac{1}{2}\ \tfrac{1}{2}\ \tfrac{1}{2})\ +$

4 U in (e) $0\ \tfrac{1}{4}\ z;\ 0\ \tfrac{3}{4}\ \bar{z};\ z/c = 0.111$

4 Al in (e) $0\ \tfrac{1}{4}\ z;\ 0\ \tfrac{3}{4}\ z;\ z/c = -0.111$

4 Al in (b) $0\ 0\ \tfrac{1}{2};\ 0\ \tfrac{1}{2}\ \tfrac{1}{2}$

8 Al in (h) $0\ y\ z;\ 0\ \bar{y}\ \bar{z};\ 0,\ \tfrac{1}{2} + y,\ \bar{z};\ 0,\ \tfrac{1}{2} - y,\ z$
$y/b = -0.033\ z/c = 0.314$

The number and kinds of nearest neighbors and the interatomic distances for the various atoms in the unit cell are given in Table I. With the exception of the Al-Al distance of 2.57A, the interatomic distances are consistent with the separations predicted by the sum of the atomic radii. Though the distances reported are not highly accurate—since the light atom positions are only approximate—it is possible that this separation may be somewhat less than the atomic diameter of aluminum given by Goldschmidt. Axon and Hume-Rothery have found that the apparent atomic radius of aluminum in its face-centered cubic structure is large.[6] They predict that the corrected atomic diameter of aluminum is probably less than 2.71A.

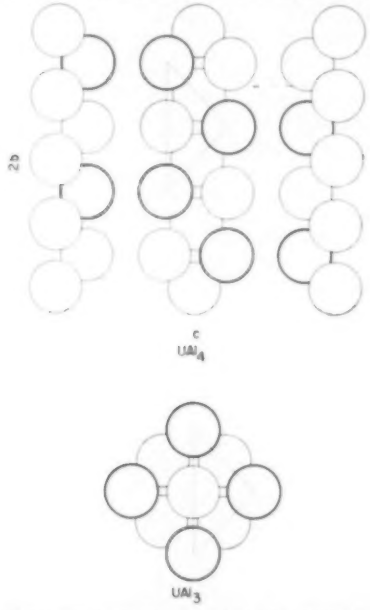

Fig. 4—Comparison of two unit cells of UAl_4 with the eight-fold Al atoms omitted, and a unit cell of UAl_3. Analogous units in the two structures are shown with dotted lines. Uranium atoms are shown in heavy outline.

The distribution of the atoms in the unit cell as viewed along the *a* axis is shown in Fig. 3. The ones shown in heavy outline are uranium. The atoms are arranged in two layers parallel to the *yz* plane at $x/a = 0$ and $x/a = \tfrac{1}{2}$. The coordination numbers are: for uranium, 13; for the aluminum atoms in (b), 12; in (e), 13; and those in (h), 11.

The chemical analyses and density measurements, which are somewhat inconsistent with the ideal structure, may be explained by assuming either that some uranium sites are unoccupied or that some are occupied by aluminum atoms.

There are numerous structures in which such lattice defects exist. CuSn, which has the nickel arsenide structure, is invariably found to have a deficiency of tin of about 4.6 atomic pct. A similar situation exists in the phase CuAl. Lead dioxide is known to retain its structure down to the composition $PbO_{1.46}$. Other compounds having defect structures are $NaWO_3$, γ-Al_2O_3, and FeS, all of which have cation deficiencies. $NaWO_3$ apparently retains its structure with less than one third of the sodium sites occupied.

An interesting similarity between this structure and the simple cubic structure of UAl_3 exists. This is illustrated in Fig. 4 which compares unit cells of the two structures. The eight-fold aluminum atoms in UAl_4 have been omitted.

It is clear from Fig. 4 that the UAl_4 unit cell, except for the eight-fold aluminum atoms, could be constructed from plates of UAl_3. The plates would have for their faces 110 planes of the cubic structure and would be of a thickness equal to the spacing of the 110 planes of UAl_3. The normal to the planes would be parallel to the c axis of UAl_4.

Actually the UAl_4 cell would have to be slightly expanded for this construction to be possible. The U-U separation in UAl_4 is about 3.5 pct greater than it is in UAl_3. However, the cubic symmetry is almost perfectly maintained. For this to be so, the U-U separation in the *bc* plane, *a*, and $b/\sqrt{2}$ would have to be equal. These three distances are respectively, 4.37A, 4.41A, and 4.43A.

Hence the structure may be thought of as UAl_4 plates held together by extra aluminum atoms.

Acknowledgment

The author is indebted to M. A. Bredig under whose direction and guidance this work was done, C. G. Shull who measured the neutron diffraction pattern, and R. O. Williams who prepared the samples used in this work.

References

[1] A. R. Kaufmann and P. Gordon: *Trans.* AIME (1950) **188**, p. 182: JOURNAL OF METALS (January 1950).

[2] R. E. Rundle and A. S. Wilson: *Acta Crystallographica* (1949) **2**, Part 3, p. 148.

[3] *Internationale Tabellen zur Bestimung von Kristallstruksturen.* (Gebruder Borntaeger, Berlin, 1935) **1**, pp. 117, 150.

[6] H. J. Axon and W. Hume-Rothery: *Proc.* Royal Society (1948) **193A**, p. 1.

Solidification of Lead-Tin Alloy Droplets

by J. H. Hollomon and D. Turnbull

THERE is a large body of evidence[1-3] indicating that solidification during the liquid-solid transition is usually induced by heterogeneities present in the liquid. By dispersing liquid metals into small droplets, the impurities responsible for catalyzing solidification are isolated within a small number of these droplets. The effect of the foreign body therefore is restricted to a single drop by this technique. Thus upon cooling below the melting temperature, solidification is initiated by homogeneous nucleation in the majority of the droplets that do not contain impurities.

In the case of solidification of liquid metals, the activation energy for nucleation is so great that its rate changes by orders of magnitude for a change in temperature of only several degrees centigrade.[4] Effectively homogeneous nucleation occurs at a critical temperature upon continuous cooling. Thus by microscopic observation of single particles during cooling, a temperature at which the rate of homogeneous nucleation becomes sensible can be determined.[3] Since at the temperatures at which nucleation occurs in the absence of impurities the rate of crystal growth is extremely rapid, the temperature at which the entire particle solidifies is very nearly the temperature at which the nucleation of the solidification occurs. Thus for liquids that freeze at high temperatures the onset of nucleation can be established by simply observing the temperature at which the marked heat evolution and increase in brightness of the particle occur. For liquids that freeze at lower temperatures the onset of nucleation can be determined by a rumpling and change in shape of the particle resulting from its solidification. The microscopic technique for observing the solidification of small particles has already been described.[3]

In earlier papers the nucleation of solidification of pure metals[5, 6] and of alloy systems[7] showing complete liquid and solid solubility have been described. In the present paper, the observations are extended to a simple eutectic system (Pb-Sn) where the possibility of the formation of two solid phases exists.

Metals for the investigation were obtained from the American Smelting and Refining Co. in the form of pure lead and pure tin, 99.8 and 99.9 pct purity, respectively. An ingot of each of the pure metals was made into shot by heating the metals at a temperature about 50°C in excess of the melting point and pouring the liquid slowly into a container of water at 15°C. Samples of the shotted pure metals were weighed out to make alloys containing 5, 10, 15, 20, 25, 30, 40, 50, 60, 70, 80, and 90 atomic pct Pb. Samples of each alloy were then melted in separate beakers. Each melt was poured through a pyrex funnel into a cylindrical mold ($\frac{5}{8}$ in. ID). The casting solidified in 10 to 20 sec. The inside of the mold as well as the funnel through which the metal was poured were coated with graphite to eliminate adherence of the metal. Analyses were performed on some of the compositions and are given in Table I.

J. H. HOLLOMON, Junior Member, and D. TURNBULL, Associate Member AIME, are associated with the Research Laboratory, General Electric Co., Schenectady.

Discussion on this paper, TP 3104E, may be sent, 2 copies, to AIME by Dec. 1, 1951. Manuscript, Jan. 30, 1951. Detroit Meeting, October 1951.

Table I. Analyses of Poured Metal

Nominal Tin, Pct	Actual Tin, Pct
90	91.4
60	60.6
40	41.7
30	31.0
20	23.0
10	10.2

The compositions also were checked for these samples and for those that were not analyzed by determining the spread between the liquidus and the solidus upon melting the small metal particles. These measurements agreed as well with the nominal compositions as the analyses listed above.

Results

The results of the supercooling experiments for the several alloys are summarized in Table II and plotted on the constitution diagram in Fig. 1. Data for the pure lead and pure tin were taken from earlier investigations.

The values for the maximum supercooling of the several alloys are the average of several determinations on a number of drops of each alloy. The maximum value in any determination was within about 2 pct of the average. For the alloys containing from 20 to 60 atomic pct Sn, inclusive, two marked changes of the surface structure were observed upon cooling. At the higher temperature, after the first appearance of the solid phase it continued to grow slowly at a constant temperature and then stopped. At the lower temperature the alteration of surface structure was abrupt. For the alloys containing from 70 to 95 atomic pct Sn, inclusive, an abrupt change in surface structure was observed at a single critical temperature.

Table II. Results of Supercooling Experiments

Tin, Atomic Pct	Temperature, °C: Liquidus	1st Solidification	2nd Abrupt Solidification
0	327	247[5]	none
10	310	275	none
20	298	256	170
30	281	238	159
40	261	230	158
50	241	205	158
60	218	170	158
70	192	148	none
75	185	135	none
80	183	120	none
85	201	142	none
90	210	150	none
95	221	145	none
100	232	127[6]	none

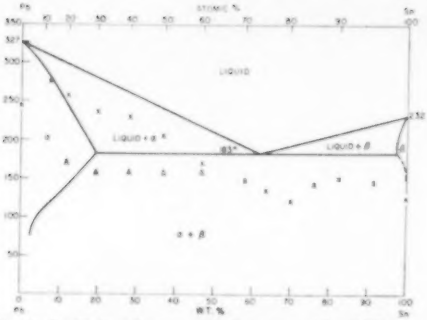

Fig. 1—Equilibrium diagram of Pb-Sn system with solidification temperature of small alloy droplets indicated.

The alloy containing 20 atomic pct Sn completed its solidification at a temperature of about 170°C. However, in all these experiments summarized in Table II and Fig. 1 the cooling time from the maximum temperature (where the drop was liquid) to the temperature of complete solidification was of the order of 10 min. It was believed that the second critical temperature for complete solidification of the 20 and 30 atomic pct alloys resulted from segregation due to lack of equilibration of the composition. Thus a second set of experiments were performed with the 20 pct alloy in which the specimen was held at a temperature of about 220°C for several hours. This treatment resulted in less segregation as determined metallographically than did the more rapid cooling, and the lower critical temperature was not observed. However, it is believed that the two critical temperatures for the 40, 50, and 60 pct alloys would be observed if the equilibration with respect to composition was complete.

A droplet from each of the several compositions was cross-sectioned and examined metallographically after solidification. Typical micrographs are presented in Figs. 2, 3, 4, and 5. Fig. 2 is the microstructure of the alloy containing 70 pct Pb. The alloy of Fig. 3 contains 25 pct Pb and that of Figs. 4 and 5, 15 pct Pb. All the micrographs are at 500 magnification excepting that Fig. 5 was taken at 100X. In Fig. 2 the light constituent is the tin phase trapped by the dendritic arms of the lead. Conversely, in Figs. 4 and 5, small particles of lead have been trapped by the dendritic arms of tin.

Discussion

In the phase diagram in Fig. 6, the liquidus lines have been extrapolated into the metastable region. In an alloy of 50 atomic pct Sn, lead nucleates homogeneously at the temperature marked x; the alloy being significantly supercooled (approximately 40°C). As the small droplet is further cooled the composition of the liquid tends to follow the α-liquidus line and its extension into the region of metastability. At the temperature marked with the triangle that liquid becomes sufficiently supercooled with respect to the β-liquidus that tin nucleates. Thereafter both lead and tin crystals grow. The actual composition of the liquid phase when tin nucleates must fall on the extended α-liquidus and is marked with a circle at the same temperature as that of the triangle. For the alloy containing 10 atomic pct Sn the droplet solidified completely as soon as nucleation of lead took place.

For the 20 and 30 atomic pct Sn alloys the solidification began with the formation of a lead-rich phase at the temperatures marked x and was completed gradually if the temperature was lowered slowly. Consider now an alloy containing 70 atomic pct Sn. Upon supercooling approximately 45°C, the alloy completely solidifies. After the formation of the lead-rich nucleus the composition of the residual liquid is given by the α-liquidus composition at that temperature. At this composition and temperature the solution is already supercooled below the temperature of rapid nucleation of the tin-rich phase in the presence of lead indicated by the circle. Thus a line joining the points marked with x in Fig. 6 represents the temperature at which the lead-rich phase

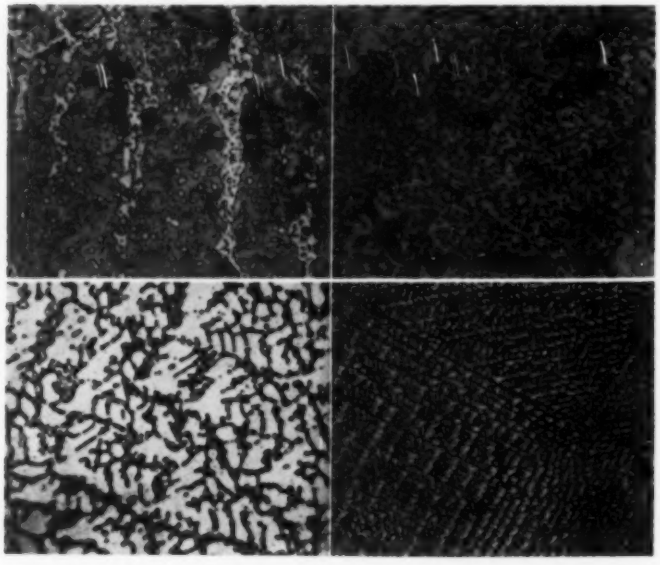

Fig. 2 (upper left)—Microstructure of alloy droplet after solidification, 30 atomic pct Sn. X500.

Fig. 3 (upper right)—Microstructure of alloy droplet after solidification, 75 atomic pct Sn. X500.

Fig. 4 (lower left)—Microstructure of alloy droplet after solidification, 85 atomic pct Sn. X500.

Fig. 5 (lower right)—Microstructure of alloy droplet after solidification, 85 atomic pct Sn. X100.

first nucleates from the liquid solution. The triangles represent the temperature at which the tin-rich phase subsequently nucleates from the supercooled liquid solution. Since the nucleation of the tin-rich phase occurs at a temperature and composition on the extended liquidus line the temperature at which the tin-rich phase first forms is independent of the compositions of the alloy for percentages less than the 70 atomic pct Sn.

Consider now an alloy containing 90 atomic pct Sn. It is noted that complete solidification is accomplished by cooling this alloy to a single temperature even though it is not supercooled below the extended α-liquidus line. The interpretation of this result is that tin nucleates first with a supercooling of approximately 75°C following which the composition of the liquid becomes that given by the extended β-liquidus line. At this composition the temperature is below that necessary to nucleate the lead-rich phase. Thus immediately upon the formation of the first tin-rich nucleus and following its growth, the liquid is supersaturated and supercooled sufficiently for the lead-rich phase to nucleate and grow. Particles of the lead-rich phase will nucleate within the liquid trapped in the interstices of the tin-rich phase as illustrated in Figs. 4 and 5. Thus the curve joining the squares gives the temperature at which the tin-rich phase first nucleates. With an alloy containing approximately 80 atomic pct Sn the temperatures at which the tin and lead-rich phase nucleate are very nearly the same.

The fact that the tin-rich phase that forms following the formation of the lead-rich phase solidifies at a temperature of about 10° above the curve of temperature of first solidification of tin-rich alloys indicates that possibly the lead-rich phase has a mild catalytic effect on the nucleation of the tin-rich phase. The effect is less than 10° and amounts to only a little more than the experimental errors. Also there is some additional error due to the extrapolation of the α-liquidus curve.

In some systems in which two solid phases may form from a single liquid solution one of the phases may catalyze the nucleation of the second phase. Experiments in other systems should be performed to determine the prevalence of such catalytic action.

The degree of supercooling is determined by the differences in free energy between the solid and the liquid and upon the interfacial free energy between that solid and the melt. An interpretation of the slight decrease in the amount of supercooling with a small addition of tin to lead or of lead to tin may be that this addition decreases the interfacial tension between the solid that nucleates and the liquid from which it forms.

In pure metals it is possible to calculate from the theory of homogeneous nucleation and from the maximum supercooling of small droplets the interfacial free energy between the liquid and solid phases. However, in an alloy system, for a liquid of a given composition both the interfacial free energy between this liquid and solid and the free energy difference between this liquid and the solid will be a function of the composition of the solid. Thus even though the free energy as a function of composition is known it is not possible to calculate the interfacial free energy unless the composition of the nucleus is known or the dependence of the interfacial free energy on the composition is known. The functional relationship between the interfacial free energy between liquid and solid and the composition of the solid can in principle be determined experimentally. Theoretical analysis of these experimental results in terms of nucleation theory will not be possible until these measurements have been made.

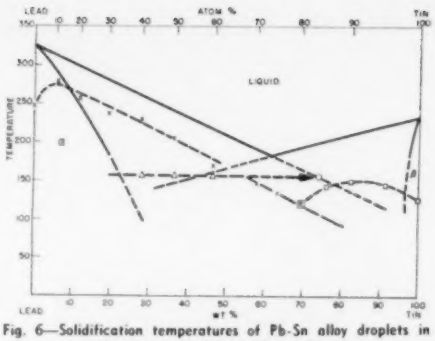

Fig. 6—Solidification temperatures of Pb-Sn alloy droplets in relation to extended equilibrium lines.

Summary

1—The solidification of Pb-Sn alloy droplets (30 to 50 micron diam) was observed as a function of composition by a microscopic technique.

2—On the lead-rich side of the eutectic the initial solidification temperature, T_i, is about 35° to 45°C below the liquidus, T, excepting that for pure lead[2] $T_m - T_i = 80°$.

3—On the tin-rich side of the eutectic $T_m - T_i \sim 60°$ to 75°C excepting that for pure tin[3] $T_m - T_i = 110°$.

4—In the lead-rich alloy a second temperature of abrupt solidification $T_f \sim 160°$ and independent of composition was observed. It is believed that T_f is the initial solidification temperature of the tin-rich solution that remains liquid after the formation and growth of the lead-rich crystalline phase.

5—There is some evidence that the lead-rich crystalline phase has a mild catalytic effect on the formation of nuclei for the growth of the tin-rich solid solution.

Acknowledgment

The authors are pleased to acknowledge the assistance of Mrs. Joyce Rowland and R. E. Cech in carrying out the experiments herein reported.

References

[1] M. Avrami: Kinetics of Phase Change. *Journal of Chemical Physics* (1939) **7**, p. 1103.

[2] D. Turnbull: Kinetics of Heterogeneous Nucleation. *Journal of Chemical Physics* (1950) **18**, p. 198.

[3] J. H. Hollomon: Heterogeneous Nucleation. Thermodynamics in Physical Metallurgy, ASM, Cleveland (1950) pp. 161-177.

[4] D. Turnbull: Isothermal Rate of Solidification of Small Droplets of Mercury and Tin. *Journal of Chemical Physics* (1950) **18**, p. 768.

[5] D. Turnbull: The Supercooling of Aggregates of Small Metal Particles. *Trans.* AIME (1950) **188**, p. 1144; JOURNAL OF METALS (September 1950).

[6] D. Turnbull and R. E. Cech: Microscopic Observation of the Solidification of Small Metal Droplets. *Journal of Applied Physics* (1950) **21**, p. 804.

[7] R. E. Cech and D. Turnbull: Microscopic Observation of the Solidification of Copper-Nickel Alloy Droplets. JOURNAL OF METALS (March 1951) *Trans.* AIME p. 242.

[8] B. Vonnegut: Variation with Temperature of the Nucleation Rate of Supercooled Tin and Water Drops. *Journal of Colloid Science* (1948) **3**, p. 563.

Creep Characteristics of Some Platinum Metals at 1382°F

by R. H. Atkinson and D. E. Furman

HITHERTO the practical creep testing of precious metals has received little or no attention. The only previous creep tests of precious metals have been made with wires under conditions such as to yield much more rapid rates of creep than in engineering tests.[1,2] Up to the present time the value of creep bars of adequate size, in the absence of real need for engineering data, has deterred investigators. However, the increasing use of platinum at high temperatures has demonstrated the need for reliable creep data for the guidance of engineers, especially those engaged in designing certain specialized chemical plant equipment. In order to supply this need, creep tests were conducted at 1382°F (750°C) on 0.290 in. diam specimens of platinum, 90 pct Pt, 10 pct Rh and palladium.

The platinum was high purity, nominally 99.95 pct Pt. The 90 pct Pt, 10 pct Rh was of the same high quality as is used for making gauzes for the catalytic oxidation of ammonia. The palladium was also of high purity; two batches of palladium bars were tested, one deoxidized with calcium boride and the other with aluminum. Spectrographic examination of the palladium confirmed its good quality; the only significant impurities apart from the residual deoxidizers were traces of silicon and lead.

Procedure

The creep bars, which were furnished by Baker and Co. to our specification, were $6\frac{3}{4}$ in. in overall length with a $4\frac{1}{2}$ in. (4 in. gage length) reduced section 0.290 in. in diam and had the ends threaded ($\frac{3}{8}$-NC16). It may be of interest that the bars were valued at up to $600 each. The specimens were supplied in a 50 pct cold-worked-condition to facilitate attachment of the creep extensometer, which was of the push rod type. Because of the softness of the platinum and palladium, the extensometer rings were secured to the test section by means of circular knife edges instead of the usual pointed set screws. The extensometer rods extended through the bottom of the furnace and readings were taken with a 0.0001 in. "Last Word" dial gage fastened to the rods for the duration of the test. The bars were directly loaded by hanging weights from the lower specimen grip. All tests were conducted at 1382°F ± 2°F, and an effort was made to maintain the temperature gradient over the test section within 2°F. The ends of the furnace tube were packed with asbestos wool, which allowed a very slow circulation of air through the tube.

Annealing was accomplished in the creep furnace before the load was applied. The platinum and palladium specimens were annealed at the test temperature for about 17 and 24 hr respectively; in the case of the rhodioplatinum it was found expedient to anneal for 1 hr at 1922°F (1050°C). Pilot samples cut from the same stock as the bars were used to check annealing procedures. Pertinent measurements of grain size and hardness were recorded.

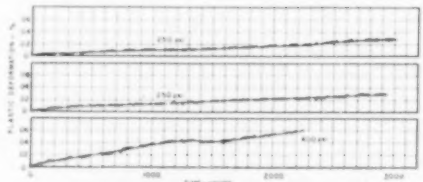

Fig. 1—Platinum creep curves at 1382°F (750°C).

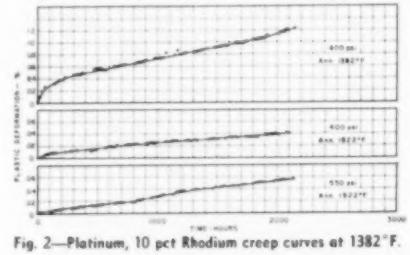

Fig. 2—Platinum, 10 pct Rhodium creep curves at 1382°F.

Results and Discussion

The creep data obtained are given in Table I and the creep curves are plotted in Figs. 1, 2, and 3.

Two platinum specimens, tested under a stress of 250 psi, had almost identical creep rates at 2000 hr, namely 0.000008 and 0.000009 pct per hr. A third platinum specimen, stressed at 400 psi, had a creep rate at 2000 hr of 0.000026 pct per hr; the reason for a rather sharp decrease in creep rate during the period from 1200 to 1600 hr is unknown.

As it was thought that 90 pct Pt, 10 pct Rh would have a lower creep rate than platinum, the first sample was tested at 400 psi; however, the creep rate was approximately 50 pct greater. Microexamination revealed that differences in grain size might be responsible for the unexpected result, as annealing at 1382°F developed an average grain diameter of 0.0021 in. in the rhodioplatinum specimen compared with 0.004 in. in the platinum bar. Annealing the alloy for 1 hr at 1922°F (1050°C) increased the average grain diameter to 0.0032 in. and materially improved the creep resistance, making it much better than platinum. A second specimen annealed at 1922°F (1050°C) and tested under a stress of 550 psi had a creep rate of 0.000022 pct per hr at 2000 hr, which was still substantially lower than that shown by the specimen annealed at 1382°F (750°C) and stressed at only 400 psi.

In contrast to the creep behavior of the platinum and rhodioplatinum specimens, the palladium bars, whether deoxidized with calcium boride or aluminum, were characterized by high first stages of creep. However, after about 1200 hr of test, the creep

[1] S. Dushman, L. W. Dunbar, and H. Huthsteiner: Creep of Metals. *Journal of Applied Physics* (1944) 15, pp. 108-124. Paper includes measurements of rate of creep of Pt wires (0.010 in. diam).

[2] R. P. Carreker, Jr.: Plastic Flow of Platinum Wires. *Journal of Applied Physics* (1950) 21, pp. 1289-1296.

R. H. ATKINSON, Member AIME, and D. E. FURMAN are Research Metallurgists, International Nickel Co., Inc., Bayonne, N. J.

Discussion on this paper, TP 3132E, may be sent, 2 copies, to AIME by Dec. 1, 1951. Manuscript, April 10, 1951. Detroit Meeting, October 1951.

rates decreased rather rapidly to much smaller values. As the changes in creep rate occurred after approximately 1200 hr regardless of whether the specimens were stressed at 250 or 150 psi, it was decided to pretreat another specimen at the test temperature for a similar length of time. This pretreatment of the unstressed creep specimen completely eliminated the high first stage of creep and may have improved the secondary creep rate too. Incidentally the specimen did not change in length during pretreatment. It was thought at first that the good effect of the extended anneal might be associated with further stress relief or an increase in grain size, but measurements of hardness and grain size did not support this view. However, something else had been happening which might affect

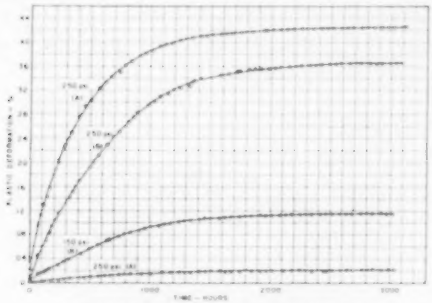

Fig. 3—Palladium creep curves at 1382°F.
A—Bar deoxidized with aluminum.
B—Bar deoxidized with calcium boride.

the creep rate. Microexamination of bars after tests of 3000 hr duration revealed intergranular attack and formation of subscale to a depth of about 0.055 in., Fig. 4, and the rate of penetration indicated that the major part of this internal oxidation probably occurred during the first thousand hours at testing temperature. The improvement effected by the extended anneal might be due to its affording an opportunity for the subsurface reaction to reach equilibrium before the load was applied.

A comparison of the creep strengths of the three materials at 1382°F (750°C) on the basis of the estimated stresses required to give a creep rate of 0.00001 pct per hr at 2000 hr (or 3000 hr in the case of palladium) may be made from the log stress-log creep rate plot of Fig. 5. For platinum and 90 pct Pt, 10 pct Rh stresses of 270 psi and 340 psi, respectively, would give creep rates of 0.00001 pct per hr at 2000 hr. In the case of palladium it is esti-

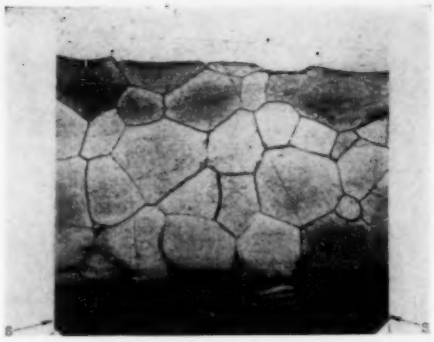

Fig. 4—Palladium creep bar after 3090 hr test. Longitudinal section shows intergranular attack and formation of subscale extending to a considerable distance below the surface (SS). True depth of attack as observed in a cross-section was 0.052 in. Etch: Electro, AC; 5 pct NaCN. X28.

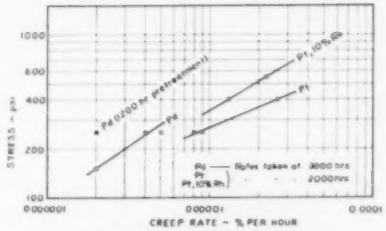

Fig. 5—Creep data at 1382°F.

mated that a stress of 440 psi would give the same creep rate at 3000 hr. The evaluation of the creep strength of palladium is made at 3000 hr because the creep data at 2000 hr are influenced by the high first stage, which it was shown later could be eliminated by suitable pretreatment.

The surprising finding that palladium is apparently more creep resistant than either platinum or 90 pct Pt, 10 pct Rh at the given temperature calls for comment. The larger grain size of the palladium does not seem to account adequately for its superiority. It would almost seem as if internal oxidation had strengthened the palladium instead of weakening it. The question also arises as to whether very pure palladium free from excess deoxidizer would also be more creep resistant than pure platinum. To answer this question it would be necessary to measure the creep rate of specimens prepared from

Table I. Creep Data for Platinum, Platinum 10 Pct Rhodium and Palladium at 1382°F (750°C)

Material	Annealing Temperature, °F	Average Grain Diam., In.	Stress, Psi	Creep Rate—Pct per Hr X10⁵ 1000 Hr	3000 Hr	3090 Hr	Length of Test, Hr	Estimated Stress for Creep Rate of 0.00001 Pct per Hr	Hardness, VHN Before Test	After Test
Platinum	1382	0.0040	250	0.08	0.08	0.04	3817			
Platinum	1382	0.0040	250	0.09	0.09		2929			
Platinum	1382	0.0040	400	0.33	0.26		2256	270		41*
Platinum	1382	0.0021	400	0.40	0.40		2153			
10 pct Rhodium	1922	0.0032	400	0.17	0.13		2107			
	1922	0.0032	550	0.38	0.22		2135	340	74*	76*
Palladium (CaB₆)†	1382	0.015	250	1.43	0.19	0.04	3090			
Palladium (CaB₆)†	1382	0.015	150	0.56	0.08	0.02	3017		43	42
Palladium (Al)†	1382	0.015	250	0.87	0.18	0.05	3118	440		
Palladium (Al)†	1382‡	0.015	250	0.09	0.03	0.02	3032		41*	42

* Pyramidal diamond, 1 kilo load. Other VHN taken with 5 kilo load. † Deoxidizer. ‡ Specimen annealed for 1200 hr before loading.

vacuum cast palladium without the use of deoxidizer.

Summary

The creep rates of pure platinum, 90 pct Pt, 10 pct Rh and pure palladium at 1382°F (750°C) have been determined using bars 0.290 in. in diam and stresses of 150 to 550 psi in tests lasting up to 3000 hr. The creep rate curves of platinum were normal for stresses of 250 and 400 psi. The creep rate of 90 pct Pt, 10 pct Rh, provided it was given a brief high temperature anneal (1 hr at 1922°F) for grain enlargement, was below that of pure platinum. The creep rate of normally annealed palladium under stresses of 150 and 250 psi was very high for the first 1200 hr but fell to a low value thereafter. Heating the palladium at 1382°F (750°C) for 1200 hr virtually eliminated the first stage of creep and also lowered the rate in the second stage.

Acknowledgment

The authors wish to take this opportunity of thanking Baker & Co., of Newark, N. J., for their cooperation both in lending the platinum metals and in preparing the specimens. The authors are grateful to N. B. Pilling, Director of Research, International Nickel Co., for permission to publish these data, to E. M. Wise for suggestions and to W. T. Coughlin and J. W. Whitney for their assistance.

Technical Note

Deformation Texture of Body-Centered Cubic Metal Wires

by W. R. Hibbard, Jr., A. E. Roswell, and A. E. Schuetz

THE drawn wire texture of body-centered cubic iron,[1] tungsten,[2] and molybdenum[3] has been determined to be a [110] direction parallel to the wire axis. The purpose of this study is to extend the available information on body-centered cubic wire textures to other metals and alloys.

Wires were produced using hand wire rolls and dies as given in Table I. In addition, attempts were unsuccessful to draw wires from chromium, vanadium (Vanadium Corp. of America), and tungsten (Cleveland Tungsten Inc.). Although it is known that wires can be made from these materials, suitable techniques were not readily adaptable.

Where necessary, wires were polished and etched to form flat ribbons 0.005 to 0.007 in. thick, and transmission X-ray patterns were taken using molybdenum radiation with the specimen tilted 0 degrees from the perpendicular toward the beam to critically cover the wire axis. Analyses were made of (110), (002), and (112) reflection circles.

Table I. Wires Used in Study

Metal	Source	Reduct. in Diam., Pct	Remarks
β brass (51.92 pct)	American Brass Co.	78.1	Hot worked at 600°C
β brass (62.5 pct)	Scovill Mfg. Co.	71.2	Quenched from 875°C, Cold formed
Iron	Armco	97	Cold formed
Molybdenum	North American Phillips	93	Hot formed starting at 550°C, finished at 110°C
Niobium	Rem-Cru	95	Cold formed
Tantalum	Fansteel	97	Cold formed

In all cases reflection maxima indicated the texture to be a single [110] deformation fiber, as illustrated by Fig. 1 for molybdenum. In the case of the hot-worked β brass, a second texture, [100], was also found, but this is believed to be the result of recrystallization since it has been reported for recrystallized molybdenum wires[4] and it was not present in the cold-drawn β brass. The difference in drawability between the 51.92 pct Cu β brass and the 62.5 pct Cu β brass (containing some grain boundary α due to incomplete quenching) is quite striking, since the latter could be cold worked readily while the former had to be hot worked to avoid cracking.

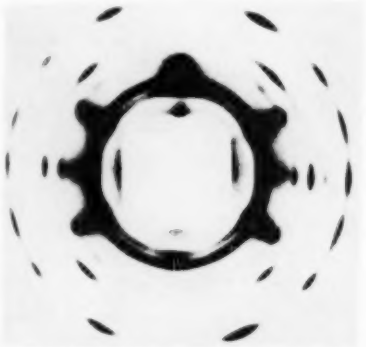

Fig. 1—Molybdenum wire drawn 93 pct reduction in diam. Wire axis vertical tilted 10° from perpendicular toward the beam. (110) ring shows maxima at 0°, 60°, and 90° from wire axis, (002) ring at 45° and 90°, and (112) ring at 30°, 55°, 73° and 90° indicating a single [110] texture.

Summary

The deformation texture of drawn body-centered cubic wires of β brass, iron, molybdenum, niobium, and tantalum is essentially a single [110] fiber as predicted by theory.[5]

Acknowledgment

The authors wish to thank the suppliers of the metals listed in the text, and the Grant-in-Aid from the Research Fund of the Society of the Sigma Xi and Scientific Research Society of America which made possible the purchase of X-ray equipment.

References

[1] C. S. Barrett and L. H. Levenson: *Trans.* AIME (1939) **135**, p. 327.

[2] M. Ettisch, M. Polyani, and K. Weissenberg: *Ztsch. Physik* (1921) **7**, p. 181.

[3] Z. Jeffries: *Trans.* AIME (1924) **70**, p. 303.

[4] T. Fujiwara: *Proc.* World Eng. Cong., Tokyo, 1929, (1931) **36**, pt. 4, p. 171.

[5] W. R. Hibbard, Jr. and M. K. Yen: *Trans.* AIME (1948) **175**, p. 126; METALS TECHNOLOGY (February 1948).

W. R. HIBBARD, JR., Member AIME, formerly Associate Professor, Department of Metallurgy, Yale University, is now with General Electric Co., Schenectady. A. E. ROSWELL and A. E. SCHUETZ are with the Department of Metallurgy, Yale University, New Haven, Conn.

TN 86E. Manuscript, May 21, 1951.

This note is based on research aided by a Grant-in-Aid from the Research Fund of the Society of the Sigma Xi and the Scientific Research Society of America.

AIME OFFICERS:

President—Willis McG. Peirce
Vice-Presidents—A. B. Kinzel, Philip Kraft, R. W. Thomas, J. L. Gillson, M. L. Haider
Vice-President and Treasurer—Andrew Fletcher

AIME STAFF:

Secretary—E. H. Robie
Ass't. Secretaries—E. J. Kennedy, Jr., Ernest Kirkendall, J. V. Beall, J. B. Alford, R. E. O'Brien
Ass't. to Secretary—H. N. Appleton
Ass't. Treasurer—H. A. Maloney

aime NEWS

Institute of Metals Div., AIME, Announces Tentative Program for Fall Meeting at Metal Congress

THE Institute of Metals Div., AIME, has formulated plans for its annual Fall Meeting to be held in conjunction with the World Metal Congress & Exposition. The Metal Congress will be held in Detroit, Oct. 13 to 19. The IMD will be headquartered at the Detroit-Leland Hotel, where all of its meetings will be held. The technical sessions will be held Oct. 15, 16, and 17, but some committee meetings will be held on Sunday, Oct. 14.

SUNDAY, OCTOBER 14

7:00 p.m., Tropical Room

IMD Program Committee Meeting
P. A. Beck, Chairman

7:00 p.m., New York Room

IMD Publications Committee Meeting
M. Gensamer, Chairman

MONDAY, OCTOBER 15

9:00 a.m. to 12:00 m., Jade Room

Grain Growth and Recrystallization
B. L. Averbach, Chairman; J. E. Burke, Secretary

Grain Structure of Aluminum-Killed Low Carbon Steel Sheets: R. L. Solter and C. W. Beattie, Armco Steel Corp. JOURNAL OF METALS, September 1951.

Theory of Grain Boundary Migration Rates: D. Turnbull, General Electric Co. JOURNAL OF METALS, August 1951.

Secondary Recrystallization in Copper Wire: G. Bassi, AB Svenska Metallverken, Sweden. JOURNAL OF METALS, July 1951.

Observations on Cleavage and Polygonization of Molybdenum Single Crystals: N. K. Chen and R. Maddin, Johns Hopkins University. JOURNAL OF METALS, July 1951.

9:00 a.m. to 12:00 m., Colonial Room

Alloy Systems I
M. Hansen, Chairman; R. S. Busk, Secretary

Systems Titanium-Molybdenum and Titanium-Columbium: M. Hansen, H. D. Kessler, D. J. McPherson, Armour Research Foundation, and E. L. Kamen, U. S. Naval Reserve.

Crystal Structure of Ti_2Si_3, Ti_5Ge_3, and Ti_5Sn_3: P. Pietrokowsky and Pol Duwez, California Institute of Technology. JOURNAL OF METALS, September 1951.

Solidification of Lead-Tin Alloy Droplets: J. H. Hollomon and D. Turnbull, General Electric Co. JOURNAL OF METALS, September 1951.

Registration

3:00 to 9:00 pm Sunday; 8:00 am to 9:00 pm Monday; 8:00 am to 5:00 pm Tuesday; 9:00 am to 4:00 pm Wednesday in lobby of Detroit-Leland Hotel.

Registration Fee $2.00 to AIME members; $4.00 to non-members.

Equilibrium Relations in Magnesium-Aluminum-Manganese Alloys: B. J. Nelson, Aluminum Co. of America. JOURNAL OF METALS, September 1951.

Constitution and Precipitation-Hardening Properties of Copper-Rich Copper-Tin-Beryllium Alloys: R. A. Cresswell and J. W. Cuthbertson, Tin Research Institute, England. JOURNAL OF METALS, September 1951.

2:00 to 5:00 p.m., Jade Room

SEMINAR: Dislocations in Metals
(The field will be reviewed, brought up-to-date, and clarified in a comprehensive manner.)

Nature of Dislocations: Frederick Seitz, University of Illinois.

Role of Dislocations in Crystal-Growth and Grain-Boundary Phenomena: W. T. Read, Bell Telephone Laboratories.

7:00 p.m., New York Room

Membership Committee Meeting
W. J. Harris, Jr., Chairman

8:00 to 10:00 p.m., Jade Room

SEMINAR: Dislocations in Metals (Cont'd)

Theory of Dislocations as Applied to Mechanical Behavior: Egon Orowan, Massachusetts Institute of Technology.

Annual Meeting Paper Deadline Sept. 15

Sept. 15, 1951 is the deadline for all IMD papers for the 1952 New York Annual Meeting and for all ISD and EMD papers to be prepublished.

TUESDAY, OCTOBER 16

9:00 a.m. to 12:00 m., Jade Room

Transformations

Rapid Tempering of High Speed Steel: A. E. Powers, General Electric Co., and J. F. Libsch, Lehigh University.

Effect of Rate of Cooling on the Alpha-Beta Transformation in Titanium and Titanium-Molybdenum Alloys: Pol Duwez, California Institute of Technology. JOURNAL OF METALS, September 1951.

Burst Phenomenon in the Martensitic Transformation: E. S. Machlin, Columbia University and Morris Cohen, Massachusetts Institute of Technology. JOURNAL OF METALS, September 1951.

Isothermal Formation of Martensite at Subzero Temperatures in a High Chromium Steel: S. C. Das Gupta, University of Notre Dame and B. S. Lement, Massachusetts Institute of Technology. JOURNAL OF METALS, September 1951.

Isothermal Transformation and Properties of a Commercial Aluminum Bronze: A. H. Kasberg, Jr., Westinghouse Electric Corp., and D. J. Mack, University of Wisconsin.

9:00 a.m. to 12:00 m., Colonial Room

Alloy Systems II

J. T. Norton, Chairman; C. E. Birchenall, Secretary

Crystal Structure of UAl_2: B. S. Borie, Jr., Oak Ridge National Laboratory. JOURNAL OF METALS, September 1951.

Intermediate Phases in Ternary Alloy Systems of Transition Elements: P. A. Beck, University of Notre Dame; Sheldon Rideout, Argonne National Laboratory; W. D. Manly, Oak Ridge National Laboratory; E. L. Kamen, U. S. Naval Research; and B. S. Lement, Massachusetts Institute of Technology.

Intermetallic Compounds in the System Molybdenum-Beryllium: S. G. Gordon, Los Alamos Scientific Laboratory; J. A. McGurty and W. K. Koshuba, NEPA Project; and G. E. Klein, Oak Ridge National Laboratory. JOURNAL OF METALS, August, 1951.

Chromium-Nickel Phase Diagram: S. Bloom and N. J. Grant, Massachusetts Institute of Technology.

Thermal Variation of Young's Modulus in Some Fe-Ni-Mo Alloys: M. E. Fine and W. C. Ellis, Bell Telephone Laboratories. JOURNAL OF METALS, September 1951.

Effects of Tungsten or Molybdenum Upon the Alpha-Beta Transformation and Gamma Precipitation in Cobalt-Chromium Alloys: A. R. Elsea and E. E. Fletcher, Battelle Memorial Institute.

12:15 p.m., New York Room

Executive Committee, IMD, Luncheon Meeting

R. M. Brick, Chairman

2:00 to 5:00 p.m., Jade Room

Light Metals

Jay Robert Burns, Secretary

Effects of Precompression on the Behavior of the Aluminum Alloy 24ST, During Cyclic Direct Stressing: S. I. Liu, Pei-Yang University, China. JOURNAL OF METALS, June 1951.

Structural Studies of Plastic Deformation in Aluminum Single Crystals: N. K. Chen, Johns Hopkins University and C. H. Mathewson, Yale University. JOURNAL OF METALS, August 1951.

Effect of Alloying Elements on the Elevated Temperature Plastic Properties of Alpha Solid Solutions of Aluminum: O. D. Sherby, R. A. Anderson, and J. E. Dorn, University of California. JOURNAL OF METALS, August 1951.

Effect of Alloying Elements on the Electrical Resistivity of Aluminum Alloys: A. T. Robinson and J. E. Dorn, University of California. JOURNAL OF METALS, June 1951.

Effect of Rare-Earth Metals on the Properties of Extruded Magnesium: T. E. Leontis, Dow Chemical Co.

2:00 to 5:00 p.m., Colonial Room

Creep

Jerome J. Kanter, Secretary

Fundamental Effects of Cold Working on the Creep Resistance of an Austenitic Alloy: D. N. Frey and J. W. Freeman, University of Michigan. JOURNAL OF METALS, September 1951.

Creep Characteristics of Some Platinum Metals at 1382°F: Ralph H. Atkinson and D. E. Furman, International Nickel Co. JOURNAL OF METALS, September 1951.

Creep Behavior of Zinc Modified by Copper in the Surface Layer: M. R. Pickus and Earl R. Parker, University of California. JOURNAL OF METALS, September 1951.

Creep and Stress Rupture Behavior of Aluminum as a Function of Purity: Italo S. Servi and N. J. Grant, Massachusetts Institute of Technology.

Structure Observations of Aluminum Deformed in Creep at Elevated Temperatures: Italo S. Servi and N. J. Grant, Massachusetts Institute of Technology.

6:00 p.m., Colonial Room and Cocktail Lounge

Cocktail Party for Dinner Guests

Compliments of Detroit members of AIME and their friends

7:00 p.m., Jade Room

Institute of Metals Div. Annual Fall Dinner

Toastmaster: R. M. Brick, Chairman, Institute of Metals Div.

Welcome: F. P. Bens, Chairman, Detroit Section, AIME

Speaker and Subject to be announced

WEDNESDAY, OCTOBER 17

12:15 p.m., New York Room

Powder Metallurgy Committee Luncheon Meeting

J. J. Cordiano, Chairman

2:00 to 5:00 p.m., Colonial Room

High Temperature Oxidation

B. Lustman, Chairman; L. A. Carapella, Secretary

Oxidation of Titanium: M. H. Davies and C. E. Birchenall, Carnegie Institute of Technology.

Thermal Stability of the Chromium, Iron and Tungsten Borides in Steaming Ammonia and the Existence of a New Tungsten Nitride: Roland Kiessling and Y. H. Liu, University of Uppsala, Sweden. JOURNAL OF METALS, August 1951.

High Temperature Oxidation of Copper-Palladium and Copper-Platinum Alloys: D. E. Thomas, Westinghouse Electric Corp.

Mechanism and Kinetics of the Scaling of Iron: M. H. Davies, M. T. Simnad, C. E. Birchenall, Carnegie Institute of Technology.

2:30 to 5:00 p.m., Jade Room

Powder Metallurgy

Role of Gases in the Production of High Density Powder Compacts: Donald Warren and J. F. Libsch, Lehigh University. JOURNAL OF METALS, September 1951.

Solubility Relationships in Some of the Ternary Systems of Refractory Monocarbides: J. T. Norton, Massachusetts Institute of Technology and A. L. Mowry, Kaiser Aluminum and Chemical Corp.

Sintered Titanium Carbide: Frank W. Glaser and W. Ivanick, American Electro-Metal Corp.

Personals

T. W. MERRILL

G. V. LUERSSEN

G. A. PETERSON

T. W. Merrill has been appointed chief metallurgical engineer for the Vanadium Corp. of America and has been transferred from the plant at Bridgeville, Pa. to the executive office in New York City. He had been metallurgical engineer since 1949.

George V. Luerssen, formerly chief metallurgist, was appointed vice-president in charge of metallurgy for the Carpenter Steel Co., Reading, Pa. He has been with the firm since 1907. **Carl B. Post** succeeds Mr. Luerssen as chief metallurgist.

G. A. Peterson has been elected president, Ferro Engineering Co., Cleveland. Mr. Peterson joined the firm as a chief engineer and in 1942 was elected a vice-president. He succeeds the late **Walter M. Charman.**

Walter Burton Johnson has joined the Kaiser Aluminum & Chemical Corp., Oakland, Calif. as a junior engineer. He was previously a metallurgist with the U. S. Bureau of Mines, Reno.

Michael C. Kopchak is now metallurgical inspector for the Inland Steel Co., East Chicago, Ind. He had been employed by Carnegie-Illinois Steel Co., Chicago.

A. Kenneth Schellinger has joined the U. S. Dept. of Interior, Bureau of Mines, College Park, Md.

Simon D. Strauss, vice-president in charge of sales for American Smelting & Refining Co., has been elected to the board of directors, Revere Copper & Brass, New York.

Carl Wagner, visiting professor of metallurgy, Massachusetts Institute of Technology, has been awarded the first Palladium Medal Award by the Electrochemical Society, Inc.

Henry D. Phillips was elected president of Hartford Electric Steel Corp., Hartford, Conn. He formerly had been executive vice-president of the company.

William C. Hagel has been appointed junior metallurgist to the staff of the metallurgical div., Oak Ridge National Laboratory, Oak Ridge.

Truman S. Fuller, engineer in charge of works laboratory, General Electric Co., was elected president of the ASTM. **Hyman Bornstein,** chief technical consultant, Deere & Co., Moline, Ill.; **H. H. Lester,** principal physicist, Watertown Arsenal, Watertown, Mass.; and **Stanton Walker,** director of engineering and research, National Sand & Gravel Assn. and National Ready Mixed Concrete Assn., Washington, D. C., have been awarded 1951 ASTM Awards of Merit.

Edson R. Packer is now mill superintendent for the Northern Peru Mining & Smelting Co., Lima.

D. G. Fraser, metallurgist, has joined the Canadian Westinghouse Co., Ltd., appliance engineering, Hamilton, Ont.

J. E. Andersen is now employed by the Sherritt Gordon Mines, Ltd., at the metallurgical research div., Ottawa, Ont.

S. H. Perry has retired as vice-president of Chase Brass & Copper Co.

Frederick Jackson is now a metallurgist at the Newark works of Kaiser Aluminum & Chemical Corp., Newark, Ohio. He had been mill metallurgist with the Riverside Metal Co., Riverside, N. J.

Walter E. Streeter, who has been president and general manager of the Paragon Aluminum Corp., Munroe, Mich., since its founding has resigned.

Robert L. Hallett is no longer associated with Arnold H. Miller. He has opened his own consulting office in New York City.

E. F. Chojnowski has accepted a position with International Harvester, Chicago, as a technician in the manufacturing research div.

I. R. Kramer has left the Office of Naval Research as head of the metallurgy branch to accept a position as assistant to the president of the Horizons Titanium Corp.

J. E. Archer has been appointed assistant director of the patent dept., American Cyanamid Co.

W. H. Maxwell was recently appointed assistant to the vice-president, Calumet & Hecla Consolidated Copper Co.

E. A. Murray was made manager, compressor div., Worthington Pump & Machinery Corp.

Obituaries

Cecil Eugene Bales (Member 1936), president of Ironton Fire Brick Co., Ironton, Ohio, died on May 26, 1951. Mr. Bales was born at Livingston, Ky. on Oct. 23, 1897. He attended both the University of Chicago and University of Kentucky. In 1920 he joined the Louisville Fire Brick Works, Louisville, as chief chemist. He was promoted to the position of assistant manager in 1926. During this time he was field assistant for the Kentucky Geological Survey on a part-time basis. He resigned from the Louisville firm and became production manager for the Ironton Fire Brick Co. In 1929 he was elected vice-president and later president. Mr. Bales was an active member of various technical societies.

Walter M. Charman (Member 1936), president and founder of the Ferro Engineering Co., Cleveland died on June 15, 1951. Born in Terre Haute, Ind. on Sept. 30, 1894, Mr. Charman received his college education at Rose Polytechnic Institute. He graduated in 1918 with the degree of B.S. in mechanical engineering. He began his business career as an assistant engineer with the Youngstown Sheet & Tube Co., Youngstown. During his years with this firm he became superintendent of the open hearth dept. He perfected his method of hot topping dioxidized steel ingots and in 1929 organized the Ferro Engineering Co. for the production of the C & D hot tops. Several years later the hot tops became recognized as a necessity in the production of quality steels and companies in Europe were licensed to manufacture them.

Herbert B. Cox (Member 1904) died on Feb. 11 at the age of 91. Mr. Cox was born at Pittston, Maine on August 10, 1860. He received his engineering education at the Institute of Technology, Boston and Spring Garden Institute, Philadelphia. He joined the Charles River Iron Works, Cambridge, Mass. as a machinist apprentice and then became superintendent of the gas engine dept., Dickoon Mfg. Co., Scranton, Pa. Later he was made manager of the Scranton Passenger Railway Co. Mr. Cox joined the Lackawanna Iron & Steel Co., Scranton as master mechanic and assistant superintendent of blast furnaces. In 1904 he was appointed superintendent of the Cornwall and Lebanon furnaces with the same firm. He joined the Ringwood Co., New York in 1918 and later became associated with the Hewitt Realty Co. In 1921 he was appointed superintendent and metallurgical engineer for the same company. He moved to Winchester, Mass. and at the time of his death was residing there.

William R. Maurer (Member 1947) died on Mar. 1 after a few days' illness. Born in Portsmouth, England on Aug. 9, 1906, he received the degree of B.Sc. in engineering from Cardiff University. He also attended the Technical School of Portsmouth and Winchester. Mr. Maurer was field engineer for Pirelli General, Southampton from 1929 to 1931. For four years he was employed by Edelenru Borsig, Magdeburg, Germany as erection engineer. He returned to England in 1937 to accept a position as research engineer for the National Oil Refineries. In 1940 he became superintendent for E. Curran Nonferrous Melting & Rolling. Mr. Maurer went to India in 1943 as works manager, production, in the Indian Ordnance Service. In 1946 he was made superintending engineer for Birla Bros., India. He remained in India for several years, returning to England in 1949. In 1950 he joined the English Steel Corp., Ltd., Vickers Works, Sheffield as technical representative.

NECROLOGY

Date Elected	Name	Date of Death
1943	Henry B. Harriman	June 13, 1950
1912	S. B. Patterson, Jr.	Unknown
1916	W. H. Whittier	June 6, 1951

Proposed for Membership

Metals Branch AIME

Total AIME membership on July 31, 1951, was 16,969; in addition 2502 Student Associates were enrolled.

ADMISSIONS COMMITTEE

Thomas G. Moore, Chairman; Carroll A. Garner, Vice-Chairman; George B. Corless, F. W. Hanson, Albert J. Phillips, Lloyd C. Gibson, R. D. Mollison, John T. Sherman. Alternates: A. C. Brinker, H. W. Hitzrot, Plato Malozemoff, Ivan Given, T. D. Jones, and W. A. Clark, Jr.

Institute members are urged to review this list as soon as the issue is received and immediately to wire the Secretary's office, night message collect, if objection is offered to the admission of any applicant. Details of the objection should follow by mail. The Institute desires to extend its privileges to every person to whom it can be of service but does not desire to admit persons unless they are qualified. Objections must be received before the 30th of the month on Metals and Mining Branches.

In the following list C/S means change of status; R, reinstatement; M, Member; J, Junior Member; A, Associate Member; S, Student Associate.

Arizona
Hayden—Sewell, George P., Jr. (M) (R, C/S—J-M)
Tucson—Heinrichs, Walter E., Jr. (M)
Warren—Meyer, Robert C. (J) (R, C/S—S-J)

Colorado
Grand Junction—Brenton, James F. (M), Toole, Robert H. (M)

Illinois
Chicago—Yamamoto, Albert S. (J) (R, C/S—S-J)
Park Forest—Burgess, Price B. (J)

Indiana
East Chicago—Hoener, Lavern G. (J)
Hammond—Linn, Thomas B. (M) (R, C/S—J-M)

Massachusetts
Cambridge—Gokcen, Nevzat A. (M)

Michigan
Berkley—Clark, Ralph A. (M)

New Mexico
Hurley—Wilkinson, T. D., III (J) (R, C/S—S-J)
Vanadium—Singleton, Robert C. (M)

New York
Ballston Lake—McKechnie, Robert K. (M) (C/S—J-M)
Bronx—Blum, Arnold (J) (R, C/S—S-J), Gross, Jason (J) (R C/S—S-J)
Flushing—de Andrade, Benedito M. (M)
Niagara—McKinsey, Charles R. (J)

Ohio
Portsmouth—Lewry, Richard W. (M)
Steubenville—Cauger, Edward H. (M)

Pennsylvania
Arnold—Zorena, Peter J. (J) (C/S—S-J)
Corry—Rainesalo, Charles R. (J) (C/S—S-J)
Pittsburgh—Glass, Robert J., Jr. (M), Nelson, Harry S. (J)

Washington
Tacoma—Somerville, Gordon R. (J)

Brazil
Belo Horizonte, Minas Gerais—Herzer, Richard W. (M)

Mexico
Mexico, D.F.—Beggs, Harry K. (M) (M, C/S—J-M)
Monterrey—Christianson, Philip L. (M)
San Luis Potosi—Olson, Arvid L. (M), Woodul, Lewis C. (M)

Ontario, Canada
Sault Ste. Marie—Hugill, Oswald H. (M)

South Australia
Port Pirie—Krysko, Wladimir (M)

The world is at your doorstep

When you see the VANCORAM trademark you can be assured of the highest quality products it is possible to produce.

The world is truly at your doorstep, for the finest raw materials from the world over contribute to the uniformity, superior quality and maximum efficiency of VANCORAM products.

To make it easier for you to identify these fine products, shipping drums are now painted a distinctive green with the VANCORAM trademark superimposed in white—your assurance of top-notch quality.

MAKERS OF ALLOYS
VANCORAM
CHEMICALS AND METALS

VANADIUM CORPORATION OF AMERICA

420 LEXINGTON AVENUE, NEW YORK 17, N. Y. • DETROIT • CHICAGO • CLEVELAND • PITTSBURGH

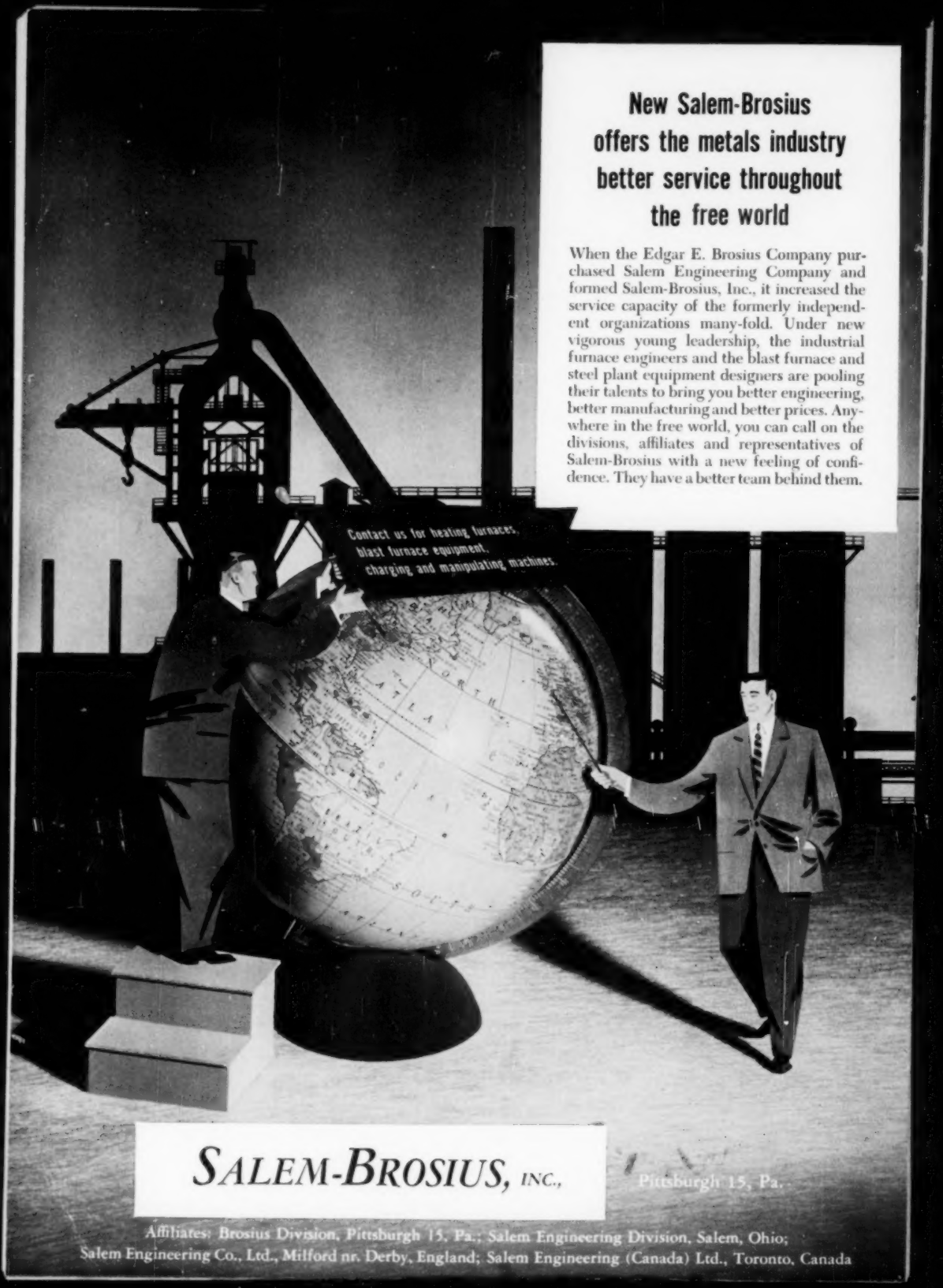

New Salem-Brosius offers the metals industry better service throughout the free world

When the Edgar E. Brosius Company purchased Salem Engineering Company and formed Salem-Brosius, Inc., it increased the service capacity of the formerly independent organizations many-fold. Under new vigorous young leadership, the industrial furnace engineers and the blast furnace and steel plant equipment designers are pooling their talents to bring you better engineering, better manufacturing and better prices. Anywhere in the free world, you can call on the divisions, affiliates and representatives of Salem-Brosius with a new feeling of confidence. They have a better team behind them.

SALEM-BROSIUS, INC., Pittsburgh 15, Pa.

Affiliates: Brosius Division, Pittsburgh 15, Pa.; Salem Engineering Division, Salem, Ohio; Salem Engineering Co., Ltd., Milford nr. Derby, England; Salem Engineering (Canada) Ltd., Toronto, Canada